Modeling compressible turbulence for explosion applications

Ali Toufaili

Aix*Marseille université
Socialement engagée

NNT/NL : 2020AIXM0001/001ED000

THÈSE DE DOCTORAT

Soutenue à Aix-Marseille Université
le 15 mars 2023 par

Ali TOUFAILI

Modélisation de la turbulence compressible pour l'explosion

Discipline
Mathématiques

École doctorale
ED 184 MATHÉMATIQUES ET INFORMATIQUE

Laboratoire/Partenaires de recherche
Institut de Mathématiques de Marseille
EDF lab Chatou-MFEE
Financement CIFRE EDF/AMU-I2M

Composition du jury

Christophe CHALONS Prof., UVSQ	Rapporteur
Samuel KOKH Dr-HdR, CEA Saclay	Rapporteur
Claire CHAINAIS Prof., Université de Lille	Examinatrice
Olivier HURISSE Dr-HdR, EDF R&D	Examinateur Encadrant industriel
Marica PELANTI MdC, ENSTA Paris	Examinatrice
Raphaèle HERBIN Prof., Aix-Marseille Université	Présidente du jury
Sergey GAVRILYUK Prof., Aix-Marseille Université	Co-directeur de thèse
Jean-Marc HÉRARD Dr-HdR, EDF R&D	Directeur de thèse
Gloria FACCANONI MdC, Université de Toulon	Invitée

Aix*Marseille université
Socialement engagée

INSTITUT de MATHÉMATIQUES de MARSEILLE

Affidavit

Je soussigné, Ali Toufaili, déclare par la présente que le travail présenté dans ce manuscrit est mon propre travail, réalisé sous la direction scientifique de Jean-Marc Hérard et Sergey Gavrilyuk, dans le respect des principes d'honnêteté, d'intégrité et de responsabilité inhérents à la mission de recherche. Les travaux de recherche et la rédaction de ce manuscrit ont été réalisés dans le respect à la fois de la charte nationale de déontologie des métiers de la recherche et de la charte d'Aix-Marseille Université relative à la lutte contre le plagiat.

Ce travail n'a pas été précédemment soumis en France ou à l'étranger dans une version identique ou similaire à un organisme examinateur.

Fait à Chatou le 05-12-2022

Liste de publications et participation aux conférences

Liste des publications réalisées dans le cadre du projet de thèse :

1. Sergey Gavrilyuk, Jean-Marc Hérard, Olivier Hurisse, and Ali Toufaili. *"Theoretical and Numerical Analysis of a Simple Model Derived from Compressible Turbulence."* Journal of Mathematical Fluid Mechanics 24, no. 2 (March 21, 2022). https ://doi.org/10.1007/s00021-022-00676-5

Participation aux conférences et écoles d'été au cours de la période de thèse :

1. Atelier, *New trends in complex flows*, Institut Henri Poincaré-Paris, 19–21 septembre 2022.
   https ://indico.math.cnrs.fr/event/8047/
2. Journées scientifiques, *GdR MaNu*, Le Croisic, 25–27 octobre 2021.
   https ://indico.math.cnrs.fr/event/6838/
3. Congrès, *10 ième Biennale Francaise des Mathématiques Appliquées et Industrielles SMAI*, La Grande Motte, du 21-25 juin 2021.
   https ://smai2021.math.univ-toulouse.fr5
4. École d'été, *ADVANCED NUMERICAL METHODS for HYPERBOLIC PDE*, Université de Trente-Italie, 01-05 février 2021.
   https ://webmagazine.unitn.it/en/evento/dicam/86729/short-course-on-advanced-numerical-methods-for-hyperbolic-equations
5. Journées scientifiques, *GdR MaNu*, en ligne, 15 octobre 2020.
   http ://gdr-manu.math.cnrs.fr/JS2020/

Résumé

Cette thèse concerne la modélisation et la simulation d'écoulements turbulents compressibles pour des applications à l'explosion.

La partie 1 considère un modèle de turbulence compressible simple proposé en 2014, où l'énergie cinétique turbulente est modélisée à l'aide d'une loi associée à un comportement uniforme en temps/espace de l'entropie turbulente. Il correspond à un modèle à trois équations de bilan masse, dynamique,énergie, en forme conservative, associé à une loi de fermeture thermodynamique prenant en compte les contributions de pression laminaire et turbulente. Les propriétés du modèle sont données, et l'analyse du problème de Riemann unidimensionnel permet d'obtenir un résultat d'existence et unicité de la solution de ce problème, pour des données initiales (presque) quelconques. Une seconde partie aborde la simulation numérique de ce modèle à l'aide d'un schéma de Godunov approché, et en examinant concrètement l'impact de l'amplitude du nombre de Mach turbulent associé aux conditions initiales.

Dans une seconde partie, on s'intéresse à un modèle de turbulence compressible proposé en 2006. Dans ce modèle, l'entropie turbulente peut varier à la traversée des chocs, avec une loi de comportement spécifiée dynamique. Le modèle proposé est analysé en détail, en examinant les conditions d'hyperbolicité, la caractérisation entropique et la structure d'ondes. C'est un modèle à 4 équations (masse/dynamique/énergie totale et entropie turbulente), intégrant un terme source sur les ondes de choc pour la dernière équation/variable. Une technique simple de Volumes finis, avec solveur de Riemann approché, intégrant le terme source dans les ondes de choc, permet d'obtenir des approximations discrètes des solutions. Ceci nécessite en particulier de mettre en place un détecteur de choc dynamique, qui est basé sur le contrôle de l'entropie et des conditions de Lax. Une analyse de convergence numérique en fonction du pas de maillage met en évidence les difficultés à simuler ce modèle.

La troisième partie propose un nouveau modèle qui comporte comme dans la partie 2 quatre EDP portant sur la masse/dynamique/énergie, mais la variable principale pour la dernière EDP est la fraction ξ_k d'entropie turbulente sur l'entropie totale (laminaire et turbulente), et le terme source intègre cette fois un terme de relaxation avec une échelle de temps de relaxation associée. La construction est différente de celle des modèles précédents et repose sur une vision diphasique de l'ensemble laminaire/turbulence. Le modèle est encore une fois analysé. Il est hyperbolique et possède une structure d'ondes proche de celle du système Euler, avec une contribution en pression totale/énergie interne totale associée aux deux contributions laminaire /

turbulente. La simulation de ce modèle est également abordée, mettant en œuvre une approche en Volumes Finis et des solveurs de Riemann de type VFRoe-ncv (Godunov approché), en variable ξ_k, ρ, U, P.

Mots clés : Turbulence, écoulements compressibles, explosion, système hyperbolique, problème de Riemann, ondes de choc, solveur de Riemann approché, volume fini.

Abstract

This thesis concerns the modeling and simulation of turbulent compressible flows for explosion applications.

Part 1 considers a simple compressible turbulence model proposed in 2014, where the turbulent kinetic energy is modeled using a law associated with a uniform behavior of turbulent entropy with respect to time/space. It corresponds to a model with three balance equations for mass / momentum / energy in conservative form, associated with a thermodynamics closure law which takes into account both laminar and turbulent pressure contributions. Model properties are given, and the analysis of the one-dimensional Riemann problem allows to obtain a result of existence and uniqueness for the solution of this problem, for (almost) arbitrary initial data. A second part deals with the numerical simulation of this model using an approximate Godunov scheme, and by investigating the impact of the turbulent Mach number amplitude associated with the initial conditions.

In the second chapter, we consider a compressible turbulence model proposed in 2006. In this model, the turbulent entropy can vary when crossing the shocks, with a dynamic specific constitutive law. The latter model is analyzed in detail, examining the hyperbolicity conditions, the entropy characterization and the wave structure. It is a four-equation model (for mass, momentum, total energy and turbulent entropy), integrating a source term on the shock waves for the last equation/variable. A simple Finite Volume technique, using an approximate Riemann solver, and integrating the source term in the shock waves, allows to obtain discrete approximations of the solutions. This requires in particular to define a dynamic shock detector, which is based on the entropy control and Lax conditions. A numerical convergence analysis as a function of the mesh size highlights the difficulties to simulate this model.

The third chapter proposes a new model which involves four partial differential equations for mass, momentum and energy balance. The fourth PDE governs the evolution of the turbulent entropy fraction ξ_k (ratio between turbulent and total entropies), and its source term integrates a relaxation term with an associated relaxation time scale. The construction relies on a diphasic vision of the laminar/turbulence interaction. The model is again analyzed. It is hyperbolic and its wave structure is close to that of the Euler system, including a contribution in total pressure / total internal energy associated with laminar/turbulent contributions. The simulation of this model is eventually discussed, using a Finite Volume approach and Riemann solvers (approximate Godunov scheme), using variables ξ_k, ρ, U, P.

Keywords: Turbulence, compressible flows, explosion, hyperbolic system, Riemann problem, shock waves, approximate Riemann solver, finite volume.

Remerciements

Table des matières

Table des figures

Introduction

0.1. Contexte industriel

Les différentes industries ou le milieu des transports sont confrontés à de nombreuses situations où des écoulements de fluides turbulents sont en jeu. Cette turbulence est générée par des inhomogénéités des domaines géométriques dans lesquels les fluides circulent (obstacles, diaphragmes, tuyères, coude, etc...) , par des éléments mécaniques (pompes, actuateurs, etc...) ou par la rencontre d'écoulements de propriétés différentes (té de mélange, vitesses co-courantes en bord de fuite d'un profil, etc ...). Les écoulements compressibles sont très présents dans l'industrie et les transports, par exemple pour : l'aérodynamisme, la combustion dans les moteurs/propulseurs, le risque d'explosion de nuages gazeux, de produits chimiques ou hydrocarbures, etc... Dans chacun de ces domaines, la turbulence peut être amenée à jouer un rôle important. C'est en particulier le cas pour tous les phénomènes où la combustion est l'élément central. On la retrouve naturellement au cœur des moteurs à combustion ou des engins de propulsion, mais elle a un rôle primordial dans le cas de l'explosion de nuages gazeux dans les milieux encombrés ou bâtis. C'est ce point en particulier qui est l'objet des travaux présentés dans cette thèse.

Le fonctionnement d'une centrale nucléaire nécessite d'utiliser une grande quantité d'hydrogène qui est stocké dans des réservoirs à haute pression. Il est bien connu qu'en présence d'oxygène (et donc d'air) cet hydrogène est hautement inflammable au-delà et en-deça de certains seuils en concentration. Cette inflammation entraîne une forte montée en température (jusqu'a plusieurs milliers de kelvin) et des déplacements brutaux et importants de masses gazeuses. Pour garantir la sûreté de ses installations, EDF doit donc démontrer la tenue du bâti à une hypothétique explosion d'un tel nuage d'hydrogène formé par une fuite du parc de réservoirs d'hydrogène. La simulation numérique de ce genre de phénomène est particulièrement sensible à la turbulence. En effet, une fois le nuage d'hydrogène allumé, le front de flamme va se propager dans le nuage sous l'action de deux phénomènes : la montée en température des gaz imbrûlés proches du front de flamme (zone extrêmement chaude) par conduction thermique, et l'activation de la réaction chimique de combustion dans les gaz imbrûlés proches du front de flamme suite à la montée en température. Ces mécanismes permettent, de proche en proche, de propager le front de combustion.

Certaines conditions de propagation de la flamme rendent le front de flamme turbulent, par exemple : lorsque celle-ci rencontre des obstacles sur sa trajectoire ou quand

des interactions d'ondes génèrent des instabilités qui plissent le front de flamme (instabilité de type Ritchmyer-Meshkov par exemple). Cette turbulence va avoir le même effet que la conduction thermique et va permettre de transférer de l'énergie thermique des gaz brûlés vers les gaz frais et donc favoriser la montée en température de ces derniers. Dans de nombreux régimes de fonctionnement, la turbulence est même prépondérante sur la conduction thermique, ce qui va entraîner une accélération du front de flamme, qui va elle-même augmenter la turbulence. La violence de l'explosion est donc plus élevée avec des conséquence potentielles plus importantes. La turbulence est donc un élément de modélisation central pour pouvoir prédire correctement l'explosion.

La modélisation de la turbulence pour les écoulements compressibles (en particulier réactifs) est donc un point sur lequel il faut porter une attention toute particulière. Si la turbulence des écoulements incompressibles, donc avec des vitesses d'écoulement faibles devant la vitesse du son, est assez bien étudiée depuis quelques décennies, les travaux sur la turbulence des écoulements compressibles sont comparativement plus rares et soulèvent encore de nombreuses questions ouvertes, telle que, par exemple, la génération de la turbulence dans une onde de choc.

0.2. Contexte scientifique

La modélisation numérique de la turbulence compressible peut être envisagée de plusieurs manières.

Une première approche consiste à rechercher des solutions approchées des équations de Navier-Stokes (NS) en formulation complète, sans modélisation ajoutée. Ceci requiert évidemment le recours à des maillages de taille rarement compatible avec les configurations industrielles devant faire l'objet d'études. On parle dans ce cas de simulation directe. Une approche assez voisine, dite LES (Large Eddy Simulation), introduit un tenseur de sous-maille qui vient s'ajouter au tenseur visqueux présent dans les équations de Navier-Stokes de base mentionnées ci-dessus. Dans la mesure où cette approche n'est pas retenue ici, nous ne la commenterons pas plus.

Dans une seconde approche, dite URANS (Unsteady Reynolds Averaged Navier Stokes equations), on introduit un opérateur de moyenne statistique, que l'on applique aux équations de Navier-Stokes en formulation complète, soit sur les bilans de masse, dynamique et énergie totale. Avec cette technique, on construit alors les équations d'évolution des moments d'ordre un relatifs à la densité moyenne, au débit moyen et à l'énergie totale moyenne. Ceci nécessite alors d'introduire les variables de densité $< \rho >$ et de pression $< P >$ moyenne (au sens de Reynolds), mais aussi de vitesse $\tilde{U}$ et d'énergie interne $\tilde{e}$ moyenne (au sens de Favre, avec pour n'importe quelle quantité ϕ la relation : $\tilde{\phi} =< \rho\phi > / < \rho >$). Il faut alors adjoindre une loi d'état reliant

les différentes variables thermodynamiques moyennes (densité, pression, énergie interne) entre elles, mais aussi des relations (dites de fermeture), soit écrites de manière locale, soit par le biais d'équations d'évolution en temps, pour "fermer" le problème (concrètement afin de disposer d'autant d'inconnues que d'équations). Les termes non linéaires des équations de NS génèrent en effet des moments d'ordre deux et plus, au sein des équations de bilan d'énergie totale moyenne et de bilan de quantité de mouvement moyen, parmi lesquels on trouve le tenseur de Reynolds $R_{ij} =< \rho u_i u_j >$, déjà présent dans le cadre incompressible à ρ constant. A ce stade, deux voies peuvent être considérées.

La plus classique consiste à relier le tenseur R_{ij} à sa trace et au tenseur vitesse de déformation moyenne, en posant :

$$R_{ij} = 2/3K\delta_{ij} \ -\mu_t\left(\partial_{x_j}(\tilde{U}_i) + \ \partial_{x_i}(\tilde{U}_j) \ -2/3\partial_{x_1}(\tilde{U}_1)\delta_{ij}\right)$$

où $K = 1/2R_{11}$ désigne l'énergie cinétique turbulente. Il faut alors écrire une équation donnant l'évolution en temps/espace de la variable K. Il est également indispensable de fournir une forme de viscosité turbulente pour μ_t, soit de manière algébrique, soit par le biais d'une équation d'évolution, qui peut par exemple porter sur la dissipation turbulente. Cette viscosité peut aussi être omise, dans une perspective d'applications comportant des ondes de pression laminaire et turbulente significatives. De nombreux travaux relatifs à cette approche de type $K-\epsilon$ existent dans la littérature, parmi lesquels on pourra au moins mentionner MOHAMMADI et PIRONNEAU 1993; SPALART et ALLMARAS 1994; LOUIS 1995; FORESTIER, Jean-Marc HÉRARD et LOUIS 1997; Christophe BERTHON 1999; POPE 2000; CHASSAING 2000 mais aussi TENNEKES et LUMLEY 1972; ERLEBACHER, HUSSAINI, KREISS et al. 1990; WILCOX 1998; GATSKI et BONNET 2013, qu'il s'agisse de travaux de modélisation ou de simulation numérique.

Dans le cas précédent, il est clair que par construction, le tenseur de Reynolds a ses axes propres alignés avec ceux du tenseur de vitesse de déformation moyenne, ce qui est assez souvent peu cohérent avec la réalité expérimentale. Une seconde possibilité consiste alors à écrire des équations d'évolution sur les composantes du tenseur de Reynolds, et de fermer les termes inconnus ainsi générés dans les nouvelles EDP afférentes. Les contraintes de réalisabilité pour le tenseur de Reynolds (garantissant le caractère défini positif de la matrice symétrique associée), l'objectivité, la consistance avec le second principe, et éventuellement d'autres éléments permettant de garantir que le problème à condition initiale pour le système complet est bien posé, peuvent alors être invoqués afin de limiter le choix des modèles aux lois de fermeture admissibles en ce(s) sens. Bien entendu, le problème de lois de fermeture n'est pas limité au seul tenseur de Reynolds, mais concerne aussi des corrélations de pression et de vitesse fluctuante, parmi d'autres. Si la littérature associée au cadre URANS est assez copieuse dans le cadre incompressible, elle est - assez paradoxalement- beaucoup plus restreinte dans le cadre compressible. On ne citera ici que quelques éléments tels que VANDROMME et MINH 1986; BRUN, J.-M HÉRARD, JEANDEL et al. 1999; C.

BERTHON, F. COQUEL, J. HÉRARD et al. 2002 ; S. GAVRILYUK et GOUIN 2012 ; AUDEBERT et Frédéric COQUEL 2006 ; RICHARD et S. L. GAVRILYUK 2013 ; NASR, GEROLYMOS et VALLET 2014 ; RICHARD et S. L. GAVRILYUK 2015.

Les méthodes décrites succinctement ci-dessus modélisent la turbulence sur la base de la dynamique de l'écoulement, à savoir la vitesse U. Or, dans le cadre des écoulements réactifs, il se trouve que c'est la température qui joue un rôle primordial pour la propagation du front de flamme. On choisit donc dans ces travaux de thèse de regarder une approche thermodynamique de la turbulence, comme celle proposée par exemple dans SAUREL, CHINNAYYA et RENAUD 2003 ; Jean-Marc HÉRARD 2014 ; Jean-Marc HÉRARD et LOCHON 2016. Pour ces modèles, ainsi que pour ceux étudiés dans la suite, l'idée de base est de voir l'écoulement comme un mélange de deux phases miscibles BARBERON et HELLUY 2005 ; H. MATHIS 2019 : une porteuse de l'énergie interne thermodynamique et une associée à la contribution turbulente de l'énergie. Le mélange de ces deux phases est alors fait en accord avec le second principe en supposant que l'énergie du système résulte de l'addition des énergies turbulente et thermodynamique. On obtient alors par construction un tenseur des contraintes isotrope et diagonal, de la forme :

$$R_{ij} = 2/3K\delta_{ij},$$

qui modifie la pression vue par l'écoulement. De la même façon, la température du système est une combinaison entre la température thermodynamique, et une température "turbulente" associée à l'énergie turbulente. Cette température de mélange vue par la réaction de combustion est ainsi plus importante en présence de turbulence et dépend directement de cette dernière. On espère ainsi pouvoir obtenir une vitesse de flamme qui dépend de la turbulence, même si ce couplage avec des termes sources réactifs n'a pas été testé au cours des travaux de cette thèse.

L'avantage d'introduire la turbulence comme une quantité thermodynamique est que l'on bénéficie de toutes les conséquences positives de la modélisation thermodynamique des mélanges basée sur le modèle d'Euler avec énergie BARBERON et HELLUY 2005. En particulier, les modèles ainsi construits sont réalisables naturellement et ils sont associés à des systèmes d'EDP hyperboliques à condition que les lois d'état soient bien choisies. Par ailleurs, le cadre Euler associé aux modèles étant conservatif, les chocs sont définis de manière unique et non-équivoque à travers des relations de Rankine-Hugoniot. Ce dernier point est particulièrement important car il constitue un point faible de beaucoup de modèles issus de la dynamique.

En revanche, le tenseur des contraintes étant extrêmement simplifié dans cette approche, elle ne permet pas, en l'état, d'être aussi précise que des modélisations de type R_{ij} plus complexes. La turbulence des écoulements fluides n'est en effet plus isotrope dès lors que l'on est en présence d'obstacles ou de singularités. De même, la notion classique de couche limite n'est ici pas prise en compte. Ce point n'a pas

été abordé dans ces travaux, mais il est possible d'introduire dans les modèles (en particulier ceux des chapitres 1 et 3) une notion de dissipation de la turbulence et une notion de création de la turbulence (par transfert entre l'énergie cinétique et l'énergie turbulente), tout en conservant les bonnes propriétés des modèles.

0.3. Objectifs des travaux

Le présent manuscrit est composé de trois chapitres, dans lesquels trois modèles de complexité croissante sont étudiés. Le premier chapitre constitue une étude théorique du modèle proposé dans Jean-Marc HÉRARD 2014. Ce modèle fait l'hypothèse que l'entropie turbulente est constante et uniforme à travers tout le domaine, y compris à travers les chocs. Cette dernière hypothèse semble peu réaliste Sergey GAVRILYUK et Richard SAUREL 2006. En effet, dans Sergey GAVRILYUK et Richard SAUREL 2006, un modèle de saut d'entropie turbulente à travers un choc a été proposé. Cette proposition a été testée numériquement dans le chapitre 2. Enfin, dans le troisième chapitre, un modèle continu permettant de gérer nativement les sauts d'entropie turbulente à la fois dans le contact et les chocs est étudié. Celui-ci est basé sur une équation de transport de l'entropie turbulente, qui est relaxée à l'aide d'un terme source. Cette relaxation, compatible avec le second principe de la thermodynamique, permet de faire varier l'entropie turbulente dans les chocs.

0.4. Synthèse des travaux

Chapitre 1 : Analyse numérique et théorique d'un modèle simple dérivé de la turbulence compressible

Les modèles de turbulence sont largement étudiés dans la littérature (cf par exemple FAVRE 1958 ; TENNEKES et LUMLEY 1972 ; ERLEBACHER, HUSSAINI, KREISS et al. 1990 ; SPALART et ALLMARAS 1994 ; WILCOX 1998). Dans ce premier chapitre, on s'intéresse à l'étude d'un modèle de turbulence simple. Cette étude comporte deux parties : théorique et numérique. Le modèle considéré ici est le modèle proposé dans Jean-Marc HÉRARD 2014 (l'extension étant Jean-Marc HÉRARD et LOCHON 2016 dans le cadre diphasique). Le système d'équations aux dérivées partielles est basé sur les équations de Euler/Navier-Stokes (à 3 équations, sans EDP supplémentaire introduite), où la turbulence est prise en compte à l'aide d'une fermeture algébrique. Le système d'EDP dans le cadre unidimensionnel est le suivant :

$$\begin{cases} \partial_t(\rho) + \partial_x(\rho u) = 0 \\ \partial_t(\rho u) + \partial_x\left(\rho u^2 + P + \dfrac{2K}{3}\right) = 0 \\ \partial_t(\rho E) + \partial_x\left(u\left(\rho E + P + \dfrac{2K}{3}\right)\right) = 0 \end{cases} \tag{0.1}$$

avec $\rho E = \rho e(P,\rho) + \frac{\rho u^2}{2} + K$.
Les quantités ρ, u, P, et E représentent respectivement la densité moyennée, la vitesse moyennée, la pression moyennée et l'énergie moyennée. K représente l'énergie cinétique turbulente :

$$K = \xi_0 \rho^{5/3},$$

avec ξ_0 une constante positive.
Dans la suite, afin de simplifier les calculs, nous introduisons la pression totale P^* :

$$P^* = P + 2/3K.$$

Dans un premier temps, une étude détaillée des propriétés du modèle est proposée. Il s'agit d'une inégalité d'entropie qui permet de choisir les solutions admissibles du problème de Riemann associé au système (0.1). La propriété d'hyperbolicité est bien vérifiée. Le système en variables $w = (\rho, u, P)$ est strictement hyperbolique et il admet 3 valeurs propres réelles distinctes associées à des champs VNL (vraiment non linéaire) et LD (linéairement dégénéré). Les invariants de Riemann associés à ces différentes natures de champs (VNL, LD) sont trouvés pour 2 variables différentes w et $Y = (s, u, P^*)$. Pour l'étude des ondes des choc, une caractérisation des relations de Rankine-Hugoniot est faite. On montre que dans le cas d'une loi d'état de type gaz parfait turbulent, on a :

$$\beta^{-1} \leq \frac{\rho_r}{\rho_l} \leq \beta,$$

avec $\beta = \frac{\gamma+1}{\gamma-1}$. On établit ainsi l'équivalence avec la formule associée aux équations d'Euler laminaire (sans la contribution turbulente) (voir SMOLLER 1983).

Dans le cas de gaz parfaits, l'existence et l'unicité de la solution du problème de Riemann unidimensionnel sans apparition de vide sont montrés, sous une condition portant sur l'écart de vitesse moyenne initial :

$$u_R - u_L < X_L + X_R, \tag{0.2}$$

avec $X_i = \int_0^{\rho_i} \frac{c_t(s,\rho')}{\rho'} \mathrm{d}\rho'$, où $c_t = c^2 + \frac{10K}{9\rho}$ est la célérité totale du mélange .
La méthode employée pour la mise en œuvre numérique est classique. Le système est résolu à l'aide d'un schéma volumes finis, en utilisant un solveur de Riemann approché, de type VFRoe-ncv BUFFARD, Thierry GALLOUËT et Jean-Marc HÉRARD 2000. Le schéma VFRoe-ncv consiste à résoudre à chaque interface le problème de Riemann linéarisé en utilisant la variable $Z = (\rho, u, P^*)$:

$$\begin{cases} \partial_t Z + B(\bar{Z})\partial_x Z = 0. \\ Z(x, t=0) = \begin{cases} Z_L \text{ si } x < 0 \\ Z_R \text{ si } x > 0 \end{cases} \end{cases}$$

avec $\bar{Z} = \frac{Z_R + Z_R}{2}$.
Pour s'assurer de la convergence numérique du schéma, des cas tests de vérification ont été mis en place : il s'agit de problèmes de Riemann unidimensionnels, en faisant varier la nature des ondes. Les cas tests unidimensionnels réalisés sont les suivants :

- un premier cas de double choc permet d'obtenir une courbe de convergence numérique.
- un second cas test correspond à une situation où les états initiaux présentent un grand écart de pression/densité ; il est représentatif de situations impliquant des ondes d'explosion ou de détonation. Ce cas test nécessite une correction entropique HELLUY, Jean-Marc HÉRARD, Hélène MATHIS et al. 2010 liée à la propagation d'une onde de raréfaction supersonique.
- un dernier cas de double raréfaction symétrique est représentatif de ce qui se passe à proximité d'une paroi en dépressurisation.

Dans le cadre bidimensionnel, une simulation en gaz parfait est effectuée, qui est représentative d'une explosion se propageant dans un espace ouvert comportant un bâtiment. La structure de l'écoulement est examinée. Ces simulations nous permettent de nous assurer de la consistance du schéma, et voir l'effet du niveau de la turbulence sur l'écoulement.

Le modèle étudié correspond à une entropie turbulente ξ constante. Dans les prochains chapitres 2 et 3, des modèles plus complexes, faisant varier l'entropie turbulente, seront présentés et analysés.

Chapitre 2 : Un solveur hybride pour calculer un modèle compressible avec une estimation dynamique de l'énergie cinétique turbulente à travers une onde de choc

Le modèle du chapitre 1 tient compte de l'énergie cinétique turbulente K de manière simple :

$$K(\rho) = \xi_0 \rho^{5/3}. \tag{0.3}$$

On peut donc soutenir que la fermeture de K (0.3) ne prend pas en compte la variation d'entropie turbulente à travers le choc. Dans ce chapitre, nous introduisons un modèle de turbulence plus pertinent, qui permettrait de présenter des écoulements compressibles turbulents avec plus de précision, l'entropie turbulente variant à travers le choc. Ce modèle est une extension (à 4 équations) du modèle proposé dans Jean-Marc HÉRARD 2014 ; Jean-Marc HÉRARD et LOCHON 2016, basé sur les équations d'Euler moyennées . Il a trois lois de conservation correspondant au bilan de masse, bilan de quantité de mouvement et bilan d'énergie. Une quatrième équation sur ξ décrit l'évolution de l'entropie turbulente, en prenant en compte sa variation à travers les ondes de choc. Les équations aux dérivées partielles dans le cadre unidimensionnel

s'écrivent comme suit :

$$\begin{cases} \partial_t(\rho) + \partial_x(\rho u) = 0 \\ \partial_t(\rho u) + \partial_x\left(\rho u^2 + P + \dfrac{2K}{3}\right) = 0 \\ \partial_t(\rho E) + \partial_x\left(u\left(\rho E + P + \dfrac{2K}{3}\right)\right) = 0 \\ \partial_t(\rho\xi) + \partial_x(\rho u\xi) + M(x,t)\delta_{(x-\sigma t=0)} = 0 \end{cases} \tag{0.4}$$

avec $\xi = K\rho^{-5/3}$, $M(x,t)$ est la masse localisée à la position du choc et σ est la vitesse d'onde de choc, et E désigne l'énergie totale :

$$E = e(P,\rho) + \frac{1}{2}u^2 + \frac{K}{\rho}.$$

Notre première partie dans ce chapitre consiste à estimer le saut d'entropie turbulente "$[\xi]_l^r$" à travers les ondes de choc, en suivant la méthodologie proposée dans l'article de Sergey GAVRILYUK et Richard SAUREL 2006. Le calcul de la masse localisée sur une onde de choc est obtenu en faisant la résolution du système de Rankine-Hugoniot associé au système (0.4). Étant donné $(\rho,u,P,\xi)_l$ et σ, on va calculer $(\rho,u,P)_r$ et M_0 tel que :

$$\begin{cases} [\rho(u-\sigma)]_l^r = 0 \\ m^2[\tau]_l^r + [P^*]_l^r = 0 \\ [e + K\tau]_l^r + \bar{P}^*_{rl}[\tau]_l^r = 0, \\ m[\xi]_l^r + M_0 = 0 \end{cases} \tag{0.5}$$

avec $m = \rho_r(u_r - \sigma)$, $P^* = P + \frac{2}{3}K$ et $\tau = \frac{1}{\rho}$.

La deuxième partie porte sur la mise en œuvre numérique. Nous proposons un schéma numérique adapté à ce modèle. Dans le cadre d'une approche volumes finis, nous avons choisi d'utiliser un solveur hybride pour calculer les solutions approchées du modèle à l'interface. Ce solveur hybride est composé de deux solveurs :

- Un solveur de Riemann approché en l'absence de choc à l'interface : VFRoe-ncv BUFFARD, Thierry GALLOUËT et Jean-Marc HÉRARD 2000.
- Un solveur de Riemann approché modifié "MARS", dédié à l'interface où on a une onde de choc.

Une technique de détection de choc est proposée (voir KANAMORI et SUZUKI 2011 ; WU, XU, WANG et al. 2013, pour les modèles stationnaires), afin de détecter les interfaces instationnaires où il apparaît des ondes de choc, et par suite, d'adapter sur cette interface le solveur "MARS". Cette technique s'appuie sur l'inégalité de l'entropie et les conditions de Lax. Le schéma numérique s'écrit :

$$\Delta x_i(Z_i^{n+1} - Z_i^n) + \Delta t(\mathscr{F}^n_{i+\frac{1}{2}} - \mathscr{F}^n_{i-\frac{1}{2}}) + \Delta t B_i^n = 0, \tag{0.6}$$

avec $Z = (\rho, \rho u, \rho E, \rho\xi)$, $B_i = (0,0,0,M_i)$, et :

$$\mathscr{F}^n_{i+\frac{1}{2}} = \begin{cases} \mathscr{F}^{lnd}_{i+\frac{1}{2}} = F(Z(W^*_{lnd}(W^n_i, W^n_{i+1})) \text{ lorsqu'aucune onde de choc n'a été détectée,} \\ \mathscr{F}^{MARS}_{i+\frac{1}{2}} = F(Z(W^*_{MARS}(W^n_i, W^n_{i+1})) \text{ si une onde de choc a été détectée.} \end{cases} \tag{0.7}$$

Des tests numériques sont réalisés :

— Un premier cas test comporte un double choc non symétrique avec M_0=0 et une entropie turbulente constante ($\xi = \xi_0$). Ce cas test est issu du chapitre 1, il vise à tester le solveur modifié "MARS" lorsque le système est conservatif, et à comparer les résultats obtenus avec ceux du chapitre 1.

— Un deuxième cas test présente une onde de choc simple (plus précisément un $u+\tilde{c}$-choc), avec M_0 non nul. Les conditions initiales de ce test ont été construites grâce à la relation de saut associée au modèle (0.4), de manière à être capable d'en exhiber une solution analytique.

Les principaux résultats obtenus sont ensuite présentés.

Chapitre 3 : Une approche de relaxation pour modéliser la turbulence dans les écoulements compressibles

Dans le chapitre 2, un modèle de turbulence compressible impliquant une entropie turbulente variant à travers les chocs a été étudié. Mais ce modèle reste à priori difficilement applicable en 3D. Dans ce chapitre, on introduit un modèle qui permet de faire varier l'entropie turbulente à travers les chocs, tout en étant adapté aux écoulements en 3D.

Ce modèle est basé sur une approche de relaxation et il utilise des caractéristiques classiques de la thermodynamique des mélanges en écoulement multiphasique BARBERON et HELLUY 2005 ; H. MATHIS 2019, et reprend certains principes utilisés dans SAUREL, CHINNAYYA et RENAUD 2003. Le modèle est d'abord décrit en forme extensive. Des hypothèses de modélisation sont proposées, telles que :

— l'entropie turbulente (η_k) et l'entropie laminaire (η_l) sont deux contributions à un mélange de deux phases miscible partageant une même masse ($\mathscr{M} = \mathscr{M}_k = \mathscr{M}_l$).

— l'entropie totale η est la somme de deux entropies : $\eta = \eta_k + \eta_l$.

— la masse "$\mathscr{M}$" de fluide possède une énergie interne à deux contributions (laminaire et turbulente) $\mathscr{E} = \mathscr{E}_k + \mathscr{E}_l$.

Nous introduisons la fraction entropique turbulente : $\xi_k = \frac{\eta_k}{\eta_k+\eta_l} \in [0,1]$.

Une écriture complète des équations aux dérivées partielles (EDP) sous forme conser-

vative est présentée :

$$\begin{cases} \partial_t \rho\xi_k + \partial_x \rho U\xi_k = \rho\mathscr{S}_k, \\ \partial_t \rho + \partial_x \rho U = 0, \\ \partial_t \rho U + \partial_x \rho U^2 + P = 0, \\ \partial_t \rho E + \partial_x U(\rho E + P) = 0, \end{cases} \tag{0.8}$$

où ρ est la densité, U la vitesse, $P = P_l + P_k$ la pression totale, $E = e + U^2/2$ l'énergie totale spécifique, et $\mathscr{S}_k$ le terme source.

Une discussion concernant la différence entre ce modèle et le modèle du chapitre 1 a été proposée. Sous les hypothèses :

— s_k est uniforme $s_k = s_k^0 \neq 0$;
— le terme source $\mathscr{S}_k = 0$;
— l'EOS pour la contribution turbulente est définie comme : $e_k(\tau, s_k) = s_k \tau^{-2/3}$;

nous retrouvons, pour les solutions régulières, le même modèle que celui introduit dans Jean-Marc HÉRARD 2014 et détaillé dans Sergey GAVRILYUK, Jean-Marc HÉRARD, Olivier HURISSE et al. 2022. Concernant les solutions chocs, les relations de saut sont différentes de celles du chapitre 1 et donc les solutions impliquant des chocs sont différentes.
Certaines des principales propriétés du système d'équations (0.8) sont fournies, telles que : l'hyperbolicité, l'inégalité d'entropie, les invariants de Riemann et les relations de saut.
Une configuration complète du problème de Riemann de la partie convective est ensuite étudiée, où l'EOS pour la contribution laminaire est une EOS de gaz parfait, tandis que pour la contribution turbulente l'EOS est dérivée de celle utilisée dans Jean-Marc HÉRARD 2014.
Le pendant de cette étude est proposé ensuite lorsque l'on considère que le fluide est en équilibre de température (c'est-à-dire en relaxation instantanée). Nous décrivons d'abord la loi de pression de mélange qui rend compte de l'équilibre de température instantané. Puis, sur la base de cette loi de pression, le cas d'un seul choc est étudié comme pour le modèle proposé en Sergey GAVRILYUK et Richard SAUREL 2006.

La méthode numérique employée est classique. Elle est fondée sur la méthode des pas fractionnaires YANENKO 1968 et utilise un splitting de Lie-Trotter. A chaque itération, le système convectif est d'abord résolu à l'aide de schémas de volumes finis explicites :

$$\begin{cases} \partial_t \rho\xi_k + \partial_x \rho U\xi_k = 0, \\ \partial_t \rho + \partial_x \rho U = 0, \\ \partial_t \rho U + \partial_x \rho U^2 + P = 0, \\ \partial_t \rho E + \partial_x U(\rho E + P) = 0, \end{cases} \tag{0.9}$$

et dans un second temps, le terme source est discrétisé en résolvant implicitement

le système suivant :

$$\begin{cases} \partial_t \xi_k = \frac{\bar{\xi}_k(\tau,e)-\xi_k}{\lambda(t)}, \\ \partial_t \rho = 0, \\ \partial_t \rho U = 0, \\ \partial_t \rho E = 0, \end{cases} \tag{0.10}$$

Afin d'assurer la consistance et la convergence du schéma numérique, plusieurs cas tests sur la base du problème de Riemann sont présentés :

1. Le premier cas test est lié à l'étude de l'équilibre de température pour une 1-onde de choc isolée.
2. Pour le deuxième cas test, le niveau de turbulence initial est choisi uniforme pour une configuration à double choc, et le terme source d'équilibre de température n'est pas pris en compte. Ce cas test a déjà été présenté avec le modèle présenté au chapitre 1.
3. Un troisième cas test correspond à une transition laminaire-turbulente. Une seule onde de choc est considérée et sépare deux zones : une dans laquelle la vitesse est nulle et la turbulence est nulle, et une seconde où l'on considère l'équilibre de température. De nombreuses configurations ont été testées, en faisant varier : le niveau de turbulence (toujours proche de zéro mais non nul), le temps de relaxation λ.

A l'issue des résultats obtenus à partir des tests numériques ci-dessus, nous avons vérifié la convergence numérique du schéma à la fois pour la partie convective et la partie terme source.

Bibliographie

[AC06] Bruno AUDEBERT et Frédéric COQUEL. « Hybrid Godunov-Glimm Method for a Nonconservative Hyperbolic System with Kinetic Relations ». In : *Numerical Mathematics and Advanced Applications*. Springer Berlin Heidelberg, 2006, p. 646-653. DOI : 10.1007/978-3-540-34288-5_62 (cf. p. 4).

[BH05] Thomas BARBERON et Philippe HELLUY. « Finite volume simulation of cavitating flows ». In : *Computers &amp Fluids* 34.7 (août 2005), p. 832-858. DOI : 10.1016/j.compfluid.2004.06.004 (cf. p. 4, 9).

[Ber+02] C. BERTHON, F. COQUEL, J.M. HÉRARD et al. « An approximate solution of the Riemann problem for a realisable second-moment turbulent closure ». In : *Shock Waves* 11.4 (jan. 2002), p. 245-269. DOI : 10.1007/s001930100109 (cf. p. 3).

[Ber99] Christophe BERTHON. « Contribution à l'analyse numérique des équations de Navier-Stokes compressibles à deux entropies spécifiques. Applications à la turbulence compressible ». Thèse de doct. Paris 6, 1999. URL : https://www.math.sciences.univ-nantes.fr/~berthon/cv_these_hdr/these.pdf (cf. p. 3).

[Bru+99] G BRUN, J.-M HÉRARD, D JEANDEL et al. « An Approximate Riemann Solver for Second-Moment Closures ». In : *Journal of Computational Physics* 151.2 (mai 1999), p. 990-996. DOI : 10.1006/jcph.1999.6190 (cf. p. 3).

[BGH00] Thierry BUFFARD, Thierry GALLOUËT et Jean-Marc HÉRARD. « A sequel to a rough Godunov scheme : application to real gases ». In : *Computers & Fluids* 29(7) (2000), p. 813-847. DOI : 10.1016/s0045-7930(99)00026-2 (cf. p. 6, 8).

[Cha00] Patrick CHASSAING. *Turbulence en mécanique des fluides*. Cépaduès-éditions, 2000 (cf. p. 3).

[Erl+90] Gordon ERLEBACHER, Mohammed Yousuff HUSSAINI, Heinz-Otto KREISS et al. « The analysis and simulation of compressible turbulence ». In : *Theoretical and Computational Fluid Dynamics* 2.2 (1990), p. 73-95. DOI : 10.1007/bf00272136 (cf. p. 3, 5).

[Fav58] Alexandre FAVRE. « Equations statistiques des gaz turbulents ». In : *Compte-Rendus de l'Académie des Sciences Paris* 246.18 (1958), p. 2576-2579 (cf. p. 5).

Bibliographie

[FHL97] Alain FORESTIER, Jean-Marc HÉRARD et Xavier LOUIS. « Solveur de type Godunov pour simuler les écoulements turbulents compressibles ». In : *Comptes Rendus de l'Académie des Sciences-Series I-Mathematics* 324(8) (1997), p. 919-926. DOI : 10.1016/s0764-4442(97)86969-8 (cf. p. 3).

[GB13] Thomas B GATSKI et Jean-Paul BONNET. *Compressibility, turbulence and high speed flow*. Academic Press, 2013. URL : https://www.researchgate.net/publication/281766815_Compressibility_Turbulence_and_High_Speed_Flow (cf. p. 3).

[GG12] S. GAVRILYUK et H. GOUIN. « Geometric evolution of the Reynolds stress tensor ». In : *International Journal of Engineering Science* 59 (oct. 2012), p. 65-73. DOI : 10.1016/j.ijengsci.2012.03.008 (cf. p. 4).

[Gav+22] Sergey GAVRILYUK, Jean-Marc HÉRARD, Olivier HURISSE et al. « Theoretical and numerical analysis of a simple model derived from compressible turbulence ». In : *Journal of Mathematical Fluid Mechanics* 24.2 (2022), p. 1-34. DOI : 10.1007/s00021-022-00676-5 (cf. p. 10).

[GS06] Sergey GAVRILYUK et Richard SAUREL. « Estimation of the turbulent energy production across a shock wave ». In : *Journal of Fluid Mechanics* 549 (2006), p. 131. DOI : 10.1017/s0022112005008062 (cf. p. 5, 8, 10).

[Hér14] Jean-Marc HÉRARD. Rapp. tech. A simple turbulent model for compressible flows, 2014. URL : https://hal.archives-ouvertes.fr/hal-02007044 (cf. p. 4, 5, 7, 10).

[HL16] Jean-Marc HÉRARD et Hippolyte LOCHON. « A simple turbulent two-fluid model ». In : *Comptes Rendus Mécanique* 344(11-12) (2016), p. 776-783. DOI : 10.1016/j.crme.2016.10.010 (cf. p. 4, 5, 7).

[KS11] Masashi KANAMORI et Kojiro SUZUKI. « Shock wave detection in two-dimensional flow based on the theory of characteristics from cfd data ». In : *Journal of Computational Physics* 230.8 (2011), p. 3085-3092. DOI : 10.1016/j.jcp.2011.01.007 (cf. p. 8).

[Lou95] Xavier LOUIS. « Modélisation numérique de la turbulence compressible ». Thèse de doct. Paris 6, 1995 (cf. p. 3).

[Mat19] H. MATHIS. « A thermodynamically consistent model of a liquid-vapor fluid with a gas ». In : *ESAIM : Mathematical Modelling and Numerical Analysis* 53.1 (2019), p. 63-84. DOI : 10.1051/m2an/2018044 (cf. p. 4, 9).

[MP93] Bijan MOHAMMADI et Olivier PIRONNEAU. *Analysis of the k-epsilon turbulence model*. Masson, 1993 (cf. p. 3).

[NGV14] N. Ben NASR, G.A. GEROLYMOS et I. VALLET. « Low-diffusion approximate Riemann solvers for Reynolds-stress transport ». In : *Journal of Computational Physics* 268 (juill. 2014), p. 186-235. DOI : 10.1016/j.jcp.2014.02.010 (cf. p. 4).

Bibliographie

[Pop00] Stephen B POPE. *Turbulent flows*. Cambridge university press, 2000. DOI : 10.1017/cbo9780511840531 (cf. p. 3).

[RG13] G. L. RICHARD et S. L. GAVRILYUK. « The classical hydraulic jump in a model of shear shallow-water flows ». In : *Journal of Fluid Mechanics* 725 (mai 2013), p. 492-521. DOI : 10.1017/jfm.2013.174 (cf. p. 4).

[RG15] G. L. RICHARD et S. L. GAVRILYUK. « Modelling turbulence generation in solitary waves on shear shallow water flows ». In : *Journal of Fluid Mechanics* 773 (mai 2015), p. 49-74. DOI : 10.1017/jfm.2015.236 (cf. p. 4).

[SCR03] R SAUREL, A CHINNAYYA et F RENAUD. « Thermodynamic analysis and numerical resolution of a turbulent-fully ionized plasma flow model ». In : *Shock Waves* 13.4 (2003), p. 283-297. DOI : 10.1007/s00193-003-0216-z (cf. p. 4, 9).

[Smo83] Joel SMOLLER. *Shock waves and reaction—diffusion equations*. Springer Science & Business Media, 1983. DOI : 10.1007/978-1-4684-0152-3 (cf. p. 6).

[SA94] Philippe SPALART et Steven ALLMARAS. « A one-equation turbulence model for aerodynamic flows ». In : *La Recherche Aérospatiale* (1994), p. 5-21. URL : https://arc.aiaa.org/doi/10.2514/6.1992-439 (cf. p. 3, 5).

[TL72] Henk TENNEKES et John Leask LUMLEY. « A First Course in Turbulence. » In : *MIT Press* (1972). DOI : 10.7551/mitpress/3014.003.0005 (cf. p. 3, 5).

[VM86] D. VANDROMME et H.Ha MINH. « About the coupling of turbulence closure models with averaged Navier-Stokes equations ». In : *Journal of Computational Physics* 65.2 (août 1986), p. 386-409. DOI : 10.1016/0021-9991(86)90214-7 (cf. p. 3).

[Wil98] David WILCOX. *Turbulence Modelling for CFD*. DCW Industries, 1998 (cf. p. 3, 5).

[Wu+13] Ziniu WU, Yizhe XU, Wenbin WANG et al. « Review of shock wave detection method in CFD post-processing ». In : *Chinese Journal of Aeronautics* 26.3 (2013), p. 501-513. DOI : 10.1016/j.cja.2013.05.001 (cf. p. 8).

[Yan68] NN YANENKO. *Méthode à pas fractionnaires : résolutions de problèmes polydimensionnels de physique mathématique*. A. Colin, 1968. URL : https://books.google.fr/books?id=JBIyvgAACAAJ (cf. p. 10).

1. Theoretical and numerical analysis of a simple model derived from compressible turbulence

Sommaire

Theoretical and numerical analysis of a simple model derived from compressible turbulence

Sergey Gavrilyuk[b], Jean-Marc Hérard[a], Olivier Hurisse[a], Ali Toufaili[a,c] :
[a] EDF R&D, 6 quai Watier, 78400 Chatou, France.
[b] IUSTI UMR CNRS 7343, Technopôle Château-Gombert, Marseille, France.
[c] I2M UMR CNRS 7373, Technopôle Château-Gombert, Marseille, France.

Abstract
Turbulent compressible flows are encountered in many industrial applications, for instance when dealing with combustion or aerodynamics. This paper is dedicated to the study of a simple turbulent model for compressible flows. It is based on the Euler system with an energy equation and turbulence is accounted for with the help of an algebraic closure that impacts the thermodynamical behavior. Thereby, no additional PDE is introduced in the Euler system. First, a detailed study of the model is proposed : hyperbolicity, structure of the waves, nature of the fields, existence and uniqueness of the Riemann problem. Then, numerical simulations are proposed on the basis of existing finite-volume schemes. These simulations allow to perform verification test cases and more realistic explosion-like test cases with regards to the turbulence level.

key words :
Turbulence, compressible flows, hyperbolicity, entropy, shock waves, Riemann problem

Introduction

The modeling of compressible turbulent flows has actually been widely investigated for many years. It is basically grounded on compressible Navier-Stokes equations, with an unsteady setting (see for instance FAVRE 1958; FAVRE 1965; TENNEKES et LUMLEY 1972; FAVRE, KOSVAZNAY, DUMAS et al. 1976; ERLEBACHER, HUSSAINI, KREISS et al. 1990; SPALART et ALLMARAS 1994; WILCOX 1998; Christophe BERTHON 1999; Christophe BERTHON et Frédéric COQUEL 2002; Sergey GAVRILYUK et Richard SAUREL 2006; GATSKI et BONNET 2013.)
Compressible turbulent models are used in many applications, for instance in the framework of combustion and aerodynamics. They always involve three conservation laws that govern the evolution of mass, momentum and total energy of the fluid. Using classical Reynolds averaging and denoting $\overline{\overline{\phi}}$ the mean value of quantity ϕ, we recall that the Favre average $\tilde{\psi}$ of any variable ψ is defined as (FAVRE 1958; FAVRE 1965; FAVRE, KOSVAZNAY, DUMAS et al. 1976) :

$$\tilde{\psi} = \frac{\overline{\overline{\rho\psi}}}{\overline{\overline{\rho}}}.$$

Hence, in the sequel, $\overline{\overline{\rho}}$, $\overline{\overline{P}}$ will represent the mean density and the mean pressure respectively, while $\tilde{u}$ and $\tilde{e}$ will stand for the Favre average of velocity and internal energy. Exact balance laws thus read :

$$\begin{cases} \partial_t(\overline{\overline{\rho}}) + \nabla.(\overline{\overline{\rho}}\tilde{u}) = 0 \\ \partial_t(\overline{\overline{\rho}}\tilde{u}) + \nabla.\left(\overline{\overline{\rho}}\tilde{u}\otimes\tilde{u} + \left(\overline{\overline{P}} + \frac{2K}{3}\right).\mathscr{I}\right) = \epsilon_0\nabla.(\Sigma^{tot}(\nabla^s\tilde{u})) \\ \partial_t(\overline{\overline{\rho}}E) + \nabla.\left(\tilde{u}\left(\overline{\overline{\rho}}E + \overline{\overline{P}} + \frac{2K}{3}\right)\right) = \epsilon_0\nabla.(\Sigma^{tot}(\nabla^s\tilde{u})\,\tilde{u}) \end{cases} \tag{1.1}$$

where $\mathscr{I}$ is the identity matrix.
The second order tensor $\Sigma^{tot}(\nabla^s\tilde{u})$ cumulates laminar and turbulent viscous contributions, ϵ_0 is a positive parameter in [0,1] and K denotes the turbulent kinetic energy. The total energy is :

$$\overline{\overline{\rho}}E = \overline{\overline{\rho}}(\frac{\tilde{u}^2}{2} + \tilde{e}) + K,$$

and $\tilde{e}$ is a function that is expected to be given through an equation of state (EOS), for instance, for a perfect gas EOS :

$$\tilde{e}(\overline{\overline{P}},\overline{\overline{\rho}}) = \frac{\overline{\overline{P}}}{(\gamma-1)\overline{\overline{\rho}}},$$

with $\gamma > 1$. Obviously, $\epsilon_0 = 0$ corresponds to the limit case of vanishing viscosity. Actually, the three-equation model (1.1) involves four main unknowns $\overline{\overline{\rho}}$, $\overline{\overline{P}}$, $\tilde{u}$ and K.

Thus one closure law is required for the latter turbulent kinetic energy K, and several strategies have been proposed in the past for that purpose, that we briefly summarize below.
The most widespread approach consists in deriving the governing equation for K, starting from Euler or Navier-Stokes equations, and focusing on smooth solutions. Setting W the state variable, this leads to the following PDE for K :

$$\partial_t(K) + \nabla.(K\tilde{u}) + \frac{2K}{3}\nabla.(\tilde{u}) = rhs_K(W, \nabla W), \tag{1.2}$$

where the right-handside term $rhs_K(W, \nabla W)$ does not include any convective (first-order differential) term. Thus, by introducing a change of variable :

$$\xi = K\,(\overline{\overline{\rho}})^{-5/3},$$

where ξ is sometimes refered to as the turbulent entropy, equation (1.2) may be rewritten as :

$$\partial_t(\xi) + \tilde{u}\nabla.(\xi) = (\overline{\overline{\rho}})^{-5/3} rhs_K(W, \nabla W),$$

or alternatively using the mass balance equation :

$$\partial_t(\overline{\overline{\rho}}\xi) + \nabla.(\overline{\overline{\rho}}\xi\tilde{u}) = (\overline{\overline{\rho}})^{-2/3} rhs_K(W, \nabla W).$$

Obviously, this only makes sense when restricting to smooth solutions. Some possible closure laws for $rhs_K(W, \nabla W)$ can be found in Spalart et Allmaras 1994; Wilcox 1998 for instance. However, as emphasized in Forestier, Jean-Marc Hérard et Louis 1997; Christophe Berthon 1999; Christophe Berthon et Frédéric Coquel 2002; Sergey Gavrilyuk et Richard Saurel 2006, in the non viscous case, it remains to define jump conditions, and this is not straightforward, due to the occurence of non-conservative products $(2K/3\ \nabla.\tilde{u})$ in (1.2), which are active in genuinely non-linear fields associated with eigenvalues $\tilde{u} \pm c_t$, noting :

$$(c_t)^2 = c^2 + \frac{10K}{9\overline{\overline{\rho}}},$$

where c stands for the speed of acoustic waves in laminar flows.
Among other possibilities, we recall that the strategy proposed in Forestier, Jean-Marc Hérard et Louis 1997 is only valid for weak enough shock waves; besides, the approach suggested in Christophe Berthon 1999; Christophe Berthon et Frédéric Coquel 2002 is expected to be meaningful for stronger shocks. The reader is refered to Sergey Gavrilyuk et Richard Saurel 2006 for a brief review. In the present paper, focus will be given on a simple turbulent model obtained while neglecting $rhs_K(W, \nabla W)$; thus, using the mass balance equation, an obvious solution is :

$$\xi = \xi_0.$$

This implies :

$$K = K(\overline{\overline{\rho}}) = \xi_0(\overline{\overline{\rho}})^{5/3}. \tag{1.3}$$

The resulting three-equation model Jean-Marc HÉRARD 2014 (whose counterpart is Jean-Marc HÉRARD et LOCHON 2016 in the two-phase framework) has thus three main unknowns $\overline{\overline{\rho}}, \overline{\overline{P}}, \tilde{u}$, that are governed by the closed system (1.1).
We will assume the following numerical strategy, which consists in computing approximate solutions of (1.1), using an explicit scheme for convective terms, and an implicit formulation for viscous terms, thus using the following time scheme :

$$\begin{cases} \dfrac{\overline{\overline{\rho}}^{n+1} - \overline{\overline{\rho}}^{n}}{\Delta t} = -\left\{\nabla.(\overline{\overline{\rho}}\tilde{u})\right\}^{n} \\ \dfrac{(\overline{\overline{\rho}}\tilde{u})^{n+1} - (\overline{\overline{\rho}}\tilde{u})^{n}}{\Delta t} - \epsilon_0 \left\{\nabla.(\Sigma^{tot}(\nabla^s \tilde{u}))\right\}^{n+1} = -\left\{\nabla.\left(\overline{\overline{\rho}}\tilde{u}\otimes\tilde{u} + \left(\overline{\overline{P}} + \dfrac{2K}{3}\right)..\mathscr{I}\right)\right\}^{n} \\ \dfrac{(\overline{\overline{\rho}}E)^{n+1} - (\overline{\overline{\rho}}E)^{n}}{\Delta t} - \epsilon_0 \left\{\nabla.(\Sigma^{tot}(\nabla^s \tilde{u})\tilde{u})\right\}^{n+1} = -\left\{\nabla.\left(\tilde{u}\left(\overline{\overline{\rho}}E + \overline{\overline{P}} + \dfrac{2K}{3}\right)\right)\right\}^{n} \end{cases}$$

The present paper only focuses on the convective part of the system, second order tensors are not considered here and it investigates the main properties of the convective system associated with :

$$\begin{cases} \partial_t(\overline{\overline{\rho}}) + \nabla.(\overline{\overline{\rho}}\tilde{u}) = 0 \\ \partial_t(\overline{\overline{\rho}}\tilde{u}) + \nabla.\left(\overline{\overline{\rho}}\tilde{u}\otimes\tilde{u} + \left(\overline{\overline{P}} + \dfrac{2K}{3}\right)..\mathscr{I}\right) = 0 \\ \partial_t(\overline{\overline{\rho}}E) + \nabla.\left(\tilde{u}\left(\overline{\overline{\rho}}E + \overline{\overline{P}} + \dfrac{2K}{3}\right)\right) = 0 \end{cases} \tag{1.4}$$

which are detailed in section 1. In particular, we will derive an entropy inequality which will enable to select admissible solutions when investigating the one-dimensional Riemann problem, and we will find the Riemann invariants associated with the LD (Linearly degenerate) and GNL (Genuinely non linear) fields and characterize the conditions of the jump associated with system (1.4) in section 2. In the case of a perfect gas EOS, the existence and uniqueness of the solution of the Riemann problem of system (1.4) will be proved in section 3 (with **Appendix** A). In section 4, we will introduce a simple approximate Riemann solver in order to compute approximate solutions of the system introduced in section 1. Some test cases for verification including shock structures will be carried out in Section 5, where it will be checked that this scheme enables to retrieve numerical convergence towards the exact solution even when shock waves occur, with the expected convergence rate. Section 6 will be devoted to the presentation of some two-dimensional computation The last section will be a conclusion of the work done in this paper.

Throughout the paper, standard $\tilde{a}$ and $\overline{\overline{b}}$ notations will be skipped.

1.1. Turbulent compressible flow model

As recalled before, the model Jean-Marc HÉRARD 2014 has been obtained by a statistical averaging of the Euler / Navier-Stokes equations, and thus the following system of partial differential equations is considered :

$$\begin{cases} \partial_t(\rho) + \partial_x(\rho u) = 0 \\ \partial_t(\rho u) + \partial_x\left(\rho u^2 + P + \dfrac{2K}{3}\right) = 0 \\ \partial_t(\rho E) + \partial_x\left(u\left(\rho E + P + \dfrac{2K}{3}\right)\right) = 0 \end{cases} \tag{1.5}$$

It governs the mean evolution of mass, momentum and energy. The quantities ρ, u, P, K, and E respectively represent the mean density, the mean velocity, the mean pressure, the turbulent kinetic energy and the mean total energy. The latter quantity is given by :

$$\rho E = \rho e(P,\rho) + \frac{\rho u^2}{2} + K, \tag{1.6}$$

where e=e(P,ρ) is the mean specific internal energy, and the turbulent kinetic energy follows the law :

$$K = \xi_0 \rho^{5/3}, \tag{1.7}$$

with ξ_0 a positive constant.

We introduce the celerity of density waves c(P,ρ) and the temperature T, such that :

$$c^2(P,\rho) = \left(\frac{P}{\rho^2} - \partial_\rho e(P,\rho)\right) / \partial_P e(P,\rho), \tag{1.8}$$

$$\frac{1}{T} = (\partial_P e)^{-1}(\partial_P s), \tag{1.9}$$

where s=$s(P,\rho)$ is the specific entropy complying with the constraint :

$$c^2(P,\rho)(\partial_p s) + (\partial_\rho s) = 0. \tag{1.10}$$

We will also define the modified pressure P^* :

$$P^* = P + \frac{2}{3}K. \tag{1.11}$$

1.2. Main properties of the flow model

In this section, we give some properties of system (1.5) in a general framework with respect to the **EOS**.

1.2.1. Entropy inequality

In order to introduce an entropy inequality, we consider a viscous perturbation of system (1.5), which is chosen as follows :

$$\begin{cases} \partial_t(\rho) + \partial_x(\rho u) = 0 \\ \partial_t(\rho u) + \partial_x\left(\rho u^2 + P + \dfrac{2K}{3}\right) = \epsilon_0 \partial_x\left(\dfrac{2}{3}\mu\partial_x u\right) \\ \partial_t(\rho E) + \partial_x\left(u\left(\rho E + P + \dfrac{2K}{3}\right)\right) = \epsilon_0 \partial_x\left(\dfrac{2}{3}\mu u\partial_x u\right) \end{cases} \tag{1.12}$$

Here μ represents the total viscosity and ϵ_0 is a constant in $]0,1]$. In the following we consider the **conservative** state variable :

$$w = (\rho, \rho u, \rho E),$$

and the flux :

$$F(w) = (\rho u, \rho u^2 + P^*, u(\rho E + P^*)).$$

We introduce the entropy-entropy flux pair (η, f_η) with :

$$\eta(w) = -\rho ln(s), \quad \text{and} \quad f_\eta(w) = u\eta. \tag{1.13}$$

Proposition 1 *Then the following inequality holds for smooth solutions of* (1.12) *:*

$$\partial_t \eta + \partial_x f_\eta \leq 0. \tag{1.14}$$

PROOF In the case of the viscous perturbed system (1.12), simple computations lead to the entropy inequality :

$$\partial_t \eta + \partial_x f_\eta = -\frac{1}{s}\frac{\partial s}{\partial P}\left(\frac{\partial e}{\partial P}\right)^{-1}\frac{2}{3}\epsilon_0\mu(\partial_x u)^2 = -\frac{1}{s}\frac{2}{3T}\epsilon_0\mu(\partial_x u)^2 \leq 0.$$

Remark 1 In the non viscous case, for a discontinuity travelling at speed σ, we will thus assume that the following inequality holds true :

$$-\sigma[\eta] + [f_\eta] \leq 0. \tag{1.15}$$

This will enable us to select the admissible solution of the Riemann problem associated with the conservative system (1.5).

1.2.2. Hyperbolicity

The system is written in the form :

$$\partial_t W + A(W)\partial_x W = 0, \tag{1.16}$$

where the primitive variable W reads :

$$W = (\rho, u, P)^t.$$

The jacobian matrix A(W) is :

$$A(W) = \begin{pmatrix} u & \rho & 0 \\ \frac{10K}{9\rho^2} & u & \tau \\ 0 & \rho c^2 & u \end{pmatrix},$$

where $\tau = 1/\rho$ denotes the specific volume.

Proposition 2 *We define c_t such that :*

$$c_t^2 = c^2 + \frac{10K}{9\rho}.$$

System (3.23) is strictly hyperbolic, it admits three real eigenvalues :

$$\lambda_1(W) = u - c_t, \quad \lambda_2(W) = u, \quad \lambda_3(W) = u + c_t, \tag{1.17}$$

and the associated eigenvectors $r_k(W)$ span the whole space $\mathbb{R}^3$ provided that $c_t \neq 0$:

$$r_1(W) = \left(\rho, -c_t, \rho c^2\right)^T, \quad r_2(W) = \left(\rho, 0, -\frac{10K}{9}\right)^T, \quad r_3(W) = \left(\rho, c_t, \rho c^2\right)^T. \tag{1.18}$$

Fields associated with $\lambda_1(W)$ and $\lambda_3(W)$ are genuinely non linear (GNL), and field associated with $\lambda_2(W)$ is linearly degenerate (LD).

PROOF The proof is simple when using the system written in the non conservative variable (s, u, P^*), see system (1.22), and it is thus left to the reader. Moreover, it should also be noted that examining the nature (GNL or LD) of the waves is more simple when using this set of variables, see the following section.

1.2.3. Riemann invariants

Proposition 3 *The two Riemann invariants associated with the LD field ($\lambda_2 = u$) are the following whatever the **EOS** is :*

$$I_1^2(W) = u \quad , \quad I_2^2(W) = P^*(P, \rho). \tag{1.19}$$

The Riemann invariants associated with the two GNL waves read :

$$1 - rarefaction\ wave: \ I_1^1(W) = s(P, \rho) \ , \ I_2^1(W) = u + \int_0^\rho \frac{c_t(I_1^1(W), \rho\prime)}{\rho\prime} \mathrm{d}\rho\prime. \tag{1.20}$$

$$3-rarefaction\ wave:\ \ I_1^3(W)=s(P,\rho)\ \ ,\ \ I_2^3(W)=u-\int_0^{\rho}\frac{c_t(I_1^3(W),\rho\prime)}{\rho\prime}\,\mathrm{d}\rho\prime. \tag{1.21}$$

PROOF I_k^i represents the k-th Riemann invariants for the i-th wave (1-rarefraction, 2-contact, 3-rarefraction). A Riemann invariant is a function that remains constant along the pathes defined by the corresponding eigenvectors, it thus complies with :

$$dI_k^i(W).r_i(W)=0.$$

It is straightforward to check that functions given by (3.32)-(3.33)-(3.34) comply with the condition above. We also note that we can express Riemann invariants with the variable :

$$Y=(s,u,P^*).$$

Actually, it may be checked that smooth solutions of (3.23) comply with :

$$\begin{cases}\partial_t s+u\partial_x s=0\\ \partial_t u+u\partial_x u+\tau\partial_x P^*=0\\ \partial_t P^*+\rho c_t^2\partial_x u+u\partial_x P^*=0\end{cases} \tag{1.22}$$

If $\bar{\tilde{r}}_i(Y)$ denote the eigenvectors associated with system (1.22) written in terms of variable Y, it may be checked that functions $\bar{\tilde{I}}_k^i$(Y) satisfying :

$$d\bar{\tilde{I}}_k^i(Y).\bar{\tilde{r}}_i(Y)=0,$$

are as follows :

$$\begin{aligned}&1-rarefaction\ wave:\ \ \bar{\tilde{I}}_1^1(Y)=s,\quad \bar{\tilde{I}}_2^1(Y)=u+\int_0^{P^*}\frac{1}{\rho(s,P^{*\prime})c_t(s,P^{*\prime})}\,\mathrm{d}P^{*\prime}.\\ &2-contact\ wave:\ \ \bar{\tilde{I}}_1^2(Y)=u,\quad \bar{\tilde{I}}_2^2(Y)=P^*.\\ &3-rarefaction\ wave:\ \ \bar{\tilde{I}}_1^3(Y)=s,\quad \bar{\tilde{I}}_2^3(Y)=u-\int_0^{P^*}\frac{1}{\rho(s,P^{*\prime})c_t(s,P^{*\prime})}\,\mathrm{d}P^{*\prime}.\end{aligned}$$

Then, the same Riemann invariants $I_k^i(W)$ and $\bar{\tilde{I}}_k^i(Y)$ are retrieved up to the variable change $W\mapsto Y$.

1.2.4. Jump conditions

We are now interested in discontinous solutions for sytem (1.5) whatever the **EOS** is. We denote

$$[f]=f_R-f_L,$$

the jump between the left and right states on each side of a discontinuity travelling at speed σ.

Proposition 4 *Jump conditions associated with system (1.5) may be written :*

$$\begin{cases} -\sigma[\rho] + [\rho u] = 0, \\ -\sigma[\rho u] + \left[\rho u^2 + P + \dfrac{2K}{3}\right] = 0, \\ -\sigma[\rho E] + \left[u\left(\rho E + P + \dfrac{2K}{3}\right)\right] = 0. \end{cases} \tag{1.23}$$

Those jump conditions may be rewritten as follows :

$$\begin{cases} \sigma = [\rho u]/[\rho], \\ \rho_R \rho_L [u]^2 = \left[P + \dfrac{2}{3}K\right][\rho], \\ \rho(u-\sigma)\left(\left[e + \dfrac{K}{\rho}\right] + \overline{P^*}\left[\dfrac{1}{\rho}\right]\right) = 0. \end{cases} \tag{1.24}$$

with $\bar{\phi} = \frac{\phi_L + \phi_R}{2}$.

Remark 2 When dealing with the LD field associated with λ_2=u the solution of the above jump conditions is equivalent to the Riemann invariants (3.32), i.e. $[I_k^2]$= 0.

PROOF By applying the Rankine-Hugoniot relation to the conservative system (1.5) :

$$-\sigma[w] + [F(w)] = 0,$$

system (1.23) is straightforwardly obtained. For the first two equations of system (3.36), we can find it thanks to simple calculations. We now detail the calculations necessary to find the third equation for system (3.36).

We first note :

$$v = u - \sigma. \tag{1.25}$$

From the first two relations of system (1.23), taking into account (1.25), we have :

$$-\sigma[\rho] + [\rho u] = [\rho v] = 0, \tag{1.26}$$

$$-\sigma[\rho u] + \left[\rho u^2 + P + \frac{2K}{3}\right] = [\rho v u] + [P^*] = 0. \tag{1.27}$$

We deduce from (1.26) that ρv is a constant across the discontinuity. By introducing v

into the third equation of system (1.23) and by using (1.26), we get the following form :

$$\rho v[e] + \rho v\left[\frac{u^2}{2}\right] + \rho v[K\tau] + \bar{P^*}[u] + \bar{u}[P^*] = 0. \tag{1.28}$$

Then, by multiplying (1.27) by $\bar{u}$, we have :

$$\rho v\left[\frac{u^2}{2}\right] = -\bar{u}[P^*]. \tag{1.29}$$

Third equation of (3.36) is finally obtained by introducing (1.29) into (1.28) :

$$\rho v[e + K\tau] + \bar{P^*}[u] = \rho v[e + K\tau] + \bar{P^*}[\rho v\tau] = \rho v([e + K\tau] + \bar{P^*}[\tau]) = 0, \tag{1.30}$$

this completes the proof.

Remark 3 In the case of a turbulent perfect gas EOS :

$$P = (\gamma - 1)\rho e,$$

jump conditions (1.23) provide bounds for the density ratio whereas the pressure ratio has no bounds, i.e. a shock wave separating two states Y_R and Y_L is such that :

$$\beta^{-1} \leq \frac{\rho_r}{\rho_l} \leq \beta,$$

with $\beta = \frac{\gamma+1}{\gamma-1}$.

PROOF For the Euler equations (i.e. without turbulent contribution) with the instantaneous perfect gas EOS :

$$P' = (\gamma - 1)\rho' e',$$

we know that (see SMOLLER 1983) the value of the ratio $\frac{max(\rho'_r,\rho'_l)}{min(\rho'_r,\rho'_l)}$ across a shock wave is bounded by :

$$\beta = \frac{\gamma + 1}{\gamma - 1}.$$

This means that in the non turbulent case :

$$\beta^{-1}\rho'_l < \rho'_r < \beta\rho'_l. \tag{1.31}$$

Since β is a constant for the perfect gas EOS, a straightforward averaging of (1.31) provides :

$$\beta^{-1}\rho_l < \rho_r < \beta\rho_l. \tag{1.32}$$

We thus may wonder whether the solution of (1.5) also satisfies (1.32). Actually, formulae (1.53) in **Appendix A.1** for the 1-shock wave provide :

$$\frac{P_r}{P_l} = \frac{\beta z_1 - 1 + g_1(z_1)}{\beta - z_1}, \qquad \text{and} \qquad g_1(z_1) > 0, \qquad \text{with} \qquad z_1 = \frac{\rho_r}{\rho_l} > 1.$$

Thus, it is staightforward to see that pressure ratio has no bound. Moreover, positive values of P_r , P_l imply $z_1 < \beta$, which means that :

$$\rho_r = max(\rho_r, \rho_l) < \beta \rho_l = \beta \; min(\rho_r, \rho_l),$$

which completes the proof, since a similar result holds using formulae (1.55) in **Appendix A.1** for the 3-shock wave.

1.3. Solution of the Riemann problem

In this section, we are interested in finding the solution of the Riemann problem associated with (1.5) in the case of a **perfect gas EOS** :

$$P = (\gamma - 1)\rho e.$$

First we have to start connecting W_L to W_R through the intermediate states W_1 and W_2, where the subscripts L and R denote respectively the left and the right states of the initial discontinuity, and the subscript 1 (respectively 2) represents the intermediate state of the solution of the Riemann problem between waves λ_1 and λ_2 (respectively between λ_2 and λ_3), see figure 1.1.

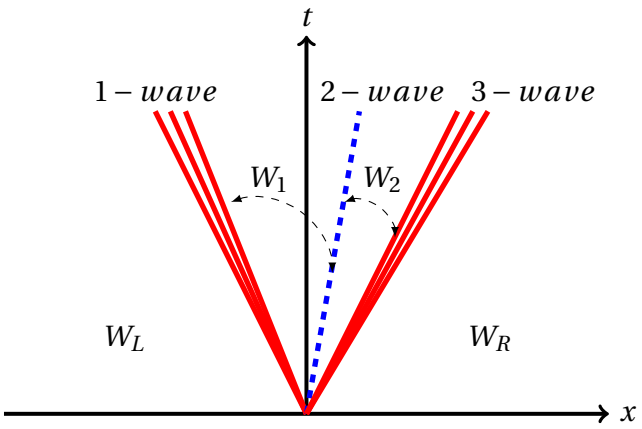

FIGURE 1.1. – Solution of the Riemann problem which consists in four constant states W_L, W_1, W_2 and W_R separated by the waves λ_i, $i = \{1,2,3\}$.

1.3.1. Waves connection

We must first distinguish 4 cases for the solution of the Riemann problem, depending on the nature of the two GNL waves associated with λ_1 and λ_3 :

- case 1 : 1-shock / 2-contact / 3-shock
- case 2 : 1-rarefaction / 2-contact / 3-rarefaction
- case 3 : 1-shock / 2-contact / 3-rarefaction
- case 4 : 1-rarefaction / 2-contact / 3-shock

Proposition 5 *We first set :*

$$z_1 = \frac{\rho_1}{\rho_L} \quad \text{and} \quad z_2 = \frac{\rho_2}{\rho_R}.$$

The solution of the Riemann problem associated with (1.5) *is as follows :*

case 1. *We have for* $z_1 > 1$ *and* $z_2 > 1$ *:*

$$u_R - u_L + c_L f_1(z_1, K_L/P_L) + c_R f_2(z_2, K_R/P_R) = 0,$$

and :

$$P_L h_1(z_1, K_L/P_L) + \frac{2K_L}{3} z_1^{5/3} = P_R h_2(z_2, K_R/P_R) + \frac{2K_R}{3} z_2^{5/3},$$

with the following definitions :

$$\begin{aligned}
f_1(z_1, K_L/P_L) &= \sqrt{\left(\tfrac{z_1-1}{\gamma z_1}\right)\left(-1 + \tfrac{2}{3}\tfrac{K_L}{P_L}(z_1^{5/3} - 1) + h_1(z_1, K_L/P_L)\right)}, \\
h_1(z_1, K_L/P_L) &= \frac{\beta z_1 - 1 + g_1(z_1, K_L/P_L)}{\beta - z_1}, \\
g_1(z_1, K_L/P_L) &= \frac{2K_L}{3P_L}\left(z_1^{8/3} - 4z_1^{5/3} + 4z_1 - 1\right),
\end{aligned}$$

and :

$$\begin{aligned}
f_2(z_2, K_R/P_R) &= \sqrt{\left(\tfrac{z_2-1}{\gamma z_2}\right)\left(-1 + \tfrac{2}{3}\tfrac{K_R}{P_R}(z_2^{5/3} - 1) + h_2(z_2, K_R/P_R)\right)}, \\
h_2(z_2, K_R/P_R) &= \frac{\beta z_2 - 1 + g_2(z_2, K_R/P_R)}{\beta - z_2}, \\
g_2(z_2, K_R/P_R) &= \frac{2K_R}{3P_R}\left(z_2^{8/3} - 4z_2^{5/3} + 4z_2 - 1\right),
\end{aligned}$$

and $K_{L,R} = \xi_0 \rho_{L,R}^{5/3}$.

case 2. *We have for* $z_1 \leq 1$ *and* $z_2 \leq 1$ *:*

$$u_R - u_L + c_L B_1(z_1, K_L/P_L) + c_R B_2(z_2, K_R/P_R) = 0,$$

and :

$$P_L Q_1(z_1) + \frac{2K_L}{3} z_1^{5/3} = P_R Q_2(z_2) + \frac{2K_R}{3} z_2^{5/3},$$

with the following definitions :

$$\begin{aligned}
&B_1(z_1, K_L/P_L) = \int_1^{z_1} \left(z^{\gamma-3} + \frac{10K_L}{9\gamma P_L} z^{-4/3} \right)^{1/2} \mathrm{d}z, \\
&Q_1(z_1) = z_1^{\gamma}, \\
&B_2(z_2, K_R/P_R) = \int_1^{z_2} \left(z^{\gamma-3} + \frac{10K_R}{9\gamma P_R} z^{-4/3} \right)^{1/2} \mathrm{d}z, \\
&Q_2(z_2) = z_2^{\gamma}.
\end{aligned}$$

case 3. *We have for* $z_1 > 1$ *and* $z_2 \leq 1$ *:*

$$u_R - u_L + c_R B_2(z_2, K_R/P_R) + c_L f_1(z_1, K_L/P_L) = 0,$$

and

$$P_L h_1(z_1, K_L/P_L) + \frac{2K_L}{3} z_1^{5/3} = P_R Q_2(z_2) + \frac{2K_R}{3} z_2^{5/3}.$$

case 4. *We have for* $z_1 \leq 1$ *and* $z_2 > 1$ *:*

$$u_R - u_L + c_L B_1(z_1, K_L/P_L) + c_R f_2(z_2, K_R/P_R) = 0,$$

$$P_L Q_1(z_1) + \frac{2K_L}{3} z_1^{5/3} = P_R h_2(z_2, K_R/P_R) + \frac{2K_R}{3} z_2^{5/3}.$$

The reader is referred to Appendices A.1 and A.2 for a proof.

1.3.2. Existence and uniqueness of the solution

Proposition 6 *The Riemann problem associated with* (1.5) *and initial states :*

$$W(x < 0, t = 0) = W_L,$$

$$W(x > 0, t = 0) = W_R,$$

admits a unique self-similar solution :

$$W(x, t) = \omega(x/t),$$

with no vacuum occurrence, provided that initial left and right states, W_L and W_R, are such that :

$$u_R - u_L < X_L + X_R, \tag{1.33}$$

with $X_i = \int_0^{\rho_i} \frac{c_t(s,\rho')}{\rho'} \mathrm{d}\rho'$.

The reader is referred to **Appendix A** for a proof which is based on the proof proposed in SMOLLER 1983.

Remark 4 For $\xi_0 = 0$, we have $c_t = c$ and condition (1.33) is equivalent to the condition of no vacuum occurrence for Euler with a perfect gas EOS.

1.4. An approximate numerical Riemann solver

Approximate Riemann solvers are commonly used in order to compute approximate solutions of hyperbolic problems, where contact waves, rarefactions and shock waves co-exist (see among others the original paper GODUNOV 1959 and the books GODLEWSKI et RAVIART 1996; TORO 1997).

We consider a classical finite volume formulation. The segment [a,b] is divided into cells I_i, where $x_{i+\frac{1}{2}}$ represents the cell interface between cells I_i and I_{i+1}, and x_i represents the cell center. We define Δt^n the time step at time t^n and Δx_i the length of I_i : $t^{n+1} = t^n + \Delta t^n$ and $\Delta x_i = x_{i+\frac{1}{2}} - x_{i-\frac{1}{2}}$.

1.4.1. VFRoe-ncv scheme

In this section, we recall an extension of the VFRoe scheme MASELLA, FAILLE et Thierry GALLOUËT 1999 called **VFRoe-ncv** which was proposed in order to deal with hyperbolic systems in BUFFARD, Thierry GALLOUËT et Jean-Marc HÉRARD 2000. The VFRoe-ncv scheme is an approximate Godunov scheme where the approximate value at the interface between two cells is computed as detailed below.

First, system (1.5) may be rewritten as follows :

$$\partial_t Z + B(Z)\partial_x Z = 0, \tag{1.34}$$

where :

$$Z = (\rho, u, P^*)^t,$$

and

$$B(Z) = \begin{pmatrix} u & \rho & 0 \\ 0 & u & \tau \\ 0 & \rho c_t^{\,2} & u \end{pmatrix},$$

and also :

$$P^* = P + \frac{2K}{3}, \qquad \tau = \frac{1}{\rho}.$$

We then consider the Riemann problem associated with system (1.34) and initial conditions :

$$Z(x<0,t=0) = Z_L, \qquad Z(x>0,t=0) = Z_R. \tag{1.35}$$

At each interface between two cells, we solve the following linearized Riemann problem :

$$\partial_t Z + B(\bar{Z})\partial_x Z = 0, \tag{1.36}$$

where $\bar{Z} = (Z_L + Z_R)/2$. System (1.36) contains 3 linearly degenerate fields, thus the solution of the one-dimensional Riemann problem is simple. Indeed, it only requires computing three real coefficients noted α_i (for i=1 to 3) and such that :

$$Z_R - Z_L = \sum_{i=1}^{3} \alpha_i \widehat{r}_i,$$

where $\widehat{r}_i$ represents the basis of right eigenvectors of the matrix $B(\bar{Z})$:

$$\widehat{r_1} = (1, -\hat{c}_t\bar{\tau}, \hat{c}_t{}^2)^T, \qquad \widehat{r_2} = (1,0,0)^T, \qquad \widehat{r_3} = (1, \hat{c}_t\bar{\tau}, \hat{c}_t{}^2)^T.$$

More details concerning the explicit computation of the intermediate states Z_1 and Z_2 can be found in **Appendix B**. Hence the exact solution $Z^*(Z_L, Z_R)$ at the initial discontinuity location, i.e. at $x/t = 0$, of the linearized Riemann problem associated with system (1.36) and initial conditions (1.35) is given by :

$$Z^*(Z_L,Z_R) = \begin{cases} Z_L \text{ if } \bar{\lambda_1} \geq 0; \\ Z_1 \text{ if } \bar{\lambda_1} < 0 \text{ and } \bar{\lambda_2} \geq 0; \\ Z_2 \text{ if } \bar{\lambda_2} < 0 \text{ and } \bar{\lambda_3} \geq 0; \\ Z_R \text{ if } \bar{\lambda_3} < 0; \end{cases} \tag{1.37}$$

where :

$$\lambda_1 = \bar{u} - \widehat{c_t}, \qquad \lambda_2 = \bar{u}, \qquad \lambda_3 = \bar{u} + \widehat{c_t},$$

and also :

$$\widehat{c_t}(\rho,P) = c_t(\bar{\rho},\bar{P}) = \sqrt{\frac{\gamma P(\bar{P^*},\bar{\rho})}{\bar{\rho}} + \frac{10}{9}\frac{K(\bar{\rho})}{\bar{\rho}}}. \tag{1.38}$$

Finally the numerical scheme reads :

$$\Delta x_i (w_i^{n+1} - w_i^n) + \Delta t(\mathscr{F}^n_{i+\frac{1}{2}} - \mathscr{F}^n_{i-\frac{1}{2}}) = 0, \tag{1.39}$$

where the numerical flux is computed thanks to the exact solution (3.70) of the linearized problem (1.36)-(1.35) with $Z_L = Z_i^n$ and $Z_R = Z_{i+1}^n$:

$$\mathscr{F}_{i+\frac{1}{2}}^n = F(w(Z^*(Z_i^n, Z_{i+1}^n))).$$

In the definition of the numerical flux above, it should be noted that we have $w = (\rho, \rho u, \rho E)$ and that $w \mapsto F(w)$ corresponds to the analytical flux of system (1.5) as defined in section 1.2.1. Moreover, we apply the **Courant-Friedrichs-Lewy** (CFL) condition :

$$\frac{\Delta t^n}{\Delta x_j} max(|\lambda_i|) < 1,$$

in scheme (1.39).

Remark 5 An entropy correction is required (see HELLUY, Jean-Marc HÉRARD, Hélène MATHIS et al. 2010) to compute shock tube problems when one sonic point is present in the rarefaction wave.

Remark 6 The alternative choice of the non-conservative variable (s, u, P^*) has not been retained here because it requires a non-explicit change of variable. The latter thus increases the computational cost of the scheme. This variable change corresponds to finding ρ such that :

$$P(\rho, s_{L,R}) + \frac{2}{3}\xi_0 \rho^{\frac{5}{3}} = P_{L,R}^*,$$

for given $s_{L,R}$ and $P_{L,R}^*$. Thus it will not be considered in the sequel.

1.5. Numerical Results

We present now some numerical results obtained for the model and scheme detailed in the previous sections. We focus here on two test cases that involve shock waves : the double-shock test case (i.e. case 1 in section 1.3.1) and a "strong shock wave" test case. The former allows to compute accurately the solution of the Riemann problem, and it is thus useful for convergence study. Indeed, the computation of an exact solution of a Riemann problem involving a rarefaction wave requires a numerical integration of the rarefaction fan. These are thus less accurately computed. The second test case corresponds to a situation where initial states present a great ratio of pressure and density. It is representative of situations involving explosion or detonation waves. It should be noted that qualitative results for a test case involving two symmetric rarefaction waves have been added in **Appendix C**.

Numerical convergence curves, at a given time, are represented by the logarithm of the relative L^1-error as a function of the logarithm of the mesh size. The relative L^1-error is computed at time t^n on the whole regular mesh as :

$$\frac{\sum_i |\phi_i^{approx,n} - \phi^{exact}(x_i, t^n)|\Delta x_i}{\sum_i |\phi^{exact}(x_i, t^n)|\Delta x_i}. \tag{1.40}$$

Obviously, when $\sum_i |\phi^{exact}(x_i, t^n)| = 0$, this definition is meaningless and we change it into :

$$\sum_i |\phi_i^{approx,n} - \phi^{exact}(x_i, t^n)|.$$

The first test case provides a comparison between the exact solution and the approximate solution and it enables to obtain a numerical convergence curve on the basis of the error (1.40). For the other test cases, only qualitative plots of the approximate solutions are presented at a given final time for the density, the velocity, the pressure P and the modified pressure P^*.

All the computations are performed for a given value of $CFL = 0.5$, and for different values of the parameter ξ_0. It should be recalled that when $\xi_0 = 0$, the modified pressure P^* is equal to the thermodynamical pressure P. Moreover, in all the tests below, we have considered the perfect gas EOS :

$$P = (\gamma - 1)\rho e,$$

where the constant γ is equal to $\frac{7}{5}$. The computational domain is $[0,1]$ and the initial discontinuity separating states W_L and W_R is located at x= 0.5. The domain $[0,1]$ is discretized using uniform cells, $\Delta x_i = \Delta x$, and the number of cells varies from 200 up to 1×10^5 cells.

1.5.1. Test 1 : Double shock wave

In this test case, we compare the exact solution of the one-dimensional Riemann problem with the approximate solution. Three different values of ξ_0 are used $\xi_0 = \{0, 10000, 50000\}$. Each value of ξ_0 leads to a different Riemann problem whose initial conditions are given below :

— For ξ_0=0 :

$$(\rho_L, u_L, P_L) = (1, 550, 10^6)$$

$$(\rho_R, u_R, P_R) = (1, -618.107550, 103990.112994)$$

— For ξ_0=10000 :

$$(\rho_L, u_L, P_L) = (1, 650, 10^6)$$

$$(\rho_R, u_R, P_R) = (1, -687.545913, 98007.273140)$$

— For ξ_0=50000 :

$$(\rho_L, u_L, P_L) = (1, 750, 10^6)$$

$$(\rho_R, u_R, P_R) = (1, -750.364690, 94038.441853)$$

Figures 3.12, 3.3 and 1.6 show qualitative comparisons between the exact solutions and the approximate solutions for a mesh that contains 500 cells and for respectively $\xi_0 = \{0, 10000, 50000\}$. Figure 3.13, 3.4 and 1.7 show the convergence curves for the set of variables $\{\rho, u, P, P^*\}$ and for the three different values of ξ_0.

First of all we notice that $\frac{\max(\rho_l,\rho_r)}{\min(\rho_l,\rho_r)} \approx 4.25$, which is less than β (for $\gamma = 1.4$ we get $\beta = 6$). This is in agreement with the theory as mentioned in remark 3. The approximated shock wave profile is monotonic; there are no spurious oscillations in the vicinity of the shock. The error varies as $\approx h^1$ for variables u and P^* on fine meshes, and as $\approx h^{1/2}$ for ρ and P on fine meshes (owing to the occurrence of the contact discontinuity), see figure 3.13. This behavior is due to the VFRoe-ncv scheme using the variable (u, P^*) and the perfect gas EOS. Indeed, thanks to the latter, profiles for the velocity and the modified pressure are almost uniform around the contact location. On fine meshes, the error on the approximated velocity and modified pressure are thus not influenced by the larger error on the contact wave. This is not the case for the density and the pressure P, which therefore have an effective convergence rate of 1/2. For $\xi_0 = 0$, the system corresponds to the classical Euler system and $P = P^*$. Then the effective convergence rate reported in BUFFARD, Thierry GALLOUËT et Jean-Marc HÉRARD 2000 is recovered for P.

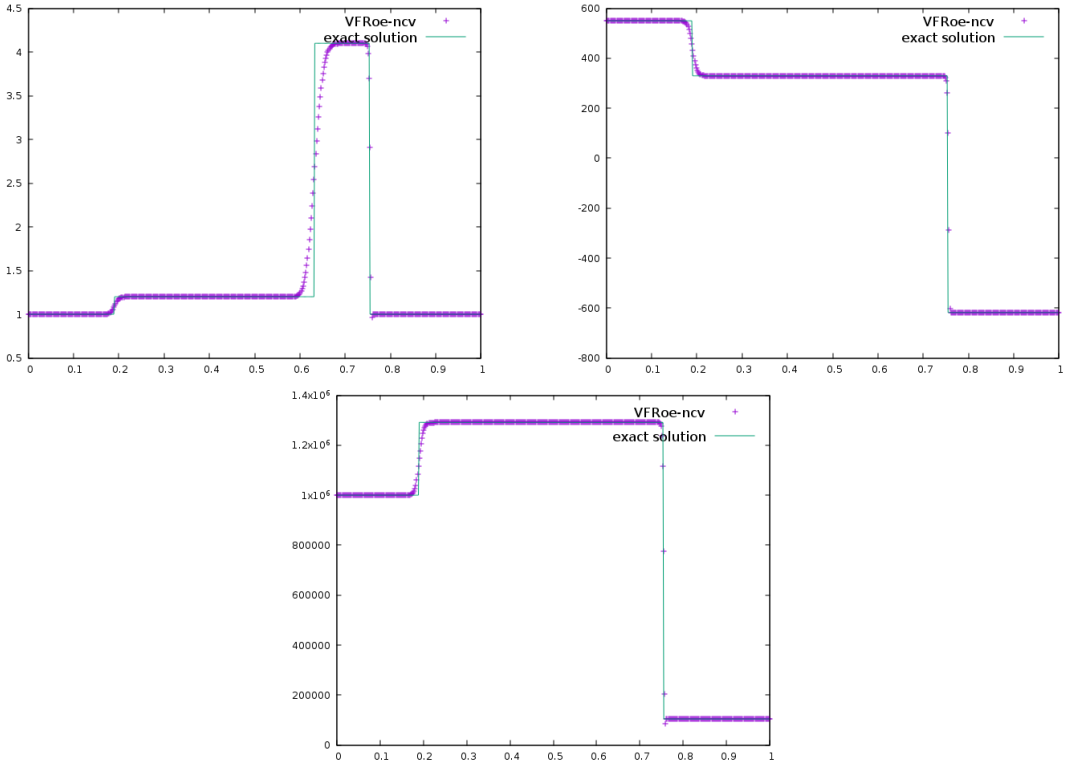

FIGURE 1.2. – Double-shock wave test case. Density (top left), velocity (top right) and pressure (bottom). Comparison between the exact solution (green) and the approximate solution (purple) at $t = 3\ 10^{-2}$ s, $CFL = 0.5$, 500 cells, $\xi_0 = 0$.

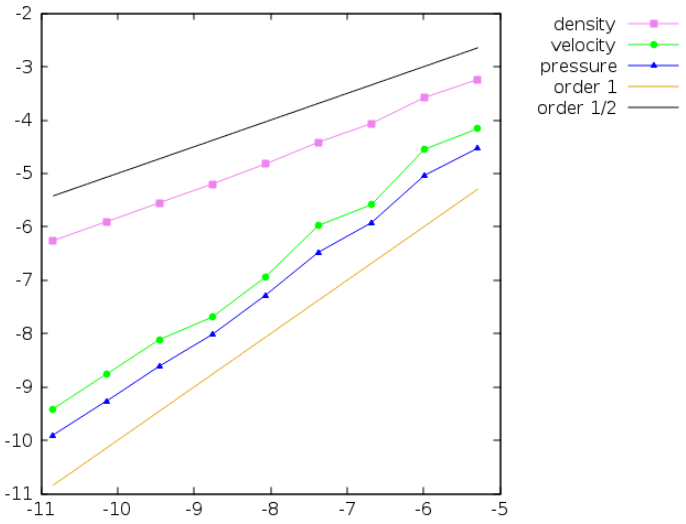

FIGURE 1.3. – Double-shock wave test case. Convergence curves : logarithm of the relative L1-error versus the logarithm of the mesh size with uniform meshes containing from 200 to 55000 cells. The error is plotted for variables, ρ, u and P^*, $\xi_0 = 0$ (recall that here $P^* = P$).

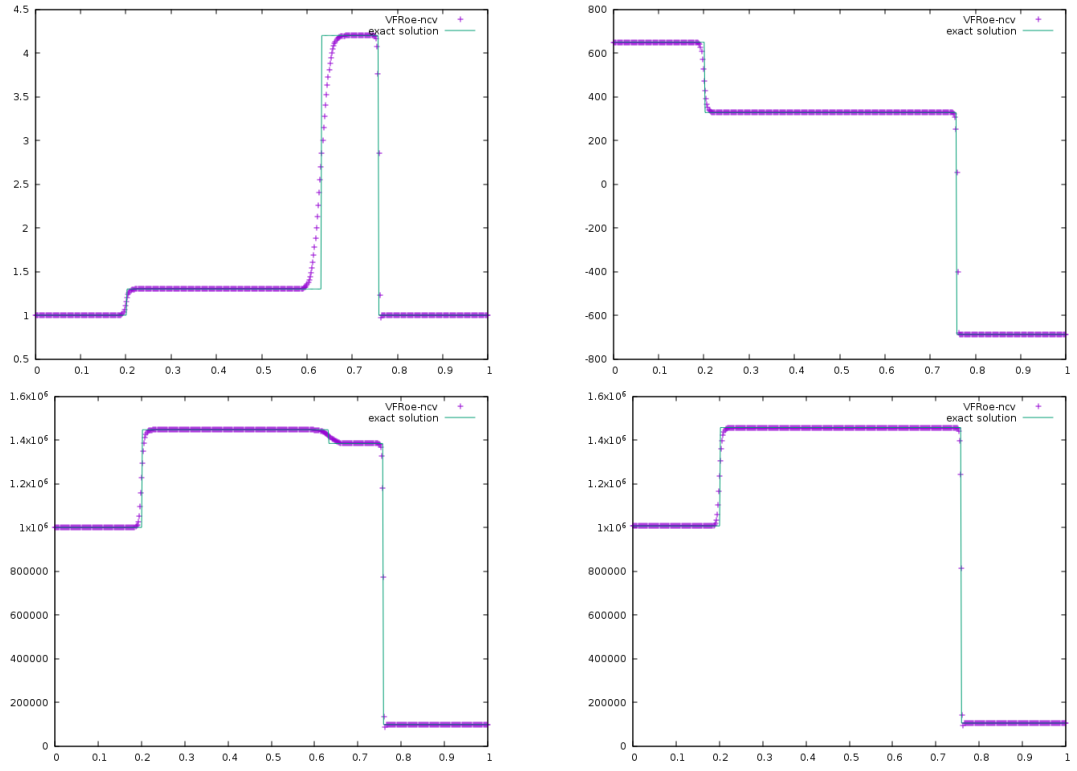

FIGURE 1.4. – Double-shock wave test case. Density (top left), velocity (top right), pressure (bottom left) and P^* (bottom right). Comparison between the exact solution (green) and the approximate solution (purple) at $t = 3\ 10^{-2}$ s, $CFL = 0.5$, 500 cells, $\xi_0 = 10000$.

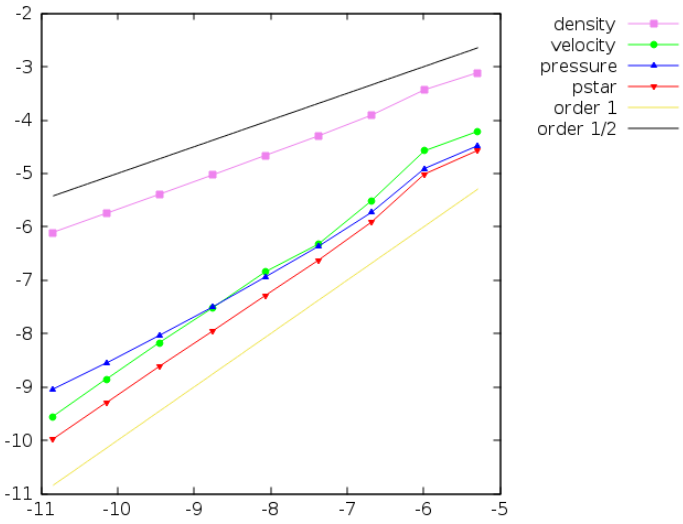

FIGURE 1.5. – Double-shock wave test case. Convergence curves : logarithm of the relative L1-error versus the logarithm of the mesh size with uniform meshes containing from 200 to 55000 cells. The error is plotted for variables, ρ, u, P and P^*, $\xi_0 = 10000$.

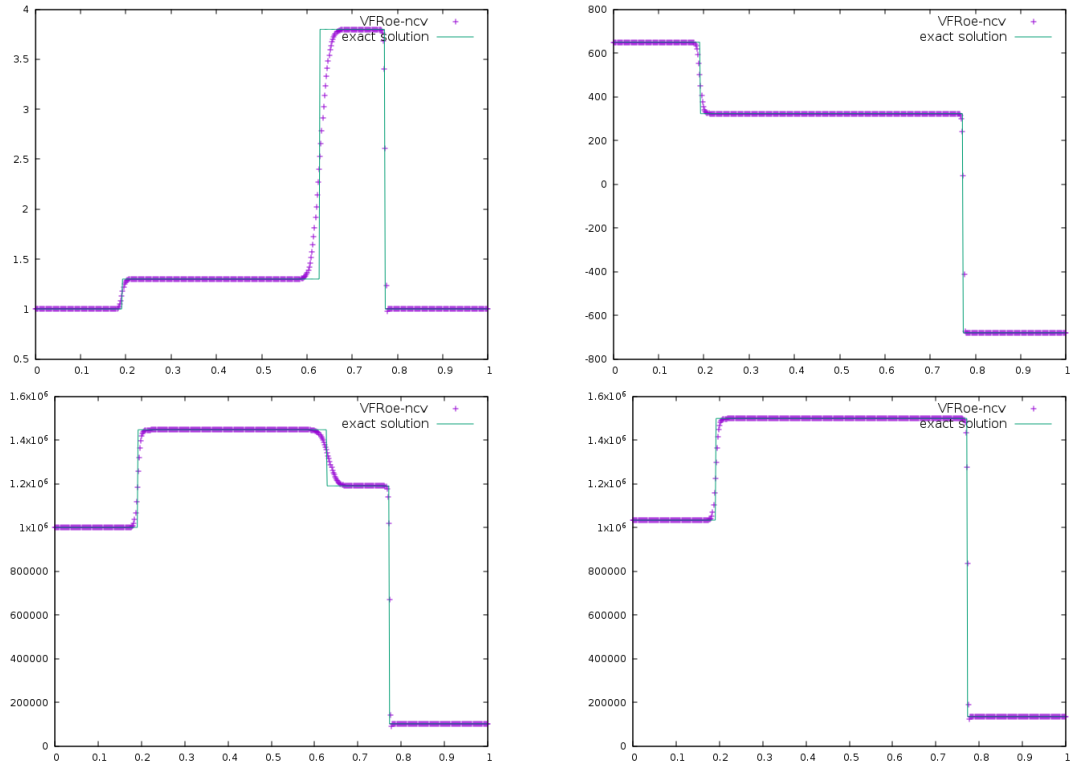

FIGURE 1.6. – Double-shock wave test case. Density (top left), velocity (top right), pressure (bottom left) and P^* (bottom right). Comparison between the exact solution (green) and the approximate solution (purple) at $t = 3\ 10^{-2}$ s, $CFL = 0.5$, 500 cells, $\xi_0 = 50000$.

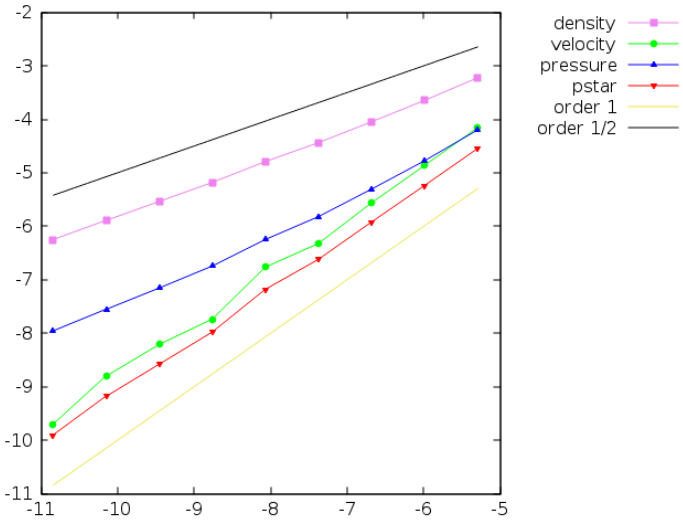

FIGURE 1.7. – Double-shock wave test case. Convergence curves : logarithm of the relative L1-error versus the logarithm of the mesh size with uniform meshes containing from 200 to 55000 cells. The error is plotted for variables, ρ, u, P and P^*, $\xi_0 = 50000$.

1.5.2. Test 2 : Strong shock wave

The propagation of strong shock waves, generated by a strong explosion is of great interest from a physical point of view due to its numerous applications in various fields. In order to mimic such situations, we consider here a Riemann problem for which the left state corresponds to a gas at very high pressure with respect to the right state, the latter representing the ambient conditions. The high pressurized gas then expands rapidly and generates strong waves. When the pressure ratios between left and right states are high enough, a supersonic rarefaction wave is observed. For the latter the two extremities of the fan of the rarefaction wave travel in opposite directions (see figure 1.8). In these situations, an entropy correction is mandatory for the VFRoe-ncv scheme, as the one proposed in HELLUY, Jean-Marc HÉRARD, Hélène MATHIS et al. 2010 and implemented here. Without the latter, computations fail because of the occurrence of a discontinuous - and non physical - pattern in the rarefaction fan (in fact at the location of the initial discontinuity). Thus this test is of interest and it shows what happens for the flows during strong variations in density, which originate from strong variations in pressure and temperature.

We propose here to examine the approximate solution for a Riemann problem with a pressure and density ratio equal to 1000. More precisely, we choose the left and right states such that :

$$(\rho, u, P)_L = (1000 \times \rho_0, 0, 1000 \times P_0), \qquad \text{and} \qquad (\rho, u, P)_R = (\rho_0, 0, P_0),$$

and where the right state corresponds to ambient gas at rest : (ρ_0, P_0)= (1, 10^5). Figures 1.9, 1.10, 1.11 and 1.12 show the behavior of the density, velocity, pressure and modified pressure at a given time $T_f = 1.25\ 10^{-4}\ s$, on different meshes with 500 cells, 5000 cells and 50000 cells. Moreover, we set $\xi_0 = 10000$ which corresponds to a high level of turbulence.

It should be noted that in this test case, the contact wave and the shock wave travel to the right with a high velocity : respectively $\sim 2168\ m/s$ (see figure 1.10) and $\sim 2680\ m/s$. Moreover, the fan of the rarefaction wave expands to the left with a velocity of $-1152\ m/s$ and to the right with a velocity of $1791\ m/s$. Hence, both the shock wave and the rarefaction wave remain very close to the contact wave (see on the density variable in figure 1.9 or on the pressure P on figure 1.11). In particular, when focusing on the present final time $T_f = 1.25\ 10^{-4}\ s$: the rarefaction fan corresponds to the interval $[0.356, 0.724]$, the contact wave is located around $x = 0.771$ and the shock wave is located around $x = 0.835$ (see figure 1.8). The distance between the two GNL waves and the contact wave is thus small. Since the numerical scheme is not very accurate on the contact wave, the approximated values for the intermediate states 1 and 2 (see figure 1.8) are not very accurate on coarse meshes. Indeed, the results of figures 1.11 clearly show that at least 5000 cells are needed in order to get a correct approximation of the intermediate state 2 ; whereas it is not yet sufficient for

intermediate state 1. As a consequence, fine meshes have to be used in order to get a correct accuracy of the location of the approximate contact wave and of the pressure level of P^* between the rarefaction wave and the shock wave. Obviously, an other solution could be to use a second order extension of the scheme based for instance on a MUSCL reconstruction with a slope limiter and a second order Runge-Kutta time-scheme, see GODLEWSKI et RAVIART 1996 or TORO 1997 among others. This is an important point because the increase of P^* across the front of the shock will determine the importance of the impact of the shock on the surroundings. Moreover, an accurate location of the front of the shock enables to get the correct time at which the surroundings would be impacted.

Due to the entropy correction implemented in the numerical scheme, the approximate profiles in the rarefaction fan remain "regular" and monotonic, even if very small perturbations may be observed on very coarse meshes around $x = 0.5$. We also notice that in the vicinity of the shock wave, we have $\frac{\rho_2}{\rho_L} \approx \frac{5.35}{1} = 5.35$. This is still less than the theoretical limit $\beta = 6$ (see figure 1.9) as pointed out by remark 3. At last, the VFRoe-ncv scheme using the variable (ρ, u, P^*) enables to maintain uniform profiles for the modified pressure P^* and the velocity u around the contact wave, see figure 1.10 and 1.12.

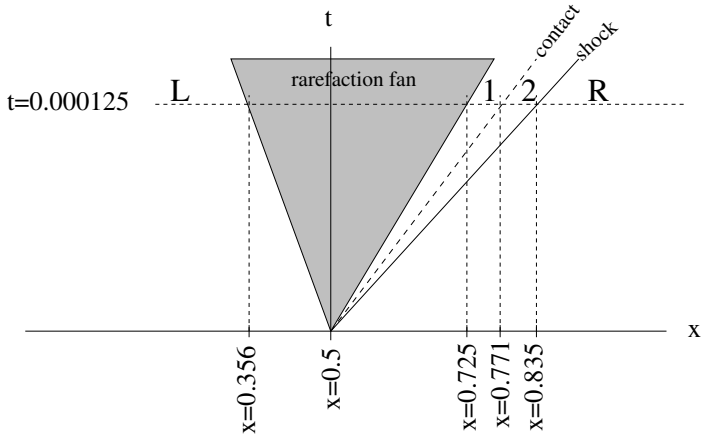

FIGURE 1.8. – Sketch of the waves in the (x, t)-plane for the strong shock test case at time $T_f = 1.25\ 10^{-4}\ s$.

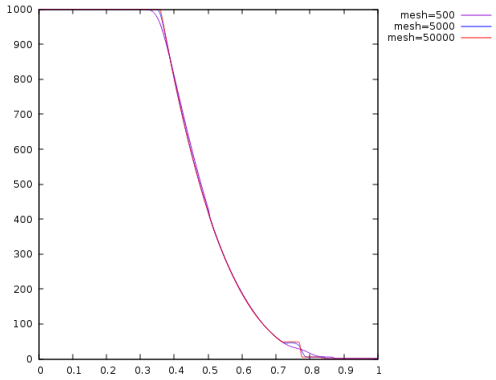

FIGURE 1.9. – Strong shock wave test case. Density for $\xi_0 = 10000$ and for meshes with 500, 5000 and 50000 cells.

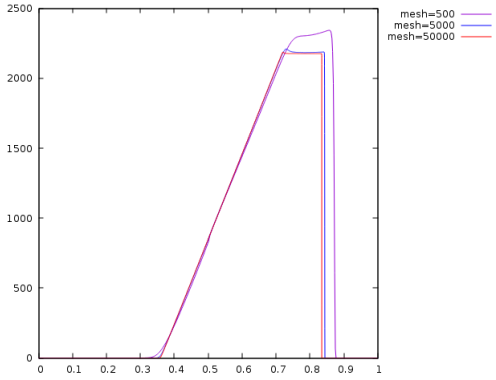

FIGURE 1.10. – Strong shock wave test case. Velocity for $\xi_0 = 10000$ and for meshes with 500, 5000 and 50000 cells.

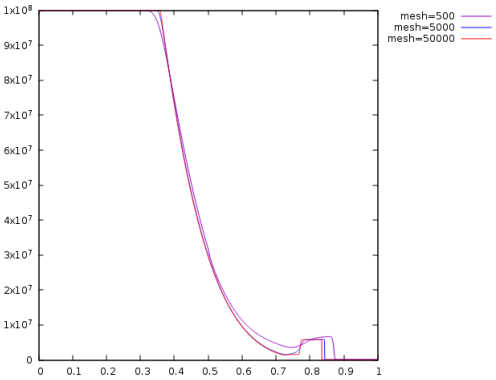

FIGURE 1.11. – Strong shock wave test case. Pressure P for $\xi_0 = 10000$ and for meshes with 500, 5000 and 50000 cells.

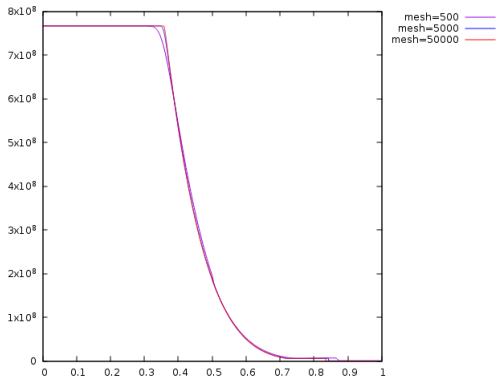

FIGURE 1.12. – Strong shock wave test case. Modified pressure P^* for $\xi_0 = 10000$ and for meshes with 500, 5000 and 50000 cells.

1.6. 2D Numerical Results

In the two-dimensional case, the numerical scheme reads :

$$vol(\Omega_i)(w_i^{n+1} - w_i^n) + \Delta t^n \sum_{j \in \mathcal{V}(i)} F(w(Z_{ij}^*), n_{ij})\Gamma_{ij} = 0, \tag{1.41}$$

where $\mathcal{V}(i)$ refers to the neighboring cells of Ω_i, Γ_{ij} is the length of the interface between cells Ω_i and Ω_j, and vol(Ω_i) is the area of Ω_i. The quantity $F(w(Z_{ij}^*), n_{ij})$ denotes the numerical flux at the interface between cells Ω_i and Ω_j, n_{ij} stands for the unit normal vector directed from Ω_i to Ω_j and Z_{ij}^* is the solution of the linearized Riemann problem at the face between cells Ω_i and Ω_j along the n_{ij}-direction. The flux for model (1.4) in 2D is given in the n_{ij}-direction by :

$$F(w, n_{i,j}) = \begin{pmatrix} (\rho U.n)_{ij} \\ (\rho(U.n)U + P^* n)_{ij} \\ ((U.n)(\rho E + P^*))_{ij} \end{pmatrix}, \tag{1.42}$$

where $w = (\rho, \rho U, \rho E)$, and where the velocity vector U gathers the two components of the velocity along the axis x and y : $U = (u_x, u_y)$. The solution Z_{ij}^* of the linearized Riemann problem is computed thanks to shceme used for 1D simulations by using Ω_i and Ω_j as L and R states, see also **Appendix B** .Indeed, it should be noted that for the 2D flux (1.42), the velocity component wich is orthogonal to n_{ij} is simply advected with velocity $U.n_{ij}$ BUFFARD, Thierry GALLOUËT et Jean-Marc HÉRARD 2000.
In order to compute the numerical fluxes at the rigid wall boundaries, we use the classical "mirror state" technique. For the numerical treatment of inlet and outlet boundary conditions the reader may also refer to BUFFARD, Thierry GALLOUËT et Jean-Marc HÉRARD 2000 for more details. Moreover, we apply the Courant-Friedrichs-Lewy (CFL) condition :

$$\frac{\Delta t^n}{vol(\Omega_i)} max(|\lambda_i|) = \frac{1}{2},$$

in scheme (1.41).

We present here a numerical simulation obtained in a two-dimensional domain for model (1.4). The parameters of the EOS are the same than those chosen for the 1D results of the previous sections. Let us consider the domain $(x, y) \in [-1, 1] \times [0, 1]$. A small rectangular obstacle with a length $L_b = 0.05\ m$ and a height $H_b = 0.1\ m$ is placed at $x = 0.15\ m$. The obstacle and the boundary $y = 0$ (i.e. the ground) are considered as rigid walls. Outlet conditions are imposed for the other boundaries. The complete setting is depicted in figure 1.13. The initial conditions of the test case carried out in this section are representative of an explosion involving hydrogen. At ambiant temperature and pressure, the AICC [1] pressure of stoechiometric mixture of air and hydrogen is close to 10 $bars$. We choose here to set a high pressure zone inside a

1. Adiabatic Isochoric Complete Combustion

half-circle, whose centre is $(0,0)$ and whose radius is 0.05 m. In the rest of the domain, ambiant conditions are set. The initial flow is assumed to be at rest everywhere in the domain. In the whole computational domain, we set $\xi_0 = 10^5$, and the perfect gas EOS :

$$P = (\gamma - 1)\rho e,$$

with the constant $\gamma = \frac{7}{5}$ is still considered. Thus, according to the EOS parameters, the initial conditions read :

$$(\rho, u, v, P) = \begin{cases} (1.2\ kg/m^3, 0\ m/s, 0\ m/s, 10^6\ Pa) & \text{if } x^2 + y^2 \leq (0.05)^2; \\ (0.8\ kg/m^3, 0\ m/s, 0\ m/s, 10^5\ Pa) & \text{if } x^2 + y^2 > (0.05)^2. \end{cases} \tag{1.43}$$

In order to highlight the influence of the turbulence for this test case, the current results (for $\xi_0 = 10^5$) are compared with the same case without turbulence (ξ_0=0). Three probes are chosen at elevation $y = 0.1$ and for different x :

— probe 1 is centered, $x = 0$,
— probe 2 is set on the left part of the domain x= -0.15,
— and probe 3 is set on the right part, just above the rectangular obstacle, at $x = 0.15$ (see also figure 1.13).

The following results have been obtained for an unstructured mesh composed of 67300 triangular cells, see in figures 1.14 and 1.15 for a view of the mesh. In figures 1.16 and 1.17, the turbulent kinetic energy, the modified pressure and the velocity field have been plotted. The influence of the obstacle can clearly be observed. The effects of turbulence can be observed in figures 1.18 and 1.19 when comparing the laminar and the turbulent cases. With $\xi_0 = 10^5$ the turbulent energy reaches an important level. In particular, the influence on the pressure P is clear : the traveling velocity of the waves is slightly different, while the amplitude of the pressure waves are noticeably modified. Most of the turbulent kinetic energy is located at the shock front, which seems quite natural owing to the model.

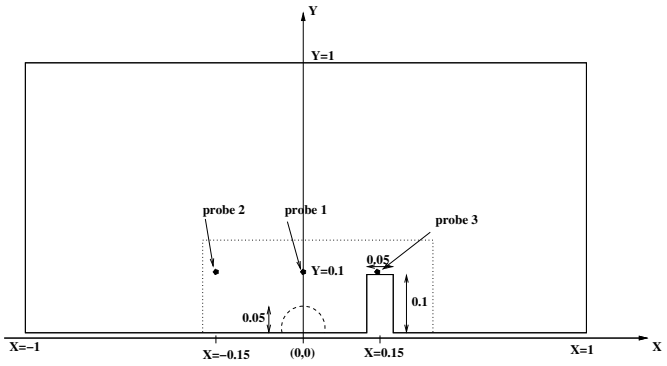

FIGURE 1.13. – Sketch of the domain for the 2D simulation. The half-circle delimited by a dashed line corresponds to the initial high pressure domain. The rectangular domain delimited by a doted line corresponds to the part of the domain where the mesh is refined. The black dots correspond to the three probes.

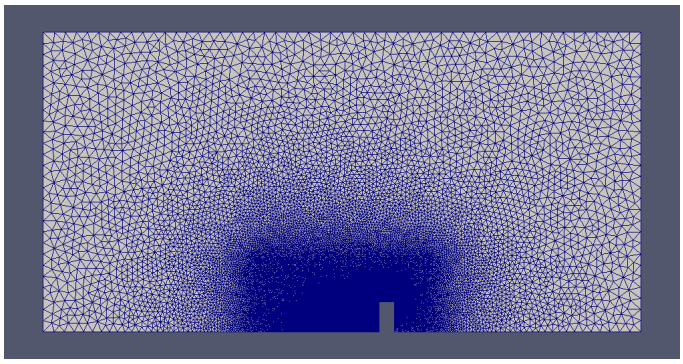

FIGURE 1.14. – Overview of the whole mesh for the 2D computational domain.

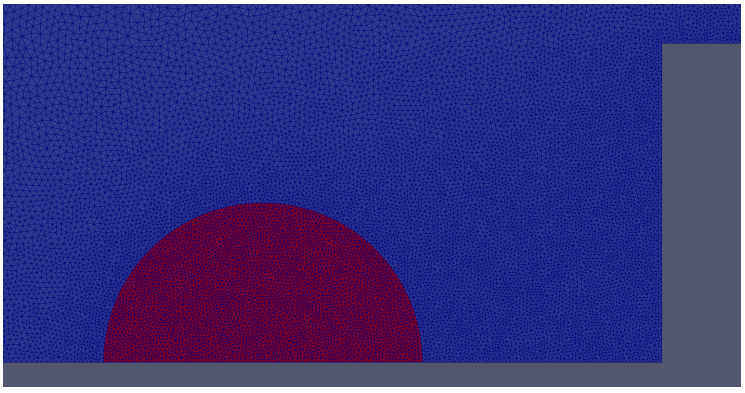

FIGURE 1.15. – Zoom of the 2D mesh around the high pressure zone (in red) and the obstacle.

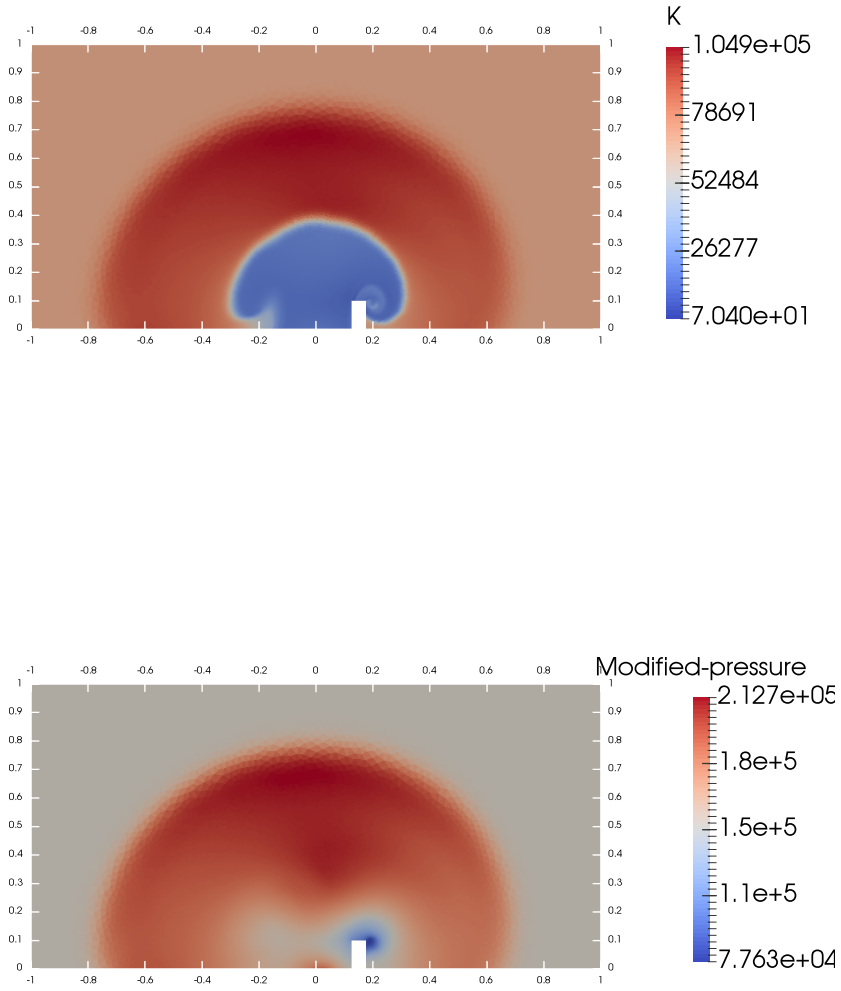

FIGURE 1.16. – Distributions of the turbulent kinetic energy K (top) and modified pressure P^* (bottom).

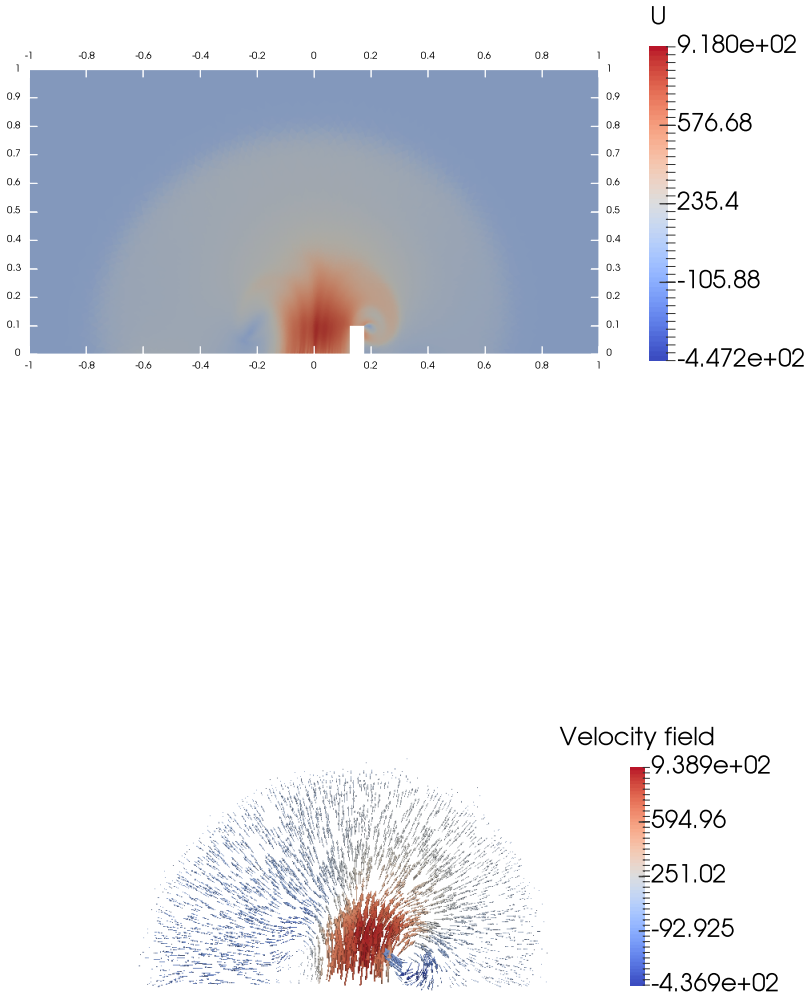

FIGURE 1.17. – Distributions of the norm of the velocity field (top) and velocity field (bottom)

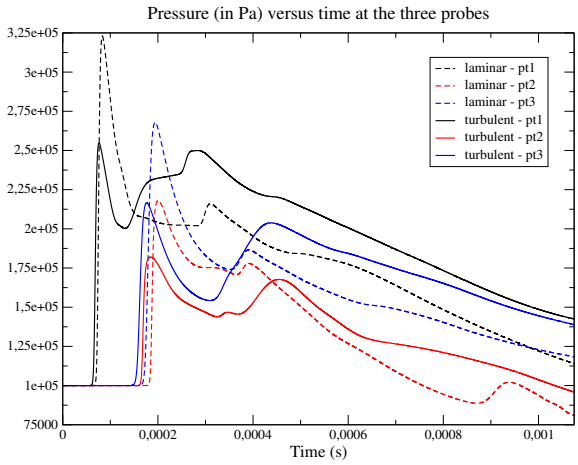

FIGURE 1.18. – Comparison between the pressure values in the turbulent ($\xi_0 = 10^5$) and laminar ($\xi_0 = 0$) cases at the three probes versus time.

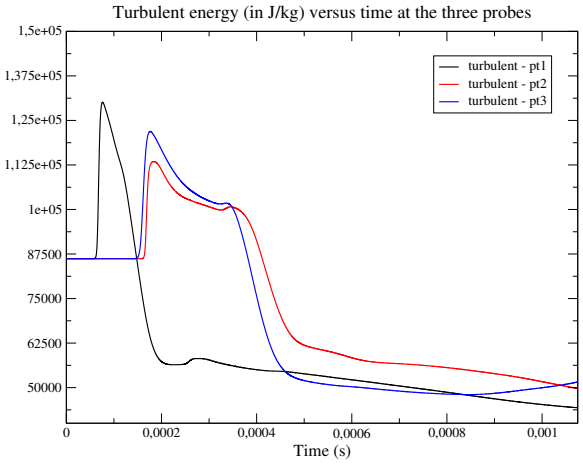

FIGURE 1.19. – Energy turbulence profile at the 3 probes versus time for $\xi_0 = 10^5$.

1.7. Conclusion

The main aim of the paper is to study a simple compressible turbulent model, with a specific behaviour in shocks waves (turbulent entropy is constant across shock waves). From a mathematical modeling point of view, an analysis of the conservative system (1.5) shows the hyperbolicity and the wave structure associated with LD and GNL (Riemann invariants) fields. In order to characterize shock waves, exact jump conditions can be defined. This analysis with a turbulent perfect gas EOS shows that the Riemann problem associated with system (1.5) admits a unique self-similar solution with no vaccum occurence. This result is the straightforward counterpart of the well-known result of existence and uniqueness in the Euler framework, while focusing on perfect gas equation of state (see for instance SMOLLER 1983; GODLEWSKI et RAVIART 1996).
An approximate Godunov solver has been implemented and some verification test cases including shock structures have been computed. A 2D hydrogen explosion test case has been computed and shown in section 6.
Ongoing work concerns a more complex model Sergey GAVRILYUK et Richard SAUREL 2006, which would allow variations of the turbulent entropy ξ through the shock waves. This one reads :

$$\begin{cases} \partial_t(\overline{\overline{\rho}}) + \nabla.(\overline{\overline{\rho}}\tilde{u}) = 0 \\ \partial_t(\overline{\overline{\rho}}\tilde{u}) + \nabla.\left(\overline{\overline{\rho}}\tilde{u}\otimes\tilde{u} + \left(\overline{\overline{P}} + \frac{2K}{3}\right).\mathscr{I}\right) = \epsilon_0\nabla.(\Sigma^{tot}(\nabla^s\tilde{u})) \\ \partial_t(\overline{\overline{\rho}}E) + \nabla.\left(\tilde{u}\left(\overline{\overline{\rho}}E + \overline{\overline{P}} + \frac{2K}{3}\right)\right) = \epsilon_0\nabla.(\Sigma^{tot}(\nabla^s\tilde{u})\tilde{u}) \\ \partial_t(\overline{\overline{\rho}}\xi) + \nabla.(\overline{\overline{\rho}}\xi\tilde{u}) = (\overline{\overline{\rho}})^{-2/3} rhs_K(W,\nabla W) + RHS^{SW} \end{cases} \tag{1.44}$$

The first term on the right-hand side of the last equation in (1.44) takes classical source terms into account (see introduction), while RHS^{SW} enables to account for turbulent entropy local variations through shock waves Sergey GAVRILYUK et Richard SAUREL 2006.

Acknowledgements
The last author receives financial support by ANRT through an EDF/CIFRE grant number 2019/1580. Computational facilities were provided by EDF. The authors thank the reviewers for their careful reading and suggestions.

ANNEXES

A. Solution of the Riemann problem

In this section, the notations depicted by figure 1.1 are used. We recall that the subscript L, 1, 2 and R respectively denote : the left state, the intermediate states between 1- and 2-wave, the intermediate states between 2- and 3-wave and the right state. The left and right states correspond to the initial states of the Riemann problem. We also recall that v stands for the velocity in the shock referential : $v = u - \sigma$, where σ is the shock speed.

The proof of existence and uniqueness of a solution of the Riemann problem associated with system (1.5) is built here following SMOLLER 1983. In reference SMOLLER 1983, the proof of the existence and uniqueness of a solution of the Riemann problem is built for the Euler system with a perfect gas EOS, but it may be extended to some suitable EOS. System of equations (1.5) corresponds in fact to the Euler system of equations with a pressure law P^* that is a correction of the perfect gas pressure law P^{pg}. We have the pressure law $P^*(\rho, e) = P^{pg}(\rho, e) + 2K(\rho)/3$ and the modified internal energy $e^*(\rho, e) = e + K(\rho)/\rho$. Actually, we show below that the proof proposed in SMOLLER 1983 can also be extended to our system of equations.

As in SMOLLER 1983, the outline of the proof in this appendix is the following. First, the paths across each wave are defined using the Riemann invariants or the Rankine-Hugoniot relations established in sections 3.3 and 1.2.4. These paths are defined through two parameters which are the density ratios : $z_1 = \rho_1/\rho_2$ and $z_2 = \rho_2/\rho_R$. Then, the connection between the different waves is performed. Afterwards, it can be proved that solving the Riemann problem is equivalent to finding a root in $]0, \beta[$ of a function $z_2 \mapsto \mathscr{H}(z_2)$ which is continuous and increasing, with $\beta = (\gamma+1)/(\gamma-1)$. It should be noted that, since $\gamma > 1$, we have $\beta > 1$. Moreover, under the assumption that void does not occur, it can be shown that this function $\mathscr{H}$ is such that :

$$\lim_{z_2 \to 0^+} \mathscr{H}(z_2) \times \lim_{z_2 \to \beta^-} \mathscr{H}(z_2) < 0.$$

At least, this allows to conclude the proof of existence and uniqueness of a solution of the Riemann problem thanks to the theorem of the intermediate values.

A.1. Paths across the waves of the system

According to section (3.2), the waves associated with the eigenvalues λ_1 and λ_3 are GNL waves. They can be either shock waves or rarefaction waves. For the former the path across the wave is defined thanks to the Rankine-Hugoniot relations, whereas for the latter the Riemann invariants are used. The field associated with the eigenvalue

λ_2 is linearly degenerated so that it can be described by both the Rankine-Hugoniot relations or the Riemann Invariants.

Definition of shock waves .

Let us first start by the case of the shock waves. The jump conditions for system (1.5) are given in section 1.2.4 by relations (3.36) and are recalled below :

$$\begin{cases} [\rho v] = 0, \\ [\rho v^2 + P^*] = 0, \\ \rho v \left(\left[e + \dfrac{K}{\rho} \right] + \overline{P^*} \left[\dfrac{1}{\rho} \right] \right) = 0. \end{cases} \tag{1.45}$$

These relations involve the square of the jump of the velocity : $[u]^2$. Hence the velocity jump is not uniquely defined and an additional information must be added to relations (3.36) in order to get a unique definition of the velocity jump across the shock. We use here the entropy inequality for that purpose. We recall the entropy inequality associated with (1.45), and given by (1.15) :

$$\mathscr{B} = -\sigma [\eta]_L^R + [u\eta]_L^R < 0, \tag{1.46}$$

with $\eta = -\rho ln(s)$.
Since $[\rho v]_L^R$ =0, we can rewrite $\mathscr{B}$ in the following form :

$$\mathscr{B} = -[\rho v ln(s)]_L^R = -\rho v \frac{[ln(s)]_L^R}{[s]_L^R} [s]_L^R < 0,$$

so that we get :

$$\mathscr{A} = \rho v [s]_L^R = [\rho v s]_L^R > 0.$$

By using the first jump relation equation of (1.45) :

$$[\rho v]_L^R = \bar{\rho} [v]_L^R + \bar{v} [\rho]_L^R = 0,$$

$\mathscr{A}$ can be rewritten :

$$\mathscr{A} = \vartheta [v]_L^R, \tag{1.47}$$

with :

$$\vartheta = \bar{\rho} s - \bar{\rho} \frac{[\rho s]_L^R}{[\rho]_L^R}.$$

In the case of a perfect gas EOS, we have $\rho s = P\tau^{\gamma-1}$. Let us define :

$$a = \frac{\tau_R}{\tau_L}, \quad R_p = \frac{P_R}{P_L},$$

so that ϑ reads :

$$\vartheta = \frac{(P\tau^{\gamma-1})_L}{1-a}(1-R_p a^\gamma). \tag{1.48}$$

In the following the sign of ϑ is studied, so that the sign of $[v]_L^R$ and then $[u]_L^R$ can be exhibited. By using the third jump relation equation of (1.45) :

$$[e+K\tau]_L^R + \bar{P}^*[\tau]_L^R = 0,$$

we get :

$$\gamma\bar{P}[\tau]_L^R + \bar{\tau}[P]_L^R + (\gamma-1)\bar{\tau}[K]_L^R + \frac{5}{3}(\gamma-1)\bar{K}[\tau]_L^R = 0.$$

Thus, we have :

$$R_p(\beta a-1) = \beta - a + \frac{K_L}{P_L}\left((a+1)(1-a^{-5/3}) + 5/3(1-a)(1+a^{-5/3})\right). \tag{1.49}$$

By replacing the formula of R_p (1.49) into that of ϑ (1.48), we get :

$$\frac{\vartheta}{(P\tau^{\gamma-1})_L} = (1-a)^{-1}(\beta a-1)^{-1}g^L(a) + \frac{2K_L}{3P_L}a^{\gamma-5/3}(1-a)^{-1}(\beta a-1)^{-1}g^T(a),$$

where :

$$\begin{cases} g^L(a) = \beta a - 1 - a^\gamma(\beta - a), \\ g^T(a) = a^{8/3} - 1 - 4a^{5/3} + 4a. \end{cases} \tag{1.50}$$

Table 3.14 gives the sign and variations of these 2 functions on the interval $[\frac{1}{\beta}, \beta]$.

a	$\frac{1}{\beta}$		1		β
βa -1		+		+	
1-a		+	0	−	
$(g^{L,T})''(a)$		−	0	+	
$(g^{L,T})'(a)$		↘	0	↗	
$(g^{L,T})(a)$		−	0	+	

FIGURE 1.20. – Variation table for g^L and g^T functions

We can deduce from table 3.14 that :

$$\frac{\vartheta}{(P\tau^{\gamma-1})_L} \leq 0 \quad \forall a \in]\frac{1}{\beta}, \beta[.$$

Since $\mathscr{A} > 0$, we deduce from (1.47) that $[v]_L^R < 0$ and thus that $[u]_L^R < 0$.
Hence, for system (1.5) the relation $[u] < 0$ holds across a shock wave, and thus the entropy inequality (1.10) allows to define shocks in a unique manner through :

$$[u]^2 + [\tau][P] = 0 \quad \text{and} \quad [u] < 0 \Longleftrightarrow [u] = -\sqrt{-[\tau][P]}.$$

Furthermore, when void does not occur, $\tilde{c}_i > 0$ for $i \in \{L, 1, 2, R\}$, we always get the same order for the eigenvalues : $\lambda_1 < \lambda_2 < \lambda_3$, so that we also have the relation :

$$u_1 = \lambda_2(W_1) > \sigma_1 \Longrightarrow v_1 = u_1 - \sigma_1 > 0 \tag{1.51}$$

and

$$u_2 = \lambda_2(W_2) < \sigma_2 \Longrightarrow v_2 = u_2 - \sigma_2 < 0 \tag{1.52}$$

Since $[u] = [v] = [\rho\tau v] = \rho v[\tau]$, and $[u] < 0$ in shocks, we have $v[\tau] < 0$ in shocks. Thus, thanks to the signs of v_1 and v_2 :

$$\tau_1 < \tau_L \quad \Longrightarrow \quad z_1 > 1,$$

in the 1-shock, and :

$$\tau_R > \tau_2 \quad \Longrightarrow \quad z_2 > 1,$$

in the 3-shock. It should be noted that the jump relations (3.36) also leads to the relation :

$$(\rho v)^2[\tau] + [P^*] = 0.$$

Therefore, using the results above on $[\tau]$, we get that $P_1^* > P_L^*$ in a 1-shock and $P_R^* < P_2^*$ in a 3-shock

Path across a 1-shock wave.

The path across a 1-shock wave is obtained through the parameter z_1 thanks to the Rankine-Hugoniot relations (3.36) and to the Lax criterion. After some calculus, it yields that a 1-shock is defined for $z_1 > 1$ by the relations :

$$\begin{cases} u_1 = u_L - c_L f_1(z_1, K_L/P_L), \\ P_1 = P_L h_1(z_1, K_L/P_L), \end{cases} \tag{1.53}$$

with the functions :

$$\begin{aligned} f_1(z_1, K_L/P_L) &= \sqrt{\left(\tfrac{z_1-1}{\gamma z_1}\right)\left(-1 + \tfrac{2}{3}\tfrac{K_L}{P_L}(z_1^{5/3} - 1) + h_1(z_1, K_L/P_L)\right)}, \\ h_1(z_1, K_L/P_L) &= \frac{\beta z_1 - 1 + g_1(z_1, K_L/P_L)}{\beta - z_1}, \\ g_1(z_1, K_L/P_L) &= \frac{2K_L}{3P_L}\left(z_1^{8/3} - 4z_1^{5/3} + 4z_1 - 1\right), \end{aligned} \tag{1.54}$$

and $K_L = \xi_0 \rho_L^{5/3}$.

Path across a 3-shock wave.

For a 3-shock, the path depends on $z_2 > 1$ and by using the Rankine-Hugoniot relations (3.36) and the Lax criterion we get :

$$\begin{cases} u_2 = u_R + c_R f_2(z_2, K_R/P_R), \\ P_2 = P_R h_2(z_2, K_R/P_R), \end{cases} \tag{1.55}$$

with the functions :

$$\begin{aligned} f_2(z_2, K_R/P_R) &= \sqrt{\left(\tfrac{z_2-1}{\gamma z_2}\right)\left(-1 + \tfrac{2}{3}\tfrac{K_R}{P_R}(z_2^{5/3}-1) + h_2(z_2, K_R/P_R)\right)}, \\ h_2(z_2, K_R/P_R) &= \frac{\beta z_2 - 1 + g_2(z_2, K_R/P_R)}{\beta - z_2}, \\ g_2(z_2, K_R/P_R) &= \frac{2K_R}{3P_R}\left(z_2^{8/3} - 4z_2^{5/3} + 4z_2 - 1\right), \end{aligned} \tag{1.56}$$

and $K_R = \xi_0 \rho_R^{5/3}$.

Path across a 1-rarefaction wave.

In a 1-rarefaction wave the Riemann Invariants $\tilde{\tilde{I}}_1^1$ and $\tilde{\tilde{I}}_2^1$ exhibited in section 3.3 remain constant. Hence, we get the following relations in a 1-rarefaction wave for $z_1 < 1$:

$$s_L = s_1, \tag{1.57}$$

and

$$u_L + \int_0^{\rho_L} \frac{c_t(s,\rho\prime)}{\rho\prime}\,\mathrm{d}\rho\prime = u_1 + \int_0^{\rho_1} \frac{c_t(s,\rho\prime)}{\rho\prime}\,\mathrm{d}\rho\prime. \tag{1.58}$$

Then, using the thermodynamical closures chosen for the model, (1.57) and (1.58) can be rewritten in the form :

$$\begin{cases} u_1 - u_L + c_L B_1(z_1, K_L/P_L) = 0, \\ P_1 = P_L Q_1(z_1), \end{cases} \tag{1.59}$$

with the following definitions :

$$\begin{aligned} B_1(z_1, K_L/P_L) &= \int_1^{z_1} \left(z^{\gamma-3} + \frac{10K_L}{9\gamma P_L} z^{-4/3}\right)^{1/2} \mathrm{d}z, \\ Q_1(z_1) &= z_1^{\gamma}. \end{aligned} \tag{1.60}$$

Path across a 3-rarefaction wave.

With the same arguments, using the Riemann Invariants $\tilde{\tilde{I}}_1^3$ and $\tilde{\tilde{I}}_2^3$, one can write for a 3-rarefaction wave for $z_2 < 1$:

$$\begin{cases} u_2 - u_R - c_R B_2(z_2, K_R/P_R) = 0, \\ P_2 = P_R Q_2(z_2), \end{cases} \tag{1.61}$$

with the following definitions :

$$\begin{aligned} &B_2(z_2, K_R/P_R) = \int_1^{z_2} \left(z^{\gamma-3} + \frac{10K_R}{9\gamma P_R} z^{-4/3} \right)^{1/2} \mathrm{d}z, \\ &Q_2(z_2) = z_2^{\gamma}. \end{aligned} \tag{1.62}$$

Path across the 2-contact wave.

In the 2-wave, the 2-Riemann invariants u and P^* are constant. Hence, the following relations arise :

$$P_1^* = P_2^*, \tag{1.63}$$

and

$$u_1 = u_2. \tag{1.64}$$

Remark 7 Functions B_1 and B_2 are defined on the basis of an integral of the form :

$$I(z) = \int_z^1 \left(x^{\gamma-3} + a_0 x^{-4/3} \right)^{1/2} \mathrm{d}x,$$

for $z \in [0,1]$, with $a_0 \geq 0$, $\gamma > 1$ and $\beta = (\gamma+1)/(\gamma-1) > 1$. Oviously, we have $I(z) \geq 0$. For $\gamma \in]1, 5/3]$ and $\gamma \geq 5/3$, the integral $I(z)$ can be respectively bounded by :

$$I(z) \leq \frac{2\sqrt{1+a_0}}{\gamma-1}(1 - z^{(\gamma-1)/2}),$$

and

$$I(z) \leq 3\sqrt{1+a_0}(1 - z^{1/3}).$$

Hence, the integral $I(z)$, and thus functions B_1 and B_2, are defined for z in $[0,1]$. Moreover, it should be noticed that :

$$I(z) = 3\sqrt{1+a_0}(1 - z^{1/3}),$$

for $\gamma = 5/3$.

A.2. Connection between the different waves

Thanks to the relations of the previous section, the left state W_L and the intermediate state W_1 are related through the 1-wave thanks to

$$\begin{cases} u_1 = u_L - c_L \mathscr{G}_L(z_1), \\ P_1 = P_L \mathscr{F}_L(z_1), \end{cases} \tag{1.65}$$

where the functions $\mathscr{F}_L$ and $\mathscr{G}_L$ are respectively defined piecewise through the relations obtained either for a rarefaction wave, $z_1 \leq 1$, or for a shock wave, $z_1 > 1$, using respectively (1.53)-(1.54) and (1.59)-(1.60). So we obtain the definitions :

$$\mathscr{F}_L(z_1) = \begin{cases} h_1(z_1, K_L/P_L) \text{ if } z_1 > 1, \\ Q_1(z_1) \text{ if } z_1 \leq 1, \end{cases} \tag{1.66}$$

and

$$\mathscr{G}_L(z_1) = \begin{cases} f_1(z_1, K_L/P_L) \text{ if } z_1 > 1, \\ B_1(z_1, K_L/P_L) \text{ if } z_1 \leq 1. \end{cases} \tag{1.67}$$

In the same way, for the 3-wave, the following relations hold between W_R and W_2 :

$$\begin{cases} u_2 = u_R + c_R \mathscr{G}_R(z_2), \\ P_2 = P_R \mathscr{F}_R(z_2), \end{cases} \tag{1.68}$$

where according to (1.55)-(1.56) and (1.61)-(1.62), we have :

$$\mathscr{F}_R(z_2) = \begin{cases} h_2(z_2, K_R/P_R) \text{ if } z_2 > 1, \\ Q_2(z_2) \text{ if } z_2 \leq 1, \end{cases} \tag{1.69}$$

and

$$\mathscr{G}_R(z_2) = \begin{cases} f_2(z_2, K_R/P_R) \text{ if } z_2 > 1, \\ B_2(z_2, K_R/P_R) \text{ if } z_2 \leq 1. \end{cases} \tag{1.70}$$

Due to the order of the different waves for system (1.5) which is always such that $\lambda_1 < \lambda_2 < \lambda_3$, the connection of the two GNL waves is easily performed through the contact wave using relations (1.63) and (1.64). Indeed, the modified pressure reads : $P^* = P + 2K/3$. Hence by combining equation (1.63) with first equation of (1.65) and first equation of (1.68), we obtain :

$$P_L \mathscr{F}_L(z_1) + \frac{2}{3} K_L z_1^{5/3} = P_R \mathscr{F}_R(z_2) + \frac{2}{3} K_R z_2^{5/3}, \tag{1.71}$$

The velocity equality (1.64) combined with second equation of (1.65) and second equation of (1.68) yields :

$$u_R + c_R \mathscr{G}_R(z_2) - u_L + c_L \mathscr{G}_L(z_1) = 0. \tag{1.72}$$

System (1.71)-(1.72) is a 2×2 non-linear system for the unknowns $(z_1, z_2) \in]0, \beta[^2$. Let us now study this system.

A.3. Existence and uniqueness of a solution for the Riemann problem

It can been proved that $\mathscr{F}_L$ and $\mathscr{G}_L$ (respectively $\mathscr{F}_R$ and $\mathscr{G}_R$) are differentiable functions of $z_1 \in]0,\beta[$ (respectively of $z_2 \in]0,\beta[$). By differentiating equation (1.71) with respect to z_1 and z_2, it can be shown that $dz_1/dz_2 > 0$. Then, thanks to (1.71) one can implicitly define a variable change $z_2 \mapsto \mathscr{Z}_1(z_2)$ which gives z_1 as a function of z_2 :

$$z_1 = \mathscr{Z}_1(z_2).$$

Relation (1.72) can thus be expressed as a function of the sole variable z_2, and finding a solution of system (1.71)-(1.72) is equivalent to finding a root of the function $z_2 \mapsto \mathscr{H}(z_2)$ defined on $]0,\beta[$ as :

$$\mathscr{H}(z_2) = u_R + c_R\mathscr{G}_R(z_2) - u_L + c_L\mathscr{G}_L(\mathscr{Z}_1(z_2)). \tag{1.73}$$

When differentiating $\mathscr{H}$ with respect to z_2, we find that :

$$\mathscr{H}'(z_2) = c_R\mathscr{G}_R'(z_2) + c_L\frac{d\mathscr{Z}_1(z_2)}{dz_2}\mathscr{G}_L'(\mathscr{Z}_1(z_2)). \tag{1.74}$$

It can be shown that $\mathscr{G}_L'$ and $\mathscr{G}_R'$ are positive functions, so that $z_2 \mapsto \mathscr{H}(z_2)$ is a continuous and increasing function on $]0,\beta[$.

By studying the definition of $\mathscr{G}_L$ and $\mathscr{G}_R$, the following limits can be found :

$$\lim_{z_2\to 0^+}(c_L\mathscr{G}_L(\mathscr{Z}_1(z_2)) + c_R\mathscr{G}_R(z_2)) = c_LB_1(0,K_L/P_L) + c_RB_2(0,K_R/P_R).$$

and

$$\lim_{z_2\to \beta^-}(c_L\mathscr{G}_L(\mathscr{Z}_1(z_2)) + c_R\mathscr{G}_R(z_2)) = +\infty$$

The variable change $\mathscr{Z}_1$ is an increasing function of z_2. Hence, when z_2 tends to zero, z_1 also tends to zero. This means that the first limit above is reached in the cases where both 1- and 3- waves are rarefaction waves. On the contrary, the second limit is reached in the cases where both 1- and 3- waves are shock waves (we recall that $\gamma > 1 \Rightarrow \beta > 1$). These two limits then give the following limits for $\mathscr{H}$:

$$\lim_{z_2\to 0^+}\mathscr{H}(z_2) = u_R - u_L + c_LB_1(0,K_L/P_L) + c_RB_2(0,K_R/P_R),$$

and

$$\lim_{z_2\to \beta^-}\mathscr{H}(z_2) = +\infty.$$

Since the function $z_2 \mapsto \mathscr{H}(z_2)$ is increasing and continuous on $]0,\beta[$, the intermediate value theorem can be applied in order to conclude that $\mathscr{H}$ admits a unique root

provided that the following condition holds :

$$u_R - u_L + c_L B_1(0, K_L/P_L) + c_R B_2(0, K_R/P_R) < 0 \tag{1.75}$$

As a consequence, the Riemann problem associated with system (1.5) possesses a unique solution if and only if condition (1.75) holds.

B. Building the intermediate states for VFRoe-ncv

As depicted in section 1.4, the VFRoe-ncv scheme is based on the computation of the exact solution of a linearized version of the Riemann problem at the interface between two cells. It thus relies on finding the two intermediate states Z_1 and Z_2 : the state Z_1 (resp. Z_2) is between the linearized waves $\bar{\lambda}_1$ and $\bar{\lambda}_2$ (resp. $\bar{\lambda}_2$ and $\bar{\lambda}_3$). We have :

$$Z_1 = Z_L + \alpha_1 \widehat{r}_1, \tag{1.76}$$

$$Z_2 = Z_1 + \alpha_2 \widehat{r}_2, \tag{1.77}$$

$$Z_R = Z_2 + \alpha_3 \widehat{r}_3, \tag{1.78}$$

where the linearized right eigenvectors are :

$$\widehat{r}_1 = (1, -\widehat{c}_t\bar{\tau}, \widehat{c}_t{}^2)^T, \quad \widehat{r}_2 = (1,0,0)^T, \quad \widehat{r}_3 = (1, \widehat{c}_t\bar{\tau}, \widehat{c}_t{}^2)^T,$$

and where the coefficients α_1 and α_3 associated with the eigenvalues $\bar{\lambda}_1$ and $\bar{\lambda}_3$ read :

$$\alpha_1 = \frac{1}{2}\frac{[P^*]_L^R}{\widehat{c}_t{}^2} - \frac{1}{2}\frac{[u]_L^R\bar{\rho}}{\widehat{c}_t},$$

$$\alpha_3 = \frac{1}{2}\frac{[P^*]_L^R}{\widehat{c}_t{}^2} + \frac{1}{2}\frac{[u]_L^R\bar{\rho}}{\widehat{c}_t}.$$

The linearized sound speed $\widehat{c}_t$ is defined by equation (1.38). It should be noted that thanks to (2.46), we have :

$$u_1 = u_2, \quad \text{and} \quad P_1^* = P_2^*.$$

After simple calculus on equations (2.45) and (2.47), the following intermediate values can be found :

$$u_1 = u_2 = \bar{u} - \frac{1}{2\bar{\rho}\widehat{c}_t}[P^*]_L^R,$$

$$P_1^* = P_2^* = \bar{P^*} - \frac{\bar{\rho}\widehat{c}_t}{2}[u]_L^R,$$

$$\rho_1 = \rho_L + \frac{[P^*]_L^R}{2\widehat{c_t}^2} - \frac{\bar{\rho}}{2\widehat{c_t}}[u]_L^R, \qquad \rho_2 = \rho_R - \frac{[P^*]_L^R}{2\widehat{c_t}^2} - \frac{\bar{\rho}}{2\widehat{c_t}}[u]_L^R.$$

C. Additional numerical results : a symmetric double rarefaction wave

This test case is representative of what happens close to a wall when the fluid flows outward or in a bluff-body. In these situations, the pressure decreases at the wall generating a rarefaction wave that propagates outwards from the wall. We reproduce such a configuration here with a symmetric double rarefaction wave test case for which the initial condition of the Riemann problem uses the "mirror state" strategy :

$$(\rho, u, P)_L = (\rho_0, -u_0, P_0), \qquad \text{and} \qquad (\rho, u, P)_R = (\rho_0, u_0, P_0),$$

with a negative normal velocity u_0 and $(\rho_0, u_0, P_0) = (1, 370, 10^5)$. The first test case ($\xi_0 = 0$) is inspired from BUFFARD, Thierry GALLOUËT et Jean-Marc HÉRARD 2000.

Profiles of the approximate solutions along the x-domain are given in figure 1.21, 1.22 and 1.23 for a mesh with 500 cells and using three values of $\xi_0 = \{0, 5000, 10000\}$. They involve a low-density state in the center of the domain, between the two rarefaction waves. This feature makes this problem a test for assessing the performance of numerical methods for low-density flows. Indeed, this test case allows to examine the stability of the scheme together with the preservation of positivity of the approximate density around $x = 0.5$ (which corresponds to the fictive wall location). The classical drawback of Godunov-type schemes on the density variable near the position of initial discontinuity $x = 0.5$ can be observed : an undershoot of the density profile which tends to vanish when the mesh is refined.

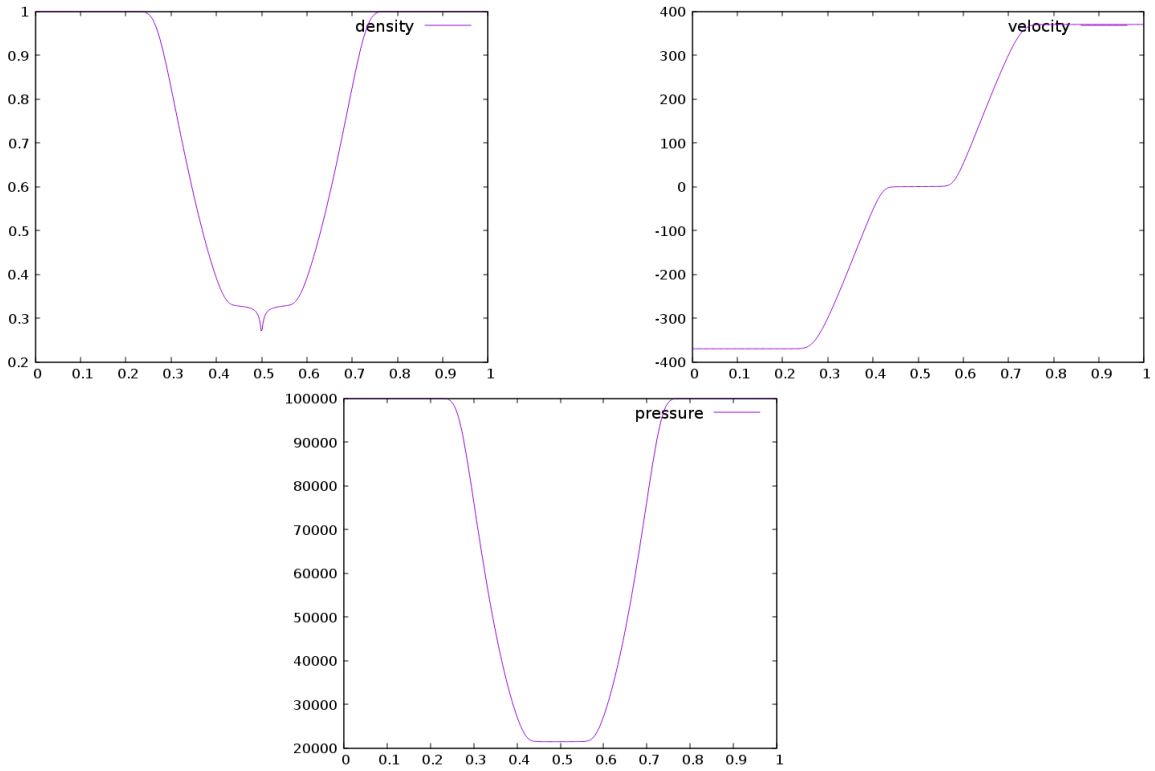

FIGURE 1.21. – Double rarefaction test case. Density (top left), velocity (top right) and pressure (bottom). Approximate solution at time $t_f = 3\ 10^{-4}$s, $CFL = 0.5$, for 500 cells and $\xi_0 = 0$.

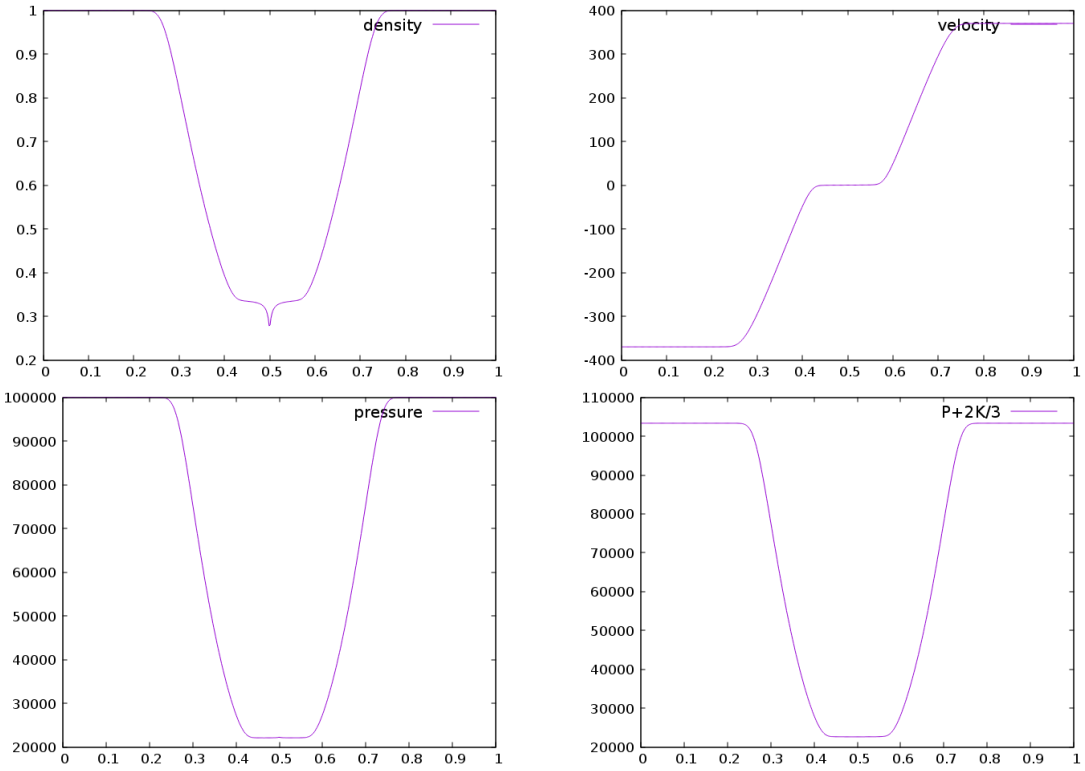

FIGURE 1.22. – Double rarefaction test case. Density (top left), velocity (top right), pressure P (bottom left) and modified pressure P^* (bottom right). Approximate solution at time $t_f = 3\ 10^{-4}$s, $CFL = 0.5$, for 500 cells and $\xi_0 = 5000$.

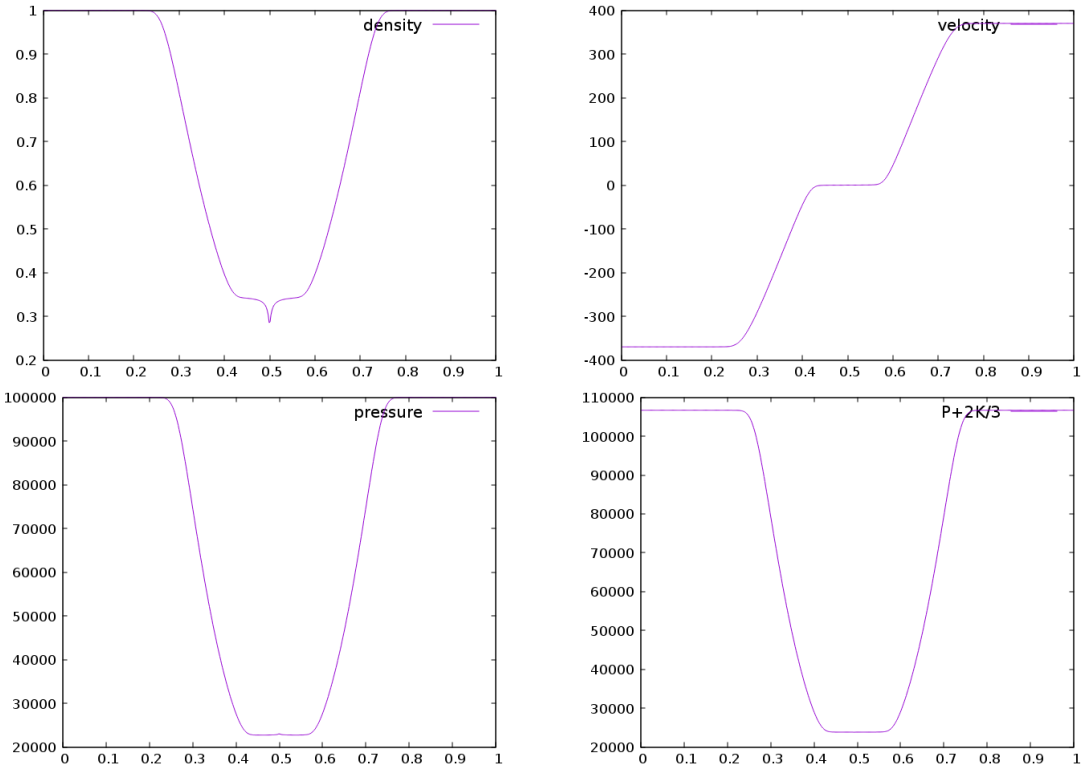

FIGURE 1.23. – Double rarefaction test case. Density (top left), velocity (top right), pressure P (bottom left) and modified pressure P^* (bottom right). Approximate solution at time $t_f = 3\ 10^{-4}$s, $CFL = 0.5$, for 500 cells and $\xi_0 = 10000$.

Bibliographie

[Ber99] Christophe BERTHON. « Contribution à l'analyse numérique des équations de Navier-Stokes compressibles à deux entropies spécifiques. Applications à la turbulence compressible ». Thèse de doct. Paris 6, 1999. URL : https://www.math.sciences.univ-nantes.fr/~berthon/cv_these_hdr/these.pdf (cf. p. 3, 4).

[BC02] Christophe BERTHON et Frédéric COQUEL. « Nonlinear projection methods for multi-entropies Navier-Stokes systems ». In : *Innovative Methods For Numerical Solution Of Partial Differential Equations* (2002), p. 278-304. DOI : 10.1142/9789812810816_0014 (cf. p. 3, 4).

[BGH00] Thierry BUFFARD, Thierry GALLOUËT et Jean-Marc HÉRARD. « A sequel to a rough Godunov scheme : application to real gases ». In : *Computers & Fluids* 29(7) (2000), p. 813-847. DOI : 10.1016/s0045-7930(99)00026-2 (cf. p. 15, 19, 30, 46).

[Erl+90] Gordon ERLEBACHER, Mohammed Yousuff HUSSAINI, Heinz-Otto KREISS et al. « The analysis and simulation of compressible turbulence ». In : *Theoretical and Computational Fluid Dynamics* 2.2 (1990), p. 73-95. DOI : 10.1007/bf00272136 (cf. p. 3).

[Fav58] Alexandre FAVRE. « Equations statistiques des gaz turbulents ». In : *Compte-Rendus de l'Académie des Sciences Paris* 246.18 (1958), p. 2576-2579 (cf. p. 3).

[Fav65] Alexandre FAVRE. « Equations des gaz turbulents compressibles. 1, Formes générales. 2, Méthode des vitesses moyennes ; méthode des vitesses macroscopiques pondérées par la masse volumique. » In : *Journal de Mécanique* 4.3 (1965) (cf. p. 3).

[Fav+76] Alexandre FAVRE, Leslie S.G. KOSVAZNAY, Raymond DUMAS et al. *La turbulence en mécanique des fluides : bases théoriques et expérimentales, méthodes statistiques.* Gauthier-Villars, 1976 (cf. p. 3).

[FHL97] Alain FORESTIER, Jean-Marc HÉRARD et Xavier LOUIS. « Solveur de type Godunov pour simuler les écoulements turbulents compressibles ». In : *Comptes Rendus de l'Académie des Sciences-Series I-Mathematics* 324(8) (1997), p. 919-926. DOI : 10.1016/s0764-4442(97)86969-8 (cf. p. 4).

[GB13] Thomas B GATSKI et Jean-Paul BONNET. *Compressibility, turbulence and high speed flow.* Academic Press, 2013. URL : https://www.researchgate.net/publication/281766815_Compressibility_Turbulence_and_High_Speed_Flow (cf. p. 3).

[GS06] Sergey GAVRILYUK et Richard SAUREL. « Estimation of the turbulent energy production across a shock wave ». In : *Journal of Fluid Mechanics* 549 (2006), p. 131. DOI : 10.1017/s0022112005008062 (cf. p. 3, 4, 36).

[GR96] Edwige GODLEWSKI et Pierre-Arnaud RAVIART. *Numerical approximation of hyperbolic sytems of conservation laws*. Springer Berlin, 1996. DOI : 10.1007/978-1-4612-0713-9 (cf. p. 15, 27, 36).

[God59] Sergueï Konstantinovitch GODUNOV. « A difference method for numerical calculation of discontinuous equations of hydrodynamics ». In : *Math sbornik (in Russian)* 47(89).3 (1959), p. 271-306. URL : https://hal.archives-ouvertes.fr/hal-01620642 (cf. p. 15).

[Hel+10] Philippe HELLUY, Jean-Marc HÉRARD, Hélène MATHIS et al. « A simple parameter-free entropy correction for approximate Riemann solvers ». In : *Comptes rendus Mécanique* 338(9) (2010), p. 493-498. DOI : 10.1016/j.crme.2010.07.007 (cf. p. 17, 26).

[Hér14] Jean-Marc HÉRARD. Rapp. tech. A simple turbulent model for compressible flows, 2014. URL : https://hal.archives-ouvertes.fr/hal-02007044 (cf. p. 5, 6).

[HL16] Jean-Marc HÉRARD et Hippolyte LOCHON. « A simple turbulent two-fluid model ». In : *Comptes Rendus Mécanique* 344(11-12) (2016), p. 776-783. DOI : 10.1016/j.crme.2016.10.010 (cf. p. 5).

[MFG99] Jean-Marie MASELLA, Isabelle FAILLE et Thierry GALLOUËT. « On an approximate Godunov scheme ». In : *International Journal of Computational Fluid Dynamics* 12(2) (1999), p. 133-149. DOI : 10.1016/j.crme.2016.10.010 (cf. p. 15).

[Smo83] Joel SMOLLER. *Shock waves and reaction—diffusion equations*. Springer Science & Business Media, 1983. DOI : 10.1007/978-1-4684-0152-3 (cf. p. 11, 15, 36, 37).

[SA94] Philippe SPALART et Steven ALLMARAS. « A one-equation turbulence model for aerodynamic flows ». In : *La Recherche Aérospatiale* (1994), p. 5-21. URL : https://arc.aiaa.org/doi/10.2514/6.1992-439 (cf. p. 3, 4).

[TL72] Henk TENNEKES et John Leask LUMLEY. « A First Course in Turbulence. » In : *MIT Press* (1972). DOI : 10.7551/mitpress/3014.003.0005 (cf. p. 3).

[Tor97] Eleuterio Francisco TORO. *Riemann solvers and numerical methods for fluid dynamics*. Springer Berlin Heidelberg, 1997. DOI : 10.1007/978-3-662-03490-3 (cf. p. 15, 27).

[Wil98] David WILCOX. *Turbulence Modelling for CFD*. DCW Industries, 1998 (cf. p. 3, 4).

2. An hybrid solver to compute a compressible model with dynamic estimation of the turbulent kinetic energy across shock waves

Sommaire

An hybrid solver to compute a compressible model with dynamic estimation of the turbulent kinetic energy across shock waves

Sergey Gavrilyuk[b], Jean-Marc Hérard[a], Olivier Hurisse[a], Ali Toufaili[a,c] :
[a] EDF R&D, 6 quai Watier, 78400 Chatou, France.
[b] IUSTI UMR CNRS 7343, Technopôle Château-Gombert, Marseille, France.
[c] I2M UMR CNRS 7373, Technopôle Château-Gombert, Marseille, France.

Abstract
We propose in this paper a numerical strategy in order to compute a turbulence model for compressible flows, including a dynamical estimation of the jump of the turbulent kinetic energy across shock waves. The model is taken from Sergey GAVRILYUK et Richard SAUREL 2006, and the Finite Volume scheme applies for a specific interface Riemann solver. The whole procedure requires the detection of shock waves in unsteady flows.

key words :
Turbulence, compressible flows, hyperbolicity, entropy, shock waves, Riemann problem

Introduction

Many industrial applications require the computation of compressible turbulence models in order to obtain a relevant representation of the mean density, mean velocity, mean pressure and turbulent kinetic energy (for instance in the framework of combustion and aerodynamics). These models classically apply for Reynolds averaging technique and Favre decomposition FAVRE 1958; FAVRE 1965; FAVRE, KOSVAZNAY, DUMAS et al. 1976, and closure laws for some correlations are mandatory. We refer for instance to TENNEKES et LUMLEY 1972; SPALART et ALLMARAS 1994; Christophe BERTHON 1999; POPE 2000; Christophe BERTHON et Frédéric COQUEL 2002; GATSKI et BONNET 2013 which recall some basic useful models and closures, and also provide some properties and theoretical investigation of the latter.

This paper aims at defining a suitable algorithm for computing approximate solutions of a turbulence model for compressible flows, while retaining the dynamic model first introduced in Sergey GAVRILYUK et Richard SAUREL 2006. It is actually the sequel of a recent work devoted to the analysis and the numerical approximation of solutions of the three-equation conservative model Sergey GAVRILYUK, Jean-Marc HÉRARD, Olivier HURISSE et al. 2022 for mass, momentum and energy. The latter model which is taken from Jean-Marc HÉRARD 2014, accounts for the turbulent kinetic energy K in a simple way, while setting :

$$K = \xi_0 \rho^{5/3}, \tag{2.1}$$

with $\xi_0 > 0$, together with the standard equation of state :

$$P = (\gamma - 1)\rho e. \tag{2.2}$$

The associated one-dimensional Riemann problem is investigated in Sergey GAVRILYUK, Jean-Marc HÉRARD, Olivier HURISSE et al. 2022, and it is shown that a Finite Volume scheme including approximate Riemann solvers enables to provide convergent approximations of solutions of the model, even when shocks occur in the flow. Nonetheless, it may be argued that the closure law (2.1) does not account for turbulent entropy variations across a shock wave. This urges the introduction of a more relevant turbulence model which would enable to represent turbulent compressible flows with more accuracy. Moreover, even when restricting to smooth solutions, it is known that classical turbulence models also account for turbulent entropy variations in regular zones.

Thus we will present herein some way to account for K variations in the whole computational domain. For that purpose, we will first recall in section 1.2 the basic dynamic model proposed in Sergey GAVRILYUK et Richard SAUREL 2006, and detail the full parametrization of shock waves. This model will then be inserted in a set of PDEs that will govern the evolution of mass, momentum and total energy, together with the

turbulent entropy $K\rho^{-5/3}$, hence providing the four unknowns ρ, P, U, K. This will be achieved in section 1.3. Afterwards, a Finite Volume scheme will be defined in section 2, that requires :

— the detection of the shock wave location in the unsteady flow at any time,
— the definition of a suitable interface Riemann-type solver in order to take turbulent entropy variations through shocks arising at an interface separating two neighboring mesh cells,
— a stable and consistent way to handle Dirac source terms occurring with shock patterns.

Eventually, some numerical results will be provided and discussed in section 3, and some conclusions will be drawn.

1. Governing equations

In this section, we present the steps used with the averaged Euler equations in order to derive a compressible model with dynamic estimation of the turbulent energy across a shock wave. This presentation consists in two different steps : (i) we start with the presentation of the global PDE formulation, (ii) we then move on to the presentation of the strategy used to estimate the jump of the turbulent entropy through a shock wave.

1.1. Global PDE formulation

The present model is an extension of the model presented in Jean-Marc HÉRARD 2014 ; Sergey GAVRILYUK, Jean-Marc HÉRARD, Olivier HURISSE et al. 2022 (the counterpart two- phase framework is presented in Jean-Marc HÉRARD et LOCHON 2016), which is based on Euler equations for a compressible flow.

It includes three conservation laws corresponding to the mass, momentum and total energy balance. The main unknowns are : the mean density ρ, the mean pressure P (in the sense of Reynolds averaging) and the mean velocity u (in the sense of Favre averaging). A fourth equation accounting for the turbulent kinetic energy K describes the evolution of the turbulent entropy ξ :

$$\xi = K\rho^{-5/3}.$$

The set of PDEs which determine the evolution of variables ρ, u, P and ξ within the flow has the following form :

$$\begin{cases} \partial_t(\rho) + \partial_x(\rho u) = 0 \\ \partial_t(\rho u) + \partial_x\left(\rho u^2 + P + \dfrac{2K}{3}\right) = 0 \\ \partial_t(\rho E) + \partial_x\left(u\left(\rho E + P + \dfrac{2K}{3}\right)\right) = 0 \\ \partial_t(\rho\xi) + \partial_x(\rho u\xi) + M(x,t)\delta_{(x-\sigma t=0)} = 0 \end{cases} \tag{2.3}$$

by noting the mean total energy E :

$$\rho E = \rho e(P,\rho) + \frac{\rho u^2}{2} + K,$$

where e(P,ρ) is the mean specific internal energy given by user. We also note :

$$P^* = P + \frac{2}{3}K, \tag{2.4}$$

the modified pressure. The Dirac mass is $\delta_{(x-\sigma t=0)}$ located in $x = \sigma t$, $M(x,t)$ is the mass located at the shock position, and σ is the velocity of the shock wave.

Remark 8 (The special case $M(x,t)=0$)
In the specific case where $M(x,t)$=0, the model associated with system (2.3) is conservative. We emphasize that (2.3) is hyperbolic (see **Appendix** A). Its real eigenvalues are :

$$\lambda_1 = u - \tilde{c}, \quad \lambda_{2,3} = u, \quad \lambda_4 = u + \tilde{c},$$

where the turbulent speed of density waves $\tilde{c}$ is given by :

$$\tilde{c}^2 = c^2 + \frac{10K}{9\rho} = c^2 + \frac{10}{9}\xi\rho^{2/3}.$$

When $M(x,t)=0$, the Rankine-Hugoniot relations associated with model (2.3) are :

$$\begin{cases} -\sigma[\rho] + [\rho u] = 0, \\ -\sigma[\rho u] + \left[\rho u^2 + P + \dfrac{2K}{3}\right] = 0, \\ -\sigma[\rho E] + \left[u\left(\rho E + P + \dfrac{2K}{3}\right)\right] = 0 \\ -\sigma[\rho\xi] + [\rho u\xi] = 0 \end{cases} \tag{2.5}$$

The first relation gives us :

$$[\rho v] = 0, \quad with \quad v = u - \sigma.$$

The fourth relation can be written in the following form :

$$[\rho v\xi] = 0 \Longrightarrow \rho v[\xi] = 0$$

Through a shock wave (GNL field), we have $\rho v \neq 0$, thus $[\xi]_L^R$=0 where L (R) respectively denote the variables ahead (behind) the shock wave.

Besides, we note that ξ is a Riemann invariant in GNL waves associated with λ_1 and λ_4. Hence, we deduce that ξ remains constant in GNL waves (shock or rarefraction). ■

However, it is usually argued that the 'closure' $[\xi]_L^R$=0 through a shock wave (or $M(x,t)=0$) is not totally realistic. Focusing for instance on hydrogen explosion, an accurate prediction of shock waves is mandatory, and thus a relevant (non zero) definition of the mass $M(x,t)$ is required.

This is discussed in the following section, while **Appendix** D gives some possible reformulation of the governing set of PDE when a sole shock wave occurring in the fluid flow.

1.2. Estimation of the turbulent entropy jump through a shock wave

We will consider in the sequel the model which has been proposed in Sergey GAVRILYUK et Richard SAUREL 2006. The latter reference proposes a methodology to evaluate the jump of turbulent entropy through shock waves.

1.2.1. Estimating $M(x,t)$

In the sequel, we will consider the following turbulent perfect gas EOS :

$$P = (\gamma - 1)\rho e.$$

with $\gamma > 1$.

For a given shock wave propagating at speed σ, we note the variables on the right side of the shock with the index 'R', and the variables of the left side of the shock with index '2' (thus focusing on the wave associated with $u + \tilde{c}$). The following Rankine-Hugoniot relations for the conservation of mass, momentum and energy can be easily obtained using (2.5)

$$\begin{cases} [\rho(u-\sigma)]_2^R = 0 \\ m^2[\tau]_2^R + [P^*]_2^R = 0 \\ [e + K\tau]_2^R + \bar{P}^*_{R,2}[\tau]_2^R = 0 \end{cases} \tag{2.6}$$

with $m = \rho_R(u_R - \sigma)$, and for any quantity ϕ : $\bar{\phi}_{a,b} = \frac{\phi_a + \phi_b}{2}$, $[\phi]_b^a = \phi_a - \phi_b$.

The fourth equation in (2.3) enables to get :

$$-\sigma[\rho\xi]_2^R + [\rho u\xi]_2^R + M_0 = 0 \Longrightarrow m[\xi]_2^R + M_0 = 0 \tag{2.7}$$

In order to determine the intermediate state '2' from the state 'R', and therefore to find the value of M_0, one more relation is needed.

— The second and the third equation of (2.6) are written in the form :

$$\begin{cases} P_2^* - P_R^* - m^2(\tau_R - \tau_2) = 0 \\ P_R^*(\beta\tau_R - \tau_2) - P_2^*(\beta\tau_2 - \tau_R) + 2\xi_R\tau_R^{-2/3}\alpha - 2\xi_2\tau_2^{-2/3}\alpha = 0 \end{cases} \tag{2.8}$$

where :

$$\alpha = \frac{(\gamma - 5/3)}{(\gamma - 1)},$$

and

$$\beta = \frac{(\gamma + 1)}{(\gamma - 1)}.$$

System (2.8) admits 2 equations with 3 unknowns : P_2^*, τ_2 and ξ_2.

The first relation in (2.8) determines the Rayleigh line, and we call the function $H(\tau_2, P_2^*, \xi_2)$ the Hugoniot function of the turbulent gas flow defined by second relation in (2.8) :

$$H(\tau_2, P_2^*, \xi_2) = P_R^*(\beta\tau_R - \tau_2) - P_2^*(\beta\tau_2 - \tau_R) + 2\xi_R\tau_R^{-2/3}\alpha - 2\xi_2\tau_2^{-2/3}\alpha \tag{2.9}$$

— **The additional relation is given by following** Sergey GAVRILYUK et Richard SAUREL 2006, the tangent of the Rayleigh line to the curve H in the plane (τ_2, P_2^*) with ξ_2 fixed, gives us the additional relation. We rewrite this constraint by solving the following equation :

$$\frac{\partial H}{\partial \tau}|_{(P^*,\xi)} d\tau|_\xi + \frac{\partial H}{\partial P^*}|_{(\tau,\xi)} dP^*|_\xi = 0, \tag{2.10}$$

which gives us the following equation :

$$\frac{4}{3}\xi_2\tau_2^{-5/3}\alpha = P_R^* + P_2^*\beta + m^2\tau_R - m^2\tau_2\beta. \tag{2.11}$$

For a given value of $(\tau, u, P, \xi)_R$ and σ, we have to find 5 unknowns $(\tau, u, P, \xi)_2$ and M_0 solution of (2.6), (2.7) and (2.11).

1.2.2. Positivity conditions

We investigate now the positivity conditions pertaining to ξ_2 (or equivalently K_2). Actually, since ξ_2 must have a positive value, conditions pertaining to the jump of τ will appear when crossing the shock, depending on the value of the parameter γ .

We denote by :

$$\mathscr{A} = P_R^* + P_2^*\beta + m^2\tau_R - m^2\tau_2\beta,$$

the right hand side of equation (2.11). Assuming that $\tau_2 > 0$ therefore $\xi_2 > 0$, then $\mathscr{A}$ will take the sign of (γ-5/3) (linked to α).

— **case** $\gamma < 5/3$:
Since (γ-5/3) has a negative sign, then $\mathscr{A}$ must be negative for ξ_2 to remain positive. Using the first relation of system (2.8) and the definition of P^* (2.4), we reformulate $\mathscr{A}$ in the following form :

$$\mathscr{A} = \tilde{c_R}^2 + \frac{2}{3}K_R\tau_R(\gamma - 5/3) - m^2\left((\gamma+1)\tau_2\tau_R - \gamma\tau_R^2\right).$$

When A <0, it is necessary that :

$$m^2\left((\gamma+1)\tau_2\tau_R - \gamma\tau_R^2\right) > \tilde{c_R}^2 + \frac{2}{3}K_R\tau_R(\gamma - 5/3). \tag{2.12}$$

Using Lax inequality :

$$\sigma > \lambda_4(W_R), \tag{2.13}$$

we deduce from (2.13) that :

$$\tilde{c_R}^2 + \frac{2}{3} K_R \tau_R (\gamma - 5/3) > 0.$$

Owing to m^2>0, a condition involving the jump $[\tau]_2^R$ appears, which is :

$$(\gamma+1)\tau_2\tau_R - \gamma\tau_R^2 > 0,$$

and eventually (τ_R>0) :

$$\tau_2 > \frac{\gamma}{(\gamma+1)}\tau_R. \tag{2.14}$$

— **case** $\gamma > 5/3$:
in the case where the shock is of low amplitude (i.e $\tau_R \approx \tau_2$) and the turbulence is weak (i.e $K_R << 1$), $\mathscr{A}$ writes :

$$\mathscr{A} = P_R(1+\beta) + m^2\tau_R(1-\beta) = (c_R^2 - (u_R - \sigma)^2)\frac{1}{\tau_R}.$$

Thanks to the Lax inequality (2.13), which gives :

$$\sigma > u_R + \tilde{c_R} > u_R + c_R,$$

we get that :

$$\sigma - u_R > c_R > 0,$$

Thus $\mathscr{A}$ must be negative. However this is in contradiction with (2.11)

$$\frac{4}{3}\xi_2\tau_2^{-5/3}\alpha = \mathscr{A},$$

when $\gamma > 5/3$, that is : $\alpha > 0$.

Remark 9 (case $\gamma > 5/3$ with $\tau_R \neq \tau_2$ and $K_R >> 1$)
In this case we will not explicitly give the positivity conditions, because in an extension of this case ($\tau_R \approx \tau_2$ and $K_R << 1$) we have found a contradiction, therefore we do not take this case into account and we just focus on the case where $\gamma < 5/3$. ■

1.2.3. Final form of M(x,t)

Using the additional relation (2.11) and system (2.8), simple calculations lead to solve a second order polynomial equation in τ_2, G(τ_2)=0, where :

$$G(\tau_2) = 2m^2\beta\tau_2^2 - \frac{5\gamma}{2(\gamma-1)}(m^2\tau_R + P_R^*)\tau_2 + P_R^*\tau_R\frac{\gamma}{\gamma-1} + \frac{1}{2}m^2\tau_R + \xi_R\tau_R^{-2/3}\alpha. \tag{2.15}$$

Equation (2.15) admits a unique solution under the two constraints :

$$\tau_2 < \tau_R \quad , \quad \tau_2 > \frac{\gamma}{(\gamma+1)}\tau_R. \tag{2.16}$$

Once τ_2 has been obtained by solving G(τ_2)=0, the first equation in (2.6) gives u_2, the second one gives P_2^*, the third one gives :

$$[\frac{P^*\tau}{(\gamma-1)} + \alpha\xi\tau^{-2/3}]_2^R + P_{2,R}^{\bar{*}}[\tau]_2^R = 0 \tag{2.17}$$

which in turn provides ξ_2. Then the jump $[\xi]_2^R$ is known, and we can calculate M_0 by equation (2.7) :

$$M_0 = -m[\xi]_2^R.$$

Of course a similar approach is used across the shock wave associated with $u - \tilde{c}$.

Remark 10 The Lax criterion applied to our system states that for an admissible shock wave with a velocity σ we have for a $(u+\tilde{c})$-shock :

$$\lambda_4(W_2) = u_2 + \tilde{c_2} > \sigma > \lambda_4(W_R) = u_R + \tilde{c_R} \tag{2.18}$$

In fact, we have :

$$(\sigma - u_2)^2 - \tilde{c_2}^2 = m^2\tau_2^2 - \gamma P_R^*\tau_2 - \gamma m^2\tau_R\tau_2 + \gamma m^2\tau_2^2 + \frac{2}{3}\xi_2\tau_2^{-2/3}(\gamma - \frac{5}{3}),$$

using the first and second equations of (2.6). By replacing ξ_2 by its value given by equation (2.11), we find that :

$$\sigma - u_2 - \tilde{c_2} = 0,$$

which means that the first inequality in (2.18) is reached. ■

2. Numerical method

In this part we will introduce a numerical method in order to cope with the compressible turbulence model (2.3) described in the previous part. The method consists in adapting a hybrid solver to compute approximate solutions of the problem. This hybrid solver consists in two solvers : a classical approximate interface Riemann solver when no shock wave is detected, and a specific interface solver dedicated to the interface where a shock wave has been detected. We will call it the modified approximate Riemann solver 'MARS'.

For this, we use a classical Finite Volume formulation in a 1D domain. The computational domain on segment [a,b] is subdivided into cells I_i, where $x_{i+1/2}$ represents the cell interface between cells I_i and I_{i+1}, and x_i represents the cell center. We define Δt^n the time step at time t^n and Δx_i the length of I_i such that : $t^{n+1} = t^n + \Delta t^n$ and

$\Delta x_i = x_{i+1/2} - x_{i-1/2}$.

In the sequel, we will define the modified solver, more particularly the interface solver applied when a shock wave is detected on an interface. Concerning the classical approximate Riemann solver we will not detail it, because it is already known in the literature, the reader is referred to GODUNOV 1959; GODLEWSKI et RAVIART 1996; TORO 1997 for more details.

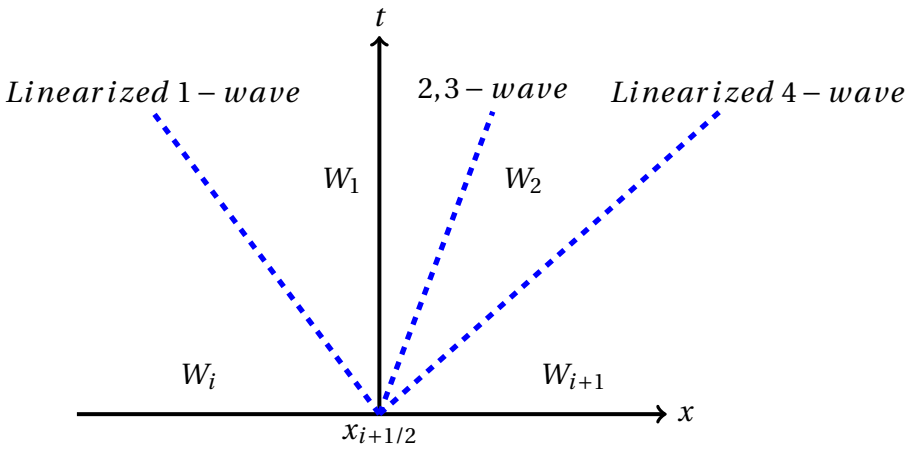

FIGURE 2.1. – Classical linearized interface solver at the interface $(i+\frac{1}{2})$ when no shock has been detected.

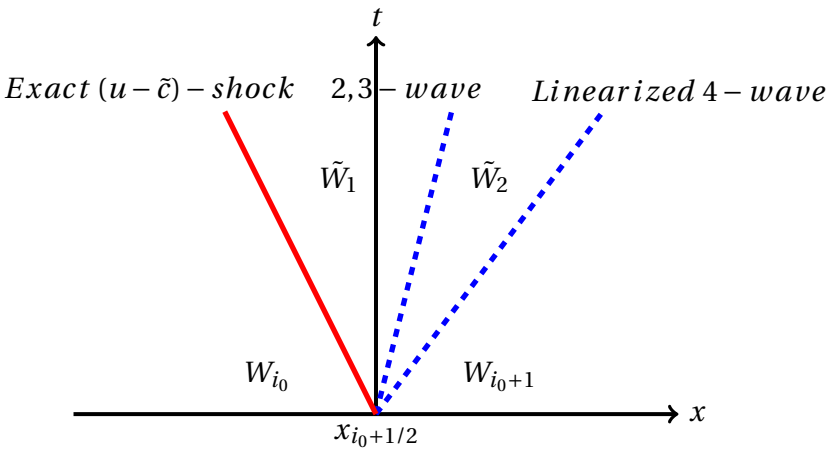

FIGURE 2.2. – Modified interface solver 'MARS', if a (u-$\tilde{c}$)-shock is detected at the interface $(i_0+\frac{1}{2})$.

2.1. Shock detector

In order to define properly the modified interface Riemann-type solver on the interface where a shock wave has been detected, a practical technique of detection of

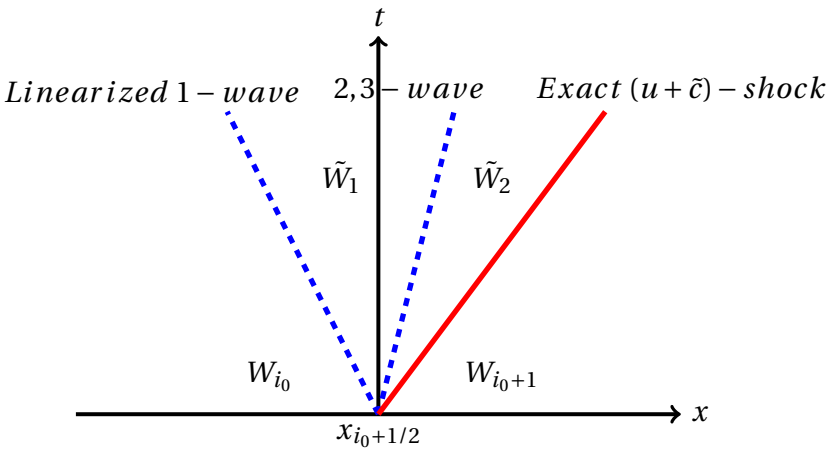

FIGURE 2.3. – Modified interface solver 'MARS', if a (u-$\tilde{c}$)-shock is detected at the interface $(i_0 + \frac{1}{2})$.

shock waves is needed. There are some methods proposed in the literature to detect shock waves (see KANAMORI et SUZUKI 2011 ; WU, XU, WANG et al. 2013 for instance for steady patterns), however only few focus on the unsteady framework, as pointed out in the conclusion of paper WU, XU, WANG et al. 2013. Thus, a different strategy will be introduced in the sequel, which basically relies on properties of the solution of the one-dimensional Riemann problem, on the entropy inequality and on associated Lax inequalities (see SMOLLER 1983).

For an interface $'i + \frac{1}{2}'$ separating the two cells i and $i+1$, we define the quantity $g_{i,i+1}$ as follows :

$$g^n_{i,i+1} = -\sigma_{i+1/2}[\eta^n]^{i+1}_i + [f^n_\eta]^{i+1}_i, \tag{2.19}$$

where (η, f_η) denotes the entropy-entropy flux pair, with $\eta = -\rho s$ and $f_\eta = u\eta$. The estimation of the shock velocity is made on the basis of the mass balance :

$$\sigma_{i+1/2} = \frac{[(\rho u)^n]^{i+1}_i}{[\rho^n]^{i+1}_i}. \tag{2.20}$$

Actually, for a discontinuity between the cells 'i' and 'i+1' travelling at speed $\sigma_{i+\frac{1}{2}}$, we have the following inequality :

$$-\sigma_{i+1/2}[\eta^n]^{i+1}_i + [f^n_\eta]^{i+1}_i < 0. \tag{2.21}$$

The use of jump relations (2.6)-(2.7) makes it possible to give a simple form of the quantity g :

$$g^n_{i,i+1} = \frac{\rho^n_i \rho^n_{i+1}[u^n]^{i+1}_i[s^n]^{i+1}_i}{[\rho^n]^{i+1}_i}.$$

We can deduce that if $g^n_{i,i+1} < 0$ then we have detected a discontinuity zone.

Though redundant, we also enforce the test :

$$[u^n]_i^{i+1} < 0,$$

where $[u^n]_i^{i+1}$ is expected to be o(1) through shock waves (unlike through 'discrete' contact discontinuities where $[u]_i^{i+1} \approx o(h)$).

Finally the test will be in the following form :

$$\textit{if } g^n_{i,i+1} < 0 \text{ and } [u^n]_i^{i+1} < 0, \textit{ then a shock wave is detected on the interface in } i + \frac{1}{2}$$

Once we have detected the interfaces with occurence of a shock wave, it remains to know whether it is a (u-$\tilde{c}$)-shock or a (u+$\tilde{c}$)-shock wave. The definition of shock waves in the sense of Lax will be used to distinguish them :

— if $u_i - \tilde{c}_i > \sigma_{i+1/2} > u_{i+1} - \tilde{c}_{i+1}$, then a $(u-\tilde{c})$-shock wave is detected on the interface in $'i + \frac{1}{2}'$

— if $u_i + \tilde{c}_i > \sigma_{i+1/2} > u_{i+1} + \tilde{c}_{i+1}$, then a $(u+\tilde{c})$-shock wave is detected on the interface in $'i + \frac{1}{2}'$

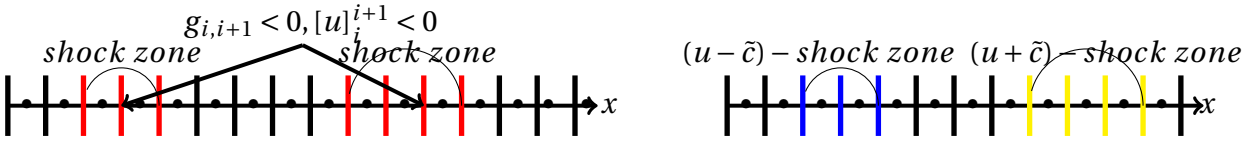

FIGURE 2.4. – Two different steps of the shock detector. Step 1 (left) shock zone detection, step 2 (right) (u-$\tilde{c}$)-shock or (u+$\tilde{c}$)-shock identification. Interface colors : shock zone (red), 1-shock (blue), 3-shock (yellow) and for other waves types (black)

In practice, most of the time the shock zone involves more than a sole interface, as depicted in figure (2.4).

2.2. Modified Approximate Riemann Solver when a shock occurs 'MARS'

This section describes the numerical resolution of the Riemann problem associated with a shock detected on the interface. More precisely we want to evaluate the numerical flux $F^{MARS}_{i_0+\frac{1}{2}}$ associated with the shock wave at interface $i_0 + \frac{1}{2}$. For the detection step, we assume that shock speeds have been estimated. Moreover the mass M_0 is given here.

In the following, we consider the general case M $\neq$ 0. In order to simplify the presentation of the modified solver, we focus on the case of an effective shock in the 4-wave

(i.e. when a (u+$\tilde{c}$)-shock appears).

First of all, we recall that (see Sergey GAVRILYUK, Jean-Marc HÉRARD, Olivier HURISSE et al. 2022, or **Appendix** A) the eigenvalues of system (2.3) are :

$$\lambda_1(W) = u - \tilde{c}, \quad \lambda_{2,3}(W) = u, \quad \lambda_4(W) = u + \tilde{c}$$

The associated eigenvectors are respectively :

$$r_1(W) = (\rho, -\tilde{c}, \rho\tilde{c}^2, 0) \quad , \quad r_2(W) = (1,0,0,0)$$

$$r_3(W) = (0,0,0,1) \quad , \quad r_4(W) = (\rho, \tilde{c}, \rho\tilde{c}^2, 0)$$

where

$$W = (\rho, u, P^*, \xi), \tag{2.22}$$

is the set of variables considered here.

The double wave associated with $\lambda_{2,3}$ is linearly degenerate (LD), and r_2 and r_3 are independent. The variables (u, P^*) are the Riemann invariants in this double wave.

The wave configuration retained for the simplified solver at the interface is depicted in figure 2.5.

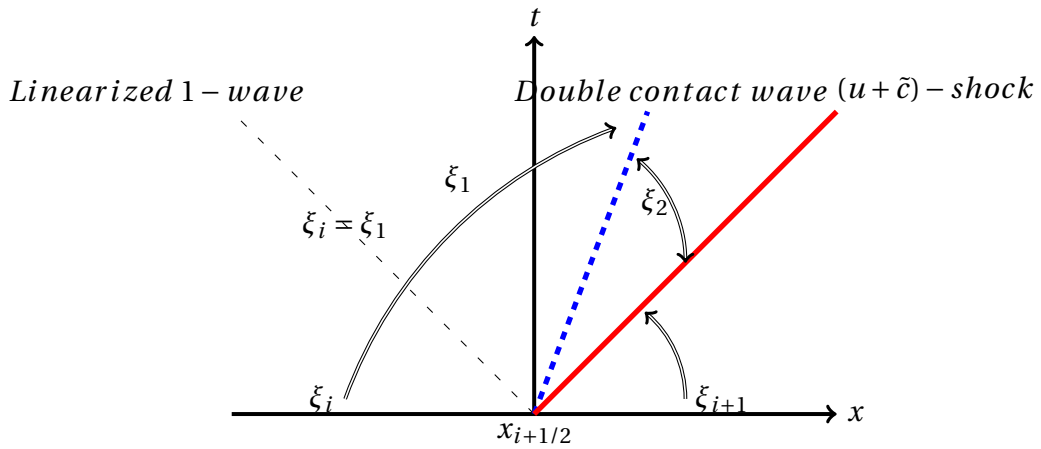

FIGURE 2.5. – Partial solution of the Riemann problem in terms of ξ. Intermediate states noted '1','2'

We note that :

$$W_1 - W_i = \mu_{i+\frac{1}{2}} \tilde{r}_1, \tag{2.23}$$

with $\tilde{r}_1 = (\bar{\rho}, -\bar{\tilde{c}}, \rho\bar{\tilde{c}}^2, 0)_{i+\frac{1}{2}}$, where $\bar{a} = \frac{a_{i+1}+a_i}{2}$ ($\mu_{i+\frac{1}{2}}$ will be given in step 3).

Concerning the wave associated with λ_4, we assume that it is a shock wave. The jump relations associated with this wave are as follows :

$$\begin{cases} \rho_R(u_R-\sigma)=\rho_2(u_2-\sigma)=m \\ m^2[\tau]_2^R+[P^*]_2^R=0 \\ [e+K\tau]_2^R+\bar{P}^*_{R,2}[\tau]_2^R=0 \\ m[\xi]_2^R+M_0=0 \end{cases} \tag{2.24}$$

where W_R=W_{i+1}.

The shock speed $\sigma_{i+1/2}$ is known numerically on the interface thanks to the detection stage (2.20). We recall that ξ_2 is known since M_0 is known, according to the formula proposed in section 1.2. We can then deduce from the jump relations (2.24) the three unknowns $(\rho,u,P)_2$ for the intermediate state '2'.

At this stage, we can propose a modified approximate Riemann solver 'MARS' adapted to the specific configuration of a (u+$\tilde{c}$)-shock wave. We calculate in three steps which are : :

1. Use of the jump relation through 4-wave.
2. Exact connection through the double contact wave $\lambda_{2,3}=u$.
3. Connection between state 'L' and '1' through linearized 1-wave.

Remark 11 The second and the third step of modified solver are the same as for the classical solver VFRoe-ncv BUFFARD, Thierry GALLOUËT et Jean-Marc HÉRARD 2000. ■

We recall that :

$$P=(\gamma-)\rho e. \tag{2.25}$$

• **Step 1((u+$\tilde{c}$)-shock)** : The jump relations (2.24) give us :

$$P_2^*(\tau_2)=P_R^*+m^2(\tau_R-\tau_2), \tag{2.26}$$

$$u_2(\tau_2)=\sigma_{i+1/2}+m\tau_2, \tag{2.27}$$

with

$$\sigma_{i+1/2}=\frac{[\rho u]_i^{i+1}}{[\rho]_i^{i+1}}=\bar{u}+\bar{\rho}\frac{[u]_i^{i+1}}{[\rho]_i^{i+1}}. \tag{2.28}$$

Using relations (2.27) (2.26), and third relation of (2.24), we have to solve a nonlinear scalar equation of unknown τ_2 :

$$\gamma(P_2^*(\tau_2)+P_R^*)(\tau_R-\tau_2)+(\tau_R+\tau_2)(P_R^*-P_2^*(\tau_2))+2(\gamma-\frac{5}{3})[K\tau]_2^R=0. \tag{2.29}$$

From a pratical point of view, the nonlinear equation (2.29) is solved using the dichotomy method, thus $\rho_2=\frac{1}{\tau_2}$ is known.

Using (2.27) (respectively (2.26)), we get the intermediate speed u_2 (the intermediate pressure P_2^*). The calculation of the intermediate state '2' guarantees that :

$$[\rho]_2^R [P^*]_2^R > 0 \text{ and } [u]_2^R < 0. \tag{2.30}$$

• **Step 2 (double contact wave) :** Knowing that the Riemann invariants associated with the contact wave are (u, P^*), we set :

$$u_1 = u_2 \text{ and } P_1^* = P_2^*. \tag{2.31}$$

• **Step 3 (Linearized 1- wave) :** u_1 and P_1^* are now known, thus using (2.23) we obtain :

$$\rho_1 = \rho_L + \frac{[P^*]_L^1}{2\tilde{\bar{c}}_{L,R}^2} - \bar{\rho}\frac{[u]_L^1}{2\tilde{\bar{c}}_{L,R}}. \tag{2.32}$$

The modified interface solver is now fully defined.The intermediate states are defined as follows :

$$W_k^{MARS} = (\rho_k, u_k, P_k^*, \xi_k),\ k = 1,2. \tag{2.33}$$

and then the numerical flux $F_{i_0+1/2}^{MARS}$ is defined through (2.36), (2.37) and (2.39). ■

Now we can move on to the presentation of the finite volume scheme that is based on these two Riemann solvers.

Remark 12 Even if M_0= 0, the 'MARS' solver is not strictly the VFRoe-ncv solver Buffard, Thierry Gallouët et Jean-Marc Hérard 2000; Sergey Gavrilyuk, Jean-Marc Hérard, Olivier Hurisse et al. 2022. ■

2.3. Global solver and numerical scheme

In this section, we present a finite volume scheme Eymard, Thierry Gallouët et Herbin 2000, for the numerical resolution of the following system of equations :

$$\begin{cases} \partial_t(\rho) + \partial_x(\rho u) = 0 \\ \partial_t(\rho u) + \partial_x\left(\rho u^2 + P + \dfrac{2K}{3}\right) = 0 \\ \partial_t(\rho E) + \partial_x\left(u\left(\rho E + P + \dfrac{2K}{3}\right)\right) = 0 \\ \partial_t(\rho\xi) + \partial_x(\rho u\xi) + M_0\delta_{(x-\sigma t=0)} = 0 \end{cases} \tag{2.34}$$

where $M_0 = 0$, or M_0 given by section (1.2).

The numerical scheme reads :

$$\Delta x_i (Z_i^{n+1} - Z_i^n) + \Delta t (\mathscr{F}^n_{i+\frac{1}{2}} - \mathscr{F}^n_{i-\frac{1}{2}}) + \Delta t B_i^n = 0, \tag{2.35}$$

with $Z = (\rho, \rho u, \rho E, \rho \xi)$, $B_i = (0, 0, 0, M_i)$, and :

$$\mathscr{F}^n_{i+\frac{1}{2}} = \begin{cases} \mathscr{F}^{lnd}_{i+\frac{1}{2}} = F(Z(W^*_{lnd}(W_i^n, W_{i+1}^n)) \text{ when no shock wave has been detected,} \\ \mathscr{F}^{MARS}_{i+\frac{1}{2}} = F(Z(W^*_{MARS}(W_i^n, W_{i+1}^n)) \text{ if a shock wave has been detected,} \end{cases} \tag{2.36}$$

where :

$$F(Z) = (\rho u, \rho u^2 + P^*, u(\rho E + P^*), \rho u \xi). \tag{2.37}$$

The solution $W^*_{lnd}(W_L, W_R)$ of the approximate Riemann problem, is found with the linearized solver VFRoe-ncv (see Buffard, Thierry Gallouët et Jean-Marc Hérard 2000; Sergey Gavrilyuk, Jean-Marc Hérard, Olivier Hurisse et al. 2022). When no shock wave is detected on the interface, the solution of the Riemann problem is given by :

$$W^*_{lnd}(W_L, W_R) = \begin{cases} W_L \text{ if } \bar{\lambda}_1 \geq 0; \\ W_1^{lnd} \text{ if } \bar{\lambda}_1 < 0 \text{ and } \bar{\lambda}_{2,3} \geq 0; \\ W_2^{lnd} \text{ if } \bar{\lambda}_{2,3} < 0 \text{ and } \bar{\lambda}_3 \geq 0; \\ W_R \text{ if } \bar{\lambda}_4 < 0; \end{cases} \tag{2.38}$$

For more details about the solution W^*_{lnd}, the reader is referred to **Appendix** B.

The solution $W^*_{MARS}(W_L, W_R)$ of the approximate Riemann problem, is found with the modified interface solver 'MARS'. If a shock wave has been detected on the interface, the solution of the Riemann problem is given thus by :

$$W^*_{MARS}(W_L, W_R) = \begin{cases} W_L \text{ if } \lambda_1 \geq 0; \\ W_1^{MARS} \text{ if } \lambda_1 < 0 \text{ and } \lambda_{2,3} \geq 0; \\ W_2^{MARS} \text{ if } \lambda_{2,3} < 0 \text{ and } \lambda_3 \geq 0; \\ W_R \text{ if } \lambda_4 < 0; \end{cases} \tag{2.39}$$

where W_1^{MARS}, W_2^{MARS} are the 2 intermediate states, calculated in the section 2.2.

M_i^n is a contribution in cell i to the global jump of turbulent entropy M_0. It appears

when a shock wave has been detected locally. In order to guarantee that $\sum_{i=1}^{N} M_i^n = M_0$ (recall that N is the total number of cells in the domain and M_0 is the global jump of turbulent entropy to be imposed on shock wave), the calculation of M_i is done as follows :

• We set $M_i^n = 0$, $\forall$ i $\in$ N, at each time step time n .

— Loop 1 : if a shock is detected at interface i+1/2 :

$$\begin{aligned} &1.\ \chi_{i+\frac{1}{2}}^n = |\rho_{i+1}^n - \rho_i^n|, \\ &2.\ Sum^n = \sum_{i=1}^{N} \chi_{i+\frac{1}{2}}^n. \end{aligned} \tag{2.40}$$

— Loop 2 : if a shock is detected at interface i+1/2 :

$$1.\ \tilde{\chi}_{i+\frac{1}{2}}^n = \frac{\chi_{i+\frac{1}{2}}^n}{Sum^n}, \tag{2.41}$$

$$2.\ \begin{cases} \text{si } \sigma_{i+1/2} < 0 \rightarrow M_i^n = M_i^n + \tilde{\chi}_{i+1/2}^n * M_0 \\ \text{si } \sigma_{i+1/2} > 0 \rightarrow M_{i+1}^n = M_{i+1}^n + \tilde{\chi}_{i+1/2}^n * M_0 \end{cases}$$

Moreover, Δt^n and Δx_i are linked by the Courant-Friedrichs-Levy (CFL) following condition :

$$\frac{\Delta t^n}{\Delta x_i} max(|\lambda_j|_{j=1,2,3,4}) < 1,$$

in scheme (2.35).

3. Numerical Results

We present now some numerical results obtained for the model and scheme detailed in the previous sections. We focus here on test cases involving shock waves. The test cases provide a comparison between the exact solution and the approximate solution and make it possible to obtain a numerical convergence curve, which gives the error in L1 norm. The profiles of the approximate solutions are presented at a given final time for the density ρ, velocity u, pressure P, modified pressure P^*, and the turbulent entropy ξ.

All the computations are performed for a given value of $CFL = 0.5$. Moreover, in all the tests below, we have considered the perfect gas EOS :

$$P = (\gamma - 1)\rho e,$$

where the constant γ is equal to $\frac{7}{5}$. The computational domain is $[0,1]$ and the initial discontinuity separating states W_L and W_R is located at x= 0.5. The domain $[0,1]$ is

discretized using uniform cells, $\Delta x_i = \Delta x$, and the number of cells varies from 200 up to 2×10^5 cells.

3.1. Test 1 : Double shock wave (ξ= ξ_0)

The first test case is a double non-symmetrical shock with a mass $M_0 = 0$. This case is used to test the modified interface solver, on the basis of the pure conservative system (turbulence entropy is constant), and to compare the results with classical solver Sergey GAVRILYUK, Jean-Marc HÉRARD, Olivier HURISSE et al. 2022.

This case test is taken from Sergey GAVRILYUK, Jean-Marc HÉRARD, Olivier HURISSE et al. 2022. The initial conditions of the Riemann problem to be solved are given below :

$$(\rho_L, u_L, P_L, \xi_L) = (1, 650, 10^6, 10^4)$$

$$(\rho_R, u_R, P_R, \xi_R) = (1, -687.545913, 98007.273140, 10^4)$$

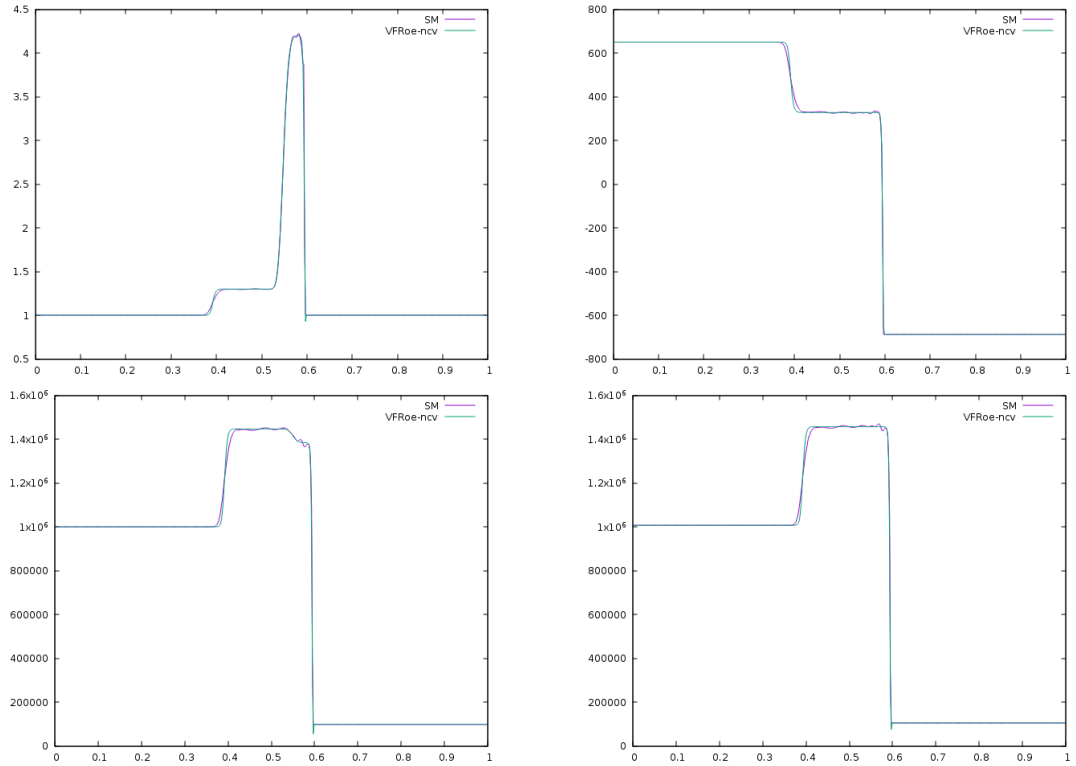

FIGURE 2.6. – Double-shock wave test case. Density (top left), velocity (top right), pressure (bottom left) and P^* (bottom right). Comparison between the modified interface solver (green) and the VFRoe-ncv solution (purple) at $t = 144 \times 10^{-3}$ s, $CFL = 0.5$, 500 cells.

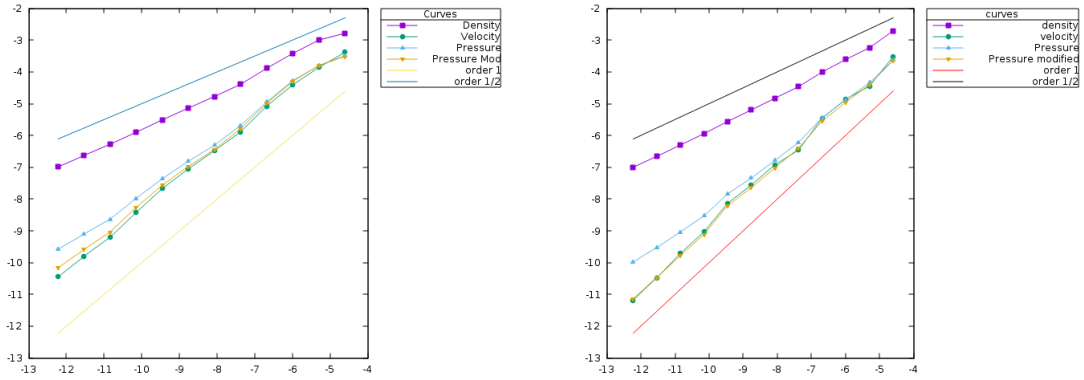

FIGURE 2.7. – Double-shock wave test case. Convergence curves, with modified interafce solver (left), VFRoe-ncv (right) : logarithm of the relative L1-error versus the logarithm of the mesh size with uniform meshes containing from 200 to 200000 cells. The error is plotted for variables, ρ, u, P and P^*.

Figure 2.6 shows qualitative comparisons between the approximate solutions calculated with the modified interface solver 'MARS' and the linearized solver VFRoe-ncv for a mesh containing 500 cells. Figure 2.7 shows the convergence curves, with the two solvers ('MARS' and VFRoe-ncv), for the set of variables $\{\rho$, u, P, $P^*\}$, and for $\xi_L = \xi_R = 10^4$, M_0=0.

First of all, the behavior of 'MARS' near the 3-shock wave around $x = 0.6$ is steep but oscillating (see figure 2.6). The error curve for VFRoe-ncv and 'MARS' on P and ρ is comparable but a little better for VFRoe-ncv on u and P^*. The error (for 'MARS') varies as $\approx h^1$ for variables u and P^* on fine meshes, and as $h^{1/2}$ for ρ and P (owing to the occurrence of the contact discontinuity), see figure 2.7. This result of the convergence was expected.

3.2. Test 2 : Simple 4-shock wave

We consider now a single 4-shock wave. We assume that $M_0 \neq 0$ is given by the user. The exact solution is shown in figure 2.8.

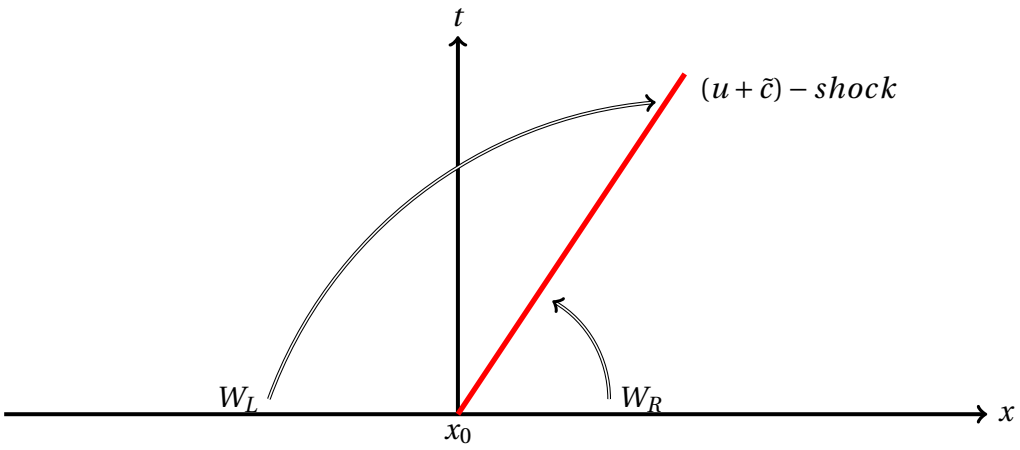

FIGURE 2.8. – The exact solution of the Riemann problem for the test 2.

We propose here to examine the approximate solution of a Riemann problem, with two different pressure ratios $\frac{P_L}{P_R}$, and with a strictly negative value for M_0 motivated from a physical point of view (turbulent entropy decreases through the shock). The initial condition of the Riemann problem is given by :

Case 1 :

$$\sigma = 580, \text{ and } M_0 = -50000,$$

$$(\rho_L, u_L, P_L, \xi_L) = (1.936, 280.451, 261265.856, 1000)$$

$$(\rho_R, u_R, P_R, \xi_R) = (1, 650, 10^5, 913.793)$$

Case 2 :

$$\sigma = 580, \text{ and } M_0 = -50000,$$

$$(\rho_L, u_L, P_L, \xi_L) = (4.487, 461.047, 268669.876, 1000)$$

$$(\rho_R, u_R, P_R, \xi_R) = (1, 650, 10^4, 913.793)$$

where W_R, σ, M_0 are given, and W_L calculated with (2.24).

The pressure ratio in test case 2 is close to 26.8 while the ratio in test case 1 is close to 2.6.

In the following we will perform these two test cases, with the standard scheme presented in 2.3, and with a modified scheme.

3.2.1. Standard scheme

In this part, we will illustrate the numerical results of test 2 (case 1, case 2) using the standard scheme 2.3.

Figure 2.9 (respectively 2.12) shows the behavior of the density ρ, velocity u, modified pressure P^* and turbulent entropy ξ for case 1 (respectively case 2) at a given time $T_f = 3\times10^{-3}$, on different meshes with 100 cells, 1000 cells and 10000 cells. Figure 2.10 (respectively 2.13) shows the convergence curve for the case 1 (respectively case 2), for the set of variables $\{\rho$, u, P, P^*,$\xi\}$. The behavior of the shock detector is shown in figure 2.11 (respectively 2.14) for case 1 (respectively case 2) on a mesh with 200000 cells.

The profiles of density ρ, velocity u, modified pressure P^*, in case 1 (rescp case 2), represented in figure 2.9 (respc figure 2.12), show a good behavior of the variable (ρ, u, P^*) through the 4-shock wave. The profiles of these 3 variables are disturbed and slightly oscillating on a coarse mesh, but by increasing the number of mesh cells, these oscillations tend to disappear. The profiles of (ρ, u, P^*) on a fine mesh take the form of the exact solution (figure 2.8) with $x_0 = 0.674$ and $T_f = 3\times10^{-3}$.

On the other hand, with regard to the profile of the turbulent entropy ξ, the latter converges towards the profile of the exact solution in case 2 and it does not converge in case 1.

The convergence curve ensures the above results (see figure 10 for case 1, and figure 13 for case 2). Figures 2.11, 2.14, show that the behavior of the shock detector in case 2 is better than that of case 1.

Remark 13 The parameter $coef_{i+\frac{1}{2}}$ taken in the standard scheme is a choice and not mandatory. We illustrate test 3.2 with another parameter :

$$coef^n_{i+\frac{1}{2}} = |P^{*n}_{i+1} - P^{*n}_i|. \tag{2.42}$$

The reader is referred to **Appendix** C for more details. ■

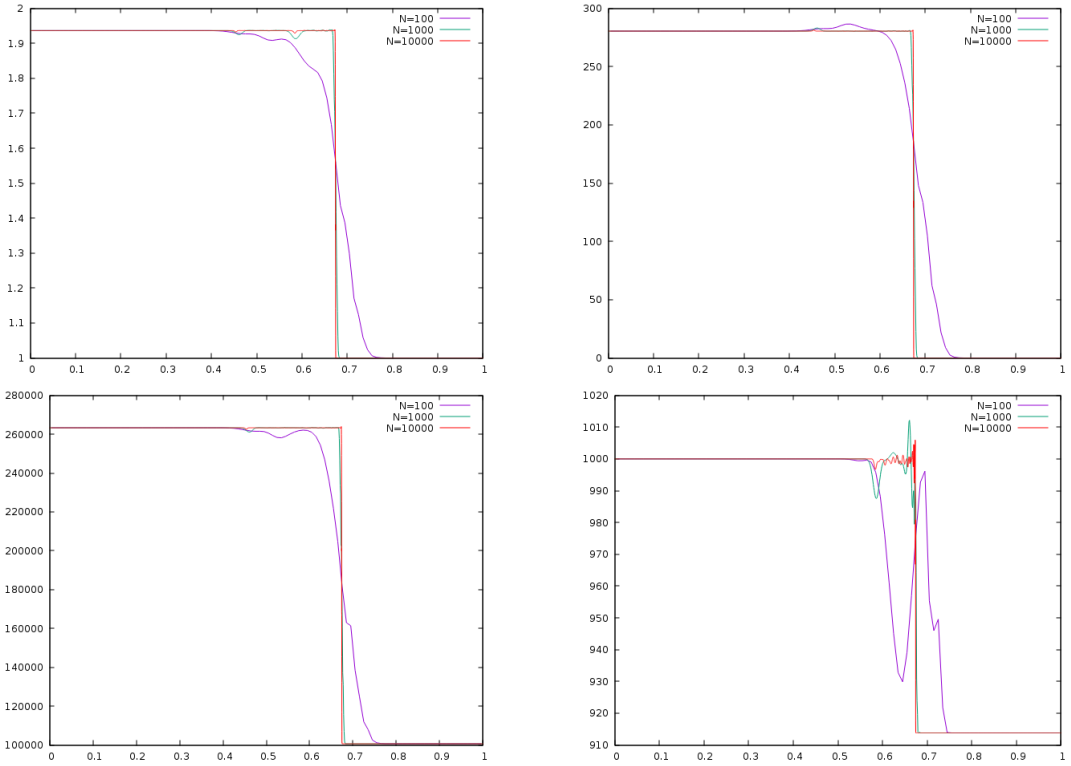

FIGURE 2.9. – Simple 4-shock wave test case 1, with **standard** scheme. Density (top left), velocity (top right), P^* (bottom left) and ξ (bottom right). Profile of the approximate solution for different meshes =100, 1000, 10000 cells at $t = 3 \times 10^{-3}$ s, $CFL = 0.5$.

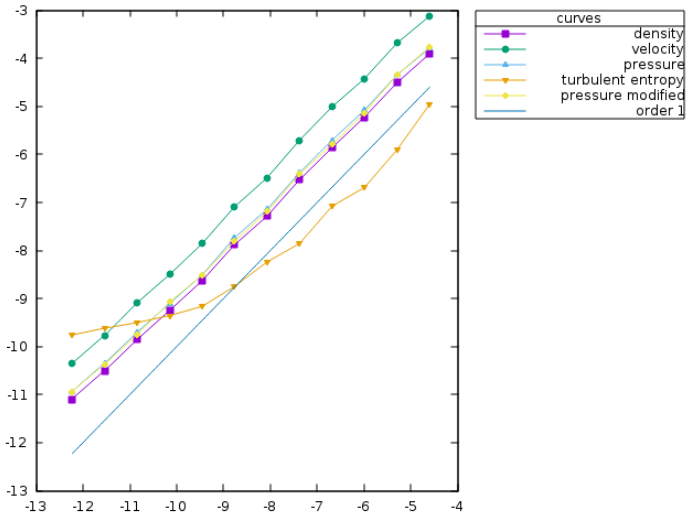

FIGURE 2.10. – Simple 4-shock wave test case 1, with **standard** scheme. Convergence curves : logarithm of the relative L1-error versus the logarithm of the mesh size with uniform meshes containing from 200 to 200000 cells. The error is plotted for variables, ρ, u, P, P^* and ξ.

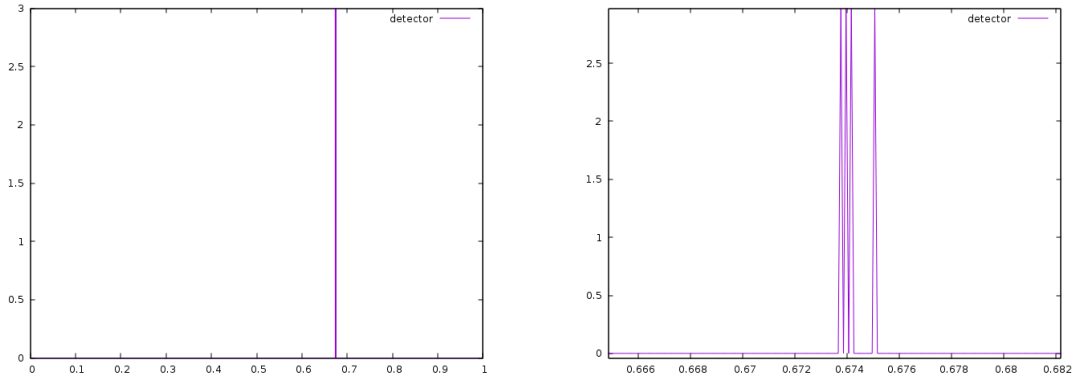

FIGURE 2.11. – Simple 4-shock wave test case 1, with **standard** scheme. Shock detector behavior on all interfaces (left), behavior of the shock detector around the detected shock (right) : it indicates 0 if it does not detect a shock, and 3 if it detects

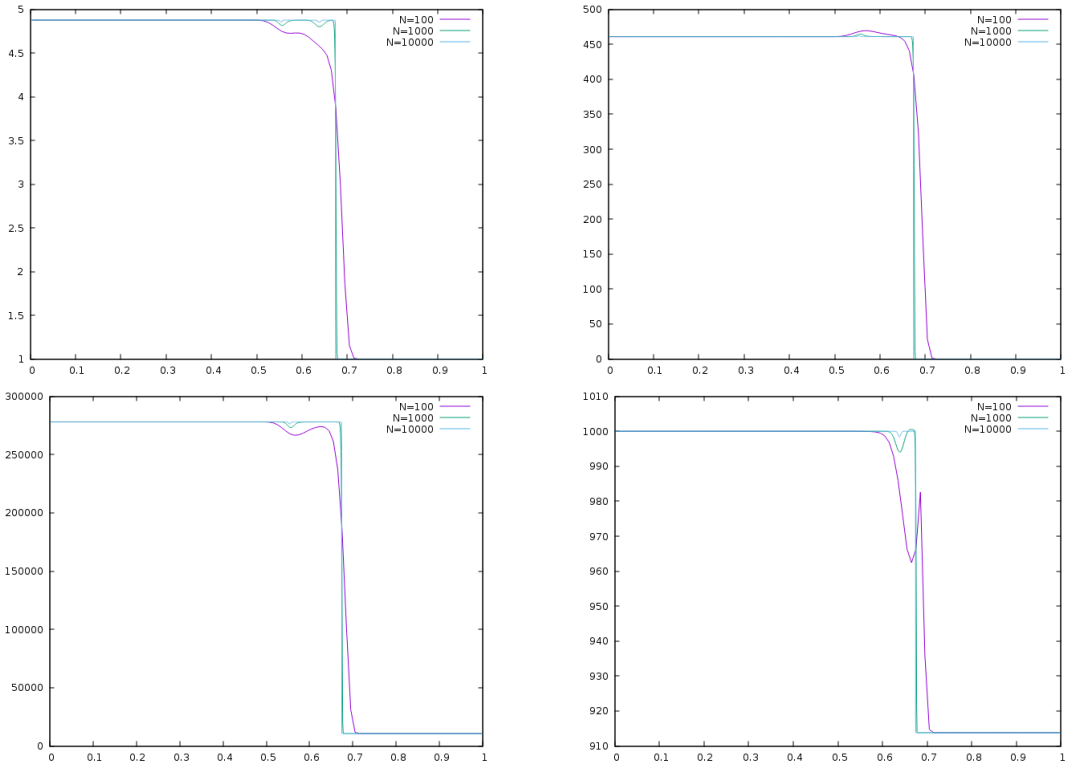

FIGURE 2.12. – Simple 4-shock wave test case 2, with **standard** scheme. Density (top left), velocity (top right), P^* (bottom left) and ξ (bottom right). Profile of the approximate solution for different meshes =100, 1000, 10000 cells at $t = 3 \times 10^{-3}$ s, $CFL = 0.5$.

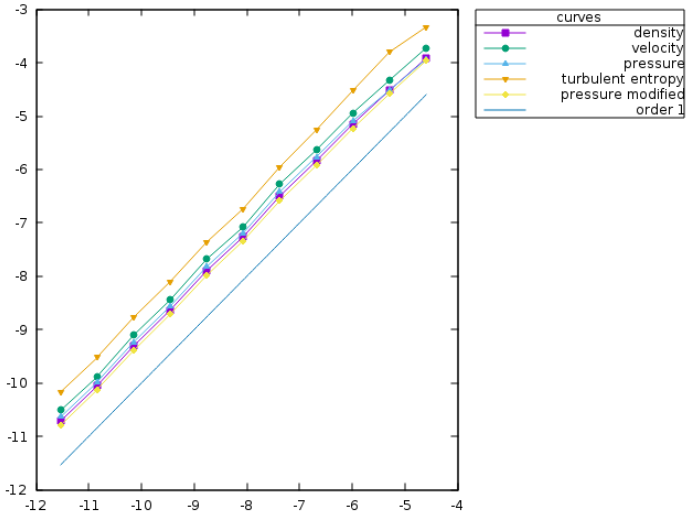

FIGURE 2.13. – Simple 4-shock wave test case 2, with **standard** scheme. Convergence curves : logarithm of the relative L1-error versus the logarithm of the mesh size with uniform meshes containing from 200 to 200000 cells. The error is plotted for variables, ρ, u, P, P^* and ξ.

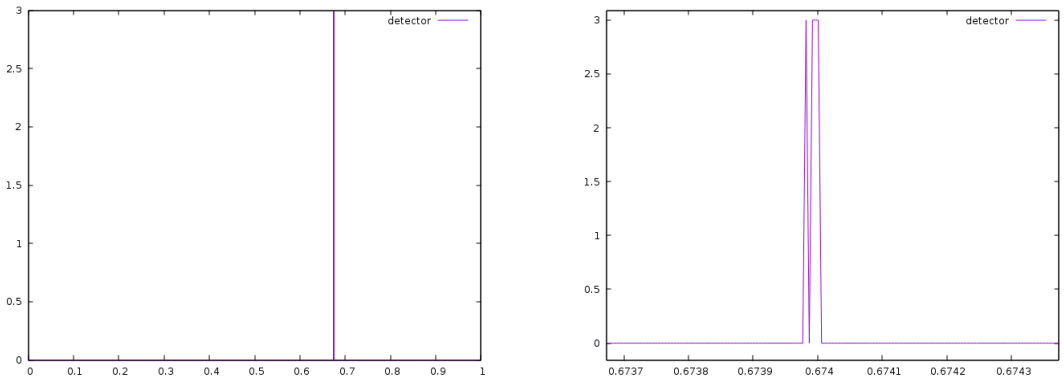

FIGURE 2.14. – Simple 4-shock wave test case 2, with **standard** scheme.Shock detector behavior on all interfaces (left), behavior of the shock detector around the detected shock (right) : it indicates 0 if it does not detect a shock, and 3 if it detects

3.2.2. Modified scheme

In this part, we assume that the shock is unique. We choose a single shock interface, looking for the greatest value of the jump of u :

$$\max_{i=1}^{N}|u_{i+1}-u_i| = |u_{i_0+1}-u_{i_0}| \Longrightarrow \text{A single shock is assumed to be located at interface } i_0+\frac{1}{2}.$$

Consequently, we modify the numerical scheme presented in 2.3, by eliminating the 2 loops (2.40,2.41), and replace it by the following one :

$$\begin{cases} M_{i_0}^n = \frac{1}{2}M_0, \\ \\ M_{i_0+1}^n = \frac{1}{2}M_0. \end{cases}$$

In the following, we will simulate test 2 case 1 with the modified scheme. The behavior of the density ρ, velocity u, modified pressure P^* and turbulent entropy ξ, are shown in figure 2.15. The results provided by the two methods are almost similar for the three profiles (ρ, u, P^*). The remarkable difference between the two methods lies in the profile of the turbulent entropy, where we notice that the oscillations around the (u+$\tilde{c}$)-shock disappear on the fine meshes, whereas this is not the case with the standard scheme. The error varies as $\approx h^1$ for all variables (ρ, u, P^*, ξ), hence the convergence of all the variables with the modified scheme holds.

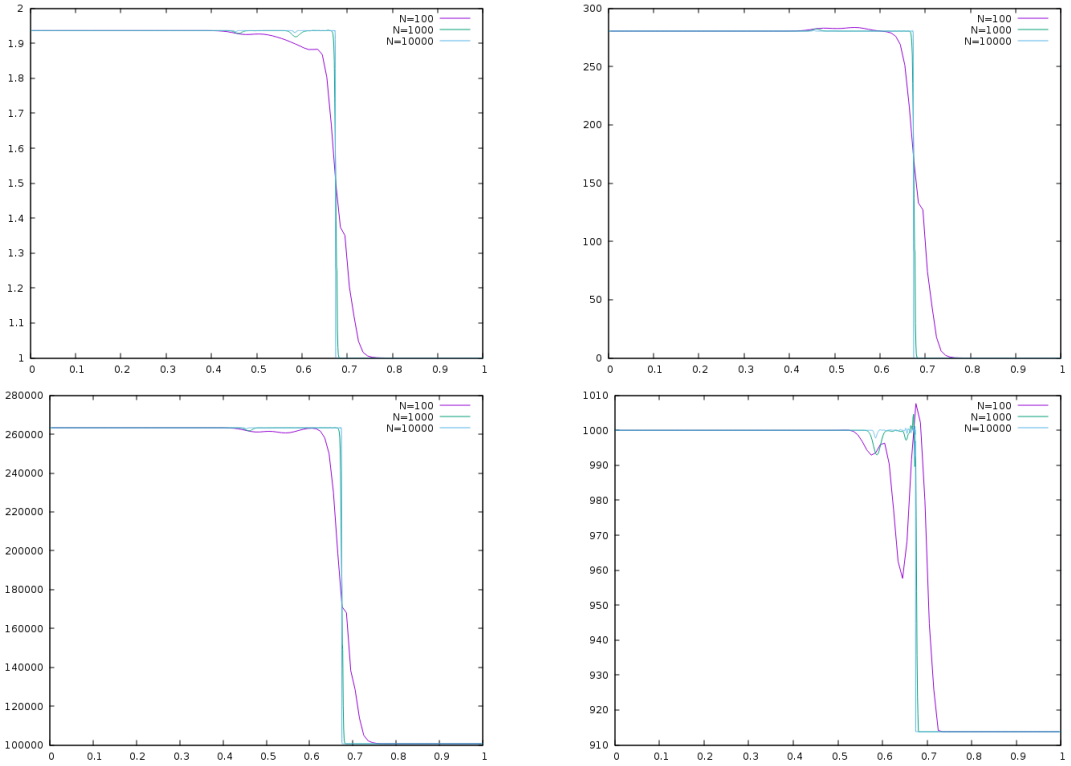

FIGURE 2.15. – Simple 4-shock wave test case 1, with **modified** scheme. Density (top left), velocity (top right), P^* (bottom left) and ξ (bottom right). Profile of the approximate solution for different meshes =100 cells, 1000 cells, 10000 cells at $t = 3 \times 10^{-3}$ s, $CFL = 0.5$.

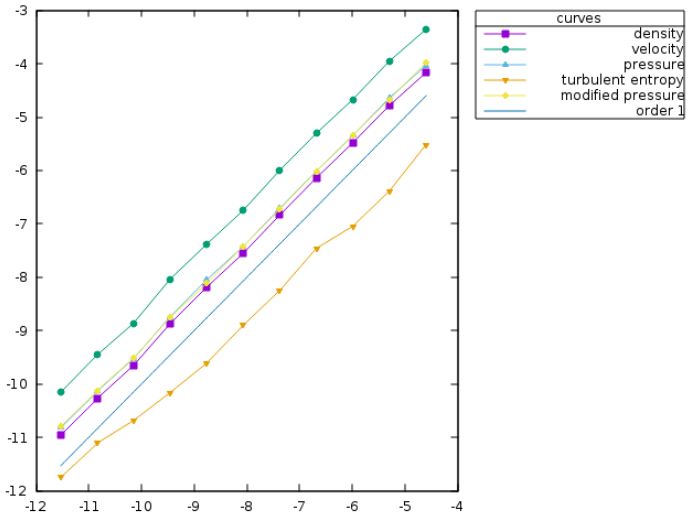

FIGURE 2.16. – Simple 4-shock wave test case 1, with modified scheme. Convergence curves : logarithm of the relative L1-error versus the logarithm of the mesh size with uniform meshes containing from 200 to 200000 cells. The error is plotted for variables, ρ, u, P, P^* and ξ.

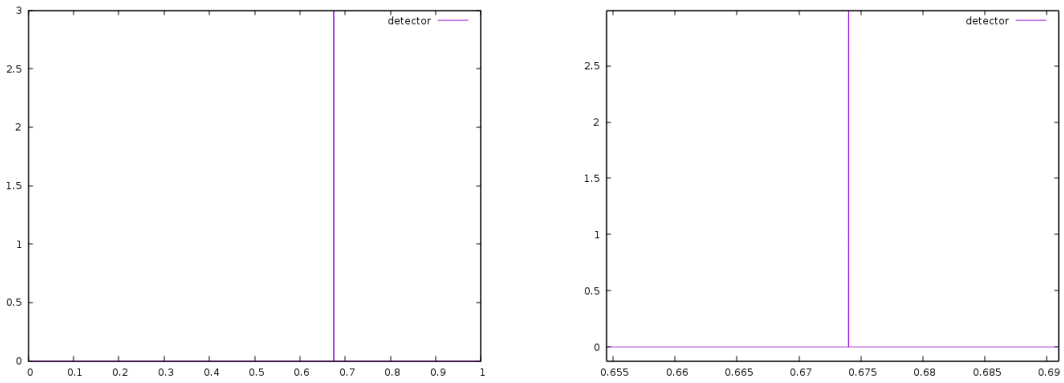

FIGURE 2.17. – Simple 4-shock wave test case 1, with **modified** scheme. Shock detector behavior on all interfaces (left), behavior of the shock detector around the detected shock (right) : it indicates 0 if it does not detect a shock, and 3 if it detects

4. Conclusion

This chapter was devoted to the analysis and numerical approximation of the turbulent compressible model introduced in Sergey GAVRILYUK et Richard SAUREL 2006. The latter model enables to take the jump of turbulent entropy across shock waves into account, and meanwhile provides some methodology in order to calculate the entropy jump. The analysis of the model comfirms it is meaningful.
A numerical technique has been proposed in order to obtain approximate solutions when a shock wave occurs in the fluid flow. This method requires a shock detector, which has been grounded on Lax conditions and the entropy inequality. Numerical results show that the present approach must be improved in order to get consistant and stable approximations in an industrial framework.

Acknowledgements The last author receives financial support by ANRT through an EDF/CIFRE grant number 2019/1580. Computational facilities were provided by EDF.

ANNEXES

A. Main properties of model 2.3 with $M(x,t)=0$

In this section, we detail the structure of system (2.3) (eigenvalues, eigenvectors, Riemann invariants) in a general framework with respect to the EOS.

A.1. Hyperbolicity

System (2.3) is written in the form :

$$\partial_t W + A(W)\partial_x W = 0, \tag{2.43}$$

where the primitive variable W reads :

$$W = (\rho, u, P^*, \xi)^t.$$

The jacobian matrix A(W) is :

$$A(W) = \begin{pmatrix} u & \rho & 0 & 0 \\ 0 & u & \tau & 0 \\ 0 & \rho\tilde{c}^2 & u & 0 \\ 0 & 0 & 0 & u \end{pmatrix},$$

where $\tau = 1/\rho$ denotes the specific volume and $\tilde{c}^2 = c^2(P,\rho) + \frac{10}{9}\xi\rho^{2/3}$.

System (3.23) is hyperbolic, it admits four real eigenvalues :

$$\lambda_1(W) = u - \tilde{c}, \quad \lambda_{2,3}(W) = u, \quad \lambda_4(W) = u + \tilde{c}, \tag{2.44}$$

and the associated eigenvectors r_k(W) span the whole space $\mathbb{R}^4$ provided that $\tilde{c} \neq 0$:

$$r_1(W) = \left(\rho, -\tilde{c}, \rho\tilde{c}^2, 0\right)^t, \quad r_2(W) = (1,0,0,0)^t,$$

$$r_3(W) = (0,0,0,1)^t, \quad r_4(W) = \left(\rho, \tilde{c}, \rho\tilde{c}^2, 0\right)^t.$$

Fields associated with $\lambda_1(W)$ *and* $\lambda_4(W)$ are genuinely non linear (GNL), and field associated with $\lambda_{2,3}(W)$ is linearly degenerate (LD).

A.2. Riemann invariants

The two Riemann invariants associated with the LD field ($\lambda_{2,3} = u$) are the following whatever the **EOS** is :

$$I_1^2(W) = u \quad , \quad I_2^2(W) = P^*(P,\rho,\xi).$$

The Riemann invariants associated with the two GNL waves read :

$$1-rarefaction\ wave: \ I_1^1(W) = s(P,\rho) \ , \ I_2^1(W) = u + \int_0^\rho \frac{\tilde{c}(I_1^1(W),\rho\prime,I_3^1(W))}{\rho\prime}\,\mathrm{d}\rho\prime,$$

$$1-rarefaction\ wave: \ I_3^1(W) = \xi.$$

$$4-rarefaction\ wave: \ I_1^4(W) = s(P,\rho) \ , \ I_2^4(W) = u - \int_0^\rho \frac{\tilde{c}(I_1^4(W),\rho\prime,I_3^4(W))}{\rho\prime}\,\mathrm{d}\rho\prime,$$

$$4-rarefaction\ wave: \ I_3^4(W) = \xi.$$

B. The intermediate states for VFRoe-ncv

The VFRoe-ncv scheme is based on the computation of the exact solution of a linearized version of the Riemann problem at the interface between two cells. It thus relies on finding the two intermediate states Z_1 and Z_2 : the state Z_1 (resp. Z_2) lies between the linearized waves $\bar{\lambda}_1$ and $\bar{\lambda}_{2,3}$ (resp. $\bar{\lambda}_{2,3}$ and $\bar{\lambda}_4$). We have :

$$Z_1 = Z_L + \alpha_1 \widehat{r_1}, \tag{2.45}$$

$$Z_2 = Z_1 + \alpha_2 \widehat{r_2} + \alpha_3 \widehat{r_3}, \tag{2.46}$$

$$Z_R = Z_2 + \alpha_4 \widehat{r_4}, \tag{2.47}$$

where the linearized right eigenvectors are :

$$\widehat{r_1} = (1, -\widehat{\tilde{c}}\tau, \widehat{\tilde{c}}^2, 0)^t, \quad \widehat{r_2} = (1,0,0,0)^t, \quad \widehat{r_3} = (0,0,0,1)^t, \quad \widehat{r_4} = (1, \widehat{\tilde{c}}\tau, \widehat{\tilde{c}}^2, 0)^t,$$

and where the coefficients α_1 and α_4 associated with the eigenvalues $\bar{\lambda}_1$ and $\bar{\lambda}_4$ read :

$$\alpha_1 = \frac{1}{2}\frac{[P^*]_L^R}{\widehat{\tilde{c}}^2} - \frac{1}{2}\frac{[u]_L^R \widehat{\rho}}{\widehat{\tilde{c}}},$$

$$\alpha_4 = \frac{1}{2}\frac{[P^*]_L^R}{\widehat{\bar{c}}^2} + \frac{1}{2}\frac{[u]_L^R\widehat{\rho}}{\widehat{\bar{c}}}.$$

It should be noted that thanks to (2.46), we have :

$$u_1 = u_2, \quad \text{and} \quad P_1^* = P_2^*.$$

After simple calculus on equations (2.45) and (2.47), the following intermediate values can be found :

$$u_1 = u_2 = \bar{u} - \frac{1}{2\bar{\rho}\widehat{\bar{c}}}[P^*]_L^R,$$

$$P_1^* = P_2^* = \bar{P^*} - \frac{\bar{\rho}\widehat{\bar{c}}}{2}[u]_L^R,$$

$$\rho_1 = \rho_L + \frac{[P^*]_L^R}{2\widehat{\bar{c}}^2} - \frac{\bar{\rho}}{2\widehat{\bar{c}}}[u]_L^R, \qquad \rho_2 = \rho_R - \frac{[P^*]_L^R}{2\widehat{\bar{c}}^2} - \frac{\bar{\rho}}{2\widehat{\bar{c}}}[u]_L^R,$$

$$\xi_1 = \xi_L, \quad \xi_2 = \xi_R.$$

Finally, the intermediate states are defined as follows :

$$W_k^{lnd} = (\rho_k, u_k, P_k^*, \xi_k), \ k = 1,2. \tag{2.48}$$

C. Additional numerical results : a simple 3-shock wave with different coefficients

The profiles of the approximate solutions along the x-domain are given in figure 2.18 (respectively 2.21) for case 1 (respectively case 2), for several meshes with 100, 1000 and 10000 cells. Figure 2.19 (respectively 2.22) represents the error curve for case 1 (respectively case 2), and the shock detector behavior is shown in figure 2.20 (respectively 2.23) for case 1 (respectively case 1).

Finally, by comparing these results (with $coef_{i+\frac{1}{2}}^n = |P_{i+1}^{*n} - P_i^{*n}|$) with the results of part 3.2.1 (with $coef_{i+\frac{1}{2}}^n = |\rho_{i+1}^n - \rho_i^n|$), we find that the solution is roughly almost the same.

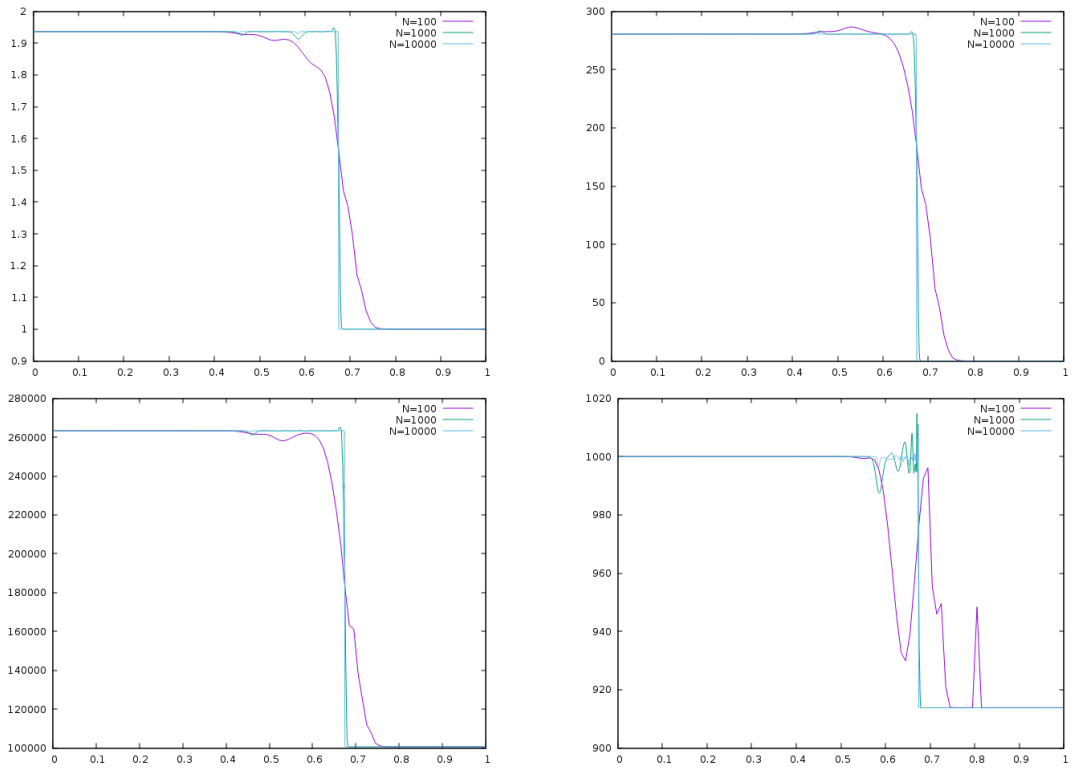

FIGURE 2.18. – Simple 3-shock wave test case 1, with standard scheme and $coef_{i+1/2} = |P^*_{i+1} - P^*_i|$. Density (top left), velocity (top right), P^* (bottom left) and ξ (bottom right). Profile of the approximate solution for different meshes =100, 1000, 10000 cells at $t = 3 \times 10^{-3}$ s, $CFL = 0.5$.

D. A tentative PDE formulation of model Sergey GAVRILYUK et Richard SAUREL 2006

Model Sergey GAVRILYUK et Richard SAUREL 2006 provides the contents of M_0 (see section 1.2). System of equations (3) presented in section 1, can be rewritten as follows :

$$\begin{cases} \partial_t \phi + \sigma \partial_x \phi = 0 \\ \partial_t(\rho) + \partial_x(\rho u) = 0 \\ \partial_t(\rho u) + \partial_x\left(\rho u^2 + P + \dfrac{2K}{3}\right) = 0 \\ \partial_t(\rho E) + \partial_x\left(u\left(\rho E + P + \dfrac{2K}{3}\right)\right) = 0 \\ \partial_t(\rho \xi) + \partial_x(\rho u \xi) + M_0 \partial_x \phi = 0 \end{cases} \tag{2.49}$$

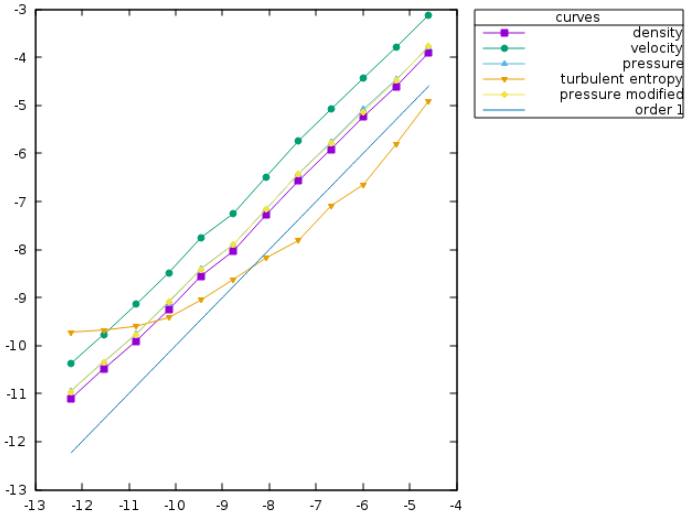

FIGURE 2.19. – Simple 3-shock wave test case 1, with standard scheme and $coef_{i+1/2} = |P^*_{i+1} - P^*_i|$. Convergence curves : logarithm of the relative L1-error versus the logarithm of the mesh size with uniform meshes containing from 200 to 200000 cells. The error is plotted for variables, ρ, u, P, P^* and ξ.

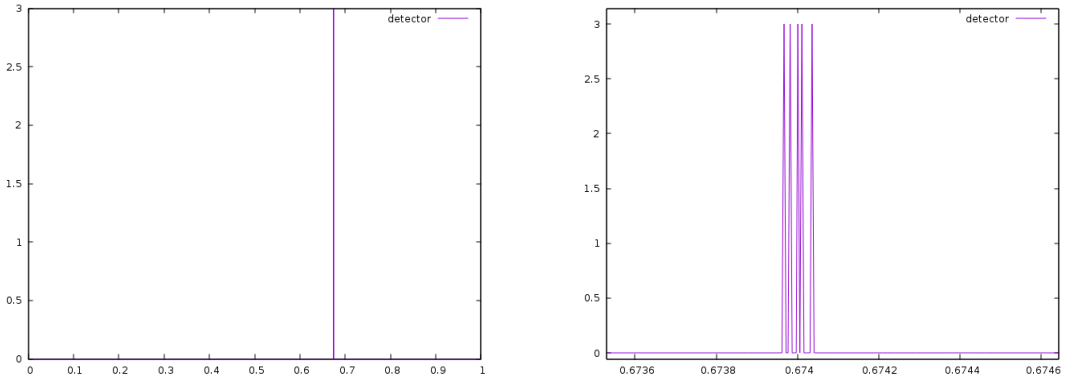

FIGURE 2.20. – Simple 3-shock wave test case 1, with standard scheme and $coef_{i+1/2} = |P^*_{i+1} - P^*_i|$. Shock detector behavior on all interfaces (left), behavior of the shock detector around the detected shock (right) : it indicates 0 if it does not detect a shock, and 3 if it detects

by noting the mean total energy E :

$$E = e + \frac{1}{2}u^2 + \frac{K}{\rho}.$$

We define the modified pressure P^* :

$$P^* = P + \frac{2}{3}K,$$

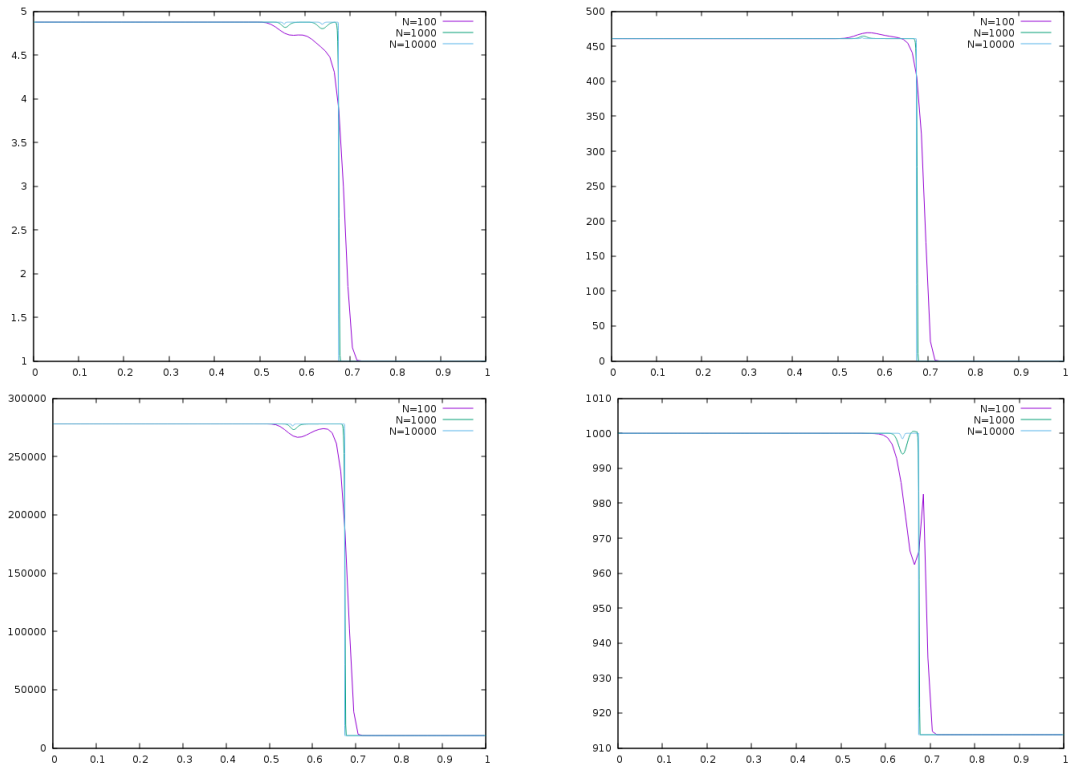

FIGURE 2.21. – Simple 3-shock wave test case 2, with standard scheme and $coef_{i+1/2} = |P^*_{i+1} - P^*_i|$. Density (top left), velocity (top right), P^* (bottom left) and ξ (bottom right). Profile of the approximate solution for different meshes =100, 1000, 10000 cells at $t = 3 \times 10^{-3}$ s, $CFL = 0.5$.

where $K = \xi\rho^{5/3} \Longleftrightarrow \xi = K\rho^{-5/3}$.

The variable ϕ denotes a colour function (see GREENBERG et LEROUX 1996; GOSSE 2001; GOATIN et LEFLOCH 2004; AMBROSO, CHALONS, Frédéric COQUEL et al. 2009 such that :

$$\phi(x,0) = \begin{cases} 0 \text{ if } x < 0 \\ 1 \text{ if } x > 0 \end{cases}$$

and σ is the shock speed. M_0 is given non zero.

System (2.49) is rewritten as follows :

$$\partial_t Y + C(Y)\partial_x Y = 0, \tag{2.50}$$

with Y the primitive variable :

$$Y = (\phi, \rho, u, P^*, \xi),$$

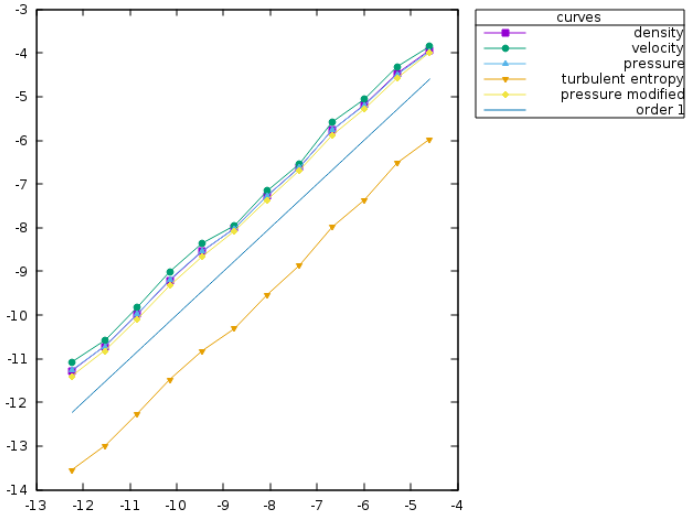

FIGURE 2.22. – Simple 3-shock wave test case 2, with **standard** scheme and $coef_{i+1/2} = |P^*_{i+1} - P^*_i|$. Convergence curves : logarithm of the relative L1-error versus the logarithm of the mesh size with uniform meshes containing from 200 to 200000 cells. The error is plotted for variables, ρ, u, P, P^* and ξ.

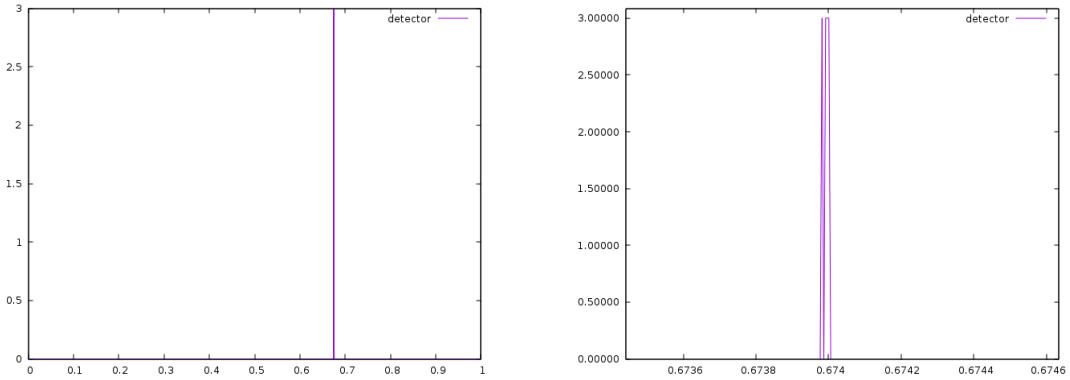

FIGURE 2.23. – Simple 3-shock wave test case 2, with **standard** scheme and $coef_{i+1/2} = |P^*_{i+1} - P^*_i|$. Shock detector behavior on all interfaces (left), behavior of the shock detector around the detected shock (right) : it indicates 0 if it does not detect a shock, and 3 if it detects

$C(Y)$ is the jacobian matrix :

$$C(Y) = \begin{pmatrix} \sigma & 0 & 0 & 0 & 0 \\ 0 & u & \rho & 0 & 0 \\ 0 & 0 & u & \tau & 0 \\ A & 0 & \rho\tilde{c}^2 & u & 0 \\ B & 0 & 0 & 0 & u \end{pmatrix},$$

with :

$$\begin{cases} A = M_0 \rho^{-1/3} \left(\frac{2}{3}\rho - (\frac{\partial e}{\partial P}|_\rho)^{-1} \right), \\ B = \frac{M_0}{\rho}. \end{cases} \tag{2.51}$$

We assume that : $M_0 \neq 0$, and $\gamma \neq \frac{5}{3}$ (in case of a perfect gas EOS) which implies that :

$$\mathbf{A \neq 0 \text{ and } B \neq 0}.$$

System (2.50) admits five real eigenvalues :

$$\lambda_0(Y) = \sigma, \quad \lambda_1(Y) = u - \tilde{c}, \quad \lambda_{2,3}(Y) = u, \quad \lambda_4(Y) = u + \tilde{c}. \tag{2.52}$$

The associated eigenvectors $r_k(Y)$ are :

$$r_0(Y) = \left(\Delta(u-\sigma), -A, (u-\sigma)\frac{A}{\rho}, -A(u-\sigma)^2, -B\Delta \right)^t,$$

$$r_1(Y) = \left(0, \rho, -\tilde{c}, \rho\tilde{c}^2, 0\right)^t, \quad r_2(Y) = (0,1,0,0,0)^t,$$

$$r_3(Y) = (0,0,0,0,1)^t, \quad r_4(Y) = \left(0, \rho, \tilde{c}, \rho\tilde{c}^2, 0\right)^t,$$

with $\Delta = (u-\sigma)^2 - \tilde{c}^2$.

In the sequel, we assume that :

$$\sigma \neq u.$$

We must distinguish two cases which depend on the value of Δ :
(i) $\Delta \neq 0$: system (2.49) is hyperbolic (eigenvectors span $\mathbb{R}^5$) ;
(ii) $\Delta = 0$: the associated eigenvector $r_0(Y) \in Vect\{r_1, r_2, r_4\} \Longrightarrow$ system (2.49) is degenerate.

The second case (ii) above corresponds to system (2.3) in section 1.1.

E. Positivity of the total pressure of the mixture P^*

In this section, we are interested in studying the condition of the positivity of the total pressure of the mixture P^*. Let us first recall the system of Rankine-Hugoniot relations associated with model (3). We assume that the variable $(\rho, u, P, \xi)_R$ on the right side of the shock 'R', the shock speed σ and M_0 are given. The system of jump

conditions is written as follows :

$$\begin{cases} [\rho(u-\sigma)]_2^R = 0 \\ m^2[\tau]_2^R + [P^*]_2^R = 0 \\ [e+K\tau]_2^R + \bar{P}^*_{R,2}[\tau]_2^R = 0 \\ m[\xi]_2^R + M_0 = 0 \end{cases} \tag{2.53}$$

with $P^* = P + \frac{2}{3}K$, $\tau = \frac{1}{\rho}$, $K = \xi\rho^{5/3}$ and $m = \rho_R(u_R - \sigma)$. The variable $(\rho, u, P, \xi)_2$ on the left side of the shock noted '2' is the main unknown.

In the sequel, we will consider the following turbulent perfect gas EOS :

$$P = (\gamma - 1)\rho e.$$

The third equation of system (2.53) can be written in the following form :

$$\begin{cases} P_2^* = P_R^* g(z) \\ g(z) = \dfrac{h(z)}{(\beta - z)} \\ h(z) = \beta z - 1 + 2\dfrac{(\gamma - 5/3)}{(\gamma - 1)}(\dfrac{K_R}{P_R^*})(z - \dfrac{K_2}{K_R}) \\ z = \dfrac{\rho_2}{\rho_R} \end{cases} \tag{2.54}$$

To study the positivity of P^*, we will examine the variation of the function $h(z)$ in the interval $[1, \beta[$. The derivative of the function h(z) is :

$$h'(z) = \beta + 2\frac{(\gamma - 5/3)}{(\gamma - 1)}\frac{K_R}{P_R^*}.$$

We distinguish 2 cases which depend on the value of γ :

— for γ>5/3 : h'(z) is positive in the interval $[1,\beta[\Longrightarrow$ h(z) is increasing over $[1,\beta[$; then for h(z) to be positive ($P_2^* > 0$), it suffices that h(1)>0, which imposes a condition on the jump of $[K]_2^R$ such that :

$$P_R^* + (\gamma - 5/3)[K]_2^R > 0 \iff h(1) > 0 \tag{2.55}$$

— for $\gamma < 5/3$: we distinguish 2 sub-cases :

1. if $(\gamma + 1) + 2(\gamma - 5/3)\frac{K_R}{P_R^*} > 0$: h'(z) is positive in the interval $[1,\beta[\Longrightarrow$ h(z) is increasing in $[1,\beta[$; condition (2.55) appears to keep the positivity of $P*$.
2. if $(\gamma + 1) + 2(\gamma - 5/3)\frac{K_R}{P_R^*} < 0$: h'(z)<0 in $[1,\beta[\Longrightarrow$ h(z) is decreasing in $[1,\beta[$; then for h(z)>0 ($P_2^* > 0$), it suffices that h(β)>0, which imposes a condition

on the jump of $[K]_2^R$ such that :

$$\gamma P_R + \frac{5}{3}(\gamma-1)K_R + \frac{(\gamma-1)(\gamma-5/3)}{2}[K]_2^R > 0.$$

F. Study of the ratio $\frac{P_2^*}{P_R^*}$ in (u+$\tilde{c}$)-shock

First of all, let us define P_k :

$$P_k = \frac{2}{3}K,$$

so that the pressure P^* reads :

$$P = P + P_k.$$

The modified pressure P^* is then composed of a 'laminar' thermodynamical pressure P and a 'turbulent' contribution P_k. In the following, the ratio $\frac{P_2^*}{P_R^*}$ is studied for the model considering a turbulent perfect gas EOS :

$$P = (\gamma-1)\rho e.$$

We assume that the right state $(\rho, u, P, \xi)_R$ and σ are known, and that $P_{k,R} > 0$ and $P_R > 0$. The jump relations associated with (u+$\tilde{c}$)-shock are :

$$\begin{cases} [\rho(u-\sigma)]_2^R = 0 \\ m^2[\tau]_2^R + [P^*]_2^R = 0 \\ [e + K\tau]_2^R + \tilde{P}_{R,2}^*[\tau]_2^R = 0 \\ m[\xi]_2^R + M_0 = 0 \\ \frac{4}{3}\xi_2\tau_R^{-2/3}\alpha = P_R^* + P_2^*\beta + m^2\tau_R - m^2\tau_2\beta \end{cases} \tag{2.56}$$

with $m = \rho_R(u_R - \sigma)$, $\alpha = \frac{(\gamma-5/3)}{(\gamma-1)}$, $\beta = \frac{(\gamma+1)}{(\gamma-1)}$, σ is the speed of the shock and $P^* = P + \frac{2}{3}\xi\rho^{5/3}$ is the total pressure.

We set :

$$z_2 = \frac{\rho_2}{\rho_R}.$$

Across a (u+$\tilde{c}$)-shock wave we have necessarily $z_2 > 1$ and $z_2 < \frac{(\gamma+1)}{\gamma}$ (see section 1.2). Using the third and fifth equations of (2.56), we get the following formula for the pressure P_2^* with respect to z_2 and to the right state :

$$P_2^* = P_R^* h_2(z_2; \xi_R, P_R^*, \rho_R), \tag{2.57}$$

with :

$$h_2(z_2;\xi_R,P_R^*,\rho_R)=\frac{2\beta z_2^2-5z_2+4z_2^2\frac{K_R}{P_R^*}\alpha-3m^2\frac{\tau_R}{P_R^*}(z_2-\beta)}{5z_2(\beta-\frac{2}{5}z_2)} \tag{2.58}$$

We note that the jump relations (2.56) can only be defined if $h_2(z_2;\xi_R,P_R^*,\rho_R)>1$ (thanks to the second equation of relations of jump). For this, we examine below the conditions to keep $\left(h_2(z_2;\xi_R,P_R^*,\rho_R)-1\right)>0$ with respect to $z_2\in[1,\frac{(\gamma+1)}{\gamma}[$.

First of all :

$$h_2(z_2;\xi_R,P_R^*,\rho_R)-1=\frac{g_2(z_2;\xi_R,P_R^*,\rho_R)}{5z_2(\beta-\frac{2}{5}z_2)},$$

with :

$$g_2(z_2;\xi_R,P_R^*,\rho_R)=2z_2^2(\beta+2\frac{K_R}{P_R^*}\alpha+1)+z_2(-5-5\beta-3m^2\frac{\tau_R}{P_R^*})+3m^2\frac{\tau_R}{P_R^*}\beta. \tag{2.59}$$

Since $5z_2(\beta-\frac{2}{5}z_2)>0$ (because$z_2<\frac{(\gamma+1)}{\gamma}$) is positive. The positivity study of g_2 is equivalent to $(h_2(z_2;\xi_R,P_R^*,\rho_R)-1)>0$.

The first and second order derivatives of g_2 are :

$$g\prime_2(z_2)=4z_2(\beta+2\frac{K_R}{P_R^*}\alpha+1)-5-5\beta-3m^2\frac{\tau_R}{P_R^*}, \tag{2.60}$$

$$g\prime\prime_2(z_2)=4(\beta+2\frac{K_R}{P_R^*}\alpha+1). \tag{2.61}$$

We distinguish 2 cases for $g\prime\prime(z_2)$ depending on the sign of α (γ) :

1. if $\alpha>0$ ($\gamma>5/3$) : we have $g\prime\prime_2(z_2)$ positive for $z_2\in[1,\frac{(\gamma+1)}{\gamma}[$
2. if $\alpha<0$ ($\gamma<5/3$) : We distinguish 2 cases depending on ratio value $\frac{P_{K,R}}{P_R^*}$:
   (a) if $\frac{P_{K,R}}{P_R^*}<\frac{2\gamma}{3(5/3-\gamma)}$: we have $g\prime\prime_2(z_2)$ positive for $z_2\in[1,\frac{(\gamma+1)}{\gamma}[$
   (b) if $\frac{P_{K,R}}{P_R^*}>\frac{2\gamma}{3(5/3-\gamma)}$: we have $g\prime\prime_2(z_2)$ negative for $z_2\in[1,\frac{(\gamma+1)}{\gamma}[$

The case $\gamma>5/3$ is not relevant (see section 1.2), we are interested in the case $\gamma<5/3$ in the following.

For $\gamma<5/3$: we have distinguished 2 sub-cases, which depend on the value of the ratio $\frac{P_{K,R}}{P_R^*}$. The limiting ratio is bounded by $\delta=\frac{2\gamma}{3(5/3-\gamma)}>1$ ($\gamma<\frac{5}{3}$), then case(b) $\frac{P_{K,R}}{P_R^*}>1$ then case (b) is impossible. For that purpose, we will consider that case 2(a) in the study of the positivity of $g_2(z_2)$.

Case 2(a) : $\gamma<\frac{5}{3}$ and $\frac{K_R}{P_R^*}<\frac{\gamma}{(5/3-\gamma)}$: we have $g\prime\prime_2(z_2)$ positive $\forall\ z_2\in[1,\frac{(\gamma+1)}{\gamma}[$, which implies that $g\prime(z_2)$ is increasing $\forall\ z_2\in[1,\frac{(\gamma+1)}{\gamma}[$.

Sign of $g\prime_2$: thanks to condition 2(a), we find that $g\prime_2(\frac{(\gamma+1)}{\gamma}) < 0$, but since $g\prime_2$ is an increasing function, then $g\prime_2(z_2)$ is negative $\forall\ z_2 \in [1, \frac{(\gamma+1)}{\gamma}[$. This implies that the function $g_2(z_2)$ is decreasing $\forall\ z_2 \in [1, \frac{(\gamma+1)}{\gamma}[$.

Finally for $\gamma < \frac{5}{3}$ and $\frac{K_R}{P_R^*} < \frac{\gamma}{(5/3-\gamma)}$: $g_2(z_2)$ is decreasing in $[1, \frac{(\gamma+1)}{\gamma}[$; then for getting $g_2(z_2) > 0$ ($P_2^* > P_R^*$), it suffices that $g_2(\frac{(\gamma+1)}{\gamma}) > 0$, which imposes the following condition :

$$2(\frac{(\gamma+1)}{\gamma})^2\left(\beta+1+2\frac{K_R}{P_R^*}\alpha\right)+\frac{(\gamma+1)}{\gamma}\left(-5-5\beta-3m^2\frac{\tau_R}{P_R^*}\right)+3m^2\frac{\tau_R}{P_R^*}\beta>0. \qquad (2.62)$$

Bibliographie

[Amb+09] Annalisa AMBROSO, Christophe CHALONS, Frédéric COQUEL et al. « Relaxation and numerical approximation of a two-fluid two-pressure diphasic model ». In : *ESAIM : Mathematical Modelling and Numerical Analysis* 43.6 (2009), p. 1063-1097. DOI : 10.1051/m2an/2009038 (cf. p. 34).

[Ber99] Christophe BERTHON. « Contribution à l'analyse numérique des équations de Navier-Stokes compressibles à deux entropies spécifiques. Applications à la turbulence compressible ». Thèse de doct. Paris 6, 1999. URL : https://www.math.sciences.univ-nantes.fr/~berthon/cv_these_hdr/these.pdf (cf. p. 4).

[BC02] Christophe BERTHON et Frédéric COQUEL. « Nonlinear projection methods for multi-entropies Navier-Stokes systems ». In : *Innovative Methods For Numerical Solution Of Partial Differential Equations* (2002), p. 278-304. DOI : 10.1142/9789812810816_0014 (cf. p. 4).

[BGH00] Thierry BUFFARD, Thierry GALLOUËT et Jean-Marc HÉRARD. « A sequel to a rough Godunov scheme : application to real gases ». In : *Computers & Fluids* 29(7) (2000), p. 813-847. DOI : 10.1016/s0045-7930(99)00026-2 (cf. p. 16-18).

[EGH00] Robert EYMARD, Thierry GALLOUËT et Raphaèle HERBIN. *Finite volume methods*. Elsevier, 2000. URL : https://hal.archives-ouvertes.fr/hal-02100732v2 (cf. p. 17).

[Fav58] Alexandre FAVRE. « Equations statistiques des gaz turbulents ». In : *Compte-Rendus de l'Académie des Sciences Paris* 246.18 (1958), p. 2576-2579 (cf. p. 4).

[Fav65] Alexandre FAVRE. « Equations des gaz turbulents compressibles. 1, Formes générales. 2, Méthode des vitesses moyennes ; méthode des vitesses macroscopiques pondérées par la masse volumique. » In : *Journal de Mécanique* 4.3 (1965) (cf. p. 4).

[Fav+76] Alexandre FAVRE, Leslie S.G. KOSVAZNAY, Raymond DUMAS et al. *La turbulence en mécanique des fluides : bases théoriques et expérimentales, méthodes statistiques*. Gauthier-Villars, 1976 (cf. p. 4).

[GB13] Thomas B GATSKI et Jean-Paul BONNET. *Compressibility, turbulence and high speed flow*. Academic Press, 2013. URL : https://www.researchgate.net/publication/281766815_Compressibility_Turbulence_and_High_Speed_Flow (cf. p. 4).

Bibliographie

[Gav+22] Sergey GAVRILYUK, Jean-Marc HÉRARD, Olivier HURISSE et al. « Theoretical and numerical analysis of a simple model derived from compressible turbulence ». In : *Journal of Mathematical Fluid Mechanics* 24.2 (2022), p. 1-34. DOI : 10.1007/s00021-022-00676-5 (cf. p. 4, 6, 15, 17, 18, 20).

[GS06] Sergey GAVRILYUK et Richard SAUREL. « Estimation of the turbulent energy production across a shock wave ». In : *Journal of Fluid Mechanics* 549 (2006), p. 131. DOI : 10.1017/s0022112005008062 (cf. p. 3, 4, 8, 9, 30, 33-37).

[GL04] Paola GOATIN et Philippe G LEFLOCH. « The Riemann problem for a class of resonant hyperbolic systems of balance laws ». In : *Annales de l'Institut Henri Poincaré C, Analyse non linéaire*. T. 21. 6. Elsevier. 2004, p. 881-902. DOI : 10.1016/j.anihpc.2004.02.002 (cf. p. 34).

[GR96] Edwige GODLEWSKI et Pierre-Arnaud RAVIART. *Numerical approximation of hyperbolic sytems of conservation laws*. Springer Berlin, 1996. DOI : 10.1007/978-1-4612-0713-9 (cf. p. 12).

[God59] Sergueï Konstantinovitch GODUNOV. « A difference method for numerical calculation of discontinuous equations of hydrodynamics ». In : *Math sbornik (in Russian)* 47(89).3 (1959), p. 271-306. URL : https://hal.archives-ouvertes.fr/hal-01620642 (cf. p. 12).

[Gos01] Laurent GOSSE. « A well-balanced scheme using non-conservative products designed for hyperbolic systems of conservation laws with source terms ». In : *Mathematical Models and Methods in Applied Sciences* 11.02 (2001), p. 339-365. DOI : 10.1142/s021820250100088x (cf. p. 34).

[GL96] Joshua M GREENBERG et Alain-Yves LEROUX. « A well-balanced scheme for the numerical processing of source terms in hyperbolic equations ». In : *SIAM Journal on Numerical Analysis* 33.1 (1996), p. 1-16. DOI : 10.1137/0733001 (cf. p. 34).

[Hér14] Jean-Marc HÉRARD. Rapp. tech. A simple turbulent model for compressible flows, 2014. URL : https://hal.archives-ouvertes.fr/hal-02007044 (cf. p. 4, 6).

[HL16] Jean-Marc HÉRARD et Hippolyte LOCHON. « A simple turbulent two-fluid model ». In : *Comptes Rendus Mécanique* 344(11-12) (2016), p. 776-783. DOI : 10.1016/j.crme.2016.10.010 (cf. p. 6).

[KS11] Masashi KANAMORI et Kojiro SUZUKI. « Shock wave detection in two-dimensional flow based on the theory of characteristics from cfd data ». In : *Journal of Computational Physics* 230.8 (2011), p. 3085-3092. DOI : 10.1016/j.jcp.2011.01.007 (cf. p. 13).

[Pop00] Stephen B POPE. *Turbulent flows*. Cambridge university press, 2000. DOI : 10.1017/cbo9780511840531 (cf. p. 4).

Bibliographie

[Smo83] Joel SMOLLER. *Shock waves and reaction—diffusion equations*. Springer Science & Business Media, 1983. DOI : 10.1007/978-1-4684-0152-3 (cf. p. 13).

[SA94] Philippe SPALART et Steven ALLMARAS. « A one-equation turbulence model for aerodynamic flows ». In : *La Recherche Aérospatiale* (1994), p. 5-21. URL : https://arc.aiaa.org/doi/10.2514/6.1992-439 (cf. p. 4).

[TL72] Henk TENNEKES et John Leask LUMLEY. « A First Course in Turbulence. » In : *MIT Press* (1972). DOI : 10.7551/mitpress/3014.003.0005 (cf. p. 4).

[Tor97] Eleuterio Francisco TORO. *Riemann solvers and numerical methods for fluid dynamics*. Springer Berlin Heidelberg, 1997. DOI : 10.1007/978-3-662-03490-3_9 (cf. p. 12).

[Wu+13] Ziniu WU, Yizhe XU, Wenbin WANG et al. « Review of shock wave detection method in CFD post-processing ». In : *Chinese Journal of Aeronautics* 26.3 (2013), p. 501-513. DOI : 10.1016/j.cja.2013.05.001 (cf. p. 13).

3. A relaxation approach for modeling turbulence in compressible flows

Sommaire

A relaxation approach for modeling turbulence in compressible flows

Sergey Gavrilyuk[b], Jean-Marc Hérard[a], Olivier Hurisse[a], Ali Toufaili[a,c] :
[a] EDF R&D, 6 quai Watier, 78400 Chatou, France.
[b] IUSTI UMR CNRS 7343, Technopôle Château-Gombert, Marseille, France.
[c] I2M UMR CNRS 7373, Technopôle Château-Gombert, Marseille, France.

Abstract
In this paper, we propose a new compressible turbulence model which involves four partial differential equations for mass, momentum and energy balance. The fourth PDE governs the evolution of the turbulent entropy fraction ξ_k (ratio between turbulent and total entropies), and its source term integrates a relaxation term with an associated relaxation time scale. We build this model on thermodynamic assumptions and we use classical mixture modeling techniques. The construction relies on a diphasic vision of the laminar/turbulence interaction. First, we study the mathematical structure of the model : hyperbolicity, wave structure, nature of the field and the entropy inequality. Then, the simulation of this model is eventually discussed, using a Finite Volume approach and Riemann solvers (approximate Godunov scheme).

key words :
Turbulence, compressible flows, hyperbolicity, entropy, shock waves, Riemann problem, source term

Introduction

In chapter 1 Sergey GAVRILYUK, Jean-Marc HÉRARD, Olivier HURISSE et al. 2022, a model involving a uniform turbulent entropy has been investigated. This simple model has then been enriched by introducing in a numerical manner a jump of the turbulent entropy in shocks on the basis of the model proposed in Sergey GAVRILYUK et Richard SAUREL 2006. This approach for introducing the modification of the turbulence in the shocks is based upon numerical schemes that are quite tricky to handle in a one-dimensional framework, and that may be not affordable for industrial 3D applications (see 2. In the present chapter, a model is proposed in order to account for jumps of the turbulent entropy in shocks.

This model is based upon a relaxation approach, which can be seen as en extension of the model studied in chapter 1 Sergey GAVRILYUK, Jean-Marc HÉRARD, Olivier HURISSE et al. 2022. It uses classical features of the thermodynamics of mixtures in mutliphase flows SAUREL, CHINNAYYA et RENAUD 2003; BARBERON et HELLUY 2005; H. MATHIS 2019. The turbulent entropy and the laminar entropy are assumed to be two contributions to a mixture of two miscible phases sharing the same mass. The properties of the mixture models are then deduced from that of each contribution (laminar and turbulent) on the basis of Gibbs relations. Such a kind of model has been proposed for instance in SAUREL, CHINNAYYA et RENAUD 2003 for turbulent plasma flows, with slightly different assumptions for the two contributions (in particular, the two contributions do not share the same mass).

The present model is based on the Euler system of equations with energy and the turbulent entropy becomes a variable, whereas it is assumed constant in the model of chapter 1 Sergey GAVRILYUK, Jean-Marc HÉRARD, Olivier HURISSE et al. 2022. The turbulent entropy fraction $\xi_k = s_k/(s_l + s_k)$ is introduced, where s_k is the turbulent entropy and s_l the laminar entropy. It is assumed that ξ_k is advected with velocity U and that a relaxation source term acts on ξ_k. This source term is written in a BGK form. It involves a relaxation time-scale $\lambda > 0$ and an equilibrium entropy fraction $\bar{\xi}_k(\tau, e)$. The latter is defined in order to maximize the entropy $(s_l + s_k)$ at a given specific volume τ and a given specific energy $e = e_k + e_l$, where e_k is the turbulent specific energy and e_l the laminar one. It is proven that this source term is in agreement with the second law of thermodynamics, and that it corresponds to the temperature equilibrium between the turbulent temperature, defined through the EOS $e_k(\tau, s_k)$, and the laminar temperature.

When the source term is not taken into account, for instance for $\lambda \to +\infty$, the turbulent fraction ξ_k is advected and it is not modified through shocks. On the contrary, when $\lambda < +\infty$, the source term is activated and its effect may be different on both sides of a shock. This implies that ξ_k, and thus the turbulent entropy, may be different on both sides of a shock. In particular, if instantaneous relaxation is considered with $\lambda \to 0^+$, ξ_k is no more an unknown of the model since we get : $\xi = \bar{\xi}_k(\tau, e)$. Since both

τ and e jump across a shock, ξ_k then also jumps across the shock. This model then allows to control the entropy variation across a shock, and in the limit case of an instantaneous relaxation a pure discontinuity is observed for the turbulent entropy in a shock, as in the model proposed in Sergey GAVRILYUK et Richard SAUREL 2006. Nevertheless, the jumps of turbulent entropy defined by these two approaches are different.

This chapter is organized as follows. The model is first described in section 1, with a particular emphasis put on the modeling assumptions. The difference with the model of chapter 1 Sergey GAVRILYUK, Jean-Marc HÉRARD, Olivier HURISSE et al. 2022 is then shortly discussed in section 2. The properties of the model are discussed in section 3, while the different waves for the Riemann problem of the convective part of the model are studied in section 4. The counterpart of this study is proposed in section 5 when considering an instantaneous relaxation (i.e. temperature equilibrium). In section 6, the numerical strategy for computing approximate solutions of the model is described and it is then assessed in section 7 on the basis of Riemann problems.

1. A simple turbulence model using a relaxation approach

1.1. Extensive description of the model

Let us consider a mass of fluid $\mathcal{M}$ that occupies a volume $\mathcal{V}$. We assume that this mass of fluid possesses an energy $\mathcal{E}$ that gathers two contributions : the internal energy $\mathcal{E}_l$ that represents the thermodynamic/laminar energy of the fluid, and $\mathcal{E}_k$ that corresponds to an additional energy due to microscopic displacement of fluid within the volume $\mathcal{V}$. The latter is classically called the turbulent energy and the term microscopic should be understood with respect of the global motion of the volume $\mathcal{V}$ in its surrounding. We then assume that we have : $\mathcal{E} = \mathcal{E}_l + \mathcal{E}_k$.

Moreover, the internal energy $\mathcal{E}_l$ and the turbulent energy $\mathcal{E}_t$, are respectively associated with an thermodynamical entropy η_l and with a turbulent entropy η_t. The total entropy of the volume of fluid η is assumed to be the sum of both entropies : $\eta = \eta_l + \eta_t$. In the following, energies are considered as the potentials that allow to define the thermodynamical behavior and the turbulent behavior of the fluid. We thus have to choose Equation of States (EoS) :

$$(\mathcal{M}, \mathcal{V}, \eta_\phi) \mapsto \mathcal{E}_\phi(\mathcal{M}, \mathcal{V}, \eta_\phi), \quad \text{for } \phi = \{l, k\}. \tag{3.1}$$

The evolution of the different quantities are supposed to be ruled by Gibbs relations, that is :

$$d\mathcal{E}_\phi = T_\phi d\eta_\phi - P_\phi d\mathcal{V} + \mu_\phi d\mathcal{M}, \quad \text{for } \phi = \{l, k\}. \tag{3.2}$$

The pressure and the temperature of the thermodynamical and turbulent contributions are then defined thanks to (3.2) and to the EoS (3.1), and they read :

$$P_\phi(\mathcal{M}, \mathcal{V}, \eta_\phi) = -\frac{\partial \mathcal{E}_\phi}{\partial \mathcal{V}}_{|\mathcal{M}, \eta_\phi}, \quad T_\phi(\mathcal{M}, \mathcal{V}, \eta_\phi) = \frac{\partial \mathcal{E}_\phi}{\partial \eta}_{|\mathcal{M}, \mathcal{V}}, \quad \text{for } \phi = \{l, k\}. \tag{3.3}$$

The Gibbs enthalpies μ_ϕ will not be used in the sequel.

Let us introduce an entropy fraction ξ_k for the turbulent contribution :

$$\xi_k = \frac{\eta_k}{\eta},$$

where η_k and η_l, and thus η, are supposed strictly positive (entropies are defined up to an additive constant). These assumptions yield that ξ_k belongs to $[0, 1]$. We also define for convenience $\xi_l = 1 - \xi_k$. Thanks to the relations $\mathcal{E} = \mathcal{E}_l + \mathcal{E}_k$ and $\eta = \eta_l + \eta_k$, and thanks to relations (3.2), we easily get a Gibbs relation for the whole volume of fluid :

$$d\mathcal{E} = (\xi_l T_l + \xi_k T_k)\, d\eta - (P_l + P_k)\, d\mathcal{V} + (\mu_l + \mu_k)\, d\mathcal{M} + \eta(T_k - T_l)\, d\xi_k, \tag{3.4}$$

from which the total pressure P and the total temperature T of the fluid can be identified from the two first terms on the right hand side :

$$T = \xi_k T_k + \xi_l T_l, \quad \text{and} \quad P = P_l + P_k. \tag{3.5}$$

The last term on the right hand side of relation (3.4) models the entropy exchange between the thermodynamical and the turbulent contributions.

Remark 14 The description above can be seen as the mixture of two miscible phases, with $\mathcal{V}_k = \mathcal{V}_l = \mathcal{V}$ and sharing the same mass $\mathcal{M}_k = \mathcal{M}_l = \mathcal{M}$ but with different energies, $\mathcal{E}_k \neq \mathcal{E}_l$ in general. Since it has been assumed that the miscibility implies that both fluids occupy the same volume, a Dalton's law is recovered for the pressures : $P = P_k + P_l$ as in CHIAPOLINO, BOIVIN et Richard SAUREL 2017; H. MATHIS 2019; J.-M. HÉRARD et H. MATHIS 2019; FACCANONI et Hélène MATHIS 2019; J.-M. HÉRARD, O. HURISSE et L. QUIBEL 2020; Olivier HURISSE et Lucie QUIBEL 2021 for instance.

We consider now the following closure for the evolution of the mass and the energy. The mass $\mathcal{M}$ of the volume of fluid is constant :

$$d\mathcal{M} = 0. \tag{3.6}$$

The first law of thermodynamics applies. When only accounting for the force due to the total pressure P on the volume, the latter reads :

$$d\mathcal{E} = -P\, d\mathcal{V}. \tag{3.7}$$

As a consequence, relation (3.4) simply gives :

$$T\, d\eta = -\eta(T_k - T_l)\, d\xi_k. \tag{3.8}$$

At last, the velocity field U is introduced. It corresponds to the velocity of the center of mass of the volume of fluid $\mathcal{V}$. For the sake of simplicity, we consider here one-dimensional flows. Accordingly to (3.7), we restrict here to the force due to the total pressure P. Therefore, the Newton's law gives that :

$$d(\mathcal{M}U) = -\mathcal{V}\partial_x P dt. \tag{3.9}$$

Moreover, the flow is compressible so that the volume $\mathcal{V}$ of the fluid is modified following the divergence of the velocity field :

$$d\mathcal{V} = \mathcal{V}\partial_x U dt. \tag{3.10}$$

At that point we have five unknowns : $\mathcal{V}$, $\mathcal{M}$, η, ξ_k and U, and we have defined four closure relations for the time evolution of the unknowns : (3.6), (3.7), (3.10) and (3.9). Indeed, we have not defined the time evolution of ξ_k. This will be achieved done in the next section.

1.2. A complete set of PDE in conservative form with intensive quantities

We turn now to a more classical description of the flow through a set of Partial Derivative Equations (PDE) whose unknowns are intensive quantities. We thus define the specific volume $\tau = \mathcal{V}/\mathcal{M}$ and the density $\rho = 1/\tau$, the specific energies $e = \mathcal{E}/\mathcal{M}$, $e_k = \mathcal{E}_k/\mathcal{M}$ and $e_l = \mathcal{E}_l/\mathcal{M}$, the specific entropies $s = \eta/\mathcal{M}$, $s_k = \eta_k/\mathcal{M}$ and $s_l = \eta_l/\mathcal{M}$.

The entropy fractions are already intensive quantities. We choose here to write : $d\xi_k = \mathscr{S}_k dt$, where the source term $\mathscr{S}_k$ must be defined. Considering the velocity field U, the derivative $d\psi$ of any quantity ψ corresponds in fact to the derivative along the streamline : $d\psi = (\partial_t\psi + U\partial_x\psi)dt$. Hence from the closure for ξ_k and from (3.6), (3.7), (3.10) and (3.9) we get the following set of four equations which is written in conservative form :

$$\begin{cases} \partial_t \rho\xi_k + \partial_x \rho U\xi_k = \rho\mathscr{S}_k, \\ \partial_t \rho + \partial_x \rho U = 0, \\ \partial_t \rho U + \partial_x \rho U^2 + P = 0, \\ \partial_t \rho E + \partial_x U(\rho E + P) = 0, \end{cases} \tag{3.11}$$

where $E = e + U^2/2$ is the specific total energy. The unknowns of the system are the four intensive quantities : $\tau = 1/\rho$, s, ξ_k and U. System (3.11) is then closed thanks to the results of the previous sections. Indeed, we have :

$$e = e_l(\tau_l, s_l) + e_k(\tau_k, s_k), \quad P = P_l(\tau_l, s_l) + P_k(\tau_k, s_k), \quad s_k = \xi_k s, \quad \text{and} \quad \tau_l = \tau_k = \tau,$$

where $(\tau, s_\phi) \mapsto e_\phi(\tau, s_\phi)$ are the EoS given in intensive form, and where :

$$P_\phi = -\frac{\partial e_\phi}{\partial \tau_{|s_\phi}}, \quad T_\phi = \frac{\partial e_\phi}{\partial s_{\phi_{|\tau}}}, \quad \text{for } \phi = \{k, l\}. \tag{3.12}$$

Moreover, the total temperature reads :

$$T = \xi_k T_k(\tau_k, \xi_k s) + \xi_l T_l(\tau_l, \xi_l s),$$

and the source terms $\mathscr{S}_k$ should be defined with respect to $\tau = 1/\rho$, s, ξ_k and U.

As noted above, it still remains to model the time evolution of ξ_k through the source terms $\mathscr{S}_k$. We then assume that the specific energies $(\tau, s_l) \mapsto e_l(\tau, s_l)$ and $(\tau, s_k) \mapsto e_k(\tau, s_k)$ are strictly convex and that the associated temperatures $T_l(\tau, s_l)$ and $T_k(\tau, s_k)$ are positive. This implies that the entropies $(\tau, e_l) \mapsto s_l(\tau, e_l)$ and $(\tau, e_t) \mapsto s_t(\tau, e_t)$ are strictly concave GODLEWSKI et RAVIART 1996. It can be proved that the total entropy $(\tau, e_t, e_l) \mapsto s(\tau, e_k, e_l) = s_k(\tau, e_k) + s_l(\tau, e_l)$ is strictly concave, see appendix A for details.

The equation (3.4) reads in intensive form :

$$(\partial_t e + U\partial_x e) = P(\partial_t \tau + U\partial_x \tau) + T\ (\partial_t s + U\partial_x s) + s(T_k - T_l)\ d\xi_k. \tag{3.13}$$

Since the entropy s is concave, the second law of thermodynamics states that s should increase along a streamline for a closed and isolated system with $\partial_t \tau + U\partial_x \tau = \partial_t e + U\partial_x e = 0$:

$$T\ (\partial_t s + U\partial_x s) \geq 0.$$

When $\partial_t \tau + U\partial_x \tau = \partial_t e + U\partial_x e = 0$, equation (3.13) simply gives :

$$0 = T\ (\partial_t s + U\partial_x s) + s(T_k - T_l)\ \mathscr{S}_k. \tag{3.14}$$

As a consequence, in order to be in agreement with the second law of thermodynamics, the source terms $\mathscr{S}_t$ should fulfill the relation : $(T_k - T_l)\ \mathscr{S}_k \leq 0$ (note that previously the entropies have been supposed to be positive). A first natural choice is to set :

$$\mathscr{S}_k = \frac{T_l - T_k}{T\lambda}, \tag{3.15}$$

where λ is a positive time-scale to be defined. Since the total energy $\xi_k \mapsto e(\xi_k, \tau, s)$ is strictly convex with respect to the entropy fraction ξ_k (see appendix A), the source term $\mathscr{S}_k$ can also be written in the form of a BGK source term :

$$\mathscr{S}_k = \frac{\overline{\xi}_k - \xi_k}{\nu}, \tag{3.16}$$

where ν is a positive time-scale, and where the equilibrium turbulent fraction $\overline{\xi}_k$ minimizes the energy at a given entropy and specific volume :

$$\overline{\xi}_k = \underset{\xi_k}{argmin}\ e(\xi_k, \tau, s). \tag{3.17}$$

The equilibrium entropy fraction $\overline{\xi}_k$ thus depends on (τ, s). The strict convexity of $\xi_k \mapsto e(\xi_k, \tau, s)$ ensures that $(\tau, s) \mapsto \overline{\xi}_k(\tau, s)$ is defined in a unique manner for all (τ, s). Moreover, when this minimum is reached for $\overline{\xi}_k \in]0, 1[$, the derivative of e with respect to ξ_k vanishes. Therefore, $\overline{\xi}_k$ can also be defined through the temperature equilibrium :

$$T_k(\tau, \overline{\xi}_k s) = T_l(\tau, (1 - \overline{\xi}_l)s).$$

The asymptotic cases with $\overline{\xi}_t = 0$ correspond to the classical Euler configurations without turbulent contribution, whereas for $\overline{\xi}_k = 1$, no thermodynamical contribution arises in the system which should be avoided in a physical point of view.

2. Revisiting a simple model of compressible turbulence

Let us now show that the model of section 1.2 can be simplified in order to recover the turbulence model introduced in Jean-Marc HÉRARD 2014, and studied in detail in Sergey GAVRILYUK, Jean-Marc HÉRARD, Olivier HURISSE et al. 2022, at least under

certain assumptions. These additional assumptions with respect to model (3.11) are the following :

— the turbulent entropy s_k is assumed to be uniform, $s_k = s_k^0 \neq 0$;
— the source terms $\mathscr{S}_k$ in model (3.11) is set to zero, $\mathscr{S}_k = 0$ (for instance by choosing formally $\lambda = +\infty$) ;
— the EOS for the turbulent contribution is defined as :

$$e_k(\tau, s_k) = s_k \tau^{-2/3}. \tag{3.18}$$

System (3.11) with the above assumptions is nicknamed in this section : "simplified model". This model is compared here to the model proposed in Jean-Marc HÉRARD 2014.

With the choice of EOS (3.18), and since the turbulent entropy is assumed uniform, the turbulent kinetic energy $K = \rho e_k$ only depends on the density (so does the internal energy e_k). It reads :

$$K(\tau) = \rho e_k(\tau, s_k^0) = s_k^0 \tau^{-5/3}.$$

From the definition of the pressure of the turbulent contribution (3.12), we get here :

$$P_k = -\frac{\partial e_k}{\tau}_{|s_k} = \frac{2}{3} s_k \tau^{-5/3} = \frac{2}{3} K,$$

hence, the pressure of the mixture and the internal energy of the mixture respectively read :

$$P = P_l + P_k = P_l + \frac{2}{3} K, \quad \text{and} \quad e = e_l + e_k = e_l + K\tau.$$

The mixture pressure and energy are then in agreement with that of the turbulent model described in Jean-Marc HÉRARD 2014 and Sergey GAVRILYUK, Jean-Marc HÉRARD, Olivier HURISSE et al. 2022. Let us now turn to the comparisons of the system of PDE.

The equations for the mass, momentum and total energy conservation are the same for both models thanks to the equivalence of the mixture pressure and of the mixture energy. It remains to examine the consistence of the equation for the entropy fraction $\xi_k = s_k / s = s_k^0 / s$. For regular solutions, first equation of system (3.11) without the source term $\mathscr{S}_k = 0$ can be written as follows :

$$\partial_t \rho \frac{s_k^0}{s} + \partial_x \rho U \frac{s_k^0}{s} = 0, \tag{3.19}$$

and since $s_k^0 \neq 0$ is constant, equation (3.19) gives :

$$\partial_x \rho s + \partial_x \rho U s = 0. \tag{3.20}$$

which is the same as for for model Jean-Marc HÉRARD 2014 ; Sergey GAVRILYUK, Jean-Marc HÉRARD, Olivier HURISSE et al. 2022.

When turning to shock solutions, we have for model (3.11) the jump relation : $[\xi_k] = [s_k/s] = 0$. For the simplified model, we have obviously by assumption : $[s_k] = 0$. But since $[s] \neq 0$ in a shock, it implies that $[s_k/s] \neq 0$ for the simplified model. The jump relations $[\xi_k] = 0$ on the one hand, and $[s_k] = 0$ on the other hand are not equivalent in shock waves. Hence, the two models define different weak solutions.

Let us state the results of this section. The simplified model deduced from system (3.11) with the three assumptions of the beginning of this section is equivalent to the the model described in Jean-Marc HÉRARD 2014 and Sergey GAVRILYUK, Jean-Marc HÉRARD, Olivier HURISSE et al. 2022 for regular solutions. For solutions involving shocks, the two models lead to different jump relations and thus to different solutions.

3. Main properties of the convection system

In the present section, some of the main properties of the system of equations (3.11) are provided considering a general framework with respect to the **EOS**. It is an important point to be quoted that all these properties are inherited from the Euler system of equations which represents the basis of the turbulent model. Indeed, the convective part of system of equations (3.11) corresponds to the Euler system of equations with a complex equation of state which depends on a fraction, ξ_k, convected with velocity U.

3.1. Entropy inequality

Let us define the entropy-entropy flux pair (η, f_η) as :

$$\eta(w) = -\rho s, \quad \text{and} \quad f_\eta(w) = U\eta, \tag{3.21}$$

where w is the conservative variable such that :

$$w = (\rho\xi_k, \rho, \rho U, \rho E).$$

If we assume that the specific internal energy $(\tau, s_k, s_l) \mapsto e(\tau, s_k, s_l)$ is convex, then the associated specific entropy $(\tau, e_k, e_l) \mapsto s(\tau, e_k, e_l)$ is concave, see GODLEWSKI et RAVIART 1996 or appendix A. Moreover, using this concave specific entropy $(\tau, e_k, e_l) \mapsto s(\tau, e_k, e_l)$, it can be shown that the volumic entropy $(\rho, \rho e_k, \rho e_l) \mapsto \rho s(\rho, \rho e_k, \rho e_l)$ is also concave GODLEWSKI et RAVIART 1996 or JUNG 2013. $(\tau, e_k, e_l) \mapsto s(\tau, e_k, e_l)$ Then, thanks to (3.14) and to definitions (3.21), the following inequality holds for smooth solutions of system (3.11) :

$$\partial_t \eta + \partial_x f_\eta \leq 0. \tag{3.22}$$

When the source terms are not accounted for in system (3.11), the classical approach of the vanishing viscosity (see GODLEWSKI et RAVIART 1996 among others) allows to

retrieve the entropy inequality (3.22). This confirms that the entropy inequality (3.22) is in agreement with the second law of thermodynamics when considering a concave physical entropy s.

3.2. Hyperbolicity

We consider here regular solutions so that the convective part of system (3.11) can be written in non-conservative form :

$$\partial_t Y + A(Y)\partial_x Y = 0, \tag{3.23}$$

where the non-conservative variable of system (3.23) is $Y = (\tau, u, s, \xi_k)^t$. In relation (3.23), the jacobian matrix $\mathrm{A}(Y)$ of the system reads :

$$A(Y) = \begin{pmatrix} u & -\tau & 0 & 0 \\ \tau \frac{\partial P}{\partial \tau|_{s,\xi_k}} & u & \tau \frac{\partial P}{\partial s|_{\tau,\xi_k}} & \tau \frac{\partial P}{\partial \xi_k|_{\tau,s}} \\ 0 & 0 & u & 0 \\ 0 & 0 & 0 & u \end{pmatrix}.$$

The celerity of the pressure waves for each contribution c_ϕ, $\phi = k, l$, is defined through the derivative of the pressure with respect to the density along an isentropic path :

$$c_\phi^2(\tau_\phi, s_\phi) = \frac{\partial P_\phi}{\partial \rho_\phi|_{s_\phi}} = -\tau_\phi^2 \frac{\partial P_\phi}{\partial \tau_\phi|_{s_\phi}} = \tau^2 \frac{\partial^2 e_\phi}{\partial \tau_\phi^2}. \tag{3.24}$$

Since it has been assumed that $(\tau_\phi, s_\phi) \mapsto e_\phi(\tau_\phi, s_\phi)$ is strictly convex, then we get that $c_\phi^2(\tau_\phi, s_\phi) > 0$.

In the same manner, the frozen sound speed in the mixture is defined through the derivative of the mixture pressure with respect to the density along an isentropic path. It can thus be computed from the mixture pressure law, and it leads to a relation that gathers the celerities of each contribution $c_\phi(\tau_\phi, s_\phi)$. The celerity of the mixture $c(\xi_k, \tau, s)$ is then :

$$c^2(\xi_k, \tau, s) = \frac{\partial P}{\partial \rho|_{s,\xi_k}} = -\tau^2 \frac{\partial P}{\partial \tau|_{s,\xi_k}}, \tag{3.25}$$

where the mixture pressure has been defined in section 1.2, and it is such that :

$$P(\xi_k, \tau, s) = P_l(\tau_l, (1-\xi_l)s) + P_k(\tau_k, s\xi_k).$$

Using the definition (3.25), it can be obtained that :

$$-\frac{c^2(\xi_k, \tau, s)}{\tau^2} = \frac{\partial P_l}{\partial \tau|_{s,\xi_k}} + \frac{\partial P_k}{\partial \tau|_{s,\xi_k}}.$$

When s and ξ_k are constant, then it implies that s_k ans s_l are also constant, hence the

relation above gives :

$$-\frac{c^2(\xi_k,\tau,s)}{\tau^2}=\frac{\partial P_l(\tau,s_l)}{\partial\tau|_{s_l}}+\frac{\partial P_k(\tau,s_k)}{\partial\tau|_{s_k}}=-\frac{c_l^2}{\tau^2}-\frac{c_k^2}{\tau^2}.$$

Then, equation (3.25) is rewritten in the following form :

$$c^2=c_l^2+c_k^2.$$

When the square of the sound speed in each phase is positive, $c_\phi^2>0$, then the square of the mixture (frozen) sound-speed is also positive :

$$c_k^2>0 \quad \text{and} \quad c_l^2>0\Longrightarrow c^2>0. \tag{3.26}$$

It should be noted that this condition is only sufficient.

When each sound speed c_ϕ^2 is strictly positive, then system (3.23) is strictly hyperbolic : it admits four real eigenvalues :

$$\lambda_1(Y)=u-c,\qquad \lambda_{2,3}(Y)=u,\qquad \lambda_4(Y)=u+c, \tag{3.27}$$

and the associated right eigenvectors $r_i(Y)$ span the whole space $\mathbb{R}^4$:

$$r_1(Y)=(\tau,c,0,0)^T, \tag{3.28}$$

$$r_2(Y)=\left(\frac{\partial P}{\partial\xi_k|_{\tau,s}},0,0,(c/\tau)^2\right)^T, \tag{3.29}$$

$$r_3(Y)=\left(\frac{\partial P}{\partial s|_{\tau,\xi_k}},0,(c/\tau)^2,0\right)^T, \tag{3.30}$$

$$r_4(Y)=(\tau,-c,0,0)^T. \tag{3.31}$$

Since the second component of r_2 and r_3 are equal to zero, and since $\lambda_{2,3}(Y)=u$, we easily get $\nabla_Y\lambda_j\cdot r_j=0$ for all Y and for $j=2,3$. Hence, the associated fields are linearly degenerate (LD) and the 2- and 3-waves are contact waves. It can be shown that for fields 1 and 4, we have :

$$\nabla_Y\lambda_1\cdot r_1=-\nabla_Y\lambda_4\cdot r_4=c-\partial_\tau c_{|\xi_k,s}.$$

In a physical point of view, the sound speed of a mixture increases when the density increases, so that we have $\partial_\tau c_{|\xi_k,s}<0$ and thus $c-\partial_\tau c_{|\xi_k,s}>0$. Hence, $\nabla_Y\lambda_1\cdot r_1$ and $\nabla_Y\lambda_4\cdot r_4$ are not equal to zero and the associated fields are genuinely non linear (GNL).

3.3. Riemann invariants

The eigenvalue U is associated with the two independent eigenvectors $r_2(Y)$ and $r_3(Y)$. Therefore, only two Riemann invariants can be found for this LD field. They

are :

$$I_1^{2,3}(Y) = u \quad , \quad I_2^{2,3}(Y) = P(\tau, s). \tag{3.32}$$

In a classical manner for Euler-likre systems, the two Riemann invariants above are the cornerstone for connecting all the intermediate states through the three waves of the system when solving a Riemann problem. Unlike for the LD fields, the two GNL fields are each associated with a single eigenvector. Therefore, three Riemann invariants can be defined for describing the profile of the rarefaction waves. They are for the field associated with λ_1 :

$$I_1^1(Y) = s \ , \ I_2^1(Y) = \xi_k, \ I_3^1(Y) = u - \int_0^\tau \frac{c(\xi_k, \tau\prime, s)}{\tau\prime} \, \mathrm{d}\tau\prime, \tag{3.33}$$

and for the field associated with λ_4 :

$$I_1^4(Y) = s \ , \ I_2^4(Y) = \xi_k, \ I_3^4(Y) = u + \int_0^\tau c\frac{(\xi_k, \tau\prime, s)}{\tau\prime} \, \mathrm{d}\tau\prime. \tag{3.34}$$

3.4. Jump conditions

The jump conditions, or Rankine-Hugoniot relations, allow to describe the variations of the variables in shock waves. These shock waves occur in the two GNL waves are they correspond to discontinuities of the variables. The solution is then a weak solution. For defining the jump of the variables across a discontinuity, let us define $[f] = f_r - f_l$. It represents the jump of the quantity f across the discontinuity between the left state denoted by l and the right state denoted by r. The speed of displacement of this discontinuity is denoted by σ. For the two genuinely non linear fields of system (3.11), the jump conditions may be written :

$$\begin{cases} -\sigma[\rho\xi_k] + [\rho u\xi_k] = 0, \\ -\sigma[\rho] + [\rho u] = 0, \\ -\sigma[\rho u] + \left[\rho u^2 + P\right] = 0, \\ -\sigma[\rho E] + \left[u\left(\rho E + P\right)\right] = 0. \end{cases} \tag{3.35}$$

They can be simplified into :

$$\begin{cases} [\xi_k] = 0, \\ \sigma = [\rho u]/[\rho], \\ \rho_R\rho_L[u]^2 = [P][\rho], \\ 2[e] + (P_R + P_L)[\dfrac{1}{\rho}] = 0. \end{cases} \tag{3.36}$$

4. Solution of the Riemann problem

This section is devoted to the solution of the Riemann problem associated with the convective part of system (3.11). The laminar contribution and the turbulent contribution fulfill respectively the following **EOS** :

$$e_l(\tau, s_l) = \frac{s_l \tau^{1-\gamma}}{(\gamma-1)}, \quad \text{and} \quad e_k(\tau, s_k) = s_k \tau^{-2/3}.$$

The **EOS** for the laminar contribution is a perfect gas **EOS**, while for the turbulent contribution the **EOS** is derived from that used in Jean-Marc HÉRARD 2014 and Sergey GAVRILYUK, Jean-Marc HÉRARD, Olivier HURISSE et al. 2022. These **EOS** give the following formulae for the pressure and for the celerity :

$$P_l(\tau, s_l) = s_l \tau^{-\gamma}, \qquad P_k(\tau, s_k) = \frac{2}{3} s_k \tau^{-5/3},$$

$$c_l^2(\tau, s_l) = \gamma s_l \tau^{1-\gamma}, \qquad c_k^2(\tau, s_k) = \frac{10}{9} s_k \tau^{-2/3}.$$

A solution of the Riemann problem for the convective part of system (3.11) is composed of four states.

— A left state w_L and a right state w_R, which correspond to the initial condition of the Riemann problem ;

— Two intermediate states w_1 and w_2, which are not present in the initial condition but which appear in the solution when time increases (as soon as $t > 0$) ;

These states are separated either by discontinuities (LD field or a shock wave in a GNL field) or by regular profiles (rarefaction wave in a GNL field). Following the abscissa x, the four states are in the order : w_L, w_1, w_2 and w_R. Hence, states L and 1 are separated by the GNL wave λ_1, states 1 and 2 are separated by the LD wave $\lambda_{2,3}$, and states 2 and R are separated by the GNL wave λ_4. Since GNL waves λ_1 and λ_4 can be either shock waves or rarefaction waves, four possible configurations should be examined depending on the nature of the the 1-wave and on the 4-wave :

- case 1 : 1-shock / 2,3-contact / 4-shock
- case 2 : 1-rarefaction / 2,3-contact / 4-rarefaction
- case 3 : 1-shock / 2,3-contact / 4-rarefaction
- case 4 : 1-rarefaction / 2,3-contact / 4-shock

Let us first denotes by z_1 and z_2 the two density ratios across the 1-wave and the 4-wave :

$$z_1 = \frac{\rho_1}{\rho_L} \quad \text{and} \quad z_2 = \frac{\rho_2}{\rho_R}.$$

The solution of the Riemann problem associated with the convective part of system (3.11) is given below for each of the four cases mentioned above. We only give here the resulting formulae. The details of the computations of each case may be found in

appendix B. Nonetheless, it should be noted that functions D_i allow to connect the laminar pressure to the total pressure. Functions h_i represent the "classical" connection functions between the total pressure on each side of a shock, and functions Q_i represent the "classical" connection functions for the total pressure between the to extremities of the rarefaction fan. In the four cases, we have :

$$\xi_{k_1} = \xi_{k_L}, \quad \xi_{k_2} = \xi_{k_R}.$$

case 1. We have for $z_1 > 1$ and $z_2 > 1$:

$$u_R - u_L + c_{l_L} f_1(z_1, \xi_{k_L}, \rho_L) + c_{l_R} f_2(z_2, \xi_{k_R}, \rho_R) = 0,$$

$$P_{l_L} h_1(z_1, \xi_{k_L}, \rho_L) D_1(z_1, \xi_{k_1}, \rho_L) = P_{l_R} h_2(z_2, \xi_{k_R}, \rho_R) D_2(z_2, \xi_{k_2}, \rho_R),$$

with the following definitions :

$$f_1(z_1, \xi_{k_L}, \rho_L) = \sqrt{\left(\frac{z_1-1}{\gamma z_1}\right)\left(-1 - \frac{2}{3}\frac{\xi_{k_L}\rho_L^{5/3-\gamma}}{(1-\xi_{k_L})} + h_1(z_1, \xi_{k_L}, \rho_L)\left(1 + \frac{2}{3}\frac{\xi_{k_L}\rho_L^{5/3-\gamma} z_1^{5/3-\gamma}}{(1-\xi_{k_L})}\right)\right)},$$

$$h_1(z_1, \xi_{k_L}, \rho_L) = \frac{\beta z_1 - 1 + \frac{2}{3}\frac{\xi_{k_L}\rho_L^{5/3-\gamma}}{(1-\xi_{k_L})}(4z_1 - 1)}{\beta - z_1 + \frac{2}{3}\frac{\xi_{k_L}\rho_L^{5/3-\gamma}}{(1-\xi_{k_L})}(4z_1^{5/3-\gamma} - z_1^{8/3-\gamma})},$$

$$D_1(z_1, \xi_{k_1}, \rho_L) = 1 + \frac{2}{3}\frac{\xi_{k_1}\rho_L^{5/3-\gamma} z_1^{5/3-\gamma}}{(1-\xi_{k_1})},$$

and :

$$f_2(z_2, \xi_{k_R}, \rho_R) = \sqrt{\left(\frac{z_2-1}{\gamma z_2}\right)\left(-1 - \frac{2}{3}\frac{\xi_{k_R}\rho_R^{5/3-\gamma}}{(1-\xi_{k_R})} + h_2(z_2, \xi_{k_R}, \rho_R)\left(1 + \frac{2}{3}\frac{\xi_{k_R}\rho_R^{5/3-\gamma} z_2^{5/3-\gamma}}{(1-\xi_{k_R})}\right)\right)},$$

$$h_2(z_2, \xi_{k_R}, \rho_R) = \frac{\beta z_2 - 1 + \frac{2}{3}\frac{\xi_{k_R}\rho_R^{5/3-\gamma}}{(1-\xi_{k_R})}(4z_2 - 1)}{\beta - z_2 + \frac{2}{3}\frac{\xi_{k_R}\rho_R^{5/3-\gamma}}{(1-\xi_{k_R})}(4z_2^{5/3-\gamma} - z_2^{8/3-\gamma})},$$

$$D_2(z_2, \xi_{k_2}, \rho_R) = 1 + \frac{2}{3}\frac{\xi_{k_2}\rho_R^{5/3-\gamma} z_2^{5/3-\gamma}}{(1-\xi_{k_2})},$$

case 2. We have for $z_1 \leq 1$ and $z_2 \leq 1$:

$$u_R - u_L + B_1(z_1, c_{k_L}, c_{l_L}, \tau_L) + B_2(z_2, c_{k_R}, c_{l_R}, \tau_R) = 0,$$

$$P_{l_L} Q_1(z_1) D_1(z_1, \xi_{k_1}, \rho_L) = P_{l_R} Q_2(z_2) D_2(z_2, \xi_{k_2}, \rho_R),$$

with the following definitions :

$$\begin{aligned}
&B_1(z_1, c_{k_L}, c_{l_L}, \tau_L) = \int_1^{z_1} \frac{1}{\tau_L} \left(c_{l_L}^2 z^{1+\gamma} + c_{k_L}^2 z^{8/3} \right)^{1/2} \mathrm{d}z, \\
&Q_1(z_1) = z_1^{\gamma}, \\
&B_2(z_2, c_{k_R}, c_{l_R}, \tau_R) = \int_1^{z_2} \frac{1}{\tau_R} \left(c_{l_R}^2 z^{1+\gamma} + c_{k_R}^2 z^{8/3} \right)^{1/2} \mathrm{d}z, \\
&Q_2(z_2) = z_2^{\gamma}.
\end{aligned}$$

case 3. We have for $z_1 > 1$ and $z_2 \leq 1$:

$$u_R - u_L + B_2(z_2, c_{k_R}, c_{l_R}, \tau_R) + c_{l_L} f_1(z_1, \xi_{k_L}, \rho_L) = 0,$$

$$P_{l_L} h_1(z_1, \xi_{k_L}, \rho_L) D_1(z_1, \xi_{k_1}, \rho_L) = P_{l_R} Q_2(z_2) D_2(z_2, \xi_{k_2}, \rho_R),$$

case 4. We have for $z_1 \leq 1$ and $z_2 > 1$:

$$u_R - u_L + B_1(z_1, c_{k_L}, c_{l_L}, \tau_L) + c_{l_R} f_2(z_2, \xi_{k_R}, \rho_R) = 0,$$

$$P_{l_L} Q_1(z_1) D_1(z_1, \xi_{k_1}, \rho_L) = P_{l_R} h_2(z_2, \xi_{k_R}, \rho_R) D_2(z_2, \xi_{k_2}, \rho_R),$$

5. Solution of the Riemann problem with temperature equilibrium

In section 4, the source term $\mathscr{S}_k$ for the turbulent entropy fraction has been set to zero by choosing for instance $\lambda \to +\infty$ or $\nu \to +\infty$, depending on the form of the source terms (3.15) or (3.16). Let us now study the other asymptotic case where the time scales λ or ν tend to zero in $\mathscr{S}_k$. We focus here on the source term (3.15), but the result would be strictly the same with source terms (3.16), since the two source terms define the same equilibrium state. Formally, the equation for the entropy fraction then reads :

$$\lambda T \left(\partial_t \rho \xi_k + \partial_x \rho \xi_k U \right) = T_l - T_k.$$

When λ tends to zero, the partial derivative equation above tends to the constraint $T_l = T_k$ and ξ_k is no more an unknown of the system. Indeed, the temperature equilibrium allows to define the equilibrium fraction $\bar{\xi}_k$, see also equation (3.17), such that :

$$T_l \left(\tau, (1 - \bar{\xi}_k) s \right) = T_k \left(\tau, \bar{\xi}_k s \right),$$

where s is the total entropy depending on τ and e. We thus get an implicit definition of the equilibrium fraction as a function of τ and e (or s) : $\overline{\xi}_k(\tau, e)$. This implies that the total pressure law is modified when considering temperature equilibrium, it now only depends on τ and e : $(\tau, e) \mapsto P(\overline{\xi}_k(\tau, e), \tau, e)$.

In this section, we first describe the mixture pressure law that accounts for the instantaneous temperature equilibrium. Then, on the basis of this pressure law, the case of a single shock is studied as for the model proposed in Sergey GAVRILYUK et Richard SAUREL 2006.

Remark 15 It is an important point to be quoted that the **EOS** for the laminar contribution is slightly different from that used in section 4. In the present section it also corresponds to a perfect gas **EOS**, but with a different temperature law. The laminar **EOS** used in present section (5) does not allow to compute explicitly the shocks, whereas the laminar **EOS** of section (4) does not allow to compute explicitly the pressure law for temperature equilibrium. Two different choices have thus been made in order to perform analytical analysis of the solutions and to build verification test cases for section (6).

5.1. Pressure law for temperature equilibrium

We describe here the pressure law that corresponds to an instantaneous temperature equilibrium. The **EOS** that are considered here are the following. For the laminar contribution we choose :

$$e_l(\tau, s_l) = \tau^{1-\gamma} exp(\frac{s_l - s_{l0}}{C_v}), \tag{3.37}$$

where $C_v > 0$ is the heat capicity, γ is the adiabtic coefficient ($\gamma > 1$), and s_{l0} is a reference specific entropy. Concerning the turbulent part, the **EOS** is the same than in section 4 :

$$e_k(s_k, \tau) = A_0 s_k \tau^{-2/3}, \tag{3.38}$$

where $A_0 > 0$ is a constant to be defined. These **EOS** have been chosen in agreement with those used in Sergey GAVRILYUK, Jean-Marc HÉRARD, Olivier HURISSE et al. 2022 or Sergey GAVRILYUK et Richard SAUREL 2006, but it should be noticed that the turbulent energy e_k is not convex with respect to (τ, s_k) and condition (3.26) can not be used in order to get the hyperbolicity of the model.

By using the Gibbs relation for each contribution, we get the temperature laws :

$$T_k = \frac{\partial e_k}{\partial s_k}|_\tau = A_0 \tau^{-2/3}, \quad T_l = \frac{\partial e_l}{\partial s_l}|_\tau = \frac{e_l}{C_v}. \tag{3.39}$$

It should be noted that the laminar temperature T_l does not depend on τ, and that the turbulent temperature T_k does not depend on the energy e_k. The temperature

equilibrium $T_l = T_k$ then imposes the following relation between e_l and τ :

$$e_l(\tau, e) = C_v A_0 \tau^{-2/3}. \tag{3.40}$$

Hence, by introducing this relation into the laminar entropy using (3.37), we obtain :

$$s_l(\tau, e) = C_v ln(C_v A_0 \tau^{\gamma-5/3}) + s_{l0}. \tag{3.41}$$

The total specific energy of the mixture is given by : $e = e_k + e_l$, therefore using (3.40) the turbulent energy is :

$$e_k(\tau, e) = e - el = e - C_v A_0 \tau^{-2/3}, \tag{3.42}$$

and the turbulent entropy s_k reads thanks to (3.38) :

$$s_k(\tau, e) = e A_0^{-1} \tau^{2/3} - C_v. \tag{3.43}$$

The entropy fraction at temperature equilibrium $\overline{\xi}_k = s_k/(s_l + s_k)$ is obtained thanks to relation (3.41) and (3.43) :

$$\overline{\xi}_k(\tau, e) = \frac{s_k}{s_k + s_l} = \frac{e A_0^{-1} \tau^{2/3} - C_v}{e A_0^{-1} \tau^{2/3} - C_v + C_v \ln\left(C_v A_0 \tau^{\gamma-5/3}\right) + s_{l0}}. \tag{3.44}$$

It should be noted that s_{l0} should be chosen large enough so that the denominator of (3.44) does not vanish; moreover C_v and A_0 should be chosen so that s_k remains positive for the problem considered. Let us now turn to the pressure law. Using the definition of the pressure laws of each contribution and equations (3.41) and (3.43), we have :

$$P_k(\tau, e) = -\frac{\partial e_k}{\partial \tau|_{s_k}} = \frac{2}{3}(e\tau^{-1} - A_0 C_v \tau^{-5/3}) \tag{3.45}$$

$$P_l(\tau, e) = -\frac{\partial e_l}{\partial \tau|_{s_l}} = (\gamma - 1)\tau^{-5/3} C_v A_0. \tag{3.46}$$

It should be remarked that P_l only depends on τ. Finally, the total pressure at equilibrium is :

$$P(\tau, e) = P_l(\tau, e) + P_k(\tau, e) = \frac{2}{3} e\tau^{-1} + (\gamma - 5/3)\tau^{-5/3} C_v A_0. \tag{3.47}$$

At last, the sound speed associated with the pressure law can be computed from (3.47) with the formula :

$$c^2(\tau, e) = \partial_\rho P_s = -\tau^2 \partial_\tau P(\tau, e)_{|e} + \tau^2 P \partial_e (P(e, \tau)_{|\tau}$$

and we obtain :

$$c^2(\tau, e) = \frac{10}{9} e + \frac{7}{3}(\gamma - 5/3) C_v A_0 \tau^{-2/3}. \tag{3.48}$$

Let us now study the domain of hyperbolicity of the model through the definition

of the sound speed (3.48). First of all, since $e > 0$ and $\tau > 0$, we obtain easily that for $\gamma \geq 5/3$ both the square of the sound speed and the pressure P are non-negative.

It thus remains to study the case where $\gamma < 5/3$. Until the end of the present section, we assume $\gamma < 5/3$. By comparing definition of the pressure (3.47) and definition of the sound speed (3.48), it can be noticed that for $\gamma < 5/3$ we have : $P(\tau, e) > 0 \Rightarrow c^2(\tau, e) > 0$. Moreover, these definitions allow to express the sound speed as a function of the pressure P and the specific volume τ :

$$c^2(\tau, e) = \frac{5}{3} P\tau + \frac{2}{3}(\gamma - 5/3) C_v A_0 \tau^{-2/3},$$

and then, using formula for the laminar pressure at temperature equilibrium (3.46) we get :

$$c^2(\tau, e) = \frac{5}{3}\, P\tau + \frac{2}{3} \frac{(\gamma - 5/3)}{\gamma - 1}\, P_l \tau. \tag{3.49}$$

We choose here to express the hyperbolicity constraint in the plane (P, P_l). It will be useful in section 5.2 for expressing jump relations in a shock. From relation (3.49), we obtain that :

$$c^2(\tau, e) > 0 \Longleftrightarrow \frac{P}{P_l} > -\frac{2}{5} \frac{(\gamma - 5/3)}{\gamma - 1}, \tag{3.50}$$

where $P_l > 0$ for $\tau > 0$ and $e > 0$, but P may be negative (since P_k can be negative). We recall that we have chosen here $\gamma < 5/3$. The model is not unconditionally hyperbolic since constraint (3.50) depends on the variables ((P, P_l) or (τ, e)). Numerical tests should be chosen carefully so that the variables of the model remain in the hyperbolicity domain.

Remark 16 Constraint (3.50) can also be written :

$$\frac{P_k}{P_l} > -1 - \frac{2}{5} \frac{(\gamma - 5/3)}{\gamma - 1} = \frac{-7/5\gamma + 5/3}{\gamma - 1}. \tag{3.51}$$

This relation states that for a given pressure $P_l > 0$ the turbulent contribution P_k can not be too small with respect to P_l. Moreover, one may want to be able to reach the limit case $P_k = 0$. This is possible if we have in (3.51) :

$$-7/5\gamma + 5/3 < 0 \Longleftrightarrow \gamma > \frac{25}{21}$$

For $\gamma \leq 25/21$, the state $P_k = 0$ does not belong to the hyperbolicity domain, which forbids purely laminar cases for the present model with temperature equilibrium.

5.2. Study of the jump relations in a 1-shock with temperature equilibrium

In the following, the jump relation across a 1-shock wave is studied for the model involving temperature equilibrium. The 1-shock wave separates the left state, denoted by a subscript L, and an intermediate state denoted by a subscript 1. The jump relations associated with a 1-shock with temperature equilibrium are :

$$\begin{cases} -\sigma[\rho]_L^1 + [\rho u]_L^1 = 0, \\ -\sigma[\rho u]_L^1 + \left[\rho u^2 + P\right]_L^1 = 0, \\ -\sigma[\rho E]_L^1 + \left[u\left(\rho E + P\right)\right]_L^1 = 0. \end{cases} \tag{3.52}$$

where $E = e + u^2/2$ is the total energy, σ is the speed of the shock, and $P = P(\tau, e)$ stands for the pressure defined in the previous section by equation (3.47). These jump relations can also be written in the following form :

$$\begin{cases} \sigma = [\rho u]_L^1 / [\rho]_L^1, \\ \rho_1 \rho_L ([u]_L^1)^2 = [P]_L^1 [\rho]_L^1, \\ 2[e]_L^1 + (P_1 + P_L)[\dfrac{1}{\rho}]_L^1 = 0. \end{cases} \tag{3.53}$$

We assume that the left state $(\tau, e, u)_L$ is known and such that the pressure P_L is non-negative : $P_L > 0$. We seek for the possible intermediate states $(\tau, e, u)_1$ that can be connected to this left state through a 1-shock. For that purpose, we set :

$$z_1 = \frac{\rho_1}{\rho_L}.$$

Across a 1-shock wave we have necessarily $z_1 > 1$. Pressure law for equilibrium temperature (3.47) can also be written :

$$e(\tau, P) = \frac{3}{2} P\tau - \frac{3}{2}(\gamma - 5/3) A_0 C_v \tau^{-2/3}. \tag{3.54}$$

Then, using the third equation of (3.53) and (3.54), we get the following formula for the pressure P_1 with respect to z_1 and to the left state :

$$P_1 = P_L h_1(z_1; P_L, P_{l,L}), \tag{3.55}$$

with :

$$h_1(z_1; P_L, P_{l,L}) = \frac{(4z_1 - 1) + B(z_1^{5/3} - z_1)}{(4 - z_1)}, \text{and } B = 3\frac{\gamma - 5/3}{\gamma - 1}\frac{P_{l,L}}{P_L}, \tag{3.56}$$

where it has been assumed that $P_L > 0$. The pressure P_1 is thus defined through (3.55) for $z_1 \in [1, 4[$. By introducing relation (3.55) into second jump relation of (3.53), we

obtain for the velocity :

$$u_1 = u_L - f_1(z_1; P_L, \tau_L), \tag{3.57}$$

with :

$$f_1(z_1; P_L, P_{l,L}) = \left(\frac{(z_1 - 1)}{z_1} (h_1(z_1; P_L, P_{l,L}) - 1) \frac{P_L}{\rho_L(P_{l,L})} \right)^{1/2}. \tag{3.58}$$

It is an important point to be quoted that this relation can be defined only if $h_1(z_1; P_L, P_{l,L}) \geq 1$. Otherwise, the product $[P]_L^1 [\rho]_L^1$ is non-positive and $([u]_L^1)^2$ is not defined in the real space, so that no admissible shock wave can be defined. It should also be recalled that, in the definition above of f_1, the density ρ_L can be expressed with respect to $P_{l,L}$ thanks to (3.46).

On the basis of these first relations, some properties of variation across a 1-shock are studied in the following subsections. Let us start by some remarks that are used in the following. First, $z_1 \in [1,4[$ and $\tau_L > 0$ imply that $\tau_1 > 0$, $P_L > 0$ and $P_{1,L} > 0$. We also assume that $P_{k,L} > 0$. Moreover, $z_1 \in [1,4[$ implies that $[\rho]_L^1 \geq 0$. So that, when focusing on the second jump relation in (3.53), the velocity jump is admissible if and only if $[P]_L^1 \geq 0$ or, equivalently, if and only if h_1 is greater or equal to 1. We obviously always have $h_1(1; P_L, P_{l,L}) = 1$. At last, let us note that, since $\gamma > 1$, the previous inequalities gives that the sign of B is the same that the sign of $\gamma - 5/3$.

5.2.1. Study of the ratio P_1/P_L in a 1-shock wave

The function $h_1 = P_1/P_L$ defined (3.56) is now studied with respect to $z_1 \in [1,4[$. Several cases can then be distinguished for h_1.

• **case 1 :** $\gamma \geq 5/3 \Longleftrightarrow B \geq 0$**.**
The function $z_1 \mapsto h_1$ is then increasing on $[1,4[$ and h_1 tends to $+\infty$ when z_1 tends towards 4. We thus have $P_1 > P_L$ for all $z_1 \in [1,4[$. it should be noticed that the choice $\gamma = 5/3$ is very peculiar since the formula for h_1 then exactly corresponds to the formula obtained for Euler system for perfect gases and without turbulence. Laminar and turbulent energies, and consequently the energy e, have then the same dependence on the specific volume, that is $\tau^{-2/3}$.

• **case 2 :** $\gamma < 5/3 \Longleftrightarrow B < 0$**.**
In this case, 2 sub-cases are distinguished depending on the value of B. For the left state and when $\gamma - 5/3 < 0$, hyperbolicity constraint (3.50) leads to :

$$\frac{P_L}{P_{l,L}} < -\frac{2}{5} \frac{(\gamma - 5/3)}{\gamma - 1} \Longleftrightarrow B > \frac{-15}{2}.$$

We thus do not consider here the case $B \leq \frac{-15}{2}$. A second threshold is introduced now : $\frac{-15}{4(4^{2/3}-1)} = \frac{-15}{2} \frac{1}{2(4^{2/3}-1)}$, which is greater than $\frac{-15}{2}$ because $2(4^{2/3} - 1) > 1$. For the two sub-cases above, examples of function h_1 are plotted in figure 3.1.

1. If $\frac{-15}{2} < B < \frac{-15}{4(4^{2/3}-1)}$, the function $z_1 \mapsto h_1$ is increasing on the interval $[1, z_1^m]$ and

decreasing on the interval $[z_1^m, 4[$. It vanishes at $z_1 = z_1^* > z_1^m$, i.e. $h_1(z_1^*; P_L, P_{l,L}) = 0$, and it tends to $-\infty$ when z_1 tends to 4. In this case, even if we are in the domain of hyperbolicity ($B > -15/2$), admissible shock waves can only be defined for $z_1 \leq z_1^M$, where z_1^M is the unique solution of the equation $h_1(z_1^M; P_L, P_{l,L}) = 1$.

2. If $B > \frac{-15}{4(4^{2/3}-1)}$, the function $z_1 \mapsto h_1$ is increasing on $[1,4[$ and it tends towards $+\infty$ when z_1 tends towards 4. Hence, for this case shock waves are always admissible in the sense that the pressure jump implies $([u]_L^1)^2 \geq 0$.

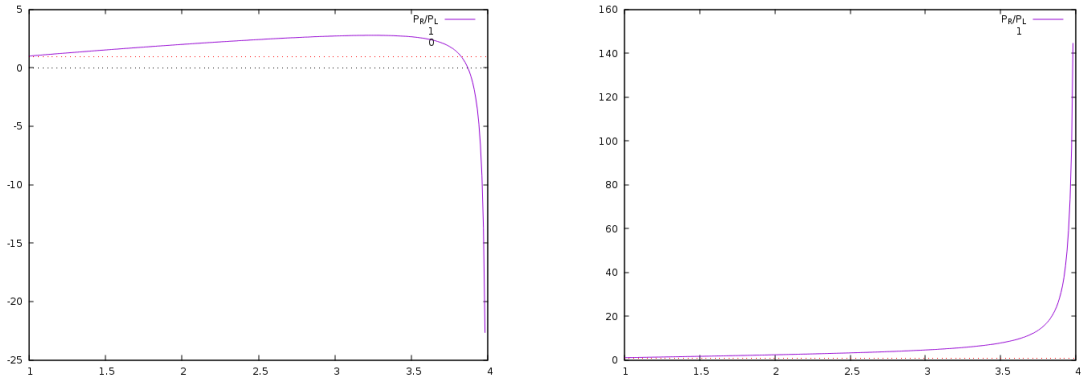

FIGURE 3.1. – Example of the behavior of the pressure ratio $h_1 = P_1/P_L$ as a function of z_1, for case 2 with $\gamma < 5/3$: case 2.1 on the left, and case 2.2 on the right.

Remark 17 When $B \leq \frac{-15}{2}$, the study of function h_1 shows that it is strictly decreasing with respect to z_1 so that shock waves cannot be defined (in that case, the sole admissible shock is for $z_1 = 1$, which corresponds to a ghost wave).

5.2.2. Study of the turbulent pressure P_k behind a 1-shock wave

It has been shown in section 5.1 that we have the relation $P > 0 \Rightarrow c^2 > 0$. Thus, since the laminar pressure P_l is always non-negative, a sufficient condition to get hyperbolicty is to have $P_k > 0$. By using pressure definitions (3.45), (3.46), (3.47) and pressure ratio (3.55), it can be shown that we have :

$$P_{k,1} = P_{k,L}\, h_1(z_1; P_L, P_{l,L}) - z_1^{5/3} P_{l,L}. \tag{3.59}$$

We define the function g_1 for $z_1 \in [1,4[$ as :

$$g_1(z_1; P_L, P_{l,L}) = \left(1 + \frac{P_{l,L}}{P_{k,L}}\right) \frac{\left(4z_1 - 1 + B(z_1^{5/3} - z_1) - 4\frac{P_{l,L}}{P_L} z_1^{5/3} + \frac{P_{l,L}}{P_L} z_1^{8/3}\right)}{4 - z_1}, \tag{3.60}$$

so that we have :

$$P_{k,1} = P_{k,L}\, g_1(z_1; P_L, P_{l,L}). \tag{3.61}$$

Studying the function $g_1(z_1; P_L, P_{lL})$ is complex because of the several different test cases that are encountered depending on the EOS parameters and on the pressure ratio $P_{l,L}/P_L$ on the left state. For the sake of readability, the details of this study have been reported in appendix D. For $\gamma > 5/3$ the function g_1 is strictly increasing with respect to z_1. While for a given ratio $P_{l,L}/P_L$ and for $\gamma < 5/3$ g_1, g_1 can be increasing or decreasing with respect to z_1 depending on the choice of the EOS parameters. Some example of plots of the function g_1 with respect to z_1 are shown in figure 3.2 for $\gamma < 5/3$.

Remark 18 The main conclusion of this study is that the turbulent pressure gap in a 1-shock has a different behavior for the present model and for the model proposed in Sergey GAVRILYUK et Richard SAUREL 2006.

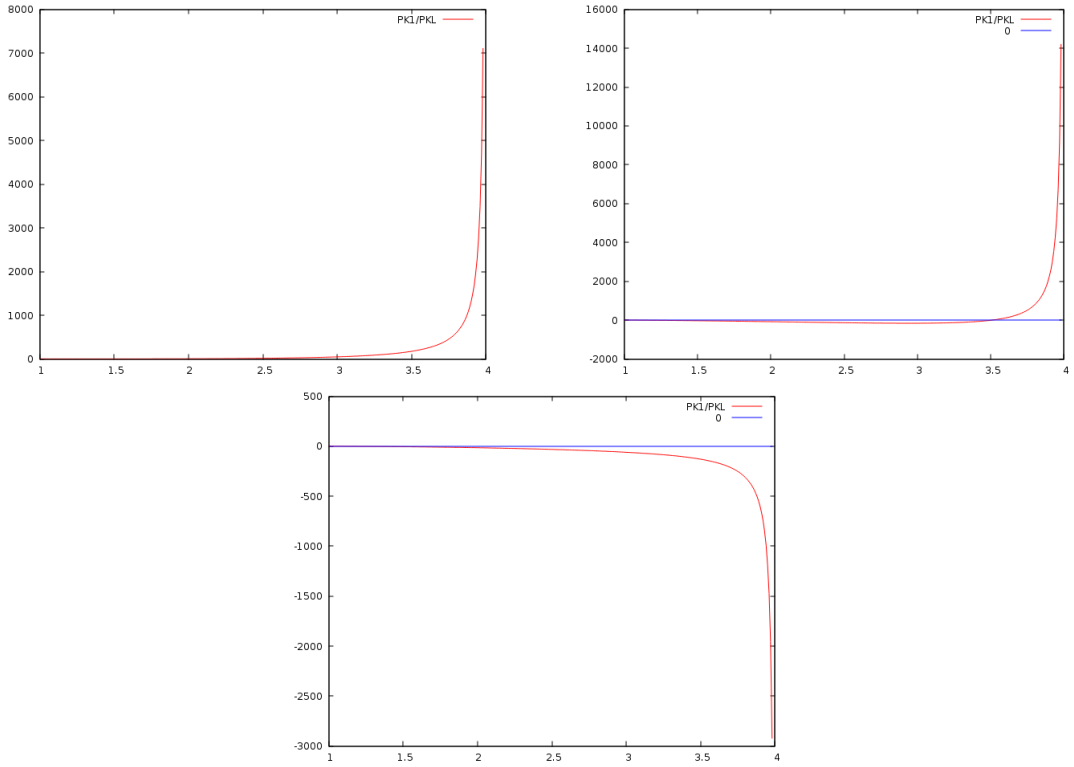

FIGURE 3.2. – Examples for the ratio Pk_1/Pk_L with respect to z_1 and for $\gamma < 5/3$.

6. Numerical scheme

The global numerical method is based on a fractional step method YANENKO 1968 using a Lie-Trotter splitting. The intial condition problem associated with system of equation (3.11) can be written :

$$\frac{\partial}{\partial t}(w) = -\frac{\partial}{\partial x}(\mathscr{F}(w)) + S(w), \quad w(t=0) = w^0, \tag{3.62}$$

where $\mathscr{F}$ corresponds to the convective flux and S to the source terms. The fractional step method used here consists in solving at time $t = t^n$ two sub-systems during a time step Δt^n. We assume that the approximated solution w^n is known at time t^n. The two problems to be solved are :

$$\frac{\partial}{\partial t}(w_a) + \frac{\partial}{\partial x}(\mathscr{F}(w_a)) = 0, \quad w_a(t=0) = w^n, \qquad \textit{(convection step)}, \tag{3.63}$$

which gives $w_a(\Delta t^n)$;

$$\frac{\partial}{\partial t}(w_b) = S(w_b), \quad w_b(t=0) = w_a(\Delta t^n), \qquad \textit{(source term step)}. \tag{3.64}$$

The approximated solution a time $t^{n+1} = t^n + \Delta t^n$ is then $w^{n+1} = w_b(\Delta t^n)$. Since this splitting is first order with respect to time, each sub-sytem is solved using first order schemes.

The first sub-system (3.63) takes into account the convective part. For that purpose, first order explicit and conservative finite volume schemes are considered. The general form for a one-dimensional framework reads as follows :

$$\Delta x_i(w_i^{n+1} - w_i^n) + \Delta t^n(F(w_{i+1}^n, w_i^n) - F(w_i^n, w_{i-1}^n)) = 0, \tag{3.65}$$

where w_i^n denotes the value of the approximated solution in cell i at iteration t^n. The time step Δt^n is computed from the variable w_i^n and from the mesh size $\Delta x_i = x_{i+1/2} - x_{i-1/2}$ ($x_{i+1/2}$ represents the cell interface between cells i and $i+1$) in order to fulfill a stability constraint. The numerical flux F depends on the numerical scheme. In the following, the **VFRoe-ncv** scheme (see BUFFARD, Thierry GALLOUËT et Jean-Marc HÉRARD 2000) using variables (ξ_k, U, P, s) has been retained. The computation of the numerical flux F according to this scheme is detailed in section 6.1.

The second sub-system (3.64) corresponds to a system of ordinary differential equations. In this sub-system, the return to the temperature equilibrium is accounted for. Since the time-step is computed to fulfill a stability constraint of the numerical scheme used for the first sub-system, this second step is achieved using an implicit scheme. The latter is detailed in section 6.3.

Remark 19 For the sake of simplicity, each sub-system is solved using a unique time-step and the time-step for solving the source-term step is the time-step computed for the convective part.

6.1. Numerical scheme for the convective fluxes

This section describes the numerical scheme used to compute the two-point numerical fluxes F at an interface separating two successive cells. The value of the different

quantities in the cell on the left (respectively right) on the interface are denoted by a subscript L (respectively R). The fluxes are computed using the VFRoe-ncv scheme using the variables (ξ_k, U, P, s) for system of equations :

$$\begin{cases} \partial_t \rho\xi_k + \partial_x \rho U\xi_k = 0, \\ \partial_t \rho + \partial_x \rho U = 0, \\ \partial_t \rho U + \partial_x \rho U^2 + P = 0, \\ \partial_t \rho E + \partial_x U(\rho E + P) = 0, \end{cases} \tag{3.66}$$

Let us define $Z = (\xi_k, U, P, s)$. When considering regular solutions, conservative system (3.66) may be rewritten in a non-conservative form using Z :

$$\partial_t Z + B(Z)\partial_x Z = 0, \tag{3.67}$$

where the convection matrix $B(Z)$ is :

$$B(Z) = \begin{pmatrix} U & 0 & 0 & 0 \\ 0 & U & \tau & 0 \\ 0 & \rho c^2 & U & 0 \\ 0 & 0 & 0 & U \end{pmatrix},$$

where c is the sound speed. System of equations (3.67) is then replaced by the following linearized system :

$$\partial_t Z + B(\bar{Z})\partial_x Z = 0, \tag{3.68}$$

where $\bar{Z} = (Z_L + Z_R)/2$. It is an important point to be quoted that, in system (3.68), the Jacobian matrix $B(\bar{Z})$ does not depend on Z (the system becomes linear). All the characteristic fields of system (3.68) are then linearly degenerate, and the solution of the associated Riemann problems can easily be computed explicitly.
Riemann problems are indeed considered now for system (3.68) with initial conditions composed of the two uniform states Z_L and Z_R :

$$Z(x < 0, t = 0) = Z_L, and Z(x > 0, t = 0) = Z_R. \tag{3.69}$$

The exact solution $Z^*(x/t = 0; Z_L, Z_R)$ of the Riemann problem at the interface $x/t = 0$ for system (3.68) with initial conditions (3.69) is :

$$Z^*(x/t = 0; Z_L, Z_R) = \begin{cases} Z_L \text{ if } \bar{\lambda}_1 \geq 0; \\ Z_1 \text{ if } \bar{\lambda}_1 < 0 \text{ and } \bar{\lambda}_{2,3} \geq 0; \\ Z_2 \text{ if } \bar{\lambda}_{2,3} < 0 \text{ and } \bar{\lambda}_4 \geq 0; \\ Z_R \text{ if } \bar{\lambda}_4 < 0; \end{cases} \tag{3.70}$$

where the eigenvalues of the linearized system (3.68) are :

$$\bar{\lambda}_1 = \bar{U} - c(\bar{Z}), \quad \bar{\lambda}_{2,3} = \bar{U}, \quad \bar{\lambda}_4 = \bar{U} + c(\bar{Z}).$$

The two intermediate states denoted here by subscripts 1 and 2 are defined by :

$$\xi_{k,1} = \xi_{k,L}, \qquad \xi_{k,2} = \xi_{k,R}, \tag{3.71}$$

$$U_1 = U_2 = \bar{U} - \frac{1}{2\rho(\bar{Z})c(\bar{Z})}(P_R - P_L), \tag{3.72}$$

$$P_1 = P_2 = \bar{P} - \frac{1}{2\rho(\bar{Z})c(\bar{Z})}(U_R - U_L), \tag{3.73}$$

$$s_1 = s_L, \qquad s_2 = s_R, \tag{3.74}$$

Finally, the numerical flux for the VFRoe-ncv scheme used here is obtained by using the approximated solution (3.70) at the interface. That is, when considering the two successive cells i and $i+1$, the fluxes in (3.65) are :

$$F(w_{i+1}^n, w_i^n) = \mathscr{F}(Z^*(x/t=0; Z_i^n, Z_{i+1}^n),$$

where $Z \mapsto \mathscr{F}(Z)$ is the analytical flux of system (3.66) written for the variable Z :

$$\mathscr{F}(Z) = \left(\rho(Z)U\xi_k,\ \rho(Z)U,\ \rho(Z)U^2 + P,\ (\rho e)(Z) + \rho(Z)UP \right).$$

6.2. Numerical scheme for the source terms

Sub-system (3.64) for the source terms corresponds to a system of ordinary differential equations. It reads :

$$\begin{cases} \partial_t \xi_k = \frac{\bar{\xi_k}(\tau,e) - \xi_k}{\lambda(t)}, \\ \partial_t \rho = 0, \\ \partial_t \rho U = 0, \\ \partial_t \rho E = 0, \end{cases} \tag{3.75}$$

where the relaxation time λ may depends on the other variables and/or on the time. By combining the last three equations of system (3.80), it can first be noted that the specific volume, the velocity and specific energy are constant : $\partial_t \tau = \partial_t U = \partial_t e = 0$. Therefore, the source term in the equation for ξ_k in (3.80) can be written in an equivalent manner :

$$\partial_t \xi_k(t) = \frac{\bar{\xi_k}(\tau(t=0), e(t=0)) - \xi_k(t)}{\lambda(t)}, \tag{3.76}$$

Obviously, when the relaxation time λ is constant, equation (3.81) can be exactly integrated. When λ is not constant, equation (3.81) can be approximated by the linearized equation :

$$\partial_t \xi_k(t) = \frac{\bar{\xi_k}(\tau(t=0), e(t=0)) - \xi_k(t)}{\lambda(t=0)}, \tag{3.77}$$

where λ has been replaced by its initial value. The approximated solutions for the computation of the source terms are built on the basis of equation (3.82). If we assume that the variable (ξ_k, ρ, U, e) is known at time t^n, the approximated solution at time $t^{n+1} = t^n + 1$ is computed thanks to the exact solution of the initial value problem :

$$\partial_t \zeta(t) = \frac{\bar{\xi_k}(\tau^n, e^n) - \zeta(t)}{\lambda^n}, with \zeta(t=0) = \xi_k^n, \tag{3.78}$$

evaluated at time $t = \Delta t^n$: $\xi_k^{n+1} = \zeta(\Delta t^n)$. We then have :

$$\begin{cases} \xi_k^{n+1} = \xi_k^n \, e^{(-\Delta t^n/\lambda^n)} + \bar{\xi}_k(\tau^n, e^n) \, \left(1 - e^{(-\Delta t^n/\lambda^n)}\right), \\ \rho^{n+1} = \rho^n, \\ U^{n+1} = U^n, \\ e^{n+1} = e^n. \end{cases} \tag{3.79}$$

This scheme has several interesting properties. Obviously, if λ is constant, the scheme performs an exact integration. When λ is not constant, the scheme is first order but it remains very accurate in particular when the time step is small with respect to the characteristic variations of λ. Moreover, ξ_k^{n+1} is a barycentric formula, so that $\xi_k^{n+1} \in [\xi_k^n, \bar{\xi}_k(\tau^n, e^n)]$ whatever the time step is. Hence, if both ξ_k^n and $\bar{\xi}_k(\tau^n, e^n)$ belong to $[0,1]$, then ξ_k^{n+1} also belongs to $[0,1]$. At last, for situations with instantaneous relaxation, i.e. with : $\lim(\lambda^n/\Delta t^n) \to +\infty$; numerical scheme (3.84) gives : $\lim_{\lambda^n/\Delta t^n \to +\infty} (\xi_k^{n+1}) = \bar{\xi}_k(\tau^n, e^n)$. This scheme allows to treat the configurations with large or small ratio $\lambda^n/\Delta t^n$.

6.3. Numerical scheme for the source terms

Sub-system (3.64) for the source terms corresponds to a system of ordinary differential equations. It reads :

$$\begin{cases} \partial_t \xi_k = \frac{\bar{\xi_k}(\tau,e) - \xi_k}{\lambda(t)}, \\ \partial_t \rho = 0, \\ \partial_t \rho U = 0, \\ \partial_t \rho E = 0, \end{cases} \tag{3.80}$$

where the relaxation time λ may depends on the other variables and/or on the time. By combining the last three equations of system (3.80), it can first be noted that the specific volume, the velocity and specific energy are constant : $\partial_t \tau = \partial_t U = \partial_t e = 0$. Therefore, the source term in the equation for ξ_k in (3.80) can be written in an equivalent manner :

$$\partial_t \xi_k(t) = \frac{\bar{\xi_k}(\tau(t=0), e(t=0)) - \xi_k(t)}{\lambda(t)}, \tag{3.81}$$

Obviously, when the relaxation time λ is constant, equation (3.81) can be exactly integrated. When λ is not constant, equation (3.81) can be approximated by the

linearized equation :

$$\partial_t \xi_k(t) = \frac{\bar{\xi_k}(\tau(t=0), e(t=0)) - \xi_k(t)}{\lambda(t=0)}, \tag{3.82}$$

where λ has been replaced by its initial value. The approximated solutions for the computation of the source terms are built on the basis of equation (3.82). If we assume that the variable (ξ_k, ρ, U, e) is known at time t^n, the approximated solution at time $t^{n+1} = t^n + 1$ is computed thanks to the exact solution of the initial value problem :

$$\partial_t \zeta(t) = \frac{\bar{\xi_k}(\tau^n, e^n) - \zeta(t)}{\lambda^n}, \text{with} \zeta(t=0) = \xi_k^n, \tag{3.83}$$

evaluated at time $t = \Delta t^n$: $\xi_k^{n+1} = \zeta(\Delta t^n)$. We then have :

$$\begin{cases} \xi_k^{n+1} = \xi_k^n \, e^{(-\Delta t^n/\lambda^n)} + \bar{\xi}_k(\tau^n, e^n) \, \left(1 - e^{(-\Delta t^n/\lambda^n)}\right), \\ \rho^{n+1} = \rho^n, \\ U^{n+1} = U^n, \\ e^{n+1} = e^n. \end{cases} \tag{3.84}$$

This scheme has several interesting properties. Obviously, if λ is constant, the scheme performs an exact integration. When λ is not constant, the scheme is first order but it remains very accurate in particular when the time step is small with respect to the characteristic variations of λ. Moreover, ξ_k^{n+1} is a barycentric formula, so that $\xi_k^{n+1} \in [\xi_k^n, \bar{\xi}_k(\tau^n, e^n)]$ whatever the time step is. Hence, if both ξ_k^n and $\bar{\xi}_k(\tau^n, e^n)$ belong to $[0,1]$, then ξ_k^{n+1} also belongs to $[0,1]$. At last, for situations with instantaneous relaxation, i.e. with : $\lim(\lambda^n/\Delta t^n) \to +\infty$; numerical scheme (3.84) gives : $\lim_{\lambda^n/\Delta t^n \to +\infty} (\xi_k^{n+1}) = \bar{\xi}_k(\tau^n, e^n)$. This scheme allows to treat the configurations with large or small ratio $\lambda^n/\Delta t^n$.

7. Numerical Results

Four numerical tests are presented in this section on the basis of Riemann problems. For all these tests, initial conditions and EOS parameters have been chosen so that the approximated solutions remain in the hyperbolicity domain (see section 4 and section 5). The computational domain is $[0,1]$ and the initial discontinuity is located at $x = 1/2$. The time step is computed for a CFL number of $1/2$. Convergence curves are then built thanks to the results of sections 4 and 5.

The first test case is directly related to the study of section 5 for an isolated 1-shock wave with temperature equilibrium. Approximated solutions obtained by using the full fractional step method described in section 6 are compared to the exact solution derived in section 5. The temperature equilibrium is thus imposed through the source term by setting the relaxation time-scale λ to zero.

In the second test case, the turbulent entropy s_k is chosen uniform while considering a double shock configuration. This situation is reminiscent from the ones tested with the model presented in chapter 1 Sergey GAVRILYUK, Jean-Marc HÉRARD, Olivier HURISSE et al. 2022. Nevertheless, it has been shown in section 2 that model (3.11) with uniform turbulent entropy is not equivalent to the model of chapter 1 Sergey GAVRILYUK, Jean-Marc HÉRARD, Olivier HURISSE et al. 2022 in the presence of a shock. Thus they can not be compared for this test case. For the third test case, the same wave configuration is tested with a non-uniform turbulent entropy. It should be added that for the second and third test case, source term for temperature equilibrium is not accounted for.

At last the fourth test case corresponds to a laminar-turbulent transition. A single shock wave is considered and separates two zones : one in which the velocity is equal to zero with a turbulent energy equal to zero, and a second one where instantaneous temperature equilibrium is considered. The relaxation time scale is chosen in order to ensure an instantaneous temperature relaxation in the turbulent domain, and no temperature relaxation in the laminar domain. Through the results of section 4 and 5, an exact solution of the associated Riemann problem can be exhibited. The speed of propagation of the approximated shock wave is then compared to the exact one.

Remark 20 In appendix C, a test case for a purely laminar situation has been added for the sake of completeness (i.e. $s_k = 0$, which corresponds to the Euler model with a perfect gas EOS).

7.1. Simple 1-shock wave with an EOS related to temperature equilbrium

For this test case, initial conditions of the Riemann problem are :

$$(\rho, U, P_l, e_k)_L = (1.185059, 0, 10^5, 12657.600000)$$

for the left state, and

$$(\rho, U, P_l, e_k)_R = (1.481323, -77.3142, 145049.651050, 373.434185)$$

for the right state. The EOS parameters are :

$$C_v = 720,\ A_0 = 261.64 \text{ and } \gamma = 1.4.$$

The associated analytical solution is a pure 1-shock wave, as studied in section 5.2. The $U + c$-wave and the contact wave are ghost waves.

The convergence curves for the approximated solutions obtained with the scheme of section 6 are plotted in figure (3.4). We recall that for this test case, temperature equilibrium is imposed for the approximated solutions by setting $\lambda \to 0^+$. The convergence rate for the finest meshes is still close to 1 for all the variables, except for the turbulent entropy fraction. For the latter, a convergence rate of 1/2 is recovered. This effective assymptotic rate of convergence should also be obtained for the other variables since the mixture EOS does not allow to preserve contact waves T. GALLOUËT, J.-M. HÉRARD et SEGUIN 2002.

In figure (3.3), the approximated solution is plotted for a mesh with 1000 uniform cells. It can be observed peaks located around the contact wave. This is a classical feature for conservative schemes that do not preserve the contact wave. Even if the $U + c$ wave is a ghost wave, it is not numerically ghost and 3-shock wave with a very small amplitude can be observed. These to features tend to disappear when the mesh is refined.

This test case shows that the fractional step approach proposed in 6 allows to compute approximate solutions for an instantaneous relaxation of the temperatures.

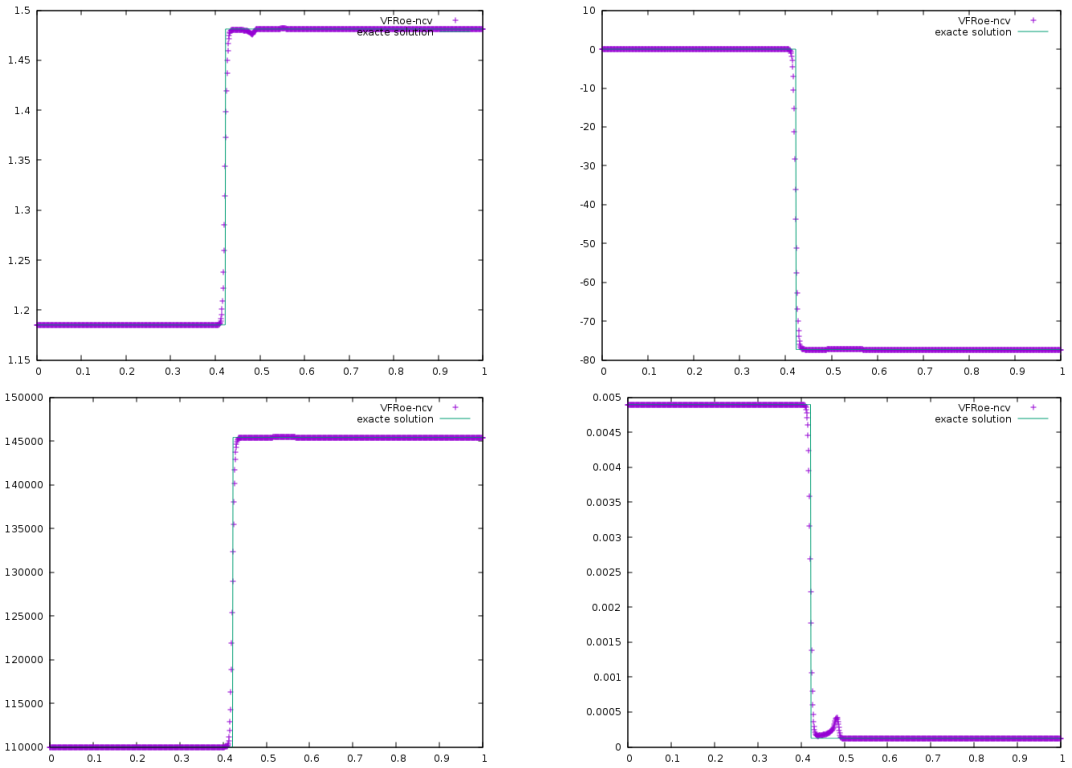

FIGURE 3.3. – Simple 1-shock test case 1. Density (top left), velocity (top right), pressure (bottom left) and ξ_k (bottom right). Comparison between the exact solution (green) and the approximate solution (purple) at $t = 2\ 10^{-4}$ s, $CFL = 0.5$, 1000 cells.

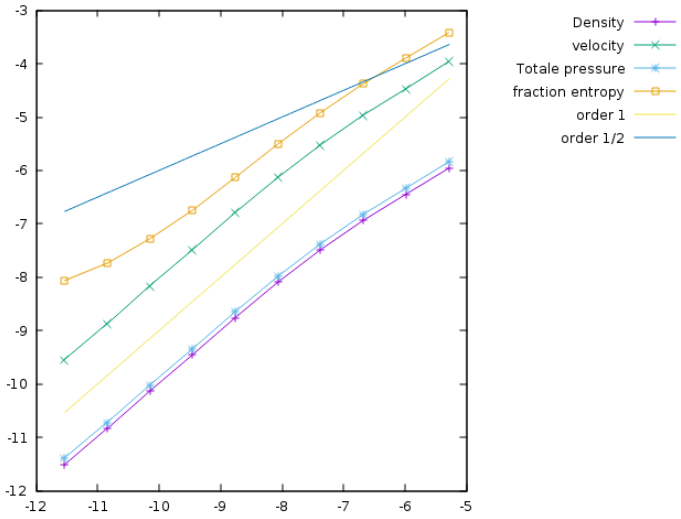

FIGURE 3.4. – Simple 1-shock test case 1. Convergence curves : logarithm of the relative L1-error versus the logarithm of the mesh size with uniform meshes containing from 200 to 100000 cells. The error is plotted for variables, ρ, u, P and ξ_k.

7.2. Double shock wave with an initial uniform turbulence level

For this test case, initial conditions of the Riemann problem are :

$$(\rho, U, P_l, e_k)_L = (1, 650, 10^6, 10^4)$$

for the left state, and

$$(\rho, U, P_l, e_k)_R = (1, -687.545913, 98007.273140, 10^4)$$

for the right state. The EOS parameters are :

$$C_v = 720,\ A_0 = 1 \text{ and } \gamma = 1.4.$$

The convergence curves for the approximated solutions obtained with the scheme of section 6 are plotted in figure 3.6 and the approximated solution is plotted for a mesh with 500 uniform cells in figure 3.5. This initial condition is such that $s_{k,L} = s_{k,R}$ and $\xi_{k,L} \neq \xi_{k,R}$. It produces two shock waves. It should be noted that the contact travels to the right of the domain. Accordingly to section 2, the turbulent entropy s_k is not uniform, i.e. $s_{k,L} \neq s_{k,1}$ and $s_{k,R} \neq s_{k,2}$ for $t > 0$. Moreover, it can be shown in figure 3.6 that the shock profiles are sharper than the contact profile, which is a classical behavior.

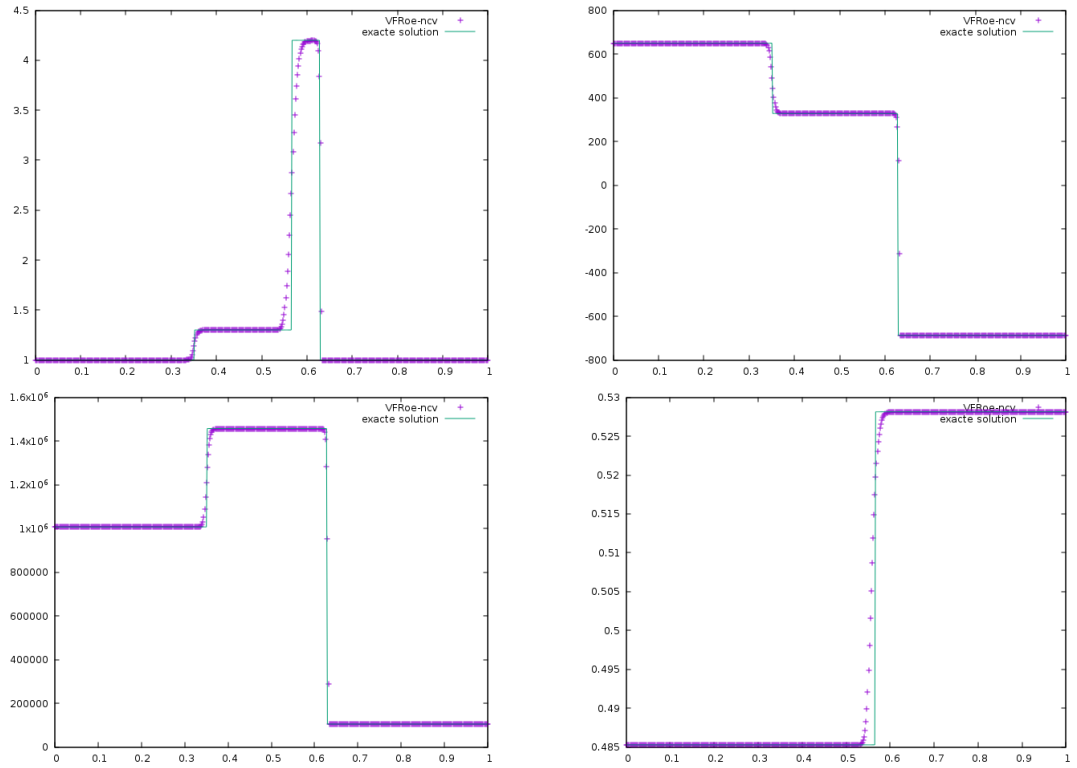

FIGURE 3.5. – Double-shock wave test case 2. Density (top left), velocity (top right), pressure (bottom left) and ξ_k (bottom right). Comparison between the exact solution (green) and the approximate solution (purple) at $t = 2\ 10^{-4}$ s, $CFL = 0.5$, 500 cells.

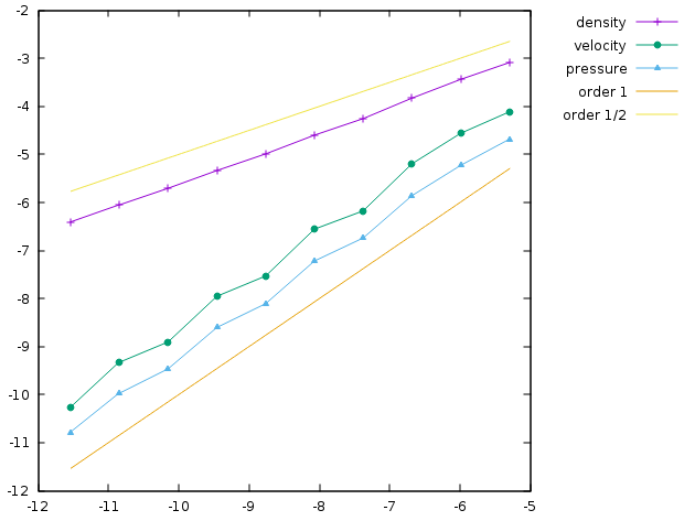

FIGURE 3.6. – Double-shock wave test case 2. Convergence curves : logarithm of the relative L1-error versus the logarithm of the mesh size with uniform meshes containing from 200 to 55000 cells. The error is plotted for variables, ρ, u, and P .

7.3. Laminar-turbulent transition through a shock wave

For this test case, initial conditions of the Riemann problem are :

$$(\rho, U, P_l, e_k)_L = (1, 0, 10^5, 0)$$

for the left state,and

$$(\rho, U, P_l, e_k)_R = (1.25, -96.432449, 145049.651050, 1735.721662)$$

for the right state. The EOS parameters are :

$$C_v = 720,\ A_0 = 198.412698 \text{ and } \gamma = 1.7 > 5/3.$$

It should be noticed that for these initial conditions, the analytical solution of the Riemann problem is only composed of two states separated by a 1-shock wave that travels from the right to the left. The left state is a purely laminar state with $e_{k,L} = 0$ with flow at rest $U_L = 0$, while for the right state the temperature equilibrium has been accounted for, and it thus contains a small amount of turbulent energy, i.e. $e_{k,R} > 0$. This test case involves a laminar-turbulent transition through the shock wave. Such a transition can only be obtained for $\gamma > 5/3$. Since the shock wave represents a pure discontinuity between left and right states, this analytical solution can be seen as the coupling of two different mixture EOS (purely laminar on the left and laminar-turbulent with temperature equilibrium on the right) through a 1-shock. It can thus be easily built on the basis of the theoretical results of the previous sections.

In a numerical point of view, this solution is approximated through the fractional step approach of section 6 by using a special law for the relaxation time-scale λ. Indeed, we set

$$\lambda(t,x) = \begin{cases} 10^{30} if |u(t,x)| < 10^{-4}, \\ 10^{-30} \quad \text{otherwise.} \end{cases}$$

In other words, if the velocity is locally high enough the temperature equilibrium is (instantaneously) enforced and turbulence is generated, whereas no turbulence is created if the flow remains at rest. The approximated solution is plotted in figure 3.7 for a mesh containing 500 uniform cells and the convergence curves are proposed in figure 3.8. From the latter, it can clearly be observed that the numerical procedure proposed in the previous sections produces convergent approximations. Since the contact wave is a ghost wave, we recover a rate of convergence of 1, as expected. Nonetheless, the results of figure 3.7 exhibit spurious over/under-shoots for the turbulent entropy fraction and for the density. They are located on the right of the position of the 1-shock and on the left of the initial discontinuity ($x = 0.5$), which corresponds to the position of the numerical contact wave. The latter is indeed not preserved by the VFRoe-ncv scheme. These spurious over/under-shoots vanish when the mesh is refined with a rate of convergence at least equal to 1, as confirmed by the convergence curves in figure 3.8.

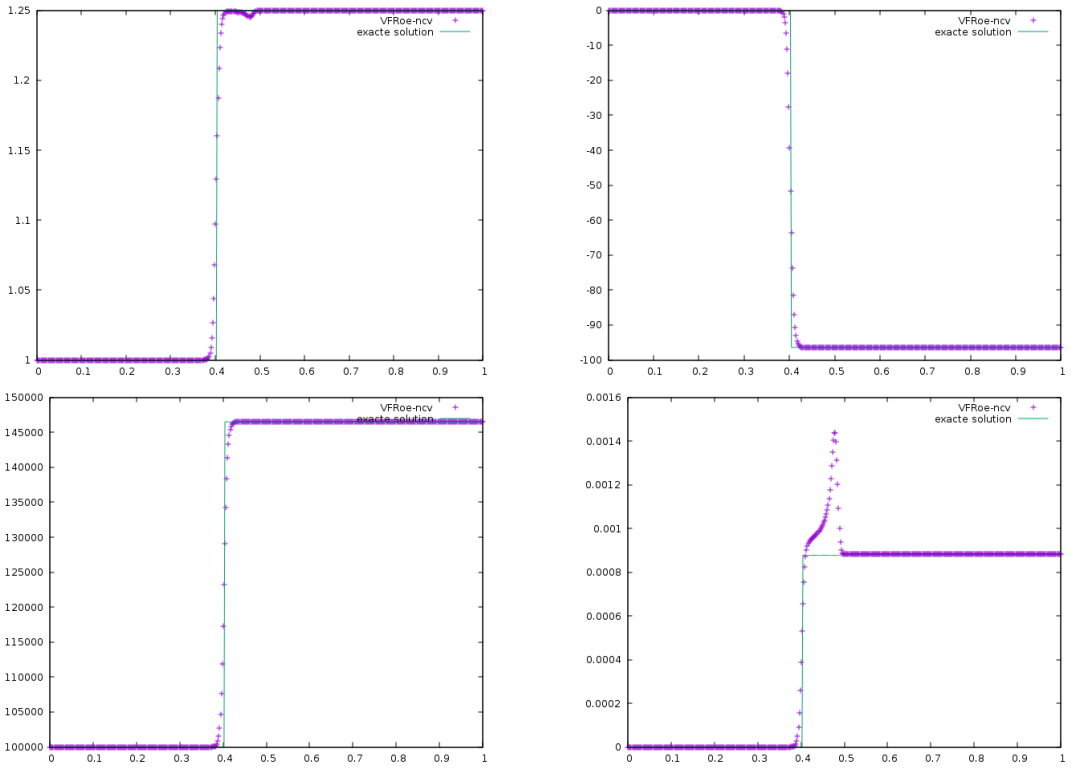

FIGURE 3.7. – Turbulent-laminar transition in a 1-shock. Density (top left), velocity (top right), pressure (bottom left) and ξ_k (bottom right). Comparison between the exact solution (green) and the approximate solution (purple) at $t = 2\ 10^{-4}$ s, $CFL = 0.5$, 500 cells.

On the basis of this Riemann problem involving a laminar-turbulent transition, some additional tests are performed. In figures 3.9 and 3.10, the sensitivity of the results to the level of e_k on the left side has been tested. With respect to the previous initial conditions, the left state is no more purely laminar. A small amount of turbulence has been introduced : $e_{k,L} = 2.169652$. The initial condition are then :

$$(\rho, U, P_l, e_k)_L = (1, 0, 10^5, 2.169652),$$

for the left state. The right states and the EOS parameters remain unchanged. It can be observed in figures 3.9 and 3.10 that the model and the numerical scheme behave continuously with respect to a small amount of turbulence in the left state. With several values of λ_0. When λ_0 is not equal to zero (or in a numerical point of view, when it becomes large enough with respect to the time-step) or $+\infty$, the solution is no more a pure 1-shock wave and the left/right states are separated by a regular profile. When λ_0 is large enough or small enough, 1-shock is recovered but with two different speeds of propagation. A classical result for convection-relaxation models is then observed : the "speed of propagation" of the gap between left and right states strongly depends

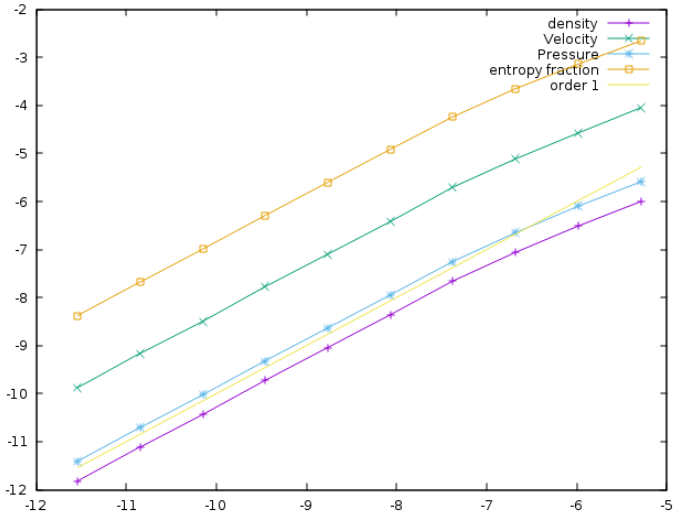

FIGURE 3.8. – Turbulent-laminar transition in a 1-shock. Convergence curves : logarithm of the relative L1-error versus the logarithm of the mesh size with uniform meshes containing from 200 to 10000 cells. The error is plotted for variables, ρ, u, P and ξ_k.

on the stiffness of the source terms, i.e. on the value of λ for the present model. In particular, the faster the creation of turbulence is (i.e. the more λ_0 is small), the faster the gap between left and right states travels.

Remark 21 Even if this has not been presented here, some sensitivity of the results has been observed with respect to the threshold of velocity in the definition of λ. Such a threshold effect is classical for stiff source terms. In our case, the transition from laminar to turbulent flow is clearly associated with the numerical diffusion. If needed, the speed of propagation of the laminar-turbulent front could be controled using techniques applied to reactive-front propagation. In particular, one may quote the *artificial thickening of the flame front* as proposed in BUTLER et O'ROURKE 1977. This method is widely used in combustion simulation and it is proven to be efficient.

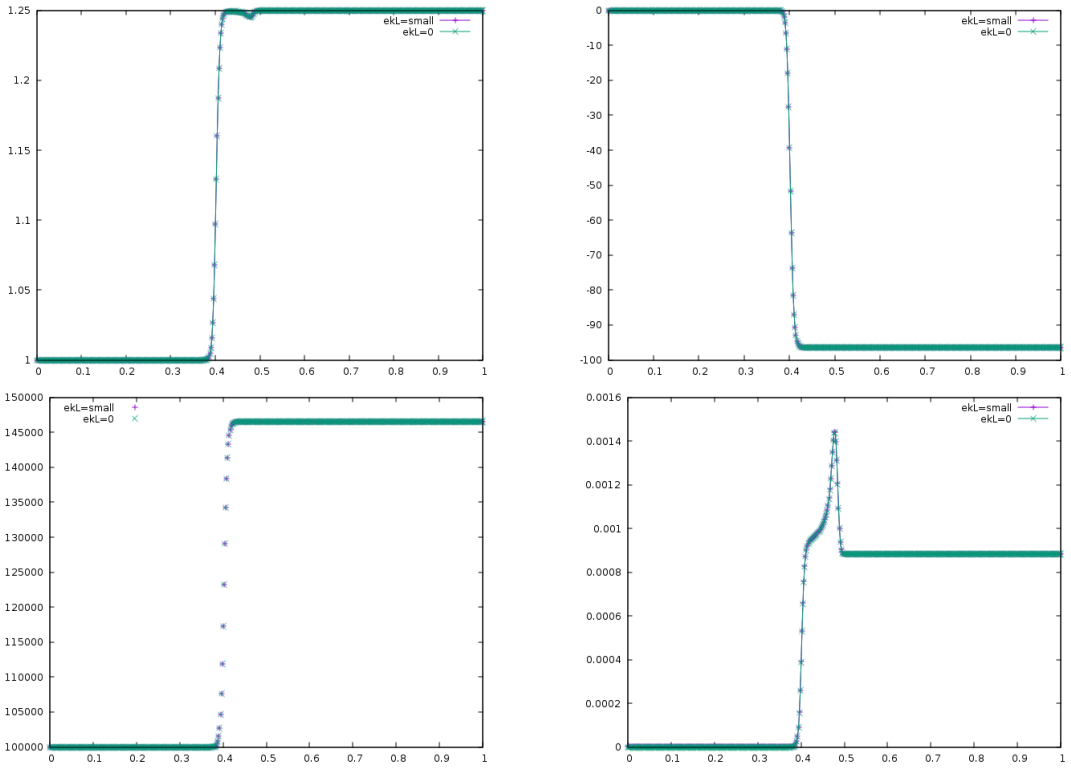

FIGURE 3.9. – Turbulent-laminar transition in a 1-shock. Density (top left), velocity (top right), pressure (bottom left) and ξ_k (bottom right). Comparison between solution of $e_{k,L} = 2.169652$ (small) (purple) and the solution of $e_{k,L} = 0$ (green) at $t = 2\ 10^{-4}$ s, $CFL = 0.5$, 500 cells.

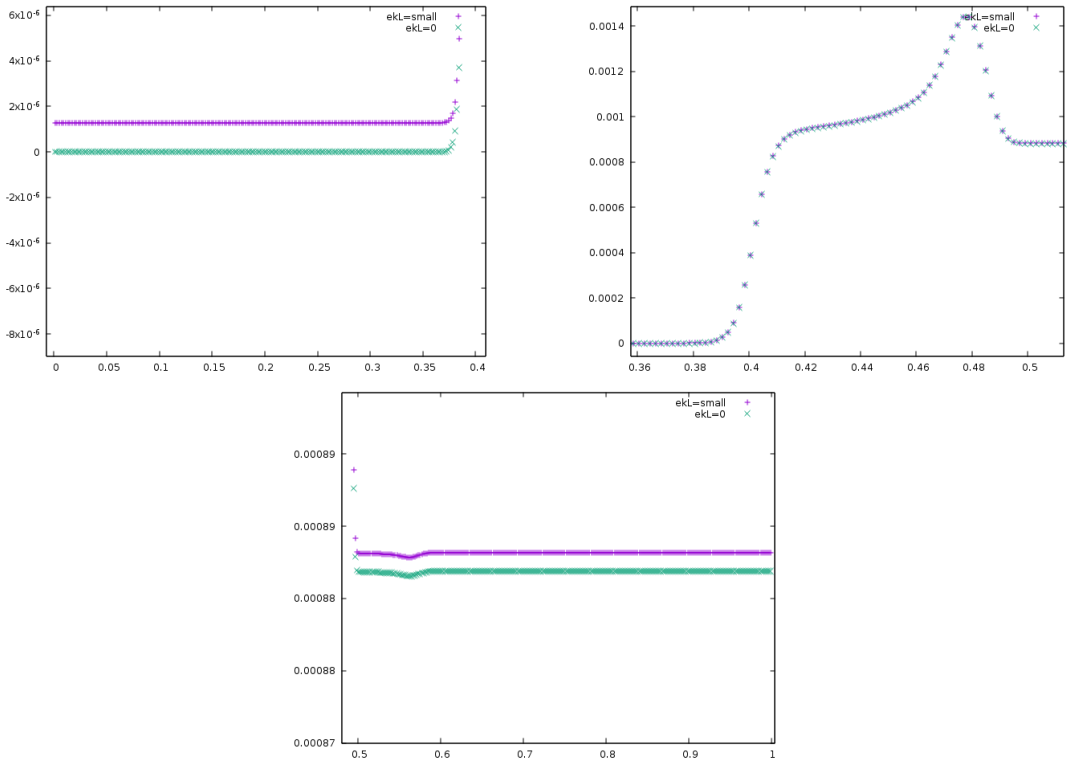

FIGURE 3.10. – Turbulent-laminar transition in a 1-shock. Zoom for entropy fraction ξ_k on multiple mesh domain at $t = 2\ 10^{-4}$ s, $CFL = 0.5$, 500 cells.

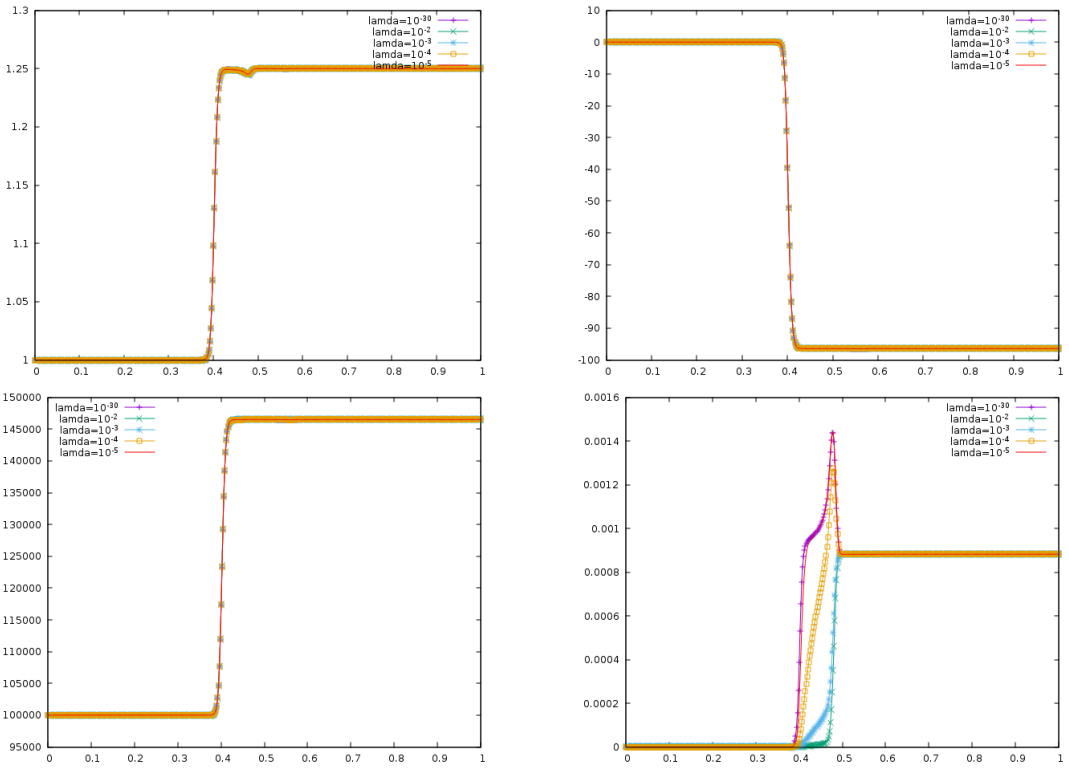

FIGURE 3.11. – Turbulent-laminar transition in a 1-shock. Density (top left), velocity (top right), pressure (bottom left) and ξ_k (bottom right). Comparison between different relaxation time scales $\lambda = 10^{-2}, 10^{-3}, 10^{-4}, 10^{-5}$ and 10^{-30} at $t = 2\ 10^{-4}$ s, $CFL = 0.5$, 500 cells.

8. Conclusion and perspectives

The model proposed in this work is built on thermodynamical assumptions. Classical techniques for mixture modelling are used and the turbulent flow is seen as a mixture of two miscible phases : a laminar phase and a turbulent phase. With regards to the models and/or numerical methods proposed in the first two chapters, the model studied here has some advantages. As for the model of the first chapter, the mathematical structure of the model is classical and no sophisticated numerical algorithms are required in order to perform numerical simulations. But, as for the work presented in chapter two, this model also enables to recover jumps of turbulent entropy across shock waves. This feature is obtained through the relaxation source term, which is defined in order to be in agreement with the second law of thermodynamics.

Nevertheless, this proposal was a first trial and several aspects still have to be improved. If the turbulent entropy jumps in the shocks, its increase or decrease does not seem in agreement with that of the proposition of Sergey GAVRILYUK et Richard SAUREL 2006, which has been studied in the second chapter. Several ways of improvements are possible. First, it should be noted that the choice of the turbulent EOS followed in the present chapter leads to some difficulties in the analysis of the property of the Rankine-Hugoniot relations. Others choices of turbulent EOS may allow better properties in the shocks. Indeed, some conditions have to be fulfilled here for defining correct shock waves, and the monotony of the evolution of the turbulent pressure in a shock depends on the initial condition and on the EOS parameters. Moreover, a less classical set for the mixture assumptions of the laminar and turbulent phases could be proposed in order to modify the mixture properties and/or the equilibirum condition. Indeed, in the present model the turbulent entropy jump in shocks are entirely defined through the Rankine-Hugoniot relations which are based on the thermodynamical mixture properties. Modifying the mixture has thus a strong impact on the turbulent entropy jump in shocks.

Acknowledgements The last author receives financial support by ANRT through an EDF/CIFRE grant number 2019/1580. Computational facilities were provided by EDF.

ANNEXES

A. Convexity properties

It has been assumed in section 1 that the specific energies $(\tau, s_l) \mapsto e_l(\tau, s_l)$ and $(\tau, s_t) \mapsto e_t(\tau, s_t)$ are strictly convex and that the associated temperatures $T_l(\tau, s_l)$ and $T_t(\tau, s_t)$ are positive. It can be shown (see GODLEWSKI et RAVIART 1996 for details) that this implies that the entropies $(\tau, e_l) \mapsto s_l(\tau, e_l)$ and $(\tau, e_t) \mapsto s_t(\tau, e_t)$ are strictly concave.

Easy computations allow to conclude that the specific energy $(\tau, s_t, s_l) \mapsto e = e_t(\tau, s_t) + s_l(\tau, s_l)$ is also strictly convex. Indeed, let us choose a non null vector $X = {}^t(X_1, X_2, X_3)$, we easily get from the Hessian of e :

$$X \cdot (\nabla^2_{(\tau,s_t,s_l)}\, e\, X) = \begin{pmatrix} X_1 \\ X_2 \end{pmatrix} \cdot \left(\nabla^2_{(\tau,s_t)}\, e_t \begin{pmatrix} X_1 \\ X_2 \end{pmatrix} \right) + \begin{pmatrix} X_1 \\ X_3 \end{pmatrix} \cdot \left(\nabla^2_{(\tau,s_l)}\, e_l \begin{pmatrix} X_1 \\ X_3 \end{pmatrix} \right). \tag{3.85}$$

Hence, the strict convexity of $(\tau, s_l) \mapsto e_l(\tau, s_l)$ and $(\tau, s_t) \mapsto e_t(\tau, s_t)$ implies that the two terms on the right hand side of equation (3.85) are positive. Moreover, since X is non null, at least one of its component is non zero and therefore at least one of the two terms on the right hand side of equation (3.85) is strictly positive. So that we can conclude that for all non null X, we have $X \cdot (\nabla^2_{(\tau,s_t,s_l)}\, e\, X) > 0$ and thus that $(\tau, s_t, s_l) \mapsto e(\tau, s_t, s_l)$ is strictly convex.

Obviously, the same proof can be used to show that the total entropy $(\tau, e_t, e_l) \mapsto s(\tau, e_t, e_l)$ is strictly concave thanks to the strict concavity of the entropies $(\tau, e_l) \mapsto s_l(\tau, e_l)$ and $(\tau, e_t) \mapsto s_t(\tau, e_t)$.

Let us now turn to the energy $(\xi_t, \tau, s) \mapsto e(\xi_t, \tau, s)$ which naturally arises in the intensive form of the model of section 1. From the previous results we know that $(\tau, s_t, s_l) \mapsto e = e_t(\tau, s_t) + s_l(\tau, s_l)$ is strictly convex. Unfortunately the change of variable between (τ, s_t, s_l) and (ξ_t, τ, s) is non-linear and partial convexity results are proved here for the variable (ξ_t, τ, s). The energy reads $e(\xi_t, \tau, s) = e_t(\tau, \xi_t s) + e_l(\tau, (1-\xi_t)s)$. Hence, we get for fixed τ and s :

$$\frac{\partial^2 e}{\partial \xi_t^2} = s^2 \left(\frac{\partial^2 e_t}{\partial s_t^2} + \frac{\partial^2 e_l}{\partial s_l^2} \right),$$

which is strictly positive thanks to the strict convexity of e_t and e_l. This implies that the energy $\xi_t \mapsto e(\xi_t, \tau, s)$ is strictly convex.

For a fixed entropy fraction ξ_t, we choose two specific volumes and two specific entropies : (τ, s) and (τ', s'). We also choose a real number $\alpha \in]0, 1[$. Then using the

strict convexity of e_t and e_l, we have the relations :

$$\begin{aligned}
&e(\xi_t, \alpha\tau + (1-\alpha)\tau', \alpha s + (1-\alpha)s') \\
&= e_t(\alpha\tau + (1-\alpha)\tau', \xi_t(\alpha s + (1-\alpha)s')) + e_l(\alpha\tau + (1-\alpha)\tau', (1-\xi_l)(\alpha s + (1-\alpha)s')) \\
&< \left\{\alpha e_t(\tau, \xi_t s) + (1-\alpha)e_t(\tau', \xi_t s')\right\} + \left\{\alpha e_l(\tau, (1-\xi_t)s) + (1-\alpha)e_l(\tau', (1-\xi_t)s')\right\} \\
&= \alpha\left\{e_t(\tau, \xi_t s) + e_l(\tau, (1-\xi_t)s)\right\} + (1-\alpha)\left\{e_t(\tau', \xi_t s') + e_l(\tau', (1-\xi_t)s')\right\} \\
&= \alpha e(\xi_t, \tau, s) + (1-\alpha)e(\xi_t, \tau', s').
\end{aligned}$$

We can then conclude that the energy $(\tau, s) \mapsto e(\xi_t, \tau, s)$ is strictly convex.

B. Paths across the waves of the system

In this appendix, the computation needed to obtain the formulae presented in section 4 for defining the paths across the different waves are detailed.

According to section 3.2, the waves associated with the eigenvalues λ_1 and λ_4 are GNL waves. They can be either rarefaction waves or shock waves. For the former Riemann invariants are used to define the path across the wave, whereas for the latter the Rankine-Hugoniot relations are used. The field associated with λ_2 is linearly degenerated so that it can be described by both the Rankine-Hugoniot relations or the Riemann invariants.

We recall that the subscript L, 1, 2 and R respectively denote : the left state, the intermediate state between the $1-$wave and $2,3-$wave, the intermediate state between $2,3-$wave and $4-$wave and the right state. The left and right states correspond to the initial states of the Riemann problem, i.e. to the left/right initial conditions of the Riemann problem. It is also recalled that the EOS is here :

$$e_l(\tau, s_l) = \frac{s_l \tau^{1-\gamma}}{(\gamma-1)}, and e_k(\tau, s_k) = s_k \tau^{-2/3}. \tag{3.86}$$

Let us now rewrite the specific internal energy e in convenient form. Thanks to (3.86) the specific internal energy e reads :

$$e(\rho, s_l, s_k) = s_k \rho^{2/3} + s_l \frac{\rho^{\gamma-1}}{(\gamma-1)}, \tag{3.87}$$

where we have : $\xi_k + \xi_l = 1$ and thus : $\xi_k = \frac{s_k}{s_k + s_l}$. It allows to find the following relation between s_k and s_l :

$$s_k = s_l \frac{(\xi_k)}{(1-\xi_k)}. \tag{3.88}$$

Using equations (3.87) and (3.88), we can rewrite e as follows :

$$e(\rho, s_l, \xi_k) = s_l \left(\frac{(\xi_k)}{(1-\xi_k)} \rho^{2/3} + \frac{\rho^{\gamma-1}}{(\gamma-1)} \right).$$

In the following, the energy e is written as a function of ρ ,ξ_k and P_l by using the s_l formula :

$$s_l = \frac{P_l}{\rho^\gamma}.$$

We then get following formula for $e(\rho, \xi_k, P_l)$:

$$e(\rho, \xi_k, P_l) = \frac{P_l}{\rho(\gamma-1)}\left(\frac{\xi_k \rho^{5/3-\gamma}(\gamma-1)}{(1-\xi_k)} + 1\right). \tag{3.89}$$

Moreover, using equation (3.88), it can be checked that the following relation holds between P_k and P_l :

$$P_k = \frac{2}{3}\frac{\xi_k}{(1-\xi_k)} P_l \rho^{5/3-\gamma}. \tag{3.90}$$

It will be seen that these relations are convenient for writing explicitly the paths across the shock waves.

Path across a 1-shock wave.
The path through a 1-shock wave is obtained using the following Rankine-Hugoniot relations :

$$\begin{cases} [\xi_k]_L^1 = 0, \\ \sigma = [\rho U]_L^1 / [\rho]_L^1, \\ \rho_1 \rho_L [U]_L^{1\,2} = [P]_L^1 [\rho]_L^1, \\ 2[e]_L^1 + (P_1 + P_L)[\frac{1}{\rho}]_L^1 = 0. \end{cases} \tag{3.91}$$

where $P = P_k + P_l$ and $e = e_k + e_l$, and where for any quantity Ψ we have set : $[\Psi]_L^1 = \Psi_1 - \Psi_L$. First equation of system (3.91) straightforwardly gives us that ξ_k is constant through 1-shock wave, so that :

$$\xi_{k,L} = \xi_{k,1}. \tag{3.92}$$

Let us now turn to the fourth equation of system (3.91). By using the internal energy formula (3.89), it yields :

$$[e]_L^1 = \frac{P_{l,1}}{\rho_1(\gamma-1)}\left(\frac{\xi_{k,1}\rho_1^{5/3-\gamma}(\gamma-1)}{(1-\xi_{k,1})} + 1\right) - \frac{P_{l,L}}{\rho_L(\gamma-1)}\left(\frac{\xi_{k,L}\rho_L^{5/3-\gamma}(\gamma-1)}{(1-\xi_{k,L})} + 1\right). \tag{3.93}$$

Let us now proceed with the second part of the fourth equation :

$$(P_1 + P_L)\left[\frac{1}{\rho}\right]_L^1 = \left(P_{k,1} + P_{l,1} + P_{k,L} + P_{l,L}\right)\left(\frac{\rho_L - \rho_1}{\rho_L \rho_1}\right) \tag{3.94}$$

In order to write the left hand side of relation (3.94) with respect to ρ, ξ_k, and P_l,

relation (3.90) between P_k and P_l is used and we obtain :

$$(P_1+P_L)\left[\frac{1}{\rho}\right]_L^1 = \left(\frac{2}{3}\frac{\xi_{k,1}}{(1-\xi_{k,1})}P_{l,1}\rho_1^{5/3-\gamma}+P_{l,1}+\frac{2}{3}\frac{\xi_{k,L}}{(1-\xi_{k,L})}P_{l,L}\rho_L^{5/3-\gamma}+P_{l,L}\right)\left(\frac{\rho_L-\rho_1}{\rho_L\rho_1}\right). \tag{3.95}$$

We now set :

$$z_1 = \frac{\rho_1}{\rho_L}.$$

By using equations (3.93) and (3.95), and the fact that ξ_k remains constant through 1-shock (3.92), we get the formula of $P_{l,1}$ as a function of z_1, ρ_L and $\xi_{k,L}$:

$$P_{l,1} = P_{l,L}h_1(z_1;\rho_L,\xi_{k,L}), \tag{3.96}$$

with

$$h_1(z_1;\rho_L,\xi_{k,L}) = \frac{\left((z_1\beta-1)+\frac{2}{3}\frac{\xi_{k,L}(1-\xi_{k,L})}{\rho}_L^{5/3-\gamma}(4z_1-1)\right)}{\left((\beta-z_1)+\frac{2}{3}\frac{\xi_{k,L}}{(1-\xi_{k,L})}\rho_L^{5/3-\gamma}(4z_1^{5/3-\gamma}-z_1^{8/3-\gamma})\right)},$$

where $\beta = \frac{(\gamma+1)}{(\gamma-1)}$.

The formula for U_1 is obtained by combining equation (3.96) with the third equation of system (3.91) :

$$U_1 = U_L - c_{l,L}f_1(z_1;\rho_L,\xi_{k,L}), \tag{3.97}$$

with

$$f_1(z_1;\rho_L,\xi_{k,L}) = \sqrt{\frac{(z_1-1)}{\gamma\, z_1}\left(h_1(z_1;\rho_L,\xi_{k,L})\left(1+\frac{2}{3}\frac{\xi_{k,L}}{(1-\xi_{k,L})}\rho_L^{5/3-\gamma}z_1^{5/3-\gamma}\right)-P_{l,L}-P_{k,L}\right)}.$$

Finally, the following relations define a 1-shock with $z_1 \in [1,4[$ as a parameter to define the amplitude of the shock :

$$\begin{cases} U_1 = U_L - c_{l,L}f_1(z_1;\rho_L,\xi_{k,L}), \\ P_{l,1} = P_{l,L}h_1(z_1;\rho_L,\xi_{k,L}), \\ \xi_{k,L} = \xi_{k,1}. \end{cases} \tag{3.98}$$

It should be noted that a 1−shock wave is correctly defined if and only if function $f_1(z_1;\rho_L,\xi_{k,L})$ is correctly defined.

Path across a 4-shock wave.
By doing the same calculations for the jump relations associated with the 4-shock wave, and by fixing z_2 :

$$z_2 = \frac{\rho_2}{\rho_R},$$

we get the following relations which define the passage through 4-shock waves for

$z_2 \in [1,4[$:

$$\begin{cases} U_2 = U_R + c_{l,R} f_2(z_2;\rho_R,\xi_{k,R}), \\ P_{l,2} = P_{l,R} h_2(z_2;\rho_R,\xi_{k,R}), \\ \xi_{k,R} = \xi_{k,2}. \end{cases} \tag{3.99}$$

with the functions :

$$f_2(z_2;\rho_R,\xi_{k,R}) = \sqrt{\frac{(z_2-1)}{\gamma z_2}\left(h_2(z_2;\rho_R,\xi_{k,R})\left(1+\frac{2}{3}\frac{\xi_{k,R}}{(1-\xi_{k,R})}\rho_R^{5/3-\gamma} z_2^{5/3-\gamma}\right) - P_{l,R} - P_{k,R}\right)},$$

and

$$h_2(z_2;\rho_R,\xi_{k,R}) = \frac{\left((z_2\beta-1) + \frac{2}{3}\frac{\xi_{k,R}(1-\xi_{k,R})}{\rho}_R^{5/3-\gamma}(4z_2-1)\right)}{\left((\beta-z_2) + \frac{2}{3}\frac{\xi_{k,R}}{(1-\xi_{k,R})}\rho_R^{5/3-\gamma}(4z_2^{5/3-\gamma} - z_2^{8/3-\gamma})\right)}.$$

It should be noted that a 4−shock wave is correctly defined if and only if function $f_2(z_2;\rho_R,\xi_{k,R})$ is correctly defined.

Path across a 1-rarefaction wave.
The Riemann invariants I_1^1, I_2^1 and I_3^1 defined in section 3.3 remain constant in a 1-rarefaction wave. As a result, in a 1-rarefaction wave, we get the following relations for $z_1 \leq 1$:

$$\xi_{k1} = \xi_{k,L} \tag{3.100}$$

$$s_1 = s_L \tag{3.101}$$

$$U_1 - \int_0^{\tau_1} \frac{c_1(I_1^1(Y), I_2^1(Y), \tau\prime)}{\tau\prime}\,\mathrm{d}\tau\prime = U_L - \int_0^{\tau_L} \frac{c_L(I_1^1(Y), I_2^1(Y), \tau\prime)}{\tau\prime}\,\mathrm{d}\tau\prime \tag{3.102}$$

By introducing our specific choices for the EOS we then obtain :

$$\begin{cases} U_1 = U_l - B_1(z_1, c_{k_L}, c_{l_L}, \tau_L), \\ P_{l,1} = P_{l,L} Q_1(z_1), \\ \xi_{k,L} = \xi_{k1}, \end{cases} \tag{3.103}$$

with the following definitions :

$$B_1(z_1, c_{k_L}, c_{l_L}, \tau_L) = \int_1^{z_1} \frac{1}{\tau_L}\left(c_{l_L}^2 z^{1+\gamma} + c_{k_L}^2 z^{8/3}\right)^{1/2}\mathrm{d}z,$$

$$Q_1(z_1) = z_1^{\gamma}.$$

Path across a 4-rarefaction wave.
In a same manner, using the Riemann invariants I_1^4, I_2^4 and I_3^4 defined in section 3.3,

we can write for a 4-rarefaction wave fo $z_2 \leq 1$:

$$\begin{cases} U_2 = U_R + B_2(z_2, c_{k_R}, c_{l_R}, \tau_R), \\ P_{l,2} = P_{l,R} Q_2(z_2), \\ \xi_{k,R} = \xi_{k,2}, \end{cases} \tag{3.104}$$

with the following definitions :

$$B_2(z_2, c_{k_R}, c_{l_R}, \tau_R) = \int_1^{z_2} \frac{1}{\tau_R} \left(c_{l_R}^2 z^{1+\gamma} + c_{k_R}^2 z^{8/3} \right)^{1/2} \mathrm{d}z,$$

and

$$Q_2(z_2) = z_2^{\gamma}.$$

Path across a 2,3-contact wave.
In this linearly degenerate wave, the Riemann invariants are U and P. As a result, the following relations hold :

$$P_1 = P_2, \tag{3.105}$$

$$U_1 = U_2. \tag{3.106}$$

By using relation (3.88) and the definition $P = P_k + P_l$, we get the following equation :

$$P_{l_1} D_1(z_1, \xi_{k_1}, \rho_L) = P_{l_2} D_2(z_2, \xi_{k_2}, \rho_R) \tag{3.107}$$

with :

$$D_1(z_1, \xi_{k_1}, \rho_L) = 1 + \frac{\xi_{k_1}}{(1-\xi_{k_1})} z_1^{5/3-\gamma} \rho_L^{5/3-\gamma},$$

and

$$D_2(z_2, \xi_{k_2}, \rho_R) = 1 + \frac{\xi_{k_2}}{(1-\xi_{k_2})} z_2^{5/3-\gamma} \rho_R^{5/3-\gamma}.$$

C. Additional test case : a laminar double shock wave

For the present test case, we consider laminar initial left and right states :

$$(\rho, U, P_l, e_k)_L = (1, 550, 10^6, 0)$$

and :

$$(\rho, U, P_l, e_k)_R = (1, -618.107550, 103990.112994, 0).$$

The EOS parameters are :

$$C_v = 720,\ A_0 = 0 \text{ and } \gamma = 1.4.$$

The 1-wave and the 4-wave are shock waves. The source term for the entropy fraction is not accounted for. Convergence curves are plotted in figure 3.13 and the approximated solution is plotted in figure 3.12. For this test case, the EOS is a mere perfect gas and the VFRoe-ncv scheme used here allow to preserve the contact wave T. GALLOUËT, J.-M. HÉRARD et SEGUIN 2002.

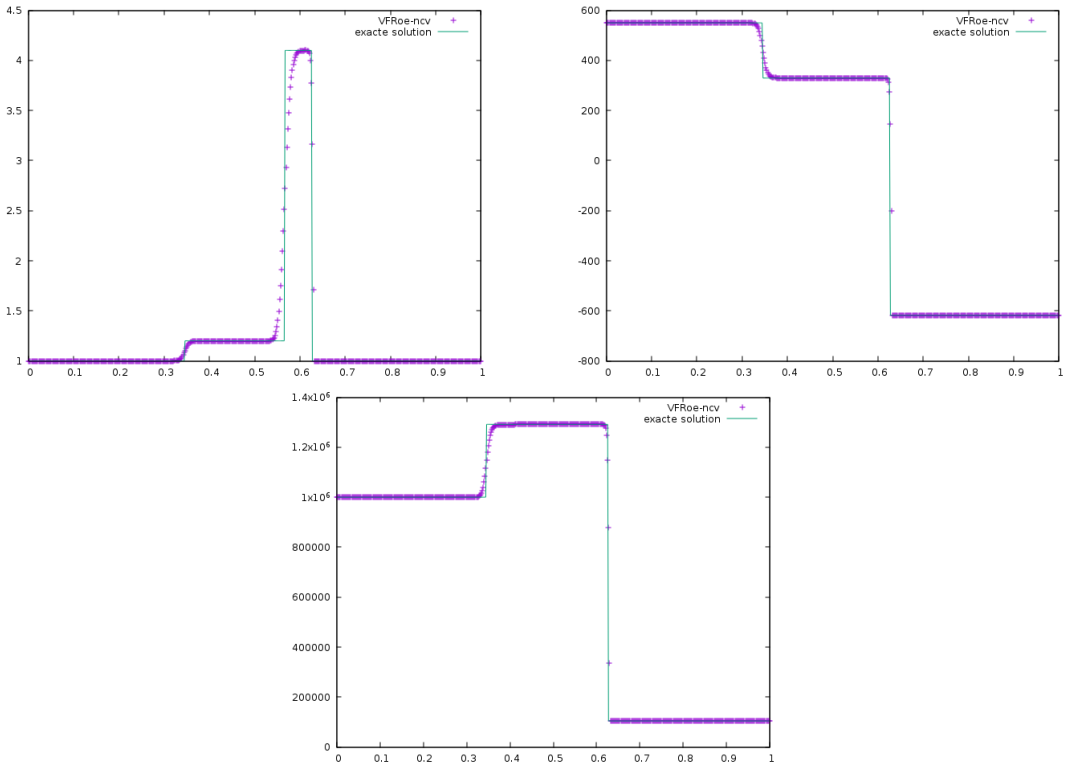

FIGURE 3.12. – Double-shock wave test case 4. Density (top left), velocity (top right) and totale pressure (bottom)Comparison between the exact solution (green) and the approximate solution (purple) at $t = 2\ 10^{-4}$ s, $CFL = 0.5$, 500 cells.

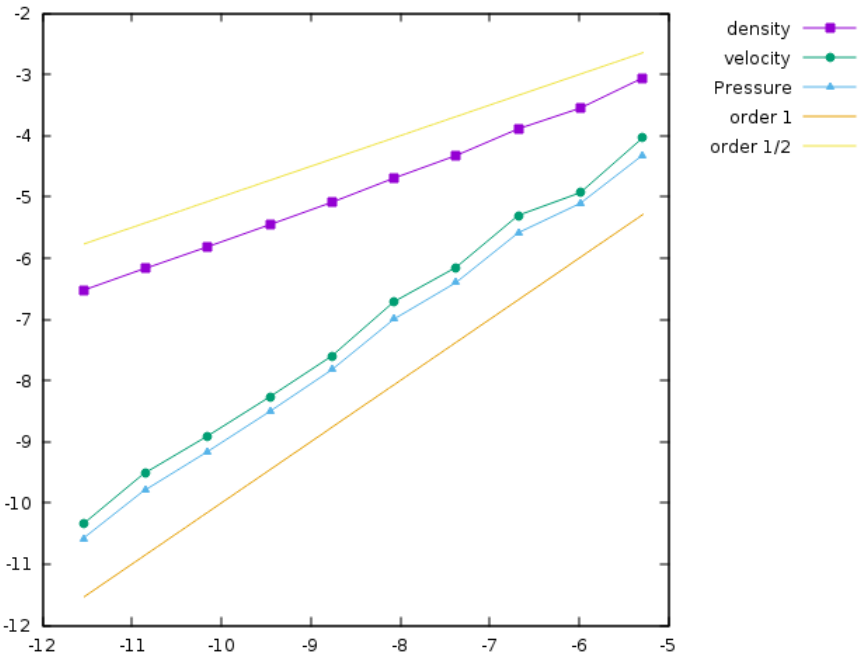

FIGURE 3.13. – Double-shock wave test case 4. Convergence curves : logarithm of the relative L1-error versus the logarithm of the mesh size with uniform meshes containing from 200 to 100000 cells. The error is plotted for variables, ρ, u and P.

D. Study of the turbulent pressure $P_{k,1}$ behind a 1-shock

In this section, the results presented in section 5.2.2 are detailed. It is assumed that $P_{l,L} > 0$ and $P_{k,L} > 0$, which implies that $P_L = P_{l,L} + P_{k,L} > 0$. The aim of the present section is to determine the sign of the turbulent pressure $P_{k,1}$ behind a 1-shock wave. The jump relations through a 1-shock and the results of the previous section enable to write $P_{K,1}$ as :

$$P_{K,1} = P_{K,L} g_1(z_1; P_L, P_{l,L}), \quad \forall z_1 \in [1,4[, \tag{3.108}$$

with

$$\begin{cases} g_1(z_1; P_L, P_{l,L}) = \left(1 + \dfrac{P_{l,L}}{P_{k,L}}\right) Q_1(z_1; P_L, P_{l,L})/(4 - z_1), \\ Q_1(z_1; P_L, P_{l,L}) = \left(4z_1 - 1 + B(z_1^{5/3} - z_1) - 4\dfrac{P_{l,L}}{P_L} z_1^{5/3} + \dfrac{P_{l,L}}{P_L} z_1^{8/3}\right), \\ z_1 = \dfrac{\rho_1}{\rho_L}. \end{cases} \tag{3.109}$$

It is recalled that in the previous sections we have set :

$$B = 3\frac{(\gamma - 5/3)}{(\gamma - 1)} \frac{P_{l,L}}{P_L} and \beta = \frac{(\gamma + 1)}{(\gamma - 1)}.$$

In the following, the sign of the function $z_1 \mapsto g_1(z_1)$ is examined on the interval $[1,4[$. Thanks to our assumptions, we have $(1 + \frac{P_{l,L}}{P_{k,L}}) > 0$, so that the sign of function $g_1(z_1)$ on $[1,4[$ is the same than the sign of function $Q_1(z_1)$ on $[1,4[$.

The first and second derivatives of $Q_1(z_1)$ are respectively :

$$Q_1'(z_1) = \left(4 + B(\frac{5}{3} z_1^{2/3} - 1) - \frac{20}{3}\frac{P_{l,L}}{P_L} z_1^{2/3} + \frac{8}{3}\frac{P_{l,L}}{P_L} z_1^{5/3}\right),$$

and

$$Q_1''(z_1) = \frac{10 P_{l,L}}{9 P_L} z_1^{-1/3} \left(4z_1 - \beta\right).$$

We have $Q_1''(z_{1,0}'') = 0$ for $z_{1,0} = \frac{\beta}{4}$, which makes it possible to distinguish 3 cases for the sign of $Q_1''(z_1)$ depending on the value of $z_{1,0}'' = \frac{\beta}{4}$:

— if $\frac{\beta}{4} < 1 \iff \gamma > 5/3 : Q_1''(z_1) > 0 \ \forall \ z_1 \in [1,4[$.

— if $1 < \frac{\beta}{4} < 4 \iff 17/15 < \gamma < 5/3$: but $\gamma > 25/21 > 17/15$ (for $P_k \neq 0$, see (6.1)), then for $25/21 < \gamma < 5/3$, we get that :

$$Q_1''(z_1) < 0 \ \ \forall \ z_1 \in [1, \beta/4], \ \ Q_1''(z_1) > 0 \ \ \forall \ \ z_1 \in]\beta/4, 4[.$$

— if $\frac{\beta}{4} > 4 \iff \gamma < 17/15 \Longrightarrow \gamma < 25/21 : Q_1''(z_1) < 0 \ \forall \ z_1 \in [1,4[$.

The third case above is not considered in the following. Indeed, it implies that $\gamma < 25/21$ and this case can be excluded since it corresponds to a domain where the model is not relevant, see the remark a the end of section 5.1. In the sequel, we thus focus on the first two cases.

Case 1 : $\gamma > 5/3$
We have $Q_1'' > 0$ on the interval $[1,4[$, which implies that Q_1' is increasing on $[1,4[$. The function $Q_1'(z_1)$ in $z_1 = 1$ gives :

$$Q_1'(1) = 4 + \frac{2}{3}B - 4\frac{P_{l,L}}{P_L} = \frac{2}{3}\left(6\left(1 - \frac{P_{l,L}}{P_L}\right) + B\right). \tag{3.110}$$

We have $\frac{P_{l,L}}{P_L} < 1$, and $B > 0$ (since $\gamma > 5/3$, $P_{l,L} > 0$ and $P_L > 0$), then we get $Q_1'(z_1) > 0$ $\forall\ z_1 \in [1,4[$. At this point, we know that $Q_1(z_1)$ is increasing in $[1,4[$, hence the sign of $Q_1(1)$ indicates the sign of $Q_1(z_1)$ $\forall z_1 \in [1,4[$.
We have $Q_1(1) = 3(1 - \frac{P_{l,L}}{P_L}) > 0$, thus we finally get :

$$\text{for } \gamma > 5/3 : Q_1(z_1) > 0 \ \ \forall z_1 \in [1,4[. \tag{3.111}$$

Case 2 : $\frac{17}{15} < \gamma < \frac{5}{3}$
In this case, Q_1'' has two different signs, for this we present the variation table for Q_1'. Table 3.14 gives the variation of the function $Q_1'(z_1)$ on the interval $[1,4[$. The values of Q_1', for $z_1 = 1$ (see equation (3.110)), $z_1 = \beta/4$ and $z_1 = 4$, determine the sign of Q_1' on the interval $[1,4[$. These values of Q_1' for the two latter points are the following :

$$Q_1'(\beta/4) = 4 + B(\frac{5}{3}(\frac{\beta}{4})^{2/3} - 1) + \frac{8}{3}\frac{P_{l,L}}{P_L}(\frac{\beta}{4})^{2/3}(\frac{\beta}{4} - \frac{5}{2}), \tag{3.112}$$

$$Q_1'(4) = 4 + B(\frac{5}{3}4^{2/3} - 1) + \frac{P_{l,L}}{P_L}4^{5/3}. \tag{3.113}$$

We distinguish several sub-cases depending on the values (3.110), (3.112) and (3.113).

z	1		$\frac{\beta}{4}$		4
Q_1''		$-$	0	$+$	
Q_1'		↘		↗	

FIGURE 3.14. – Variation table for Q_1' function (case 2)

Case 2.1 : we assume that $Q_1'(1) > 0$

$Q_1'(1) > 0$ under the condition that :

$$B > 6\left(\frac{P_{l,L}}{P_L} - 1\right) \Longleftrightarrow \frac{P_{l,L}}{P_L} < 2\frac{\gamma - 1}{\gamma - 1/3}. \tag{3.114}$$

Since $P_{l,L}/P_L < 1$ and since $\gamma \in [25/21, 5/3]$, we get that $Q_1'(\beta/4) > 0$. The function Q_1' is increasing on $[\frac{\beta}{4}, 4[$, which gives us that $Q_1'(4) > 0$, therefore $Q_1'(z_1) > 0 \ \forall \ z_1 \in [1,4[$. This implies that Q_1 is an increasing function in the interval $[1,4[$. We have $Q_1(1) > 0$, then :

$$\text{for } \frac{P_{l,L}}{P_L} < 2\frac{\gamma - 1}{\gamma - 1/3} : \ Q_1(z_1) > 0 \ \ \forall z_1 \in [1,4[\tag{3.115}$$

Case 2.2 : we assume that $Q_1'(1) < 0$
$Q_1'(1) < 0$ under the condition that :

$$B < 6\left(\frac{P_{l,L}}{P_L} - 1\right) \Longleftrightarrow \frac{P_{l,L}}{P_L} > 2\frac{\gamma - 1}{\gamma - 1/3}. \tag{3.116}$$

The function Q_1' is decreasing in $[1, \frac{\beta}{4}]$, which gives us that $Q_1'(\frac{\beta}{4}) < 0$. We distinguish 2 cases which depend on the sign of $Q_1'(4)$.

Case 2.2.1 : we assume that $Q_1'(4) < 0$
$Q_1'(4) < 0$ under the condition that :

$$B < \frac{\left(-4 - 4^{5/3}\frac{P_{l,L}}{P_L}\right)}{\left(4^{2/3}\frac{5}{3} - 1\right)} \Longleftrightarrow \frac{P_{l,L}}{P_L}(\gamma - \gamma_{lim}) < -\frac{4}{3}(\gamma - 1), \tag{3.117}$$

with $\gamma_{lim} = -4^{5/3}/3 + 5/3(5/34^{2/3} - 1) \sim 4.493$. With these conditions (3.116) and (3.117), we obtain that $Q_1'(z_1) < 0 \ \forall \ z_1 \in [1,4[$. This implies that Q_1 is a decreasing function in the interval $[1,4[$ and we get :

$$\text{for } \frac{P_{l,L}}{P_L} > 2\frac{\gamma - 1}{\gamma - 1/3} \text{ and } \frac{P_{l,L}}{P_L}(\gamma - \gamma_{lim}) < -\frac{4}{3}(\gamma - 1) \ : \ \forall z_1 \in [1, z_{1,0}[, Q_1(z_1) < 0 \ \ \forall z_1 \in]z_{1,0}, 4[, \tag{3.118}$$

with $Q_1(z_{1,0}) = 0$.

Case 2.2.2 : we assume that $Q_1'(4) > 0$
$Q_1'(4) > 0$ under the condition that :

$$B > \frac{\left(-4 - 4^{5/3}\frac{P_{l,L}}{P_L}\right)}{\left(4^{2/3}\frac{5}{3} - 1\right)} \Longleftrightarrow \frac{P_{l,L}}{P_L}(\gamma - \gamma_{lim}) > -\frac{4}{3}(\gamma - 1). \tag{3.119}$$

Table 3.15 gives the variation of the function $Q_1(z_1)$ on the interval $[1,4[$. The values of

Q_1 at the points $z_1 = 1$, $z_1 = z'_{1,0}$ and $z_1 = 4$, determine the sign of Q_1 on the interval $[1,4[$. We distinguish several sub-cases depending on the values of $Q_1(1)$, $Q_1(z'_{1,0})$ and $Q_1(4)$.

z	1	$z'_{1,0}$	4
Q'_1	$-$	0	$+$
Q_1	↘		↗

FIGURE 3.15. – Variation table for Q_1 function (case 2.2.2)

Case 2.2.2.1 : we assume that $Q_1(z'_{1,0}) > 0$. This implies that $Q_1(4) > 0$ (see table 3.15).
We then get :

$$\text{for } \frac{P_{l,L}}{P_L} > 2\frac{\gamma-1}{\gamma-1/3} \text{ and } \frac{P_{l,L}}{P_L}(\gamma-\gamma_{lim}) > -\frac{4}{3}(\gamma-1) \text{ and } Q_1(z'_{1,0}) > 0 : \; Q_1(z_1) > 0 \;\; \forall z_1 \in [1,4[\tag{3.120}$$

Case 2.2.2.2 : we assume that $Q_1(z'_{1,0}) < 0$ and $Q_1(4) > 0$.
We then get :

$$\text{for } \frac{P_{l,L}}{P_L} > 2\frac{\gamma-1}{\gamma-1/3} \text{ and } \frac{P_{l,L}}{P_L}(\gamma-\gamma_{lim}) > -\frac{4}{3}(\gamma-1) \text{ and } Q_1(z'_{1,0}) < 0 \text{ and } Q_1(4) > 0 : \tag{3.121}$$

$$Q_1(z_1) > 0 \;\; \forall z_1 \in [1, z_{1,0}] \cup [z_{1,1}, 4[, \quad Q_1(z_1) < 0 \;\; \forall z_1 \in]z_{1,0}, z_{1,1}[\tag{3.122}$$

with $Q_1(z_{1,0}) = Q_1(z_{1,1}) = 0$ and $z_{1,0} < z'_{1,0} < z_{1,1}$

Case 2.2.2.3 : we assume that $Q_1(4) < 0$.
We then get :

$$\text{for } \frac{P_{l,L}}{P_L} > 2\frac{\gamma-1}{\gamma-1/3} \text{ and } \frac{P_{l,L}}{P_L}(\gamma-\gamma_{lim}) > -\frac{4}{3}(\gamma-1) \text{ and } Q_1(4) < 0 : \tag{3.123}$$

$$Q_1(z_1) > 0 \;\; \forall z_1 \in [1, z^{\#}_{1,0}[, \quad Q_1(z_1) < 0 \;\; \forall z_1 \in]z^{\#}_{1,0}, 4[, \tag{3.124}$$

where in this case, $z^{\#}_{1,0}$ is the unique solution of $Q_1(z^{\#}_{1,0}) = 0$ on $[1,4[$.

Bibliographie

[BH05] Thomas BARBERON et Philippe HELLUY. « Finite volume simulation of cavitating flows ». In : *Computers &amp Fluids* 34.7 (août 2005), p. 832-858. DOI : 10.1016/j.compfluid.2004.06.004 (cf. p. 4).

[BGH00] Thierry BUFFARD, Thierry GALLOUËT et Jean-Marc HÉRARD. « A sequel to a rough Godunov scheme : application to real gases ». In : *Computers & Fluids* 29(7) (2000), p. 813-847. DOI : 10.1016/s0045-7930(99)00026-2 (cf. p. 25).

[BO77] Daniel T. BUTLER et Peter J. O'ROURKE. « A numerical method for two dimensional unsteady reacting flows ». In : *Symposium (international) on combustion*. T. 16. 1. Elsevier. 1977, p. 1503-1515. DOI : 10.1016/s0082-0784(77)80432-3 (cf. p. 37).

[CBS17] Alexandre CHIAPOLINO, Pierre BOIVIN et Richard SAUREL. « A simple and fast phase transition relaxation solver for compressible multicomponent two-phase flows ». In : *Computers & Fluids* 150 (2017), p. 31-45. DOI : 10.1016/j.compfluid.2017.03.022 (cf. p. 7).

[FM19] Gloria FACCANONI et Hélène MATHIS. « Admissible Equations of State for Immiscible and Miscible Mixtures ». In : *ESAIM : Proceedings and Surveys* 66 (2019), p. 1-21. DOI : 10.1051/proc/201966001 (cf. p. 7).

[GHS02] T. GALLOUËT, J.-M. HÉRARD et N SEGUIN. « Some recent finite volume schemes to compute Euler equations using real gas EOS ». In : *International journal for numerical methods in fluids* 39.12 (2002), p. 1073-1138. DOI : 10.1002/fld.346 (cf. p. 31, 48).

[Gav+22] Sergey GAVRILYUK, Jean-Marc HÉRARD, Olivier HURISSE et al. « Theoretical and numerical analysis of a simple model derived from compressible turbulence ». In : *Journal of Mathematical Fluid Mechanics* 24.2 (2022), p. 1-34. DOI : 10.1007/s00021-022-00676-5 (cf. p. 4, 5, 9-11, 15, 18, 30).

[GS06] Sergey GAVRILYUK et Richard SAUREL. « Estimation of the turbulent energy production across a shock wave ». In : *Journal of Fluid Mechanics* 549 (2006), p. 131. DOI : 10.1017/s0022112005008062 (cf. p. 4, 5, 18, 24, 41).

[GR96] Edwige GODLEWSKI et Pierre-Arnaud RAVIART. *Numerical approximation of hyperbolic sytems of conservation laws*. Springer Berlin, 1996. DOI : 10.1007/978-1-4612-0713-9 (cf. p. 8, 11, 42).

Bibliographie

[HHQ20] J.-M. HÉRARD, O. HURISSE et L. QUIBEL. « A four-field three-phase flow model with both miscible and immiscible components ». In : *ESAIM : Mathematical Modelling and Numerical Analysis* (2020). DOI : 10.1051/m2an/2020037 (cf. p. 7).

[HM19] J.-M. HÉRARD et H. MATHIS. « A three-phase flow model with two miscible phases ». In : *ESAIM : Mathematical Modelling and Numerical Analysis* 53.4 (2019), p. 1373-1389. DOI : 10.1051/m2an/2019028 (cf. p. 7).

[Hér14] Jean-Marc HÉRARD. Rapp. tech. A simple turbulent model for compressible flows, 2014. URL : https://hal.archives-ouvertes.fr/hal-02007044 (cf. p. 9-11, 15).

[HQ21] Olivier HURISSE et Lucie QUIBEL. « Simulations of liquid-vapor water flows with non-condensable gases on the basis of a two-fluid model. » In : *Applied Mathematical Modelling* (2021). DOI : 10.1016/j.apm.2021.06.020 (cf. p. 7).

[Jun13] J. JUNG. « Numerical simulations of two-fluid flow on multicores accelerator ». PhD Thesis. Université de Strasbourg, oct. 2013. URL : https://tel.archives-ouvertes.fr/tel-00876159 (cf. p. 11).

[Mat19] H. MATHIS. « A thermodynamically consistent model of a liquid-vapor fluid with a gas ». In : *ESAIM : Mathematical Modelling and Numerical Analysis* 53.1 (2019), p. 63-84. DOI : 10.1051/m2an/2018044 (cf. p. 4, 7).

[SCR03] R SAUREL, A CHINNAYYA et F RENAUD. « Thermodynamic analysis and numerical resolution of a turbulent-fully ionized plasma flow model ». In : *Shock Waves* 13.4 (2003), p. 283-297. DOI : 10.1007/s00193-003-0216-z (cf. p. 4).

[Yan68] NN YANENKO. *Méthode à pas fractionnaires : résolutions de problèmes polydimensionnels de physique mathématique*. A. Colin, 1968. URL : https://books.google.fr/books?id=JBIyvgAACAAJ (cf. p. 24).

Conclusion et perspectives

Cette thèse est consacrée à la modélisation, la simulation et l'analyse des écoulements turbulents compressibles monophasiques, en se concentrant sur l'application de l'explosion, un phénomène qui a suscité beaucoup d'intérêt scientifique depuis de nombreuses années, notamment dans le domaine de la sûreté nucléaire.

Dans un premier temps, un modèle simple de turbulence compressible proposé quelques années auparavant est étudié. Ceci fait l'objet du chapitre 1 Sergey GAVRILYUK, Jean-Marc HÉRARD, Olivier HURISSE et al. 2022. Ce modèle a été proposé dans Jean-Marc HÉRARD 2014 en faisant l'hypothèse que l'entropie turbulente « ξ » est uniforme dans tout le domaine, y compris à travers les ondes de choc. Ce modèle est basé sur les équations de Euler/Navier-Stokes moyennées, avec une fermeture algébrique pour l'énergie cinétique turbulente $K = \xi_0 \rho^{5/3}$. Ce modèle est caractérisé par une inégalité d'entropie qui permet de choisir les solutions admissibles dans les ondes de choc. Le modèle résultant a une structure hyperbolique. Il admet 3 valeurs propres distinctes (avec un champ LD et deux champs VNL), et sa structure conservative garantit des relations de saut uniques. Un résultat d'existence et d'unicité de la solution du problème de Riemann unidimensionnel est obtenu de manière classique, et les sauts de densité à la traversée des chocs sont compatibles avec le cadre laminaire. Pour la simulation numérique de ce modèle, un schéma de volume finis est mis en œuvre en utilisant un solveur de Riemann approché de type VFRoe-ncv BUFFARD, Thierry GALLOUËT et Jean-Marc HÉRARD 2000. Des cas tests de vérification 1D, qui attestent de la convergence numérique, sont présentés, ainsi qu'un cas test bidimensionnel plus réaliste qui représente le phénomène d'explosion.

Dans le second chapitre, un modèle de turbulence plus complexe est examiné, qui permet de faire varier l'entropie turbulente à travers le choc. Ce modèle comporte trois lois de conservation correspondant au bilan de masse, bilan de quantité de mouvement, bilan d'énergie, et une quatrième équation sur ξ qui décrit l'évolution de l'entropie turbulente. En suivant la méthodologie proposée dans Sergey GAVRILYUK et Richard SAUREL 2006, une estimation du saut d'entropie turbulente "$[\xi]$" à travers les ondes de choc est obtenue. Un schéma numérique de type volume finis est développé, incluant un solveur interfacial hybride, pour calculer les solutions approchées du modèle à l'interface, mais également un détecteur de choc aux interfaces. Des résultats numériques 1D, qui représentent des ondes de chocs, sont présentés.

Dans le dernier chapitre 3, on introduit un troisième modèle qui permet lui aussi de faire varier l'entropie turbulente à travers les chocs. Une écriture du modèle sous

forme extensive est réalisée dans un premier temps, puis une forme intensive est présentée. Le modèle du chapitre 1 est retrouvé pour les solutions régulières sous certaines hypothèses. Les principales propriétés mathématiques du système d'équations sont présentées. Par la suite, on examine ce modèle lorsque l'on considère que le fluide est en équilibre de température. Pour réaliser la mise en œuvre numérique, la stratégie à pas fractionnaires est employée. Le système convectif est d'abord discrétisé à l'aide d'un schéma de volumes finis explicite. Le terme source est discrétisé en résolvant implicitement le système d'EDO présenté dans le chapitre. Plusieurs cas tests basés sur des problèmes de Riemann sont présentés. La convergence numérique du schéma est vérifiée à la fois pour la partie convective et la partie associée aux termes sources.

En termes de perspectives :

1. Dans le chapitre 1, il paraît naturel d'envisager l'introduction des effets de dissipation d'énergie turbulente (de type Spalart, avec une échelle de temps associée), et des effets à caractère dissipatif sur le mouvement moyen. Les résultats seraient à confronter aux modèles de turbulence classique.
2. Concernant le chapitre 2, cette partie montre la difficulté d'intégration du modèle Sergey GAVRILYUK et Richard SAUREL 2006 dans un cadre EDP dynamique. La formulation proposée doit être améliorée dans sa déclinaison numérique (détecteur de choc à améliorer, ainsi que la prise en compte de la masse associée au saut d'entropie turbulente), mais aussi revisité sur le plan EDP. De fait, le chantier engagé actuellement ne permet pas d'envisager une mise en oeuvre dans le cadre industriel et multi-dimensionnel.
3. Dans le chapitre 3, le modèle proposé sur une base thermodynamique permet de définir de manière unique le saut d'entropie turbulente dans les chocs. Les méthodes numériques à mettre en œuvre pour calculer des solutions approchées sont donc relativement simples et classiques, contrairement à l'approche suivie dans le chapitre 2 qui nécessite de développer des schémas numériques adaptés et pointus. Par ailleurs, l'application à des cas 3D industriels est clairement plus aisée. Le saut d'entropie obtenu dans le modèle du chapitre 3 dépend directement de la loi d'état choisie pour l'entropie turbulente, mais aussi de la loi de mélange entre les phases laminaire et turbulente. De nouvelles propositions concernant ces deux points pourraient permettre d'obtenir d'autres comportements de la turbulence à la traversée des chocs.

Bibliographie

[Amb+09] Annalisa AMBROSO, Christophe CHALONS, Frédéric COQUEL et al. « Relaxation and numerical approximation of a two-fluid two-pressure diphasic model ». In : *ESAIM : Mathematical Modelling and Numerical Analysis* 43.6 (2009), p. 1063-1097. DOI : 10.1051/m2an/2009038 (cf. p. 115).

[AC06] Bruno AUDEBERT et Frédéric COQUEL. « Hybrid Godunov-Glimm Method for a Nonconservative Hyperbolic System with Kinetic Relations ». In : *Numerical Mathematics and Advanced Applications*. Springer Berlin Heidelberg, 2006, p. 646-653. DOI : 10.1007/978-3-540-34288-5_62 (cf. p. 20).

[BH05] Thomas BARBERON et Philippe HELLUY. « Finite volume simulation of cavitating flows ». In : *Computers &amp Fluids* 34.7 (août 2005), p. 832-858. DOI : 10.1016/j.compfluid.2004.06.004 (cf. p. 20, 25, 128).

[Ber+02] C. BERTHON, F. COQUEL, J.M. HÉRARD et al. « An approximate solution of the Riemann problem for a realisable second-moment turbulent closure ». In : *Shock Waves* 11.4 (jan. 2002), p. 245-269. DOI : 10.1007/s001930100109 (cf. p. 19).

[Ber99] Christophe BERTHON. « Contribution à l'analyse numérique des équations de Navier-Stokes compressibles à deux entropies spécifiques. Applications à la turbulence compressible ». Thèse de doct. Paris 6, 1999. URL : https://www.math.sciences.univ-nantes.fr/~berthon/cv_these_hdr/these.pdf (cf. p. 19, 33, 34, 83).

[BC02] Christophe BERTHON et Frédéric COQUEL. « Nonlinear projection methods for multi-entropies Navier-Stokes systems ». In : *Innovative Methods For Numerical Solution Of Partial Differential Equations* (2002), p. 278-304. DOI : 10.1142/9789812810816_0014 (cf. p. 33, 34, 83).

[Bru+99] G BRUN, J.-M HÉRARD, D JEANDEL et al. « An Approximate Riemann Solver for Second-Moment Closures ». In : *Journal of Computational Physics* 151.2 (mai 1999), p. 990-996. DOI : 10.1006/jcph.1999.6190 (cf. p. 19).

[BGH00] Thierry BUFFARD, Thierry GALLOUËT et Jean-Marc HÉRARD. « A sequel to a rough Godunov scheme : application to real gases ». In : *Computers & Fluids* 29(7) (2000), p. 813-847. DOI : 10.1016/s0045-7930(99)00026-2 (cf. p. 22, 24, 45, 49, 58, 74, 95-97, 149, 180).

[BO77] Daniel T. BUTLER et Peter J. O'ROURKE. « A numerical method for two dimensional unsteady reacting flows ». In : *Symposium (international) on combustion*. T. 16. 1. Elsevier. 1977, p. 1503-1515. DOI : 10.1016/s0082-0784(77)80432-3 (cf. p. 161).

[Cha00] Patrick CHASSAING. *Turbulence en mécanique des fluides*. Cépaduès-éditions, 2000 (cf. p. 19).

[CBS17] Alexandre CHIAPOLINO, Pierre BOIVIN et Richard SAUREL. « A simple and fast phase transition relaxation solver for compressible multicomponent two-phase flows ». In : *Computers & Fluids* 150 (2017), p. 31-45. DOI : 10.1016/j.compfluid.2017.03.022 (cf. p. 131).

[Erl+90] Gordon ERLEBACHER, Mohammed Yousuff HUSSAINI, Heinz-Otto KREISS et al. « The analysis and simulation of compressible turbulence ». In : *Theoretical and Computational Fluid Dynamics* 2.2 (1990), p. 73-95. DOI : 10.1007/bf00272136 (cf. p. 19, 21, 33).

[EGH00] Robert EYMARD, Thierry GALLOUËT et Raphaèle HERBIN. *Finite volume methods*. Elsevier, 2000 (cf. p. 96).

[FM19] Gloria FACCANONI et Hélène MATHIS. « Admissible Equations of State for Immiscible and Miscible Mixtures ». In : *ESAIM : Proceedings and Surveys* 66 (2019), p. 1-21. DOI : 10.1051/proc/201966001 (cf. p. 131).

[Fav58] Alexandre FAVRE. « Equations statistiques des gaz turbulents ». In : *Compte-Rendus de l'Académie des Sciences Paris* 246.18 (1958), p. 2576-2579 (cf. p. 21, 33, 83).

[Fav65] Alexandre FAVRE. « Equations des gaz turbulents compressibles. 1, Formes générales. 2, Méthode des vitesses moyennes ; méthode des vitesses macroscopiques pondérées par la masse volumique. » In : *Journal de Mécanique* 4.3 (1965) (cf. p. 33, 83).

[Fav+76] Alexandre FAVRE, Leslie S.G. KOSVAZNAY, Raymond DUMAS et al. *La turbulence en mécanique des fluides : bases théoriques et expérimentales, méthodes statistiques*. Gauthier-Villars, 1976 (cf. p. 33, 83).

[FHL97] Alain FORESTIER, Jean-Marc HÉRARD et Xavier LOUIS. « Solveur de type Godunov pour simuler les écoulements turbulents compressibles ». In : *Comptes Rendus de l'Académie des Sciences-Series I-Mathematics* 324(8) (1997), p. 919-926. DOI : 10.1016/s0764-4442(97)86969-8 (cf. p. 19, 34).

[GHS02] T. GALLOUËT, J.-M. HÉRARD et N SEGUIN. « Some recent finite volume schemes to compute Euler equations using real gas EOS ». In : *International journal for numerical methods in fluids* 39.12 (2002), p. 1073-1138. DOI : 10.1002/fld.346 (cf. p. 155, 172).

[GB13] Thomas B GATSKI et Jean-Paul BONNET. *Compressibility, turbulence and high speed flow*. Academic Press, 2013. URL : https://www.researchgate.net/publication/281766815_Compressibility_Turbulence_and_High_Speed_Flow (cf. p. 19, 33, 83).

[GG12] S. GAVRILYUK et H. GOUIN. « Geometric evolution of the Reynolds stress tensor ». In : *International Journal of Engineering Science* 59 (oct. 2012), p. 65-73. DOI : 10.1016/j.ijengsci.2012.03.008 (cf. p. 20).

[Gav+22] Sergey GAVRILYUK, Jean-Marc HÉRARD, Olivier HURISSE et al. « Theoretical and numerical analysis of a simple model derived from compressible turbulence ». In : *Journal of Mathematical Fluid Mechanics* 24.2 (2022), p. 1-34. DOI : 10.1007/s00021-022-00676-5 (cf. p. 26, 83, 85, 94, 96, 97, 99, 128, 129, 133-135, 139, 142, 154, 180).

[GS06] Sergey GAVRILYUK et Richard SAUREL. « Estimation of the turbulent energy production across a shock wave ». In : *Journal of Fluid Mechanics* 549 (2006), p. 131. DOI : 10.1017/s0022112005008062 (cf. p. 21, 24, 26, 33, 34, 64, 82, 83, 87, 88, 109, 113-116, 128, 129, 142, 148, 165, 180, 181).

[GL04] Paola GOATIN et Philippe G LEFLOCH. « The Riemann problem for a class of resonant hyperbolic systems of balance laws ». In : *Annales de l'Institut Henri Poincaré C, Analyse non linéaire*. T. 21. 6. Elsevier. 2004, p. 881-902. DOI : 10.1016/j.anihpc.2004.02.002 (cf. p. 115).

[GR96] Edwige GODLEWSKI et Pierre-Arnaud RAVIART. *Numerical approximation of hyperbolic sytems of conservation laws*. Springer Berlin, 1996. DOI : 10.1007/978-1-4612-0713-9 (cf. p. 45, 55, 64, 91, 132, 135, 166).

[God59] Sergueï Konstantinovitch GODUNOV. « A difference method for numerical calculation of discontinuous equations of hydrodynamics ». In : *Math sbornik (in Russian)* 47(89).3 (1959), p. 271-306. URL : https://hal.archives-ouvertes.fr/hal-01620642 (cf. p. 45, 91).

[Gos01] Laurent GOSSE. « A well-balanced scheme using non-conservative products designed for hyperbolic systems of conservation laws with source terms ». In : *Mathematical Models and Methods in Applied Sciences* 11.02 (2001), p. 339-365. DOI : 10.1142/s021820250100088x (cf. p. 115).

[GL96] Joshua M GREENBERG et Alain-Yves LEROUX. « A well-balanced scheme for the numerical processing of source terms in hyperbolic equations ». In : *SIAM Journal on Numerical Analysis* 33.1 (1996), p. 1-16. DOI : 10.1137/0733001 (cf. p. 115).

[Hel+10] Philippe HELLUY, Jean-Marc HÉRARD, Hélène MATHIS et al. « A simple parameter-free entropy correction for approximate Riemann solvers ». In : *Comptes rendus Mécanique* 338(9) (2010), p. 493-498. DOI : 10.1016/j.crme.2010.07.007 (cf. p. 23, 47, 54).

[HHQ20] J.-M. HÉRARD, O. HURISSE et L. QUIBEL. « A four-field three-phase flow model with both miscible and immiscible components ». In : *ESAIM : Mathematical Modelling and Numerical Analysis* (2020). DOI : 10.1051/m2an/2020037 (cf. p. 131).

[HM19] J.-M. HÉRARD et H. MATHIS. « A three-phase flow model with two miscible phases ». In : *ESAIM : Mathematical Modelling and Numerical Analysis* 53.4 (2019), p. 1373-1389. DOI : 10.1051/m2an/2019028 (cf. p. 131).

[Hér14] Jean-Marc HÉRARD. Rapp. tech. A simple turbulent model for compressible flows, 2014. URL : https://hal.archives-ouvertes.fr/hal-02007044 (cf. p. 20, 21, 23, 26, 35, 36, 83, 85, 133-135, 139, 180).

[HL16] Jean-Marc HÉRARD et Hippolyte LOCHON. « A simple turbulent two-fluid model ». In : *Comptes Rendus Mécanique* 344(11-12) (2016), p. 776-783. DOI : 10.1016/j.crme.2016.10.010 (cf. p. 20, 21, 23, 35, 85).

[HQ21] Olivier HURISSE et Lucie QUIBEL. « Simulations of liquid-vapor water flows with non-condensable gases on the basis of a two-fluid model. » In : *Applied Mathematical Modelling* (2021). DOI : 10.1016/j.apm.2021.06.020 (cf. p. 131).

[Jun13] J. JUNG. « Numerical simulations of two-fluid flow on multicores accelerator ». PhD Thesis. Université de Strasbourg, oct. 2013. URL : https://tel.archives-ouvertes.fr/tel-00876159 (cf. p. 135).

[KS11] Masashi KANAMORI et Kojiro SUZUKI. « Shock wave detection in two-dimensional flow based on the theory of characteristics from cfd data ». In : *Journal of Computational Physics* 230.8 (2011), p. 3085-3092. DOI : 10.1016/j.jcp.2011.01.007 (cf. p. 24, 92).

[Lou95] Xavier LOUIS. « Modélisation numérique de la turbulence compressible ». Thèse de doct. Paris 6, 1995 (cf. p. 19).

[MFG99] Jean-Marie MASELLA, Isabelle FAILLE et Thierry GALLOUËT. « On an approximate Godunov scheme ». In : *International Journal of Computational Fluid Dynamics* 12(2) (1999), p. 133-149. DOI : 10.1080/10618569908940819 (cf. p. 45).

[Mat19] H. MATHIS. « A thermodynamically consistent model of a liquid-vapor fluid with a gas ». In : *ESAIM : Mathematical Modelling and Numerical Analysis* 53.1 (2019), p. 63-84. DOI : 10.1051/m2an/2018044 (cf. p. 20, 25, 128, 131).

[MP93] Bijan MOHAMMADI et Olivier PIRONNEAU. *Analysis of the k-epsilon turbulence model*. Masson, 1993 (cf. p. 19).

[NGV14] N. Ben NASR, G.A. GEROLYMOS et I. VALLET. « Low-diffusion approximate Riemann solvers for Reynolds-stress transport ». In : *Journal of Computational Physics* 268 (juill. 2014), p. 186-235. DOI : 10.1016/j.jcp.2014.02.010 (cf. p. 20).

[Pop00] Stephen B POPE. *Turbulent flows*. Cambridge university press, 2000. DOI : 10.1017/cbo9780511840531 (cf. p. 19, 83).

[RG13] G. L. RICHARD et S. L. GAVRILYUK. « The classical hydraulic jump in a model of shear shallow-water flows ». In : *Journal of Fluid Mechanics* 725 (mai 2013), p. 492-521. DOI : 10.1017/jfm.2013.174 (cf. p. 20).

[RG15] G. L. RICHARD et S. L. GAVRILYUK. « Modelling turbulence generation in solitary waves on shear shallow water flows ». In : *Journal of Fluid Mechanics* 773 (mai 2015), p. 49-74. DOI : 10.1017/jfm.2015.236 (cf. p. 20).

[SCR03] R SAUREL, A CHINNAYYA et F RENAUD. « Thermodynamic analysis and numerical resolution of a turbulent-fully ionized plasma flow model ». In : *Shock Waves* 13.4 (2003), p. 283-297. DOI : 10.1007/s00193-003-0216-z (cf. p. 20, 25, 128).

[Smo83] Joel SMOLLER. *Shock waves and reaction—diffusion equations*. Springer Science & Business Media, 1983. DOI : 10.1007/978-1-4684-0152-3 (cf. p. 22, 41, 45, 64, 65, 92).

[SA94] Philippe SPALART et Steven ALLMARAS. « A one-equation turbulence model for aerodynamic flows ». In : *La Recherche Aérospatiale* (1994), p. 5-21. URL : https://arc.aiaa.org/doi/10.2514/6.1992-439 (cf. p. 19, 21, 33, 34, 83).

[TL72] Henk TENNEKES et John Leask LUMLEY. « A First Course in Turbulence. » In : *MIT Press* (1972). DOI : 10.7551/mitpress/3014.003.0005 (cf. p. 19, 21, 33, 83).

[Tor97] Eleuterio Francisco TORO. *Riemann solvers and numerical methods for fluid dynamics*. Springer Berlin Heidelberg, 1997. DOI : 10.1007/978-3-662-03490-3 (cf. p. 45, 55, 91).

[VM86] D. VANDROMME et H.Ha MINH. « About the coupling of turbulence closure models with averaged Navier-Stokes equations ». In : *Journal of Computational Physics* 65.2 (août 1986), p. 386-409. DOI : 10.1016/0021-9991(86)90214-7 (cf. p. 19).

[Wil98] David WILCOX. *Turbulence Modelling for CFD*. DCW Industries, 1998 (cf. p. 19, 21, 33, 34).

[Wu+13] Ziniu WU, Yizhe XU, Wenbin WANG et al. « Review of shock wave detection method in CFD post-processing ». In : *Chinese Journal of Aeronautics* 26.3 (2013), p. 501-513. DOI : 10.1016/j.cja.2013.05.001 (cf. p. 24, 92).

[Yan68] NN YANENKO. *Méthode à pas fractionnaires : résolutions de problèmes polydimensionnels de physique mathématique*. A. Colin, 1968. URL : https://books.google.fr/books?id=JBIyvgAACAAJ (cf. p. 26, 148).